

Syracuse University

SURFACE

Dissertations - ALL

SURFACE

May 2014

PATTERNED BIOFILM FORMATION TO INVESTIGATE BACTERIA-SURFACE INTERACTIONS

Huan Gu
Syracuse University

Follow this and additional works at: <https://surface.syr.edu/etd>



Part of the [Engineering Commons](#)

Recommended Citation

Gu, Huan, "PATTERNED BIOFILM FORMATION TO INVESTIGATE BACTERIA-SURFACE INTERACTIONS" (2014). *Dissertations - ALL*. 91.
<https://surface.syr.edu/etd/91>

This Dissertation is brought to you for free and open access by the SURFACE at SURFACE. It has been accepted for inclusion in Dissertations - ALL by an authorized administrator of SURFACE. For more information, please contact surface@syr.edu.

ABSTRACT

Bacterial adhesion to surfaces and subsequent formation of microcolonies play important roles in biofilm formation, which is a major cause of chronic infections and persistent biofouling. Despite the significance, mechanistic understanding of biofilm formation is still hindered by the structural heterogeneity in biofilms; and effective control of biofilm formation remains challenging. Biofilm formation is a dynamic process that involves numerous changes in bacterial gene and protein expression. These changes are highly sensitive to environmental factors such as surface chemistry, topography, charge, and hydrophobicity. To better control biofilm morphology and specifically investigate the effects of these factors, a platform was developed in this study to obtain patterned biofilm formation using surfaces with well-defined patterns of chemistry and topography.

By modifying surfaces with systematically varied square patterns of self-assembled monolayers (SAMs) of functional alkanthiols, the size of cell clusters and inter-cluster distance were well controlled. By following biofilm formation of *Escherichia coli* on these surfaces, it was found that multicellular connections were formed between adjacent cell clusters when the clusters were within a threshold distance (10 μm); and such connections were influenced by the size of interacting cell clusters. It was also found that the connections were formed by active interactions of cell clusters, rather than nonspecific binding of planktonic cells on the bioinert background. Interestingly, the mutants of *luxS* and *motB* exhibited major defects in interaction between cell clusters. The phenotype of the *luxS* mutant was successfully restored by both complementing the *luxS* gene on a plasmid and by adding the precursor of

autoinducer-2 (AI-2) signal in the culture. These results suggest that AI-2 mediated quorum sensing and motility are involved in the interaction among cell clusters. Based on these findings, a model was proposed to explain the intrinsic heterogeneity in biofilm structures. Consistently, cells attached between interacting clusters were found to be more sensitive to the antibiotic ampicillin.

Besides surfaces with patterns of surface chemistry, poly(dimethylsiloxane) (PDMS) surfaces with microtopographic patterns of different shapes, dimensions and inter-pattern distances were used to understand the effects of surface topography on bacteria-surface interactions and biofilm formation. *E. coli* was found to preferentially attach and form biofilms in the valleys between square shaped plateaus. In addition, there appeared to be a threshold dimension of a plateau to allow bacterial attachment and biofilm formation on top of the plateaus. The threshold was found to be $40\ \mu\text{m} \times 40\ \mu\text{m}$ for inverted patterns used in this study. Inspired by this finding, we created PDMS surfaces with hexagon shaped patterns and found that the ones with $15\ \mu\text{m}$ side width and $2\ \mu\text{m}$ inter-pattern distance can reduce biofilm formation by 7-fold compared to flat PDMS surfaces.

These results were integrated with additional tests to better understand the resistance of biofilm cells to antibiotics. Specifically, the biofilm formation of fluorescently labeled donors and recipients on PDMS surfaces with square shaped microtopographic patterns was followed to investigate the effects of cell density on bacterial conjugation. PDMS surfaces with microtopographic patterns were found to promote both biofilm formation and bacterial conjugation. This result was found to be due to the aggregation of biofilm cells on the side of plateaus, providing “hot spots” for

bacterial conjugation. Bacterial motility was also found to play an important role in biofilm formation and bacterial conjugation. Collectively, these results are helpful for understanding the mechanism of biofilm formation and associated drug resistance, as well as the design of nonfouling surfaces.

Keywords: Patterned biofilm, bacterial-surface interaction, biofilm heterogeneity, high drug resistance, conjugation, surface chemistry, surface topography.

**PATTERNED BIOFILM FORMATION TO INVESTIGATE
BACTERIA-SURFACE INTERACTIONS**

By

Huan Gu

B.S. China University of Mining and Technology, Beijing, P. R. of China, 2006

M.S. China University of Mining and Technology, Beijing, P. R. of China, 2009

DISSERTATION

Submitted in the partial fulfillment of the requirements for

the degree of Doctors of Philosophy in Chemical

Engineering in the Graduate School of Syracuse University

May 2014

Copyright 2014 Huan Gu

All Rights Reserved

ACKNOWLEDGEMENTS

First, I would like to thank my advisor Dr. Dacheng Ren, who brought me into Syracuse University and this fascinating research area. Without him, I will not be part of such a great project and gain so much knowledge and experience in five years. He is always willing to give suggestions on scientific problems and personal issues. He is very supportive and a good listener. Under his instruction with patience, knowledge, and talent, I am able to fulfill my Ph.D. with accomplishments and publications.

I wish to express profound gratitude to our great collaborator, Dr. Yang-Yeung Luk. Thank him for allowing us to access his equipment. I also want to thank Dr. John S. Parkinson (University of Utah), Dr. Søren Molin (Technical University of Denmark), Dr. Howard C. Berg (Harvard University) for generously sharing many useful strains. I also want to thank Robert P. Smith (N.C. Brown Center for Ultrastructure Studies) and Malcolm Thomas (Cornell Center for Materials Research) for providing valuable suggestions on operating scanning electron microscope.

I thank Syracuse University for supporting me with one year of teaching assistantship and the National Science foundation for funding the projects.

I sincerely appreciate my committee members and other professors and staffs at Syracuse University, Dr. Roy D. Welch, Dr. James H. Henderson, Dr. Patrick T. Mather, Dr. Ashok S. Sangani, Dr. Pranav Soman, Dr. Rebecca Bader, Dr. Julie M. Hasenwinkel, Dr. George Martin, Dr. Radhakrishna Sureshkuma, Dr. Lawrence L. Tavlarides, Dawn M. Long, Kristin Lingo, Sabina Redington, and Lynore de la Rosa for helping me with my projects and graduate study. Especially, I want to thank Dr. Jacques Lewalle and Dr. Paula Rosenbaum for their friendship and support.

I want to thank all my colleagues in the Ren Laboratory, Dr. Shuyu Hou, Dr. Jiachuan Pan, Dr. Tagbo Herman Roland Niepa, Dr. Xiangyu Yao, Dr. Hashimul Ehsan, Jing Wang, Srujana Govindarajulu, Chanokpon Yongat, Kris Kolewe, Shanelle Simone Gayle, Cassi Smith, Tom Russell, Henry Lars Peterson, Ginger Star Gunnip, Aaron Chen, Fangchao Song, Wen-Hsuan Huang, Ali Adam Bahar, Geetika Choudary, Li Zhang, Shuyuan Ma, Meagan Garafalo, and Robert Joseph Neiberger. They are very generous and supportive. It was a great pleasure to work with them.

I want to express my sincerest appreciation to my parents, Qisheng Gu and Chunmei Li, my parents-in-law Xin Wang and Chenghai Yin for their love and support. My greatest gratitude goes to my lovely husband Ran Yin. Thank him for his love, patience, sacrifice, and encouragement. Without him, I will not be able to finish my study.

TABLE OF CONTENTS

ACKNOWLEDGMENTS.....	VI
TABLE OF CONTENTS.....	VII
LIST OF TABLES.....	XI
LIST OF FIGURES.....	XII
CHAPTER 1 MOTIVATION, RATIONALE, RESEARCH HYPOTHESIS, AND OBJECTIVES	1
1.1 MOTIVATION	2
1.2 RATIONALE.....	4
1.2.1 <i>Heterogeneity in biofilm structure</i>	4
1.2.2 <i>Biofilm resistance to antibiotics</i>	5
1.2.3 <i>Effects of surface topography on biofilm formation</i>	6
1.3 CENTRAL HYPOTHESIS AND RESEARCH OBJECTIVES	7
1.4 TABLES.....	9
1.5 REFERENCES	12
CHAPTER 2 INTRODUCTION	16
2.1 BIOFILM FORMATION	18
2.2 GENES INVOLVED IN BIOFILM FORMATION.....	20
2.3 BIOFILM HETEROGENEITY	24
2.4 BIOFILM-ASSOCIATED ANTIBIOTIC RESISTANCE.....	25
2.5 MATERIALS USED IN TRADITIONAL BIOFILM STUDIES	27
2.6 NEW TECHNIQUES TO CONTROL CELL DENSITY AND CREATE PATTERNED CELL CLUSTERS	28
2.6.1 <i>Lipid-silica structures</i>	29
2.6.2 <i>Microwells</i>	29
2.6.3 <i>Microfluidic devices</i>	30
2.6.4 <i>Direct printing</i>	32
2.6.5 <i>Hydrogels</i>	32
2.6.6 <i>Chemical modification using microcontact printing</i>	34
2.7 PHYSICAL SURFACE MODIFICATION FOR BIOFILM CONTROL	36
2.8 FIGURE CAPTIONS.....	39
2.9 FIGURES	43
2.10 TABLES.....	51
2.11 REFERENCES	53
CHAPTER 3 PATTERNED BIOFILM FORMATION REVEALS A MECHANISM FOR STRUCTURAL HETEROGENEITY IN BACTERIAL BIOFILMS AND IMPORTANT INFORMATION OF BIOFILM-ASSOCIATED ANTIBIOTIC RESISTANCE.....	64
3.1 ABSTRACT.....	66
3.2 INTRODUCTION	68

3.3 MATERIALS AND METHODS.....	70
3.3.1 Bacterial strains and growth media.....	70
3.3.2 Genetic complementation of the luxS mutant.....	70
3.3.3 Chemicals.....	71
3.3.4 Preparation of the surfaces.....	71
3.3.5 Biofilm formation.....	72
3.3.6 Fluorescence microscopy.....	73
3.3.7 Definition of Cell Cluster Interaction Index (CII).....	74
3.3.8 Differentiating seeding cells from those formed during biofilm growth.....	75
3.3.9 Flow cell experiment.....	75
3.3.10 Long-term biofilm experiment.....	76
3.3.11 Antibiotic treatment.....	77
3.3.12 Antibiotic susceptibility of biofilm cells on patterned surfaces.....	78
3.3.13 Sample preparation for scanning electron microscopy.....	79
3.3.14 Statistics.....	80
3.4 RESULTS.....	80
3.4.1 Patterned biofilm formation revealed interaction among cell clusters.....	80
3.4.2 Pattern size and inter-pattern distance affected interactions among cell clusters.....	81
3.4.3 Interactions between cell clusters are involved in biofilm structural organization.....	83
3.4.4 Imaging cell surface structures with scanning electron microscopy (SEM).....	85
3.4.5 Mutation of key genes affected interaction among cell clusters.....	86
3.4.6 Interaction among cell clusters involves quorum sensing.....	87
3.4.7 E. coli cells exhibited changes in antibiotic susceptibility during the early stage biofilm formation.....	89
3.4.8 Location of biofilm cells and antibiotic susceptibility.....	89
3.5 DISCUSSION.....	92
3.7 FIGURE CAPTIONS.....	94
3.8 FIGURES.....	98
3.9 TABLES.....	122
3.10 REFERENCES.....	125

CHAPTER 4 MICROTOPOGRAPHIC PATTERNS AFFECT <i>ESCHERICHIA COLI</i> BIOFILM FORMATION ON POLY(DIMETHYLSILOXANE) SURFACES	129
4.1 ABSTRACT.....	131
4.2 INTRODUCTION.....	132
4.3 MATERIALS AND METHOD.....	134
4.3.1 Bacterial strains and medium.....	134
4.3.2 PDMS surfaces preparation.....	134
4.3.3 Biofilm formation and imaging analysis.....	134
4.4 RESULTS.....	136
4.4.1 Effects of surface topography on bacterial cell-surface interaction.....	136
4.4.2 Reducing biofouling by changing surface topography.....	137
4.5 DISCUSSION.....	139

4.6 ACKNOWLEDGMENTS	141
4.7 FIGURE CAPTIONS.....	143
4.8 FIGURES	146
4.9 REFERENCES	155

CHAPTER 5 CONJUGATION IN *ESCHERCHIA COLI* BIOFILMS ON POLY(DIMETHYLSILOXINE) SURFACES WITH MICROTOPOGRAPHIC PATTERNS **157**

5.1 ABSTRACT.....	158
5.2 INTRODUCTION.....	159
5.3 MATERIALS AND METHODS.....	161
5.3.1 <i>Bacterial strains and growth media</i>	161
5.3.2 <i>PDMS surfaces</i>	161
5.3.3 <i>Biofilm formation and conjugation</i>	162
5.3.4 <i>Conjugation frequency</i>	163
5.4 RESUTLS	164
5.4.1 <i>Surface topography affected E. coli conjugation in biofilm</i>	164
5.4.2 <i>Conjugation at different locations of the microtopographic patterns</i>	165
5.4.3 <i>E. coli motility mutant exhibited defects in conjugation</i>	166
5.5 DISCUSSION	168
5.6 FIGURE CAPTIONS.....	170
5.7 FIGURES	174
5.8 TABLE.....	184
5.9 REFERENCES	185

CHAPTER 6 CONCLUSIONS AND RECOMMENDATIONS FOR FUTURE WORK..... **188**

6.1 CONCLUSIONS.....	189
6.2 RECOMMENDATIONS FOR FUTURE WORK	193
6.2.1 <i>Role of bacterial motility in the bacteria-surface, bacterial cell-cell interactions, and bacterial conjugation</i>	193
6.2.2 <i>Role of bacterial surface structures during interaction between cell clusters</i> ..	194
6.2.3 <i>Effects of surface topography on bacterial cell-surface interaction and biofilm formation</i>	194
6.2.4 <i>Biofilm resistance to antibiotics</i>	195
6.3 REFERENCES	196

APPENDICES..... **197**

I. PROTOCOL FOR FABBRICATING SILICON WAFERS WITH MICROTOPOGRAPHIC FEATURES.....	198
II. PROTOCOL FOR GOLD SURFACE MODIFICATION.....	207
III. PROTOCOL FOR LABELING BACTERIA WITH ACRIDINE ORANGE.....	209
IV. PROTOCOL FOR THIN LAYER GOLD DEPOSITION ON COVERSLEIPS.....	210

VITA.....	212
-----------	-----

LIST OF TABLES

Table 1-1.	Current techniques to immobilize bacteria.....	9
Table 2-1.	Summary of <i>E. coli</i> genes involved in biofilm formation.....	51
Table 3-1.	List of <i>E. coli</i> strains and plasmids used in this study.....	122
Table 3-2.	Pearson correlation coefficients between Cell Cluster Interaction Index (CII) and pattern size.....	123
Table 3-3.	Biofilm formation of <i>E. coli</i> RP437 and its isogenic mutants on patterned surfaces.....	124
Table 5-1.	Pearson correlation coefficients between percentage of transconjugation and inter-pattern distance; as well as biomass of recipient cells and inter-pattern distance. All data were acquired on PDMS surfaces with 10 μm tall 20 μm \times 20 μm topographic patterns and varying inter-pattern distance.....	185

LIST OF FIGURES

- Figure 2-1.** Representative images of 24, 48, and 72 h *E. coli* RP437 biofilms on glass, gold (without chemical modification), and stainless steel surfaces.....43
- Figure 2-2.** Cell confinement using lipid-silica structures. (A) Schematic description of the cell-directed integration of microbes in lipid templated silica films. The insert image (a5) is an atomic force microscopy (AFM) image of a *Saccharomyces cerevisiae* cell encapsulated in a lipid-silica shell. Reproduced with permission from Ref. [117]. Copyright 2010 American Chemical Society. (B) Single *Staphylococcus aureus* cells in lipid-silica droplets on glass surfaces. (b1) Schematic description of a cell incorporated in an endosome-like lipid vesicle within a lipid-silica droplet on glass surface. (b2) Scanning electron microscopy (SEM) image of the lipid-silica structure. (b3) and (b4) Left: plan-view optical image of individual cells in droplets. Right top: differential interference contrast (DIC) image of the confined cells. Right center: red fluorescence image of a stained cell. Right bottom: green fluorescence image of lipid on cell surface labeled with 7-nitro-2, 1, 3-benzoxadiazol-4-yl (NBD). (b3) Image of localized pH labeled with Oregon Green pH-sensitive dye (Bar = 5 μm). Reproduced with permission from Ref. [119]. Copyright 2010 Nature Publishing Group.....44
- Figure 2-3.** Individual cells trapped in microwells or microchambers. (A) Comparison of *Pseudomonas aeruginosa* adhesion on flat and modified surfaces. (a1) Top: fluorescence image of bacterial adhesion on flat surfaces. Bottom: fluorescence image of bacterial adhesion on a periodically structured epoxy surface. SYTOX[®] green nucleic acid stain was used to label cells (Bar = 10 μm). a2 and a3) Cross-sectional SEM image of *P. aeruginosa* PA14 cells on flat (a2) and structured surfaces (a3) (Bar = 1 μm). Reproduced with permission from Ref. [123]. Copyright 2010 American Chemical Society. (B) Controlling the shape of filamentous *E. coli* cells in microchambers fabricated in agarose containing growth media. (b1) Schematic description of the microchambers. (b2) A single *E. coli* cell confined in a microchamber. (b3) Growth of a filamentous cell in the presence of cephalexin. (b4) Cell is released into solution. (b5) and (b6) Phase-contrast microscopy images of donut-shaped microchambers with cells before (b5) and after (b6) the growth of filamentous *E. coli* cells (Bar = 50 μm). (b7) Phase-contrast image of spiral, filamentous *E. coli* cells in solution (Bar = 10 μm). Reproduced with permission from Ref. [122]. Copyright 2005 American Chemical Society.....45
- Figure 2-4.** Schematic description of the techniques of soft lithography: (a). replica moulding; (b). micromoulding in capillaries; (c). microfluidics; d. microcontact printing. Reproduced with permission from Ref. [109]. Copyright 2007 Nature Publishing Group.....46

- Figure 2-5.** Bacterial microcontact-printing. (A-E) Schematic description of the process. (F) Image of an agarose stamp (Bar = 10 mm). (G) Circle-shaped patterns of *Vibrio fischeri* colonies (Bar = 2 mm). (H) Checkerboard patterns of *V. fischeri* colonies (Bar = 2 mm). (I) Honeycomb patterns *V. fischeri* colonies (Bar = 250 μ m). Reproduced with permission from Ref. [143]. Copyright 2005 American Chemical Society.....47
- Figure 2-6.** Small groups of bacterial cells confined in hydrogel microchambers or microstructures. (A) The confinement of *P. aeruginosa* cells in lobster traps with walls consisted of various proteins. (a1) Schematic description of the optical setup. (a2) Heart-shaped, 2-picoliter traps with (left and right) and without (middle) *P. aeruginosa* cells (Bar = 5 μ m). (a3) Confocal images of traps with *P. aeruginosa* cells after 2 h gentamicin treatment at the minimal inhibitory concentration (MIC). Reproduced with permission from Ref. [149]. Copyright 2010 American Society for Microbiology. B) *P. aeruginosa* microcolonies in 3D gelatin structures. (b1) Confocal images of *P. aeruginosa* microcolonies in a surface-anchored 2-pL pyramid (top) and an untethered 3-pL torus (bottom). (b2) Confocal images of six physically segregated *P. aeruginosa* populations in 3D spheroid cavities tethered to the glass substrate. (b3) Three connected spheroid cavities tethered to the glass surface by cylindrical posts. The top-down DIC image (left), side-on confocal image (center) and top-down confocal image (right) are shown. Reproduced with permission from Ref. [150]. Copyright 2013 National Academy of Sciences. (C) Diffusion of HSL between *P. aeruginosa* biofilm cell clusters confined in hydrogel chambers. Reproduced with permission from Ref. [82]. Copyright 2011 American Chemical Society.....48
- Figure 2-7.** A corral array of trapped *E. coli* cells (Bar = 20 μ m). Reproduced with permission from Ref. [167], Copyright 2012 American Chemical Society...49
- Figure 2-8.** Representative SEM images of *S. aureus* biofilm formation on smooth (left column) and Sharklet AF (right column) PDMS surfaces. (A) and (B) day 0, (C) and (D) Day 2, (E) and (F) Day 7, (G) and (H) Day 14, and (I) and (J) Day 21. Reproduced with permission from Ref. [177]. Copyright 2007 Springer.....50
- Figure 3-1.** Representative images of *E. coli* RP437 biofilms. (A) Heterogeneous biofilms formation on glass, gold (without chemical modification), and stainless steel surfaces (Bar = 50 μ m). (B) Patterned biofilms formed on gold surfaces modified with self-assembled monolayers (SAMs) presenting functional groups (Bar = 50 μ m).....98
- Figure 3-2.** Genetic complementation of the *luxS* mutant. (A) Map of the pCR[®]2.1 TOPO[®] vector. (B) The gel image indicating the the *luxS* gene and its promoter were obtained. (C) PCR product of the *luxS* gene amplified from the cloned plasmid.....99

Figure 3-3. Schematic description of the pattern generation through photolithograph, soft lithography and microcontact printing.....	100
Figure 3-4. Schematic description of gold surfaces modified with square patterns of CH ₃ -SAM and background of TEG-SAM.....	101
Figure 3-5. Representative fluorescence images of 24 h <i>E. coli</i> RP437 biofilms on 20 μm × 20 μm patterns with inter-pattern distance of 2 (A), 5 (B), 10 (C), or 15 (D) μm (Bar = 50 μm).	102
Figure 3-6. Interaction between <i>E. coli</i> cell clusters: representative cell clusters with 5 (A) or 10 (B) μm distance; and schematic illustration of interaction between adjacent cell clusters (C) (Bar = 10 μm).....	103
Figure 3-7. Effects of inter-pattern distance on CII values of <i>E. coli</i> RP437 biofilms. N=3 biological repeats averaged; at least 15 images were analyzed for each data point.....	104
Figure 3-8. Effects of pattern size on CII values. N=3 biological repeats averaged; at least 15 images were analyzed for each data point.....	105
Figure 3-9. Ratios of surface coverage on TEG-SAM (EB) of 20μm×20μm pattern surfaces (with varying inter-pattern distance) to that on pattern-free TEG-SAM surfaces. N=3 biological repeats averaged; at least 15 images were analyzed for each data point.....	106
Figure 3-10. Connections between cell clusters (W = 20 μm; D = 10 μm) were formed due to growth of cells from adjacent clusters rather than settlement of seeding cells. Representative cell clusters after 3 h of initial attachment (A) and 7 h of growth (B) are shown (Bar = 10 μm).....	107
Figure 3-11. Representative images of cell growth during early stage of patterned biofilm formation in a flow cell (Bar = 10 μm).....	108
Figure 3-12. Representative images of cell growth in early stage of patterned biofilm formation in batch culture (Bar = 10 μm).....	109
Figure 3-13. SEM image of <i>E. coli</i> RP437 cells in 24 h biofilms formed on a gold surface modified with size 20 μm × 20 μm patterns. Images were taken using JEOL 5800LV SEM.....	110
Figure 3-14. SEM images of <i>E. coli</i> RP437 cells in 2h (A) and 4h (B) biofilms formed on a gold surface modified with size 20 μm × 20 μm patterns. Images were obtained using JEOL 5800LV SEM.....	111
Figure 3-15. SEM images of <i>E. coli</i> RP437 cells in a 4 h biofilm formed on a gold surface modified with size 20 μm × 20 μm patterns. Samples were	

- dehydrated with tetramethylsilane (TMS) as the last step of dehydration. Images were obtained using JEOL 5800LV SEM.....112
- Figure 3-16.** SEM images of *E. coli* RP437 cells in a 4 h biofilm formed on a gold surface modified with size 20 μm \times 20 μm patterns. Images were obtained using LEO 1550 FESEM.....113
- Figure 3-17.** Patterned biofilm formation of the wild-type *E. coli* RP437 and its four isogenic mutants. (A) Representative fluorescence images of biofilms formed on surfaces modified with 20 μm \times 20 μm CH₃-SAM patterns with varying inter-pattern distance (Bar = 50 μm). (B) CII values of biofilms shown in Figure 3-17A. N=3 biological repeats averaged for this graph; at least 15 images were analyzed for each data point.....114
- Figure 3-18.** Attachment of *E. coli* BL-19 (RP437 Δ *motB*) on a surface with 20 μm \times 20 μm SAM patterns after 24 h of incubation (Bar = 50 μm).....115
- Figure 3-19.** Genetic complementation of the *luxS* mutant. (A) Representative fluorescence images of patterned biofilms of *E. coli* RP437, its *luxS* mutant KX1485, and the complemented *luxS* mutant KX1485/pRHG01 (Bar = 50 μm). (B) CII values of biofilms shown in Figure 3-19A. N=3 biological repeats averaged for this graph; at least 15 images were analyzed for each data point.....116
- Figure 3-20.** Chemical complementation of the *luxS* mutant with AI-2 precursor DPD. (A) Representative fluorescence images of patterned biofilms of *E. coli* RP437, its *luxS* mutant KX1485, and KX1485 supplemented with 50 or 100 μM DPD (Bar = 50 μm). (D) CII values of biofilms shown in Figure 3-20A. N=3 biological repeats averaged for this graph; at least 15 images were analyzed for each data point.....117
- Figure 3-21.** Co-culture biofilms on 20 μm \times 20 μm patterns. (A) Representative fluorescence images of 48 h biofilms with *E. coli* RP437/pRSH109 and KX1485/pDsRed inoculated as 4:1, 1:1, and 1:4 ratios (Bar = 50 μm). (B) Relative surface coverage of the above co-culture biofilms.....118
- Figure 3-22.** Viability of biofilm cells after treatment with 200 $\mu\text{g}/\text{ml}$ ampicillin for 3h *E. coli* HM22 biofilms were formed on glass wool. The CFU of untreated cells for each condition was normalized as 100%. N=3 biological repeats averaged for this graph.....119
- Figure 3-23.** Ampicillin susceptibility of *E. coli* RP437 cells in patterned biofilms. (A) Representative images of the patterned *E. coli* RP437 biofilms (2, 4, 6, and 24 h after inoculation) on gold surfaces modified with 20 μm \times 20 μm square shaped patterns with 15 μm inter-pattern distance. The biofilms were treated with 200 $\mu\text{g}/\text{mL}$ ampicillin for 1 h and labeled with LIVE/DEAD[®] BackLight[™] Bacteria Viability Kit before imaging (Bar = 10 μm). (B)

Viability of cells in patterned <i>E. coli</i> RP437 biofilms (2, 4, 6, and 24 h) analyzed using COMSTAT.....	120
Figure 3-24. Schematic description of early stage bacterial biofilm formation on uncontrolled surfaces (A) and well-defined surfaces (B).....	121
Figure 4-1. SEM picture of a representative patterned PDMS surface with size 50 μm \times 50 μm patterns and 30 μm inter-pattern distance (Bar = 20 μm).....	146
Figure 4-2. Biofilm formation of <i>E. coli</i> RP437/pRSH103 on upright PDMS surfaces with square shaped microtopographic patterns. (A) Three dimensional view of biofilm formation on a PDMS surface with 100 μm (W) \times 100 μm (W) \times 10 μm (H) patterns and 20 μm inter-pattern distance. (B) Representative fluorescence images of <i>E. coli</i> RP437/pRSH103 biofilms on upright PDMS surfaces with systematically varied topographies (D = 10 μm) (B1-B6) and on smooth PDMS surface (B7) (Bar = 10 μm). (C) The surface coverage (mean \pm one standard error) of <i>E. coli</i> RP437/pRSH103 biofilms formed on top of face-up protruding patterns. The side width of tested square features (W) was 5, 10, 15, 20, 30, 40, 50, or 100 μm . The surface coverage was calculated using COMSTAT software.....	147
Figure 4-3. Representative fluorescence images of <i>E. coli</i> RP437/pRSH103 biofilms on inverted PDMS surfaces with systematically varied microtopography (D = 10 μm) (A-G) and on inverted smooth PDMS surface (H) (Bar = 10 μm).....	148
Figure 4-4. Surface coverage (mean \pm one standard error) of <i>E. coli</i> RP437/pRSH103 biofilms formed on top of inverted protruding patterns. The side width of square features (W) tested was 5, 10, 15, 20, 30, 40, 50, or 100 μm and the inter-pattern distance was 5, 10, 15, or 20 μm . The surface coverage was calculated using COMSTAT software. N=3 biological repeats averaged; at least 15 images were analyzed for each data point.....	149
Figure 4-5. Biofilm formation of <i>E. coli</i> RP3087/pRSH103 on PDMS surfaces with 100 μm \times 100 μm topographic patterns. (A) Representative fluorescence image of <i>E. coli</i> RP3087/pRSH103 on upright PDMS surfaces (Bar = 20 μm). (B) The surface coverage (mean \pm one standard deviation) of <i>E. coli</i> RP3087/pRSH103 biofilms formed on top of upright protruding patterns. The distance was set to be 5, 10, 15, or 20 μm . The surface coverage was calculated using COMSTAT software. (C) Representative fluorescence images of <i>E. coli</i> 3087/pRSH103 on inverted PDMS surfaces. N=3 biological repeats averaged; at least 15 images were analyzed for each data point....	150
Figure 4-6. Representative fluorescence images of <i>E. coli</i> RP437/pRSH103 biofilms on upright PDMS surfaces modified with hexagon shaped topographic features with different size but the same 2 μm inter-pattern distance (A-E) and on smooth PDMS surfaces (F) (Bar = 10 μm).....	151

- Figure 4-7.** Biofilm formation of *E. coli* RP437/pRSH103 on upright PDMS surfaces with microtopographic patterns. (A) The biomass (mean \pm one standard deviation) of *E. coli* RP437/pRSH103 biofilms formed on PDMS surfaces with hexagon shaped topographic patterns. The width of hexagon shaped features (W) was set to be 2, 5, 10, 15, or 20 μm and inter-pattern distance (D) was set to be 2, 5, 10, 15, or 20 μm . All combinations were tested. Biomass was calculated using COMSTAT software. N=3 biological repeats averaged; at least 15 images were analyzed for each data point. (B) Comparison between the biomass (mean \pm one standard deviation) of biofilms formed on PDMS surfaces with 15 $\mu\text{m} \times 15 \mu\text{m}$ square shaped topographic patterns (225 μm^2) and on PDMS surfaces with hexagon shaped topographic patterns with side width of 10 μm (259 μm^2). Biomass was calculated using COMSTAT software. N=3 biological repeats averaged; at least 15 images were analyzed for each data point.....152
- Figure 4-8.** Representative fluorescence images of *E. coli* RP437/pRSH103 biofilms on inverted PDMS surfaces modified with hexagon shaped patterns with side width of 20 μm and different inter-pattern distance (A-E) (Bar = 10 μm)..153
- Figure 4-9.** The number per unit area (mean \pm one standard error) of *E. coli* RP437/pRSH103 cells on inverted PDMS surfaces with systematically varied hexagon shaped microtopographic patterns. The side width (W) of the hexagon patterns was set to be 2, 5, 10, 15, or 20 μm and inter-pattern distance (D) was set to be 2, 5, 10, 15, or 20 μm . All combinations were tested. N=3 biological repeats averaged; at least 15 images were analyzed for each data point.....154
- Figure 5-1.** Bacterial conjugation on PDMS surfaces with microtopographic patterns. (A) Schematic presentation of the PDMS surfaces with microtopographic patterns. (B) Three-dimensional image of the donors and recipients co-culture biofilms on PDMS surfaces with 50 $\mu\text{m} \times 50 \mu\text{m}$ topographic patterns and 50 μm inter-pattern distance. IPTG (1mM) was used to induce the expression of green fluorescence protein in donors. (C) Top-down view of the donors and recipients co-culture biofilms on PDMS surfaces with 50 $\mu\text{m} \times 50 \mu\text{m}$ topographic patterns and 50 μm inter-pattern distance. The expression of green fluorescence protein in donors was not induced. (Bar = 20 μm) Left: the image combines green and red fluorescence channels. Right: the image combines Differential Interference Contrast (DIC) channel, green fluorescence, and red fluorescence channel.....175
- Figure 5-2.** The comparison between the biomass in biofilms formed on PDMS surfaces modified with 20 $\mu\text{m} \times 20 \mu\text{m}$, 50 $\mu\text{m} \times 50 \mu\text{m}$, and 100 $\mu\text{m} \times 100 \mu\text{m}$ microtopographic patterns with various inter-pattern distances (10, 15, 20, 30, 40, or 50 μm) and that on flat PDMS surfaces. Standard deviations are presented. N=6 biological repeats averaged; at least 30 images were analyzed for each data point.....176

- Figure 5-3.** The comparison between the unit area of conjugation frequency on PDMS surfaces modified with size 20 μm \times 20 μm , 50 μm \times 50 μm , and 100 μm \times 100 μm microtopographic patterns with various inter-pattern distances (10, 15, 20, 30, 40, or 50 μm) and that on flat PDMS surfaces. Standard errors are presented. N=6 biological repeats averaged; at least 30 images were analyzed for each data point.....177
- Figure 5-4.** Biomass of *E. coli* CSH26/pKJK (donor) and *E. coli* RP437/pRSH103 (recipient) co-culture biofilms on the side and on the top of the size 20 μm \times 20 μm , 50 μm \times 50 μm , and 100 μm \times 100 μm microtopographic patterns with various inter-pattern distances (10, 15, 20, 30, 40, or 50 μm), in the channel between close patterns, and on flat PDMS surfaces. Standard deviations are presented. N=6 biological repeats averaged; at least 30 images were analyzed for each data point.....178
- Figure 5-5.** Biofilms of *E. coli* CSH26/pKJK (donor) and *E. coli* RP437/pRSH103 (recipient) co-culture biofilms on inverted PDMS surfaces modified with size 20 μm \times 20 μm microtopographic patterns with 10 μm inter-pattern distance. (A) Donor and transconjugant cell clusters on the side of protruding patterns. (B) Donor and recipient cells on the side of protruding patterns. Left: the image combines Differential Interference Contrast (DIC) channel, green fluorescence, and red fluorescence channels. Right: the image combines green and red fluorescence channels.....179
- Figure 5-6.** The percentage of bacterial conjugation at different geometric locations (on the side and top of topographic patterns and in the channel between close patterns) around size 20 μm \times 20 μm , 50 μm \times 50 μm , and 100 μm \times 100 μm microtopographic patterns with various inter-pattern distances (10, 15, 20, 30, 40, or 50 μm). Standard errors are presented. N=6 biological repeats averaged; at least 30 images were analyzed for each data point.....180
- Figure 5-7.** Representative fluorescence images of motility mutant biofilms (A) and wild-type biofilms (B) on PDMS surfaces with size 20 μm \times 20 μm topographic patterns with 15 μm inter-pattern distance.....181
- Figure 5-8.** Effects of motility on biofilm formation and bacterial conjugation. (A & B) The biomass of motility mutant (A) and wild-type (B) biofilms at different geometric locations (on the side and top of plateaus and in the channel between close plateaus) around size 20 μm \times 20 μm topographic patterns with various inter-pattern distances (10, 15, 20, 30, 40, or 50 μm). (C) The comparison between the unit area conjugation frequency of wild-type strain, the unit area conjugation frequency of motility mutant in co-culture biofilms formed on PDMS surfaces with size 20 μm \times 20 μm topographic patterns with various inter-pattern distances (10, 15, 20, 30, 40, or 50 μm), and the unit area conjugation frequency of wild-type biofilms on flat PDMS surfaces. N=3 biological repeats averaged; at least 15 images were analyzed for each data point.....182

Figure 5-9. The biomass of donors in biofilms formed on PDMS surfaces modified with 20 $\mu\text{m} \times 20 \mu\text{m}$ (A), 50 $\mu\text{m} \times 50 \mu\text{m}$ (B), and 100 $\mu\text{m} \times 100 \mu\text{m}$ (C) microtopographic patterns with various inter-pattern distances (10, 15, 20, 30, 40, or 50 μm). N=6 biological repeats averaged; at least 30 images were analyzed for each data point.....183

Figure 5-10. The biomass of donors in biofilms formed on PDMS surfaces modified with 20 $\mu\text{m} \times 20 \mu\text{m}$ (A), 50 $\mu\text{m} \times 50 \mu\text{m}$ (B), and 100 $\mu\text{m} \times 100 \mu\text{m}$ (C) microtopographic patterns with various inter-pattern distances (10, 15, 20, 30, 40, or 50 μm). N=6 biological repeats averaged; at least 30 images were analyzed for each data point.....184

I dedicate this work to my parents, Qisheng Gu and Chunmei Li, my husband, Ran Yin, my child and my friends.

CHAPTER 1

MOTIVATION, RATIONALE, RESEARCH HYPOTHESIS, AND OBJECTIVES

1.1 MOTIVATION

Microbes are well known to grow on both biotic and abiotic surfaces and develop multicellular communities embedded in extracellular polymeric matrix secreted by these attached cells¹. These complex structures, known as biofilms², cause contamination, corrosion and biofouling in virtually every industrial water-based process, and chronic infections in humans with high motility^{3,4}. Biofilm cells are up to 1000 times more tolerant to antimicrobial treatment than their planktonic counterparts⁵. Thus, biofilm-associated problems put a heavy burden on the health care system and economy; e.g., biofilms are responsible for 65% of bacterial infections in humans and treatment of biofilm-based infections cost more than \$1 billion annually in united states⁶. The significance of biofilm has stimulated increasing interests in understanding the mechanisms of biofilm formation and development of more effective techniques for biofilm prevention and removal⁶⁻⁸. However, despite some exciting progresses in fundamental research, the factors that govern biofilm formation are still poorly understood at the molecular and genetic levels, hindered by the heterogeneity in biofilm structure and associated spatial variation in gene expression⁹⁻¹¹.

Biofilm formation is a dynamic process that involves initial attachment, microcolony formation, maturation and dispersion¹². These processes are influenced by many factors such as the surface structure of bacterial cells (e.g., flagella, curli and fimbriae), material characters of the surfaces that biofilms are formed on (e.g., surface chemistry, topography, charge and hydrophobicity) and environmental conditions (e.g., flow condition, medium composition, and temperature)^{2,13-16}. Consequently, a typical biofilm in currently available experimental systems has significant heterogeneity in its

structure, e.g., uneven coverage of the surface with cell clusters of various sizes and shapes. This grand challenge causes difficulties to comparing findings from different systems in different laboratories¹⁷, leading to inconsistent results^{15,17,18} which hinders the mechanistic understanding of biofilm formation^{9,10} especially with the roles of flagella^{15,17,19}, motility^{15,19,20}, stress response^{21,22}, and quorum sensing^{17,23}. Meanwhile, biofilm heterogeneity is also one of the causes of biofilm resistance to antibiotics, since the biofilm environment is ideal for bacterial conjugation and the formation of slow-growing cells^{6,10,24}. A thorough mechanistic understanding of biofilm heterogeneity requires the biofilm morphology to be controlled to allow a direct characterization of interaction between cell clusters. To achieve this goal, it is necessary to precisely control the size and shape of cell clusters and the distance between them, which cannot be achieved by using conventional system with regular surfaces.

Recent developments in materials science and engineering have brought an exciting opportunity to address the above challenges in biofilm control (Table 1-1). Recently, Ren lab has developed a platform using patterned surface chemistry and topography to control the size and shape of bacterial colonies and the distance between colonies²⁵⁻²⁷. These well-defined surfaces can direct bacterial initial attachment and allow us to quantitatively investigate bacterial surface and bacterial cell-cell interaction. These results motivated us to further investigate bacterial biofilm formation at the genetic level and develop new biofilm control methods.

1.2 RATIONALE

1.2.1 Heterogeneity in biofilm structure

It is well recognized that biofilms are multicellular structures with heterogeneity in both the structure and gene expression of biofilm cells^{1,7,11,28}. Physiological status of each biofilm cell is decided by its local environment including pH, concentration of nutrients and wastes, flow condition, and interaction with neighboring cells; all are affected by the biofilm structure and associated heterogeneity^{10,11}. Thus, individual cells in a common biofilm could be different from each other in gene expression, metabolism, and other cellular activities⁹. Due to the technical limits, traditional biofilm research has been focused on studying the collective behavior and biochemistry of the entire biofilm populations, which overlooks the differences between individual cells in biofilm and leads to inconsistent results reported from different laboratories⁹. For example, synthesis of the signal autoinducer 2 (AI-2) by *luxS* has been found important for flagellar synthesis, motility, and chemotaxis in *E. coli*^{29, 30-34}. However, deletion of *luxS* in *E. coli* W3110 has no effects on cell growth, motility, and biofilm formation compared to the wild-type *E. coli* W3110³⁵. Such discrepancy may be caused by the differences between the experimental system and associated biofilm structures, which hinders the mechanistic understanding of biofilm formation. While the effects of biofilm structure on bacterial physiology is understudied, even less is known about the mechanism of such structural heterogeneity in biofilms due to the lack of techniques that can control biofilm morphology.

In this thesis research, the density and location of cell clusters on gold surfaces were controlled by rigorously tailoring surface chemistry with square-shaped patterns of

self-assembled monolayers (SAMs) of long-chain alkanethiols presenting functional groups. Both the size of patterns and inter-pattern distance were systematically varied. These well-defined surfaces provide a useful platform to obtain important information about bacterial cell-surface and cell-cell interactions as well as the spatial organization during biofilm formation, which cannot be obtained using methods with uncontrolled surfaces.

1.2.2 Biofilm resistance to antibiotics

Biofilm cells are less susceptible to antibiotics compared to planktonic cells with the same genetic makeup, which makes biofilms hard to eradicate leading to chronic infections in humans³⁶ and biofouling of industrial settings³⁷. The significance of biofilm resistance to antimicrobial agents has stimulated increasing interests in understanding the mechanisms of biofilm resistance to antibiotics. The reduced antibiotic susceptibility of biofilm cells is thought to be a consequence of multiple factors, including the formation of slow-growing biofilm cells, protection of the extracellular matrix, activities of efflux pumps, and the spread of antibiotic resistance genes by conjugation²⁴. Slow-growing cells can contribute to biofilm resistance against antibiotics because essentially all antibiotics are more effective in killing rapidly growing cells and less effective against slow-growing cells⁶. The formation of slow-growing biofilm cells is probably due to general stress response or chemical (nutrients, waste products, and signaling factors) gradient developed as a result of biofilm heterogeneity^{6,10,24,38}. A systematic study using the well-defined surfaces can shed new light on the formation of slow-growing cells during biofilm formation and reveal their roles in the development of biofilm resistance to antibiotics.

Another important but less studied mechanism of biofilm-associated antibiotic resistance is conjugation³⁸. Bacterial conjugation occurs when the mobile genetic materials such as conjugative plasmids are transferred from donor to recipient cells through directly cell-to-cell interaction using sex pili³⁹. The adaptive traits such as antibiotic resistance gene encoded by the mobile plasmid can allow the survival of transconjugants in harsh environments and commonly lead to the resistance of biofilm cells to antibiotics³⁹. Biofilms may provide an ideal environment for bacterial conjugation due to the high density and close proximity of the sessile biofilm cells³⁸. However, how biofilm formation promotes conjugation is still unknown. In this work, the well-defined surfaces are able to control biofilm morphology in defined locations were used with fluorescent reporter strains to study bacterial conjugation in real time.

1.2.3 Effects of surface topography on biofilm formation

In addition to surface chemistry, surface topography has also been well known to affect biofilm formation^{15,18,27,40-44}. For instance, Chung *et al.*⁴⁴ reported that the shark skin-inspired PDMS surfaces with micron scale ribs organized in parallel diamond shaped patterns can reduce the surface coverage of *Staphylococcus aureus* by 47% compared to smooth PDMS surfaces 14 days after inoculation. Friedlander *et al.*⁴¹ observed that the biomass of *E. coli* biofilms on PDMS surfaces with an array of hexagonal features was approximately 1.3 times higher than the biomass on smooth PDMS surfaces after 2 h of incubation. In addition to the shape of topographic features, the length scale of topography, including the size, height, and inter-pattern distance, can also affect biofilm formation by altering surface wettability⁴⁵.

Understanding how surface topography influences bacteria-surface interaction is critical to the development of antiadhesive surfaces or materials. This information is also important to the understanding of biofilm formation in natural environment, because most surfaces in nature are not smooth. To systematically exam the effects of surface topography on cell adhesion and biofilm formation, PDMS surfaces with topographic features of different shapes, sizes, heights, and inter-pattern distances were designed and fabricated. Specifically, we were interested in how surface topography affects *E. coli* adhesion, biofilm formation, and conjugation, as well as the roles of bacterial extracellular structures, such as flagella and pili, during these processes. The obtained information can be used to guide the engineering of antifouling surfaces.

1.3 CENTRAL HYPOTHESIS AND RESEARCH OBJECTIVES

The overall goal of this study is to improve the mechanistic understanding of biofilm heterogeneity and biofilm resistance to antibiotics. As described above, well-defined surfaces with chemical and topographical patterns can be obtained via soft lithography and microcontact printing. We hypothesize that interaction among cell clusters is important to biofilm heterogeneity and biofilm resistance to antibiotics. To test this hypothesis, we created a series of surfaces with various pattern sizes and inter-pattern distances; and used these surfaces to obtain new insights in bacterial cell-surface and cell-cell interaction. This study has the following objectives:

Objective 1. To investigate the effects of cell cluster size and the distance between cell clusters on the interaction among cell clusters and biofilm morphology,

Surfaces with chemical and topographical patterns were used to form biofilms.

Objective 2. To study the roles of key genes that are involved in the cell-surface and cell-cell interaction during interaction, including representative genes of bacterial chemotaxis, motility, and cell-to-cell signaling.

Objective 3. To corroborate the results by investigating the roles of bacterial outer membrane apertures such as the bacterial flagella, curli and fimbriae in the interaction between cell clusters.

Objective 4. To understand biofilm associated antibiotic resistance using patterned surfaces. First, the tolerance of biofilm cells to ampicillin was examined and the effects of metabolic activities were investigated. Second, bacterial conjugation on PDMS surfaces modified with microtopographic patterns was studied using fluorescently labeled donors and recipients.

1.4 TABLES

Table 1-1. Current techniques to immobilize bacteria

Technology	Surface	Ligands/Functional groups	Resolution	Cells/Proteins	Ref.
Fast replication molding technique	Poly(ethylene glycol) (PEG)	N/A	10 μm	Protein: Fluorescein isothiocyanate-labeled bovine serum albumin (FITC-BSA) Cells: NIH-3T3 murine embryonic fibroblasts	46
Photolithography and soft lithography	Poly(dimethylsiloxane) (PDMS)	N/A	Post pitch with height of 2 μm tall, diameter of 300 nm, and inter-pattern distance varied from 4 to 0.9 μm .	<i>P. aeruginosa</i> (PA14), <i>Bacillus subtilis</i> (strain 3610), and <i>E. coli</i> (strain W3110)	47
Soft lithography	PDMS	N/A	Rectangular grooves with dimension of $1.5 \times 0.5 \mu\text{m}$	<i>E. coli</i> wild-type strain and <i>hip</i> mutant	48
Colloid lithography	PEG	N/A	Dots with diameter around 1.4 μm and honeycomb with bridge width around 0.85 μm	<i>Serratia marcescens</i>	49
Photolithography and soft lithography	PEG	N/A	Square shaped patterns with 60 μm and 30 μm side width	<i>E. coli</i> and Murine fibroblasts	50
Capillary lithography	PEG	Antibodies	Lines with height about 367 nm, width of 800 nm, and a spacing of 1 or 2 mm	<i>E. coli</i>	51

Technology	Surface	Ligands/Functional groups	Resolution	Cells/Proteins	Ref.
Micromolding in capillaries (MIMIC)	PEG and polyelectrolyte (PEL)	Antibodies	Square shaped patterns with side width of 50 μm and lines with width of 50 μm	<i>E. coli</i> and NIH-3T3 murine embryonic fibroblasts	52
Projection lithography and reactive ion etching	Parylene	Antibodies	Lines with length of 5mm, width of 2 μm to 20 μm	<i>E. coli</i> and rat basophilic leukemia (RBL) cells	53
Microcontact printing	Agarose gel	N/A	Feature size varied from 200 μm^2 to 50 cm^2	<i>Vibrio fischeri</i>	54
Soft lithography	SiO_2 substrate	OTS solution	Oval patterns (12 $\mu\text{m} \times 8 \mu\text{m}$)	<i>E. coli</i>	55
Microcontact printing	Agarose gel	N/A	Hexagon patterns with diameter of 6, 12, and 24 μm and inter-pattern distance of 30, 60, and 120 μm	<i>E. coli</i>	56
Reactive wet stamping (r-WETS)	Gold surface	$\text{COOH}(\text{CH}_2)_{11}\text{-SS}(\text{CH}_2)_{11}\text{COOH}$ and $\text{COOH}(\text{CH}_2)_{11}\text{SS}(\text{CH}_2)_{11}\text{CON-Fluorescein}$	Squares with side width of 50 μm	Chinese hamster ovary	57
Electrophoretic deposition	Electrode	N/A	Randomly deposition	<i>Saccharomyces cerevisiae</i>	58

Technology	Surface	Ligands/Functional groups	Resolution	Cells/Proteins	Ref.
Direct printing using electrospray pulsed jet	Charged surfaces	N/A	Spots with diameter of 10 μm	<i>Staphylococcus epidermidis</i>	59
Direct printing using inkjet printer	Agarose gel	N/A	The size of cell colonies was set to be 0.35, 0.5, 1, or 2 mm	<i>E. coli</i>	60
Soft lithography	PEG	Hexadecanethiol (C16SH) and 11-mercaptoundecanoic acid (MUA)	Corrals with size of 12 or 63 μm square	<i>E. coli</i>	61
Local crosslinking	PEG	N/A	The size of cell clusters was set to be 1, 5, or 10 μm .	<i>S. epidermidis</i>	62

1.5 REFERENCES

- 1 **Stewart, P. S., Costerton, J. W.** 2001. Antibiotic resistance of bacteria in biofilms. *The Lancet* **358**: 135-138.
- 2 **Van Houdt, R.** 2005. Role of bacterial cell surface structures in *Escherichia coli* biofilm formation. *Res Microbiol* **156**: 626-633.
- 3 **Gilbert, P. A. D., McBain, A. J.** 2002. Biofilms in vitro and in vivo: do singular mechanisms imply cross-resistance? *J. Appl. Microbiol. Symp. Suppl.* **92**: 98S–110S.
- 4 **Walker, J. S. S., Jass, J.** 2000. Biofilms and Biofouling. In *Industrial Biofouling: Detection, Prevention and Control* 1-12.
- 5 **Mah, T. F.** 2003. A genetic basis for *Pseudomonas aeruginosa* biofilm antibiotic resistance. *Nature* **426**: 306-310.
- 6 **Mah, T. F., O'Toole, G. A.** 2001. Mechanisms of biofilm resistance to antimicrobial agents. *Trends Microbiol* **9**: 34-39.
- 7 **Wimpenny, J., Manz, W., Szewzyk, U.** 2000. Heterogeneity in biofilms. *FEMS Microbiol Rev* **24**: 661-671.
- 8 **Lee, B., Haagensen, J. A., Ciofu, O., Andersen, J. B., Hoiby, N., and Molin, S.** 2005. Heterogeneity of biofilms formed by nonmucoid *Pseudomonas aeruginosa* isolates from patients with cystic fibrosis. *J Clin Microbiol* **43**: 5247-5255.
- 9 **Weibel, D. B., Diluzio, W.R., Whitesides, G. M.** 2007. Microfabrication meets microbiology. *Nature Rev. Microbiol.* **5**: 209-218.
- 10 **Stewart, P. S., Franklin, M. J.** 2008. Physiological heterogeneity in biofilms. *Nat Rev Microbiol* **6**: 199-210.
- 11 **Wessel, A. K., Hmelo, L., Parsek, M. R., Whiteley, M.** 2013. Going local: technologies for exploring bacterial microenvironments. *Nat Rev Microbiol* **11**: 337-348.
- 12 **Stoodley, P., Sauer, K., Davies, D. G., Costerton, J. W.** 2002. Biofilms as complex differentiated communities. *Annu Rev Microbiol* **56**: 187-209.
- 13 **MacKintosh, E. E., Patel, J. D., Marchant, R. E., and Anderson, J. M.** 2006. Effects of biomaterial surface chemistry on the adhesion and biofilm formation of *Staphylococcus epidermidis* in vitro. *J Biomed Mater Res A* **78A**: 836-842.
- 14 **Katsikogianni, M., Missirlis, Y. F.** 2004. Concise review of mechanisms of bacterial adhesion to biomaterials and of techniques used in estimating bacterial-material interactions. *Eur. Cell Mater.* **8**: 37-57.
- 15 **O'Toole, G. A., Kolter, R.** 1998. Flagellar and twitching motility are necessary for *Pseudomonas aeruginosa* biofilm development. *Mol Microbiol* **30**: 295-304.
- 16 **Agladze, K. Wang, X., Romeo, T.** 2005. Spatial periodicity of *Escherichia coli* K-12 biofilm microstructure initiates during a reversible, polar attachment phase of development and requires the polysaccharide adhesin PGA. *J. Bacteriol.* **18**: 8237-8246.
- 17 **Heydorn, A., Ersboll, B., Kato, J., Hentzer, M., Parsek, M. R., Tolker-Nielsen, T., Givskov, M., Molin, S.** 2002. Statistical analysis of *Pseudomonas aeruginosa* biofilm development: impact of mutations in genes involved in

- twitching motility, cell-to-cell signaling, and stationary-phase sigma factor expression. *Appl. Environ. Microbiol.* **68**: 2008-2017.
- 18 **Klausen, M., Heydorn, A., Ragas, P., Lambertsen, L., Aaes-Jorgensen, A., Molin, S., and Tolker-Nielsen, T.** 2003. Biofilm formation by *Pseudomonas aeruginosa* wild type, flagella and Type IV pili mutants. *Mol Microbiol* **48**: 1511-1524.
- 19 **Reisner, A., Haagensen, J. A., Schembri, M. A., Zechner, E. L., Molin, S.** 2003. Development and Maturation of *Escherichia coli* K-12 Biofilms. *Mol Microbiol* **48**: 933–946.
- 20 **Prigent-Combaret, C. G. P., Thi, T. T. L., Vidal, O., Lejeune, P., Dorel, C.** 2000. Developmental Pathway for Biofilm Formation in Curli-producing *Escherichia coli* Strains: Role of Flagella, Curli and Colanic acid. *Environ. Microbiol.* **2**: 450-464.
- 21 **Corona-Izquierdo, F. P., Membrillo-Hernandez, J.** 2002. Mutation in *rpoS* enhances biofilm formation in *Escherichia coli* during exponential phase of growth. *FEMS Microbiol. Lett.* **211**: 105-110.
- 22 **Schembri, M. A., Kjaergaard, K., Klemm, P.** 2003. Global gene expression in *Escherichia coli* biofilms. *Mol Microbiol* **48**: 253–267.
- 23 **Davies, D. G., Parsek, M. R., Pearson, J. P., Iglewski, B. H., Costerton, J. W., Greenberg, E. P.** 1998. The involvement of cell-to-cell signals in the development of a bacterial biofilm. *Science* **280**: 295-298.
- 24 **Lewis, K.** 2001. Riddle of biofilm resistance. *Antimicrob Agents Ch* **45**: 999-1007.
- 25 **Hou, S. Y., Burton, E. A., Simon, K. A., Blodgett, D., Luk, Y. Y., and Ren, D. C.** 2007. Inhibition of *Escherichia coli* biofilm formation by self-assembled monolayers of functional alkanethiols on gold. *Appl. Environ. Microbiol.* **73**: 4300-4307.
- 26 **Burton, E. A., Simon, K. A., Hou, S. Y., Ren, D. C., Luk, Y. Y.** 2009. Molecular gradients of bioinertness reveal a mechanistic difference between mammalian cell adhesion and bacterial biofilm formation. *Langmuir* **25**: 1547-1553.
- 27 **Hou, S., Gu, H., Smith, C., Ren, D.** 2011. Microtopographic patterns affect *Escherichia coli* biofilm formation on Poly(dimethylsiloxane) surfaces. *Langmuir* **27**: 2686-2691.
- 28 **Drenkard, E.** 2003. Antimicrobial resistance of *Pseudomonas aeruginosa* biofilms. *Microbes Infect.* **5**: 1213-1219.
- 29 **González Barrios, A. F., Zuo, R., Hashimoto, Y., Yang, L., Bentley, W. E., Wood, T. K.** 2006. Autoinducer 2 controls biofilm formation in *Escherichia coli* through a novel motility quorum-sensing regulator (MqsR, B3022). *Journal of bacteriology* **188**: 305–316.
- 30 **Ren, D. C., Bedzyk, L. A., Ye, R. W., Thomas, S. M., Wood, T. K.** 2004. Stationary-phase quorum-sensing signals affect autoinducer-2 and gene expression in *Escherichia coli*. *Appl Environ Microb.* **70**: 2038-2043.
- 31 **Ren, D. C., Bedzyk, L. A., Thomas, S. M., Ye, R. W., Wood, T. K.** 2004. Gene expression in *Escherichia coli* biofilms. *Appl Microbiol Biot.* **64**: 515-524.

- 32 **Jones, M. B., Jani, R., Ren, D. C., Wood, T. K., Blaser, M. J.** 2005. Inhibition of bacillus anthracis growth and virulence-gene expression by inhibitors of quorum-sensing. *J Infect Dis* **191**: 1881-1888.
- 33 **Taga, M. E., Semmelhack, J. L., Bassler, B. L.** 2001. The LuxS-dependent autoinducer AI-2 controls the expression of an ABC transporter that functions in AI-2 uptake in *Salmonella typhimurium*. *Molecular Microbiology*. **42**: 777-793.
- 34 **Ahmed, N. A., Petersen, F. C., Scheie, A. A.** 2007. AI-2 quorum sensing affects antibiotic susceptibility in *Streptococcus anginosus*. *J Antimicrob Chemoth.* **60**: 49-53.
- 35 **Wang, L., Li, J., March, J. C., Valdes, J. J., Bentley, W. E.** 2005. LuxS-dependent gene regulation in *Escherichia coli* K-12 revealed by genomic expression profiling. *Journal of bacteriology* **187**: 8350-8360.
- 36 **Donlan, R. M.** 2001. Biofilm formation: a clinically relevant microbiological process. *Clin Infect Dis* **33**: 1387-1392.
- 37 **Walker, J., Surman, S., Jass, J.** 2000. Industrial Biofouling: Detection, Prevention and Control. 1-12.
- 38 **Stewart, P. S.** 2002. Mechanisms of antibiotic resistance in bacterial biofilms. *Int J Med Microbiol* **292**: 107-113.
- 39 **Sorensen, S. J., Bailey, M., Hansen, L. H., Kroer, N., Wuertz, S.** 2005. Studying plasmid horizontal transfer in situ: A critical review. *Nature Rev Microbiol* **3**: 700-710.
- 40 **Rana, D., Matsuura, T.** 2010. Surface modifications for antifouling membranes. *Chem Rev* **110**: 2448-2471.
- 41 **Friedlander, R. S. et al.** 2013. Bacterial flagella explore microscale hummocks and hollows to increase adhesion. *Proceedings of the National Academy of Sciences of the United States of America* **110**: 5624-5629.
- 42 **Whitehead, K. A., Verran, J.** 2006. The effect of surface topography on the retention of microorganisms. *Food and Bioproducts Processing* **84**: 253-259.
- 43 **Crawford, R. J., Webb, H. K., Truong, V. K., Hasan, J., Ivanova, E. P.** 2012. Surface topographical factors influencing bacterial attachment. *Advances in colloid and interface science* **179-182**: 142-149.
- 44 **Chung, K. K. et al.** 2007. Impact of engineered surface microtopography on biofilm formation of *Staphylococcus aureus*. *Biointerphases* **2**: 89-94.
- 45 **Oner, D., McCarthy, T. J.** 2000. Ultrahydrophobic surfaces. Effects of topography length scales on wettability. *Langmuir* **16**: 7777-7782.
- 46 **Suh, K. Y., Seong, J. Y., Khademhosseini, A., Laibinis, P. E., Langer, R.** 2004. A Simple Soft Lithographic Route to Fabrication of Poly(ethylene glycol) Microstructures for Protein and Cell Patterning. *Biomaterials* **25**: 557-563.
- 47 **Hochbaum, A. I., Aizenberg, J.** 2010. Bacteria pattern spontaneously on periodic nanostructure arrays. *Nano Lett* **10**: 3717-3721.
- 48 **Balaban, N. Q., Merrin, J., Chait, R., Kowalik, L., Leibler, S.** 2004. Bacterial persistence as a phenotypic switch. *Science* **305**: 1622-1625.
- 49 **Yi, D. K., Kim, M. J., Turner, L., Breuer, K. S., Kim, D. Y.** 2006. Colloid lithography-induced polydimethylsiloxane microstructures and their application to cell patterning. *Biotechnol Lett* **28**: 169-173.

- 50 **Koh, W. G., Revzin, A., Simonian, A., Reeves, T., Pishko, M.** 2003. Control of mammalian cell and bacteria adhesion on substrates micropatterned with poly(ethylene glycol) hydrogels. *Biomed Microdevices* **5**: 11-19.
- 51 **Suh, K. Y. J. S., Khademhosseini, A., Laibinis, P. E., Langer, R.** 2004. A Simple Soft Lithographic Route to Fabrication of Poly(ethylene glycol) Microstructures for Protein and Cell Patterning. *Biomaterials* **25**: 557-563.
- 52 **Shim, H. W., Lee, J. H., Hwang, T. S., Rhee, Y. W., Bae, Y. M., Choi, J. S., Han, J., Lee, C. S.** 2007. Patterning of proteins and cells on functionalized surfaces prepared by polyelectrolyte multilayers and micromolding in capillaries. *Biosens Bioelectron* **22**: 3188-3195.
- 53 **Ilic, B., Graighead, H. G.** 2000. Topographical patterning of chemically sensitive biological materials using a polymer-based dry lift off. *Biomed* **2**: 317-322.
- 54 **Weibel, D. B., Lee, A., Mayer, M., Brady, S. F., Bruzewicz, D., Yang, J., DiLuzio, W. R., Clardy, J., Whitesides, G. M.** 2005. Bacterial printing press that regenerates its ink: contact-printing bacteria using hydrogel stamps. *Langmuir* **21**: 6436-6442.
- 55 **Cerf, A., Cau, J. C., Vieu, C.** 2008. Controlled assembly of bacteria on chemical patterns using soft lithography. *Colloid Surface B* **65**: 285-291.
- 56 **Xu, L. P., Robert, L., Qi, O. Y., Taddei, F., Chen, Y., Lindner, A. B., Baigl, D.** 2007. Microcontact printing of living bacteria arrays with cellular resolution. *Nano Lett* **7**: 2068-2072.
- 57 **Campbell, C. J., Smoukov, S. K., Bishop, K. J. M., Grzybowski, B. A.** 2005. Reactive Surface Micropatterning by Wet Stamping. *Langmuir* **21**: 2637-2640.
- 58 **Brisson, V., Tilton, R. D.** 2002. Self-assembly and two-dimensional patterning of cell arrays by electrophoretic deposition. *Biotechnol Bioeng* **77**: 290-295.
- 59 **Kim, K., Lee, B. U., Hwang, G. B., Lee, J. H., Kim, S.** 2010. Drop-on-demand patterning of bacterial cells using pulsed jet electro spraying. *Anal Chem* **82**: 2109-2112.
- 60 **Merrin, J., Leibler, S., Chuang, J. S.** 2007. Printing multistrain bacterial patterns with a piezoelectric inkjet printer. *Plos One* **2**.
- 61 **Rowan, B., Wheeler, M. A., Crooks, R. M.** 2002. Patterning bacteria within hyperbranched polymer film templates. *Langmuir* **18**: 9914-9917.
- 62 **Krsko, P., Kaplan, J. B., Libera, M.** 2009. Spatially controlled bacterial adhesion using surface-patterned poly(ethylene glycol) hydrogels. *Acta Biomater* **5**: 589-596.

CHAPTER 2

INTRODUCTION

This chapter presents an overview of the topics related to my project. Since some of following chapters are from published journal articles and some chapters are written for journal submission, they also carry their own introductions with more details about specific topics. Sections, 2.1, 2.5, and 2.6 of this chapter have been published in an invited review article as Huan Gu and Dacheng Ren. 2014. Material and surface engineering to control bacterial adhesion and biofilm formation a review of recent advances. *Frontiers of Chemical Science and Engineering*. 8(1): 20-33. Reproduced by permission of Springer.

2.1 BIOFILM FORMATION

Bacteria have developed complex mechanisms to attach to surfaces and form sessile communities, known as biofilms, as a strategy to survive in adverse environmental conditions and to establish infections¹. Commonly, biofilms are ubiquitous in aqueous environments and biofilm cells are highly tolerant to antibiotics compared to their planktonic counterparts. The high-level drug tolerance of biofilm cells leads to chronic infections in humans¹ and biofouling of industrial settings², which contribute to the raising health care costs and economic loss. For example, a typical treatment of medical device associated biofilm infection involves surgical replacement of the contaminated device and intensive antibiotic therapy, which is often associated with high health care cost and long period of post-surgical recovery. Unfortunately, even with aggressive therapy, mortality of such infections remains high and biofilm formation also facilitates the development of antibiotic resistant strains³. The significance of biofilms has stimulated research efforts to understand the mechanism of biofilm formation and to engineer more efficient antimicrobial surfaces.

Biofilm formation is a dynamic process comprising of five stages including reversible attachment, irreversible attachment, microcolony formation, maturation and dispersion⁴⁻⁷. During the first stage of biofilm formation, free-living bacteria are brought to the solid surface by fluid stream or bacterial motility⁸. Extracellular organelles, such as flagella, curli, fimbriae (or pili), and outer membrane proteins, have been shown to help bacteria sense and interact with surfaces⁸⁻¹¹. Such interactions can help bacterial cells to overcome long-range repulsive forces along the surface. This process is critical for bacterial adhesion and is influenced by the properties of both bacterial cells and the

substrate surface (e.g. charge, hydrophobicity, and stiffness)¹². At this stage, bacterial cells still show Brownian motion and can be relatively easily removed by shear force¹³. After the initial attachment is made, flagellar arrest and the attached cells start the production of extracellular polymeric substance (EPS) consisting of polysaccharides, and in some strains, DNA, proteins, and lipids¹⁴. These processes promote the transition of bacterial attachment from reversible to irreversible^{11,15}. Permanently attached bacterial cells are hard to detach because these cells are attached using extracellular adhesive organelles, such as EPS, curli, and fimbriae (or pili)¹¹. The secretion of EPS is stimulated by the chemical communication between cells in clusters, which are typically tens to hundreds of micrometers in size. Quorum sensing (QS) is the best-characterized cell-to-cell communication system and is known to regulate a variety of cellular functions besides the production of EPS such as motility and production of secondary metabolites¹⁵⁻¹⁷. The components of EPS vary between species and growth conditions. As cells replicate and the EPS accumulates, these micrometer communities grow into three-dimensional (3D) structures of mature biofilms. In a mature biofilm, adhesive EPS acts as “glue” between embedded bacterial cells to support the 3D structure of biofilm, allowing the transport of nutrients and removal of wastes. Triggered by some intrinsic cues, such as cell death and autolysis in *Pseudomonas aeruginosa* biofilms, cells in some mature biofilms can also detach and return to the bulk flow¹⁸. These released cells may reattach to surface and form biofilms in a new environmental niche. Biofilm dispersion is believed to be crucial for the propagation and self-renewal of bacterial communities¹⁵.

2.2 GENES INVOLVED IN BIOFILM FORMATION

Apparently, the initial adhesion of bacteria onto a surface involves multiple extracellular structures, such as flagellum, pili and curli. For obtaining these functions at the proper time and in a right order, the expression of related genes needs to be coordinated in response to the signals from the surface, host cells, and environment at the proper time. Many studies have been conducted attempting to understand the mechanism of such regulation and identify the key biofilm genes. *E. coli* have been intensively used as a model organism to study biofilm formation. Here, we review the current knowledge of genes and pathways involved in its biofilm formation, as well as the regulation of these elements (Table 2-1).

The reversible attachment step of biofilm formation often requires bacterial flagella, which allow the planktonic cells to swim toward a solid surface. During this stage, the expression of other cell surface organelles such as fimbriae and curli is repressed⁸. Over 40 flagella genes have been identified to date. These genes cluster in three regions in *E. coli* genome chromosome and control the assembly, structure, and function of flagella¹⁹. Among these genes, *flhDC* encodes a master regulator of the class II flagella genes involved in flagellar assembly (e.g., *fliC*, encoding flagellar filaments), motor assembly (e.g., *motAB*, encoding the flagellar rotary motor), and chemotaxis (e.g., *cheA-Z*, controlling bacterial chemotaxis) in *E. coli*¹⁹. Therefore, FlhDC is the central regulator and plays a critical role in the initial stage of biofilm formation when bacterial cells are approaching a solid surface. The expression level of *flhDC* is sensitive to environmental factors such as temperature^{20,21}, pH^{22,23}, osmolarity^{24,25}, availability of carbon sources²⁶, and the presence of certain small molecules^{25,27-33}. At the genetic level,

the complex of H-NS (histone-like nucleoid-structuring protein)³⁴ and CRP (cyclic adenosine monophosphate (cAMP) catabolite activator protein or cAMP receptor protein)³⁵ control flagellar motility by repressing or activating the expression of *flhDC*. Involving CRP allows bacteria to form biofilm in response to changes in nutrient concentration in the environment. Biofilm formation can also be affected by changes in environmental osmolarity. The phosphorylated OmpR represses the expression of flagella by activating the *csgD* promoter, which promotes the switch from planktonic cells to biofilm formation by repressing bacterial motility and promoting cell-cell and cell-surface interactions³⁶. In addition to the above systems, LrhA induces the transition from planktonic cells to biofilm formation by repressing numerous genes involved in flagellation, motility and chemotaxis³⁷. Meanwhile, phosphorylated RcsB facilitates the settlement of bacteria by activating cell division and colanic acid synthesis, and at the same time inhibiting virulence, and flagella motility³⁸. The above and other results revealed that flagella gene expression is reversely regulated with the biofilm matrix synthesis, which is commonly observed not only in *E. coli* but also in other bacterial species. For example, in *P. aeruginosa*, the central regulator of flagella genes, FleQ, is indirectly inhibited by the alternative sigma factor AlgT, which is a positive regulator of biofilm matrix synthesis³⁹. When *Vibrio cholerae* was mutated to lose flagellar filaments, it synthesized biofilm matrix even without a surface⁴⁰. Thus, the arrest of flagella can promote the transition from reversible attachment to irreversible attachment¹¹.

Among the surface organelles, Type I fimbriae or pili that are approximately 1 µm long and 7 nm wide, rod-shaped adhesive structures, are important for bacterial

adhesion to mannose-containing receptors and causing urinary tract infections⁴¹⁻⁴³. The expression of *fim* gene cluster (*fimABCDEFGH*) is regulated by the promoter of fimbriae subunit *fimA*^{8,44}. The activation of *fimA* is controlled by an upstream reversible switch that is a two-component system, *fimE* and *fimB*. FimE can turn off the expression of *fim* genes cluster, while FimB can either turn on or turn off the expression of *fim* gene cluster. This two-component system is subject to tight environment control, mediated by at least five global regulators (LrpA^{45,46}, IHF^{45, 47}, H-NS⁴⁸, LrhA⁴⁹, and EnvZ/OmpR⁵⁰). Among those regulators, LrhA, a repressor of flagellar, motility, and chemotaxis genes, can turn off the expression of fimbriae by activating the expression of protein FimE and suppress biofilm formation^{49,51}. The integration host factor (IHF) and leucine-responsive regulatory protein (LrpA) affect the expression of type I fimbriae by controlling the production of both recombinases (FimE and FimB)⁴⁵, while H-NS controls only the FimB-mediated inversion and has an overall positive effect on the expression of the *fim* genes. In addition, the two-component system EnvZ/OmpR has a negative effect on the *fim* operon expression⁵⁰.

Curli are another type of surface structures that can facilitate bacterial cell-surface and cell-cell interactions and is highly expressed during bacterial adhesion to solid surfaces⁵². The environmental factors that can influence the curli expression include temperature^{53,54}, oxygen tension^{54,55}, starvation^{56,57}, osmolarity^{52,57,58}, iron⁵⁸, and pH⁵⁸. The curli genes are clustered into two divergent operons, *csgDEFG* and *csgBA*⁵⁹. To date, at least seven regulators have been found to affect curli expression including EnvZ/OmpR⁶⁰, RcsBCD^{61,62}, CpxAR^{36,63}, CRP⁶⁴, H-NS^{48,57}, MlrA⁶⁵, and FlhDC⁶⁶. In addition to its roles in flagella control, the two-component system EnvZ/ompR is also

involved in the expression of curli genes. However, unlike the flagellar system, in which the reduction of *csgD* represses flagella, the expression of curli genes is positively regulated by *csgD* (through the induction of *flhDC*). The RcsB/CD two component system is also known to promote biofilm formation by repressing flagellar synthesis, inducing curli formatting, and increasing the synthesis of colanic acid⁶². The phosphorylated CpxAR has a similar function as phosphorylated RcsB through controlling the expression of *csgA*.

In summary, the regulators of bacterial outer membrane structures, FlhDC⁶⁷, EnvZ/OmpR⁶⁸, and RcsCDB⁶⁹ control the expression of the majority of genes involved in *E. coli* biofilm formation, especially those with functions in the synthesis of flagella, curli, and type I fimbriae. FlhDC regulates the expression of flagellar genes during the very early phase of biofilm formation when bacterial cells approach a solid surface. Following this, the two component system, EnvZ/OmpR, can facilitate the formation of reversible attachment of bacteria through the repression of flagella genes and induction of adhesive surface structures, primarily curli and type I fimbriae (pili). The transition between free-swimming bacteria and sessile life style occurs when the extracellular matrix composed of colanic acids is produced, which promotes irreversible adhesion and the formation of biofilm with multiple layers of cells. These processes are influenced by signaling molecules and environmental factors⁴⁴. For example, the second messengers cAMP can interact with CRP, which activates the biogenesis of flagella and curli^{35,64,70}. The phosphorylation of OmpR⁷¹ and RcsB by acetyl phosphate controls the biosynthesis of flagella, curli, type I fimbriae, and capsules^{24,31,38,50,62,72}.

2.3 BIOFILM HETEROGENEITY

It is well known that biofilm formation is a dynamic process involving numerous factors, which contribute to the heterogeneity in biofilm structure⁷³ (Fig. 2-1). During the past three decades, biofilm structures have been extensively studied thanks to new technologies such as advanced microscopy [e.g., electron microscopy including transmission electron microscopy (TEM) and scanning electron microscopy (SEM), atomic force microscopy, and confocal laser scanning microscopy (CLSM)], microelectrodes (e.g., microelectrode for measuring nitrous oxide, oxygen, H₂S, and pH), and more powerful molecular methods [e.g., in situ hybridization with 16S or 23S rRNA-directed oligonucleotide probes and fluorescence in situ hybridization (FISH)]⁷⁴. These studies have revolutionized our view of biofilm structure from planar⁷⁴ to homogeneous film⁷⁵ to appreciate the complexity of heterogeneous structures with mushroom shape colonies and water channels between cell clusters^{6,74}. The composition of biofilm matrix is also well studied.

In biofilms, bacterial cells aggregate together with adhesive EPS acting as “glue”. The high cell density and presence of EPS within biofilms arrest the flow of water and retard the diffusion of solutes, leading to the formation of gradients of nutrients and other substances (e.g., antibiotics) across the biofilm structure^{73,76}. With the application of microelectrodes, the microscale concentration profiles of a number of solutes (e.g., nitrate, nitrate ammonium, and pH) have been determined⁷⁴. Moreover, to quantitatively assess the chemical environment surrounding small bacterial colonies, the advances techniques such as scanning electrochemical microscopy (SECM), imaging mass spectrometry (IMS), nanoSIMS, desorption electrospray ionization (DESI) mass

spectrometry, and matrix-assisted laser desorption-ionization (MALDI) – mass spectrometry have all been applied to biofilm research. These studies provide new insights into the micron environment within biofilms⁷⁷. It is now recognized that the microscale heterogeneity in the chemical environment in biofilms can cause corresponding heterogeneity in the biological activity among biofilm cells including growth, gene expression, and stress response⁷³. Such heterogeneity has been demonstrated by measuring respiratory activity of biofilm cells using 5-cyano-2,3-ditoly tetrazolium chloride (CTC) staining; by characterizing membrane permeability using differential membrane permeability staining; by monitoring extracellular product formation; and by directly following gene expression and DNA synthesis using reporter strains⁷³. These techniques help answer the fundamental question about how chemical heterogeneity affects microbial physiology in biofilm; however, there are still many unanswered questions and the development of the spatial heterogeneity in biofilm structure itself is still not fully understood.

Besides chemical gradients, biofilm structure can also be affected by bacterial cell-cell signaling⁷⁸⁻⁸² (e.g., quorum sensing) and physical interactions between cells (e.g., those through colanic acids⁸³ and pili⁸⁴). However, the role of cell-cell interaction during the development of heterogeneity in biofilm structure is not fully understood.

2.4 BIOFILM-ASSOCIATED ANTIBIOTIC RESISTANCE

A primary concern about biofilms is the high level resistance to antibiotics. The mechanisms of such antibiotic resistance include the reduced penetration of antibiotic molecules, slow growth of biofilm cells, general stress response, enhanced extrusion of

antibiotics from biofilm cells, and the spread of antibiotic resistance gene due to close contact between biofilm cells^{85,86}. Among these mechanisms, the biofilm structure and associated heterogeneity are the leading factors to the failure of some antibiotics to penetrate biofilms, slow growth of biofilm cells, and general stress. Due to the high density of biofilm cells and the presence of EPS, the diffusion rate of antibiotics into biofilm is significantly reduced, e.g. the diffusion coefficient of solutes in biofilm matrix is 60% lower than that in water^{76,85}. In addition, the absorption of antibiotics by the outer layer biofilm cells could contribute to the reduced availability of antibiotics to cells in the center of biofilm⁷⁶. Moreover, slow growth rate of biofilm cells has been observed in biofilms in response to nutrient limitation^{85,86}. The slow growth rate of biofilm cells lead to significant resistance to antibiotics because almost all antibiotics kill bacteria by targeting growth-related activities such as the synthesis of DNA, protein, and cell wall⁸⁶. Furthermore, general stress response is governed by central regulators and is induced by high cell density in biofilms through quorum sensing. Such response can protect cells from various environmental stresses including antimicrobial agents⁸⁵.

Other than the mechanisms mentioned above, biofilm formation also provides an ideal environment for spreading antibiotic resistance genes through bacterial conjugation due to the spatial stability and proximity of bacteria in biofilms⁸⁷. Bacterial conjugation is a well-documented phenomenon in which mobile genetic materials such as plasmids are transferred from donor to recipient cells through direct cell-cell contact involving sex pili. The resulting transconjugants can obtain new functions based on the genetic traits carried by the mobile plasmids, which commonly lead to antibiotic resistance⁸⁷. Furthermore, conjugative plasmids have also been found to facilitate biofilm formation^{84,87,88}. Recently,

with the application of fluorescently tagged plasmids and bacterial cells, the localization and distribution of transconjugants within biofilms have been studied⁸⁹⁻⁹². In a system of *Pseudomonas putida*, more transconjugants were found on top of the recipient microcolonies and did not spread in biofilm, which indicates that new transconjugants rarely become donors^{90,93}. Transconjugants was also observed inside biofilms formed in flow cells, suggesting that donor cells are able to penetrate the outer layer of a biofilm⁸⁷. Moreover, the 3D imaging analysis of bacterial conjugation in *Sphingomonas sp.* biofilms revealed that most transconjugants are formed in the interior part of cell clusters, which was thought to be a result of open channels and pores that enable more frequent cell-cell contact⁸⁷. Collectively, these results indicate that the spatial structure of biofilm plays an important role in bacterial conjugation. The frequency of conjugation in biofilm was also found to be affected by the availability of cell-cell contact between donors and recipients, time of biofilm growth, and biofilm structure, but not by the concentration of nutrients^{88,90}.

2.5 MATERIALS USED IN TRADITIONAL BIOFILM STUDIES

Traditional biofilm research has been based on biofilms formed on conventional materials, such as metal⁹⁴, plastic^{80,95} or glass^{80,96-98} surfaces in test tubes⁸⁰, 96-well plates^{81,84,99-103}, or flow cells^{18,81,98,104,105}. As discussed above, biofilm formation can be affected by multiple factors (e.g., bacterial surface structures, physiochemical properties of the surface that a biofilm is formed on, and environmental conditions)^{8,12,15,106-108}. Thus, a typical biofilm formed on a conventional surface has substantial heterogeneity in its spatial organization, with uneven surface coverage and cell clusters of varying size,

shape and cell density. Even on the same surface, individual cells in such heterogeneous biofilms could be different from each other in gene expression, metabolism, and other cellular activities^{73,74}. Such heterogeneity hinders the mechanistic understanding of biofilm formation^{73,109} and can lead to different results in different experimental systems^{11,104,110,111}, regarding the roles of flagella¹¹⁰⁻¹¹², motility^{95,110,112}, stress response^{112,113}, and cell-to-cell signaling^{108,111,114,115}. To understand the physiology of biofilm cells and the underlying mechanism, novel techniques and materials that can rigorously control the density and spacing of biofilm cells need to be developed.

2.6 NEW TECHNIQUES TO CONTROL CELL DENSITY AND CREATE PATTERNED CELL CLUSTERS

Interactions between bacterial cells and cell clusters are crucial to the development of multicellular biofilm structures. Such interactions are difficult to study due to the intrinsic heterogeneity in biofilm structures. Thus, new techniques that can control the location of biofilm cells, spacing between cell clusters, and the cell density in these clusters are needed to decouple the biological factors, chemical factors, and physical structure of biofilms. Two strategies have been applied to control cell density including surface guided pattern formation and cell trapping. A number of new methods have also been developed to deposit bacterial cells on surfaces with designed patterns. In this section, we will briefly introduce the principle of these methods and their applications in studying bacterial cell-to-cell communication, antibiotic resistance, and biofilm formation.

2.6.1 Lipid-silica structures

Porous lipid-silica structures formed by evaporation-induced self-assembly^{116,117} (Fig. 2-2A), an aerosol-assisted approach using dihexanoylphosphatidylcholine^{117,118} (Fig. 2-2B), and pre-formed lipid-templated silica films¹¹⁷ can be used to trap single cells or small groups of cells. Upon evaporation of the solvent, individual cells or small groups of cells are encapsulated in 3D lipid-silica structures. Such confinement of cells in a fairly small volume can be used to trap single cells or to create high density cell clusters, e.g. 10^9 to 10^{12} cells / mL⁷⁷, providing an ideal system for studying cell density associated phenotypes such as quorum sensing. In a study by Carnes *et al.*¹¹⁹, a single *Staphylococcus aureus* cell was trapped in an endosome-like lipid vesicle within a lipid/silica droplet on glass surface. It was found that single *S. aureus* cells start the production of QS signals after 10 h of incubation at 37 °C without growth and the QS signals were found to accumulate over time inside the diffusion-limited lipid silica structures (Fig. 2-2B).

2.6.2 Microwells

Another approach to trap single bacterial cells is using surfaces modified with arrays of microwells¹²⁰⁻¹²⁶. In this approach, surfaces are patterned with microwells that have defined shape and size. To trap single cells, wells are designed to be just enough to house individual cells. In some cases, the surfaces can be directly seeded with a cell suspension to allow the spontaneous deposition of single cells into wells^{121,123,125,126} (Fig. 2-3A). Kim *et al.*¹²⁴ trapped *E. coli* cells with positive dielectrophoresis into microwells, each with a diameter of 3 μm . Although the purpose of this study was to lyse the trapped single bacterial cells by applying concentrated electric potential on cell membrane, this

system can also be used to separate cells from a mixed population if the cells have different sizes. Trapping cells can also be used to follow cell growth in a confined geometry with controlled flow of media and stimuli. For example, Takeuchi *et al.*¹²² successfully trapped single *E. coli* cells in agarose microchambers by placing a flat and flexible slab of agarose or PDMS on top of microchambers (1.5-2.5 μm deep and 2-20 μm wide). These microchambers were prepared via replica molding against a master plate that contained features derived from photolithography or soft lithography^{77,109,120}. With the growth medium contained in agarose gel and the presence of cephalixin, circular-shaped filamentous *E. coli* cells were obtained by confining them in donut-shaped microchambers. The shape of these cells was retained after being released from the microchambers into solution (Fig. 2-3B). By controlling cell shape, this method can be used to study stress response of bacterial cells as well.

2.6.3 Microfluidic devices

Poly(dimethylsiloxane) (PDMS) based microfluidics have been applied to confine single bacterial cells in channels¹²⁷⁻¹²⁹, wells¹³⁰, or droplets¹³¹⁻¹³⁶ (Fig. 2-4). These microfluidic devices are fabricated via photolithography and soft lithography^{77,109,120}. Microfluidic devices with the bottom surface modified with 1.5 μm long and 0.5 μm wide grooves were used to immobilize individual *E. coli* cells and study the relationship between bacterial metabolic activity and their persistence phenotype¹²⁹. Heterogeneity in growth rate was observed among individual cells under the same growth condition, which was linked to the persister phenotype since slow-growing cells showed higher resistance to the β -lactam antibiotic ampicillin. In another study, Boedicker *et al.*¹³⁰ created an array of approximately 100 fL droplets with different cell densities by

introducing air bubbles over the wells made with biocompatible¹³⁷ resin SU-8 (photoresist)¹³⁸. *P. aeruginosa* cells were inoculated by passing a low-density cell culture through PDMS channels on top of resin wells. Bacterial cell density in the droplets was controlled by adjusting the time for settlement of bacteria in PDMS channels. This strategy allows the cell density in each droplet to be controlled varying from single cell to 10^{10} ~ 10^{11} cells/mL. In addition to QS in bacterial populations with high cell density, the expression of QS-controlled gene *lasB* was also observed in droplets with single cells¹³⁷. Another approach of confining single cells or small groups of cells in microfluidic systems involves droplet-based microfluidic systems. Droplets in microfluidic systems can be generated using a T-junction¹³⁹ or a flow-focusing microfluidic device¹³⁴, in which the droplet size can be controlled by adjusting the flow of immiscible liquids¹³⁶. Droplets are detected based on the fluorescence marker carried by cells¹⁴⁰ and can be sorted using fluorescence-activated droplet sorter (FADS)¹⁴¹. To investigate the effects of signal diffusion and cell confinement on QS, Bai *et al.*¹³⁴ confined single bacterial cells using a droplet-based microfluidic system. In this approach, droplets of surfactant monolayers are created in a microfluidic device. The droplets are organized in pairs with one containing a trapped individual *E. coli* cell and the other containing either a single cell or specific signaling molecules. This system is useful for studying bacteria at single cell level. By continuously monitoring the communication between bacteria, QS was observed at the single cell level when *E. coli* was exposed to a droplet containing either the autoinducer N-(3-oxododecanoyl)-L-homoserine lactone (OdDHL) or another *E. coli* cell. This result indicates that the confinement of individual cells by droplets led to restricted diffusion of signaling molecules and the buildup of its concentration beyond the threshold for

triggering bacterial QS in the droplets, which was found to be 1 μ M in that study¹³⁴. In addition to this application, the advances in droplet microfluidics also enabled many other high-throughput studies at single cell level^{77,132}, such as bacterial antibiotic resistance^{131,136}, comparative genomics^{77,142}, and cell isolation from natural populations¹³³.

2.6.4 Direct printing

Weibel *et al.*¹⁴³ directly printed *Vibrio fischeri* cells on agar plates, glass slides, and nylon membranes using micropatterned agarose stamps prepared by molding against PDMS masters (Fig. 2-5). Recently, inkjet printing, including variations of drop-on-demand technology employing thermal printing and piezoelectric actuation, has been used to deposit bacterial cells in cellular microarrays¹⁴⁴⁻¹⁴⁷. Merrin¹⁴⁵ and Choi¹⁴⁷ *et al.* used a piezoelectric drop-on-demand inkjet printer to print *E. coli* cells onto flat surface with up to 98.5% cells remained viable. The center-to-center drop spacing ranged from 5 μ m to 2 mm. The advantage of this methodology is its capability of controlling cell density in each droplet as well as the distance between droplets on surfaces.

2.6.5 Hydrogels

With permeability to small hydrophobic molecules, hydrogels can be created with desired mass transfer properties to mimic the environment in natural biofilms. Hence, hydrogels have been used for immobilizing bacterial cells in semi-solid media and studying bacterial physiology in biofilms^{82,148-152}. Multiphoton lithography (MPL) has been used to produce stimuli responsive lobster traps with walls composed of crosslinked proteins to confine bacterial cells¹⁴⁹ (Fig. 2-6A). Various proteins can be used to fabricate these microchambers, including bovine serum albumin (BSA), avidin,

lysozyme, and cytochrome c^{153,154}. Since these microchambers are protein-based structures, the geometry and size of the microchambers can be altered by manipulating environmental conditions such as pH, temperature, osmolarity, and light intensity^{149,155}. Moreover, the porous walls of these microchambers composed of proteins enable the diffusion of nutrients and waste products. By fabricating microchambers on coverslips in flow cells, cellular activities in microchambers can be followed in real time. Using this approach, Connell *et al.*¹⁴⁹ demonstrated that bacterial communication via QS is influenced not only by cell density but also by population size and mass transfer rate of QS signals. Cells in the lobster traps also exhibited high resistance to antibiotics; interestingly, it cannot be explained by growth rate because the cells in traps did not show different growth rate compared with cells grown in laboratory flasks¹⁵⁶. To further study bacterial QS and bacterial resistance to antibiotics, Connell *et al.*¹⁵⁰ expanded the lobster traps fabricated with MPL to a microscopic 3D printing strategy that can organize multiple populations of bacteria into any 3D geometry (Fig. 2-6B). Microstructures with defined geometry were fabricated via laser induced focal cross-linking of polypeptide molecules. Bacteria were suspended in the mixture of gelatin and BSA at 37°C. By lowering temperature to 18-22 °C, bacteria were immobilized in a gel and localized within sealed cavities formed by crosslinked gelatin. Gelatin is a highly porous material that not only can support the rapid growth of enclosed bacteria but also allow the diffusion of polypeptides, antibiotics, and QS signals. Using this approach, Connell *et al.*¹⁵⁰ demonstrated that a small population of *S. aureus* enclosed in a shell of *P. aeruginosa* cells was not killed by ampicillin. This result suggests that the shell of *P. aeruginosa* cells (2 cells/pL) can effectively degrade ampicillin as it diffuses toward *S.*

aureus cells. Since hydrogels are permeable to QS signals, Flickinger *et al.*⁸² examined the diffusion of homoserine lactones (HSLs), QS signals used by Gram-negative bacteria, between small colonies of *P. aeruginosa* confined in arrays of 1.5 mm wide chambers embossed in a layer of poly(ethylene glycol) diacrylate (PEGDA) (Fig. 2-6C). These hydrogel walls were used to study chemical communication between biofilm cells since they are permeable to small molecules such as QS signals, but prohibit physical cell-cell interactions in biofilms. Experiments using this platform showed that, during static growth, HSLs produced by *P. aeruginosa* biofilms formed a gradient in hydrogel and was detected by biofilm cells up to 8 mm away. HSLs that have no effect on cell growth in liquid culture promoted the growth of biofilm cells within 3 mm. These results corroborate those obtained by embedding QS strain in a narrow agar lane¹⁵⁷ and reveal new information about signaling over distance.

2.6.6 Chemical modification using microcontact printing

Microcontact printing has been widely used to chemically modify surfaces by transferring biomolecules from the surface of a topographically patterned polymer stamp¹⁰⁹. Recently, this method has been successfully used to control the pattern, shape, spacing, and orientation between colonies of different bacteria. Various biomolecules, chemicals, proteins, and polyelectrolytes can be used as ‘ink’ to modify a surface using microcontact printing^{143,158-160}. Several groups covalently patterned antibodies to immobilize bacteria¹⁶¹⁻¹⁶⁴. For example, Sun *et al.*¹⁶⁵ patterned polydopamine (PDA) on poly(ethylene glycol) (PEG) using microcontact printing to direct the adhesion of *E. coli* and *S. epidermidis* cells. Among all the chemicals used to immobilize bacterial cells, alkanthiols are a particularly useful group of chemicals for tailoring surfaces with specific

chemistry¹⁶⁶. To immobilize small groups of *E. coli* cells, methyl-terminated n-alkanethiol (hydrophobic) that promotes bacterial adhesion was used by Rowan *et al.*¹⁶⁷ to modify the bottom of 3D corrals, whereas the walls of these 3D corrals consisted of hydrophilic poly (acrylic acid) / PEG layered nanocomposites that inhibit adhesion. The 3D corrals were fabricated on gold, titanium, or silicon surfaces through a four-step microcontact printing mediated soft lithography. The size of corrals ranged from 12 to 63 μm^2 . Using this approach, small groups of *E. coli* cells were successfully confined in corrals (Fig. 2-7). Rozhok *et al.*¹⁶⁸ immobilized *E. coli* K12 cells in patterns of lines and circles using anti-lipopolysaccharide antibodies or poly-L-lysine, which were bound to 16-Mercaptohexadecanoic acid (MHA) (introduced by using patterned PDMS stamps). The bioinert SAM presenting (11-mercaptoundecyl-penta-(ethylene glycol) (PEG-SH) or 11-mercapto-1-undecanol (MOU)) was used as background to create 2 μm wide lines with 2 μm distance between lines, as well as 3 μm holes with 3 μm spacing. SAM surfaces can also be used to create synthetic biofilms with patterned geometry. Hou *et al.*^{160,169} directed the adhesion of *E. coli* RP437 cells in square patterns of non-inert methyl-terminated SAM (CH_3 -SAM) surrounded by bioinert tri(ethylene glycol)-terminated SAM (TEG-SAM). Using such patterned biofilms in this thesis research, it was found that the size of cell clusters and distance between adjacent clusters are important to cell-cell interactions in biofilms. Also, quorum sensing and motility were found to play a role in such interactions (more details in Chapter 3)¹⁷⁰.

2.7 PHYSICAL SURFACE MODIFICATION FOR BIOFILM CONTROL

Biofilm formation is a dynamic process that involves hundreds of proteins and genes. The expression of these genes and protein is very sensitive to the physical and chemical properties of the solid surface that a biofilm is formed on^{171,172}. Recently, the topographic features of surfaces were intensively studied as an environmental factor that can potentially influence biofilm formation. The surface structure can be represent by the roughness (2-dimensional measurement based on the mean distance between peak and valley) and topography (3-dimensional measurement) For example, Taylor *et al.*¹⁷³ reported that the attachment of *P. aeruginosa* and *S. epidermidis* to poly(methyl methacrylate (PMMA) increased significantly with a relatively small increase in surface roughness value Ra from 0.04 μm to 1.24 μm . However, when the roughness Ra increased from 1.86 to 7.89 μm , bacterial adhesion decreased, suggesting an optimal Ra exists for cell attachment in this experimental system. In comparison, Hilbert *et al.*¹⁷⁴ reported that changing the surface roughness (Ra) from 0.9 to 0.01 μm has no effects on the adherence of *Pseudomonas sp.*, *Listeria monocytogenes* and *Candida lipolytica* to stainless steel surfaces. The different effects of surface roughness on bacterial adhesion could be caused by the differences in the property of surfaces and the intrinsic characteristics of biofilms formed by different bacterial strains.

Whitehead *et al.*¹⁷⁵ reported that bacterial adhesion on surfaces with microtopographic features depends on the scale of topography. The scale of topography can also affect the retention of microorganisms on the surface if the scale of topographic features is comparable to that of microorganisms. When the size of features becomes nanoscale, the surface can significantly affect bacterial behavior. Machado *et al.*¹⁷⁶

demonstrated that the nanoscale roughness on poly(vinyl chloride) (PVC) introduced via chemical etching can alter surface energy and reduce bacterial adhesion. Another surface topography that can reduce bacterial adhesion is the Sharklet AF surfaces. These are PDMS surfaces with 2 μm -wide and 3 μm -tall rod-shaped topographic features organized in a diamond geometry with 2 μm spacing between adjacent features (Fig. 2-8). The biofilm colonization of *S. aureus* on such modified surfaces was significantly inhibited for 21 days¹⁷⁷.

It is important to note that surfaces with topographic features or increased roughness do not always reduce biofilm formation compared to smooth surfaces. For example, certain roughness and topography were found to promote bacterial adhesion by providing extra space for bacterial adhesion^{171,178}. For instance, Mitik- Dineva¹⁷⁹ and Satriano¹⁸⁰ *et al.* reported that nanoscale topography on glass and poly(hydroxymethylsiloxane) (PHMS) surfaces can promote bacterial adhesion with increase in EPS production and change in cell morphology. Friedlander *et al.*¹⁷⁸ demonstrated, while topography (hexagon, 3 μm in diameter and 2.7 μm in height) on PDMS surfaces can reduce bacterial adhesion due to the Cassie-Baxter wetting state^{181,182}, the resistance was lost after 2 h incubation with *E. coli* cells with even more cells attached than the flat surfaces. Thus, the effects of topography depends on the size and shape of such features as well as the species of bacteria^{183,175}.

The mechanism by which bacteria sense the surface and make a decision between adhesion and planktonic growth is still unknown. The impact of surface roughness and topography on the adhesion of mammalian cells is partially due to the flexibility of mammalian cells that allows these cells to spread on features. In comparison, bacterial

cells are a lot smaller. In addition, by measuring the stiffness of bacterial cells, it is found out that bacterial cells are more rigid than mammalian cells and the cells in biofilms are even stiffer than planktonic cells¹⁸⁴. The differences in cell size and stiffness may contribute to the different effects of surface roughness and topography on cell adhesion. Although bacterial cells are less flexible than mammalian cells, *E. coli* and *Proteus mirabilis* have been shown to alter their surface morphology such as flagella density, cell density, flexibility and adhesion potential on rough surfaces¹⁸⁵. This suggested that bacterial flagella may play a role in surface adhesion. However, no direct evidence has been reported regarding bacterial flagella as a sensor of environment and surface condition. Using SEM, Friedlander *et al.*¹⁷⁸ reported that flagella of *E. coli* cells reach the micrometer scale valleys between 2, 3 μm -tall topographic pattern. Although these studies provided invaluable insights, the mechanism of biofilm formation and how bacteria sense the environment are still not fully understood. To obtain a better understanding of biofilm formation, especially the roles of bacterial surface structures, experimental systems with well-defined surfaces and imaging capabilities at nanoscale are needed.

2.8 FIGURE CAPTIONS

Figure 2-1. Representative images of 24, 48, and 72 h *E. coli* RP437 biofilms on glass, gold (without chemical modification), and stainless steel surfaces.

Figure 2-2. Cell confinement using lipid-silica structures. (A) Schematic description of the cell-directed integration of microbes in lipid templated silica films. The insert image (a5) is an atomic force microscopy (AFM) image of a *Saccharomyces cerevisiae* cell encapsulated in a lipid-silica shell. Reproduced with permission from Ref. [117]. Copyright 2010 American Chemical Society. (B) Single *S. aureus* cells in lipid-silica droplets on glass surfaces. (b1) Schematic description of a cell incorporated in an endosome-like lipid vesicle within a lipid-silica droplet on glass surface. (b2) Scanning electron microscopy (SEM) image of the lipid-silica structure. (b3) and (b4) Left: plan-view optical image of individual cells in droplets. Right top: different interference contrast (DIC) image of the confined cells. Right center: red fluorescence image of a stained cell. Right bottom: green fluorescence image of lipid on cell surface labeled with 7-nitro-2, 1, 3-benzoxadiazol-4-yl (NBD) (b3); image of localized pH labeled with Oregon green pH-sensitive dye (Bar = 5 μm). Reproduced with permission from Ref. [119]. Copyright 2010 Nature Publishing Group.

Figure 2-3. Individual cells trapped in microwells or microchambers. (A) Comparison of *P. aeruginosa* adhesion on flat and modified surfaces. (a1) Top: fluorescence image of bacterial adhesion on flat surfaces. Bottom: fluorescence image of bacterial adhesion on a periodically structured epoxy

surface. SYTOX[®] green nucleic acid stain was used to label cells (Bar = 10 μm). a2 and a3) Cross-sectional SEM image of *P. aeruginosa* PA14 cells on flat (a2) and structured surfaces (a3) (Bar = 1 μm). Reproduced with permission from Ref. [123]. Copyright 2010 American Chemical Society.

(B) Controlling the shape of filamentous *E. coli* cells in microchambers fabricated in agarose containing growth media. (b1) Schematic description of the microchambers. (b2) A single *E. coli* cell confined in a microchamber. (b3) Growth of a filamentous cell in the presence of cephalixin. (b4) Cell is released into solution. (b5) and (b6) Phase-contrast microscopy images of donut-shaped microchambers with cells before (b5) and after (b6) the growth of filamentous *E. coli* cells (Bar = 50 μm). (b7) Phase-contrast image of spiral, filamentous *E. coli* cells in solution (Bar = 10 μm). Reproduced with permission from Ref. [122]. Copyright 2005 American Chemical Society.

Figure 2-4. Schematic description of the techniques of soft lithography: (a). replica moulding; (b). micromoulding in capillaries; (c). microfluidics; d. microcontact printing. Reproduced with permission from Ref. [109]. Copyright 2007 Nature Publishing Group.

Figure 2-5. Bacterial microcontact-printing. (A-E) Schematic description of the process. (F) Image of an agarose stamp (Bar = 10 mm). (G) Circle-shaped patterns of *V. fischeri* colonies (Bar = 2 mm). (H) Checkerboard patterns of *V. fischeri* colonies (Bar = 2 mm). (I) Honeycomb patterns *V. fischeri* colonies

(Bar = 250 μm). Reproduced with permission from Ref. [143]. Copyright 2005 American Chemical Society.

Figure 2-6. Small groups of bacterial cells confined in hydrogel microchambers or microstructures. (A) The confinement of *P. aeruginosa* cells in lobster traps with walls consisted of various proteins. (a1) Schematic description of the optical setup. (a2) Heart-shaped, 2-picoliter traps with (left and right) and without (middle) *P. aeruginosa* cells (Bar = 5 μm). (a3) Confocal images of traps with *P. aeruginosa* cells after 2 h gentamicin treatment at the minimal inhibitory concentration (MIC). Reproduced with permission from Ref. [149]. Copyright 2010 American Society for Microbiology. B) *P. aeruginosa* microcolonies in 3D gelatin structures. (b1) Confocal images of *P. aeruginosa* microcolonies in a surface-anchored 2-pL pyramid (top) and an untethered 3-pL torus (bottom). (b2) Confocal images of six physically segregated *P. aeruginosa* populations in 3D spheroid cavities tethered to the glass substrate. (b3) Three connected spheroid cavities tethered to the glass surface by cylindrical posts. The top-down DIC image (left), side-on confocal image (center) and top-down confocal image (right) are shown. Reproduced with permission from Ref. [150]. Copyright 2013 National Academy of Sciences. (C) Diffusion of HSL between *P. aeruginosa* biofilm cell clusters confined in hydrogel chambers. Reproduced with permission from Ref. [82]. Copyright 2011 American Chemical Society.

Figure 2-7. A corral array of trapped *E. coli* cells (Bar = 20 μm). Reproduced with permission from Ref. [167], Copyright 2012 American Chemical Society.

Figure 2-8. Representative SEM images of *S. aureus* biofilm formation on smooth (left column) and Sharklet AF (right column) PDMS surfaces. (A) and (B) day 0, (C) and (D) Day 2, (E) and (F) Day 7, (G) and (H) Day 14, and (I) and (J) Day 21. Reproduced with permission from Ref. [177]. Copyright 2007 Springer.

2.9 FIGURES

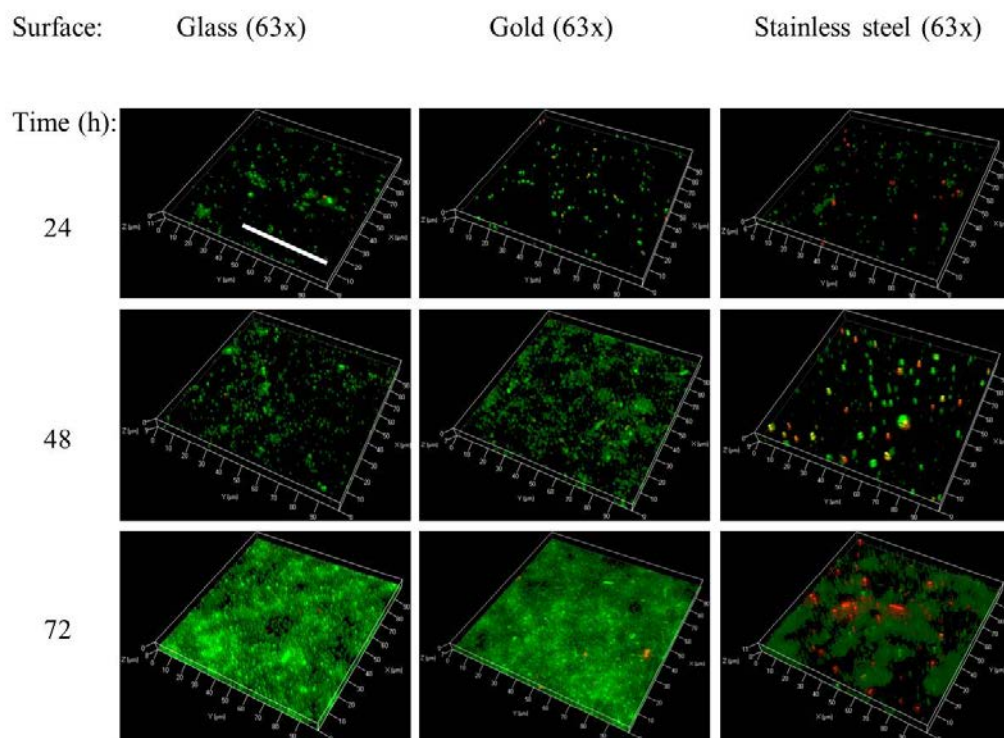


Figure 2-1

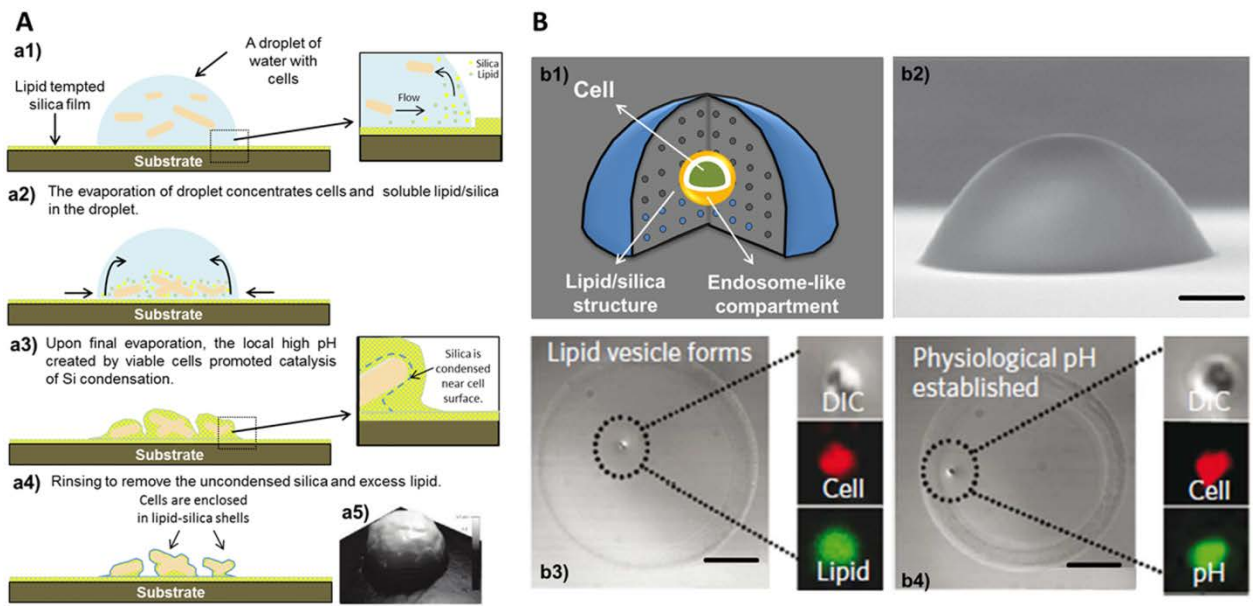


Figure 2-2

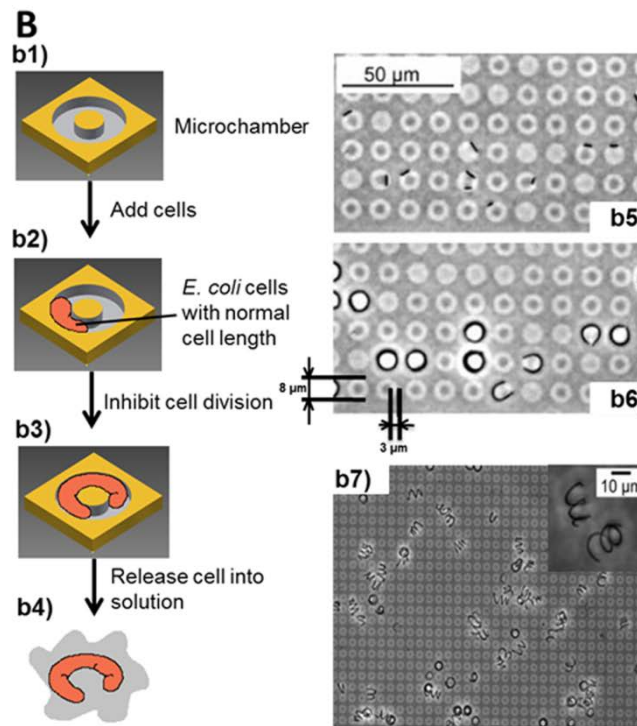
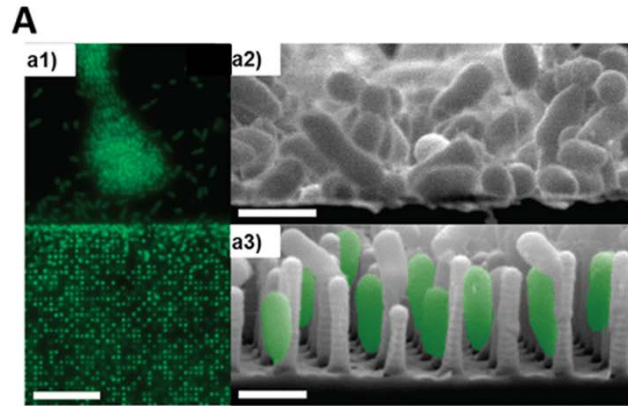


Figure 2-3

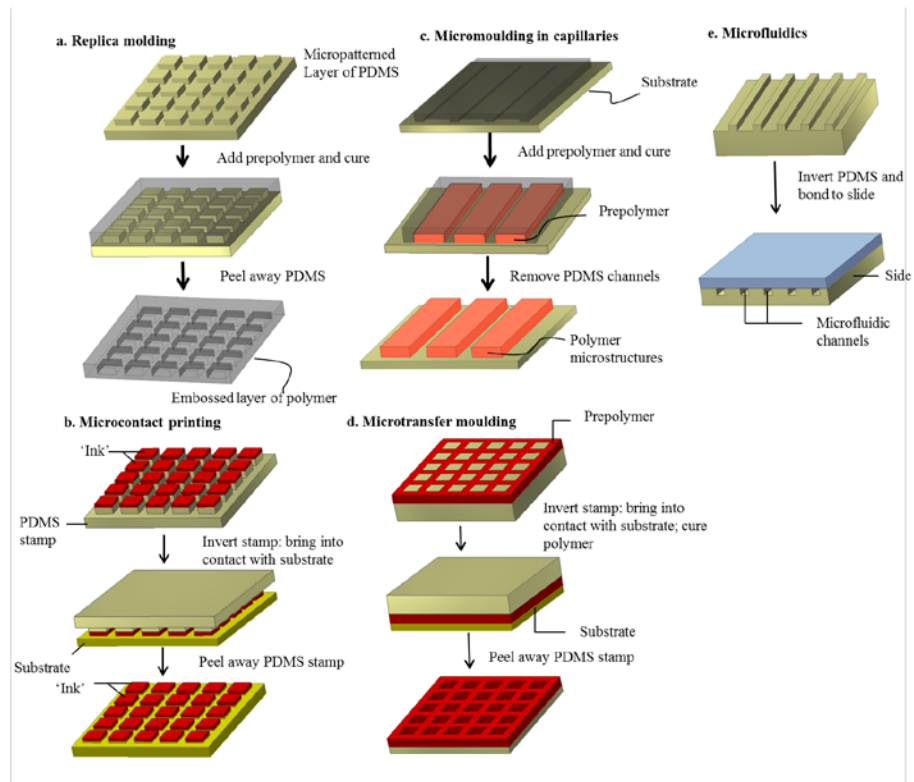


Figure 2-4

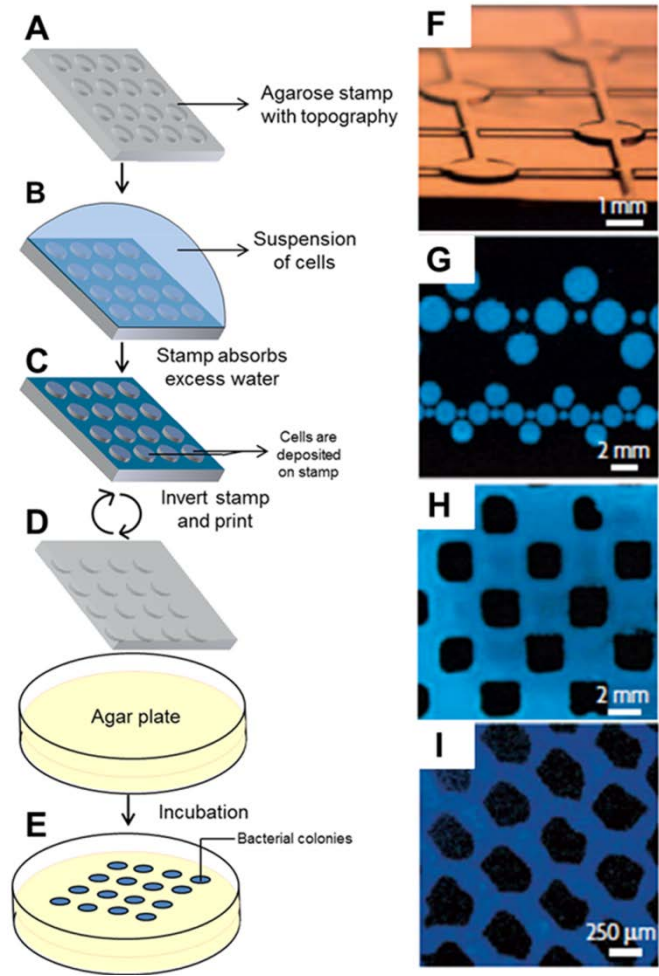


Figure 2-5

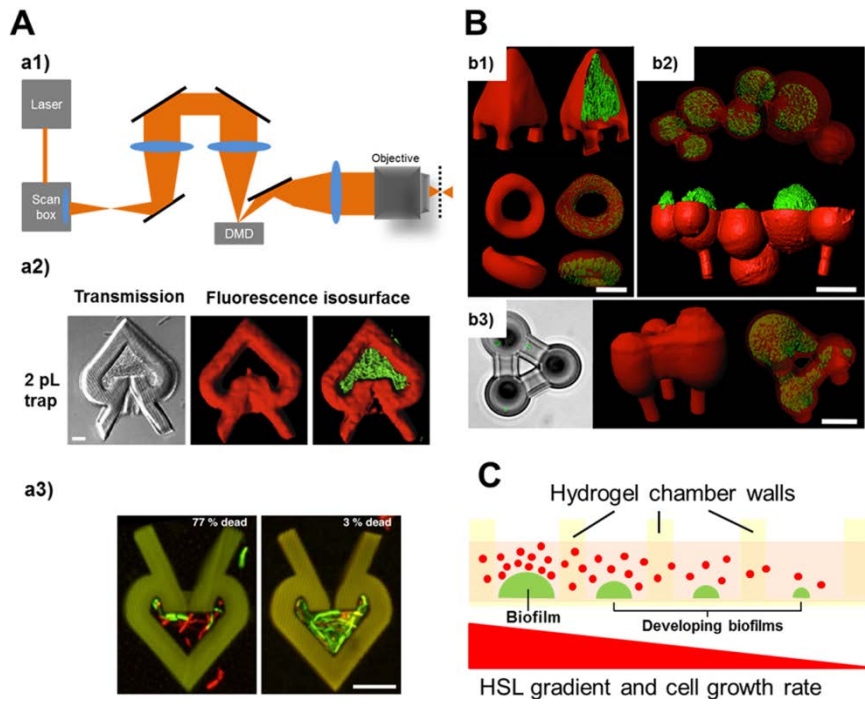


Figure 2-6

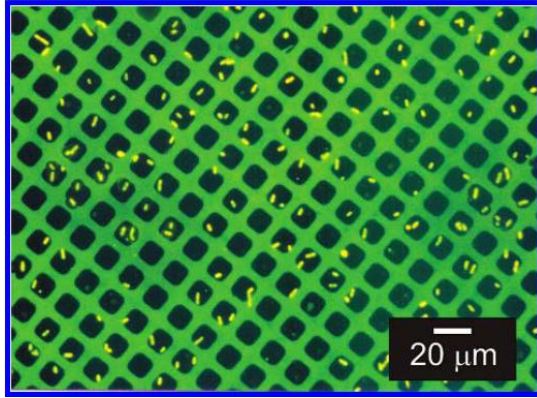


Figure 2-7

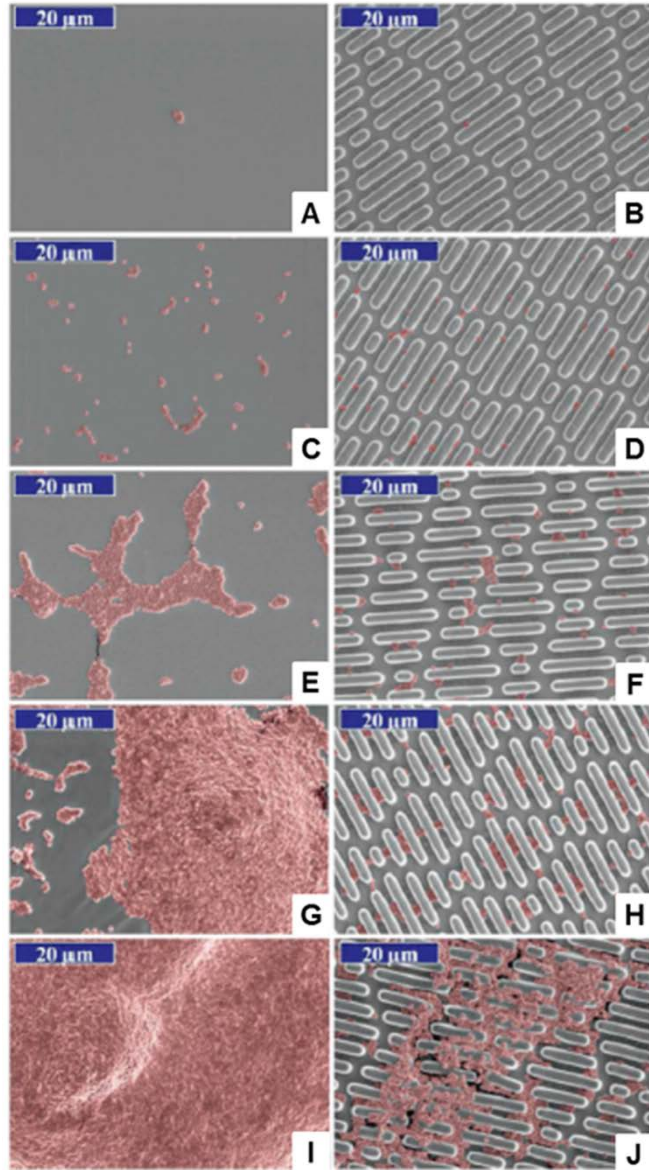


Figure 2-8

2.10 TABLES

Table 2-1 Summary of *E. coli* genes involved in biofilm formation

Gene Name	Function	Roles in Biofilm Formation
<i>cstA</i>	Carbon storage regulator ^{100,186}	This global regulation of central carbon flux serves both as a repressor of biofilm formation and an activator of biofilm dispersal under a variety of culture conditions ^{100,186} .
<i>ompR</i>	Part of an osmolarity-sensing regulatory system ^{36,186}	OmpR/EnvZ, a two-component regulatory system, senses environmental osmolarity and regulates biofilm formation. OmpR protein can promote curli production by activating <i>csgD</i> ^{36,186} .
<i>rpoS</i>	Stationary-phase-specific sigma factor RpoS ^{36,186}	RpoS controls the transcription of the transcription regulator CpxR ^{36,186} . RpoS coordinates the negative regulation between <i>csgDEFG</i> and <i>csgBA</i> , which is achieved by direct interaction between the CpxR protein and the promoters of <i>csgD</i> and <i>csgB</i> ^{36,186} .
<i>cpxR</i>	Transcription regulator CpxR ^{36,186}	CpxR represses motility and chemotaxis genes and is involved in the regulation of pili ^{36,186} .
<i>barA</i>	A member of the subclass of tripartite sensor kinases and a cognate kinase of UvrY that is a response regulator of the FliJ family ¹⁸⁷	BarA/UvrY, a two component system, promotes biofilm formation ^{186,187} .
<i>rcsB</i>	A cytoplasmic response regulator ¹⁸⁸	RcsB activates biofilm formation through remodeling of cell surface composition via two-component system, RcsB-YojN-RcsC ¹⁸⁶ .

Gene Name	Function	Roles in Biofilm Formation
<i>crp</i>	Catabolite gene Activator Protein(CRP) or cyclic AMP receptor protein ¹⁹⁰	CRP represses biofilm formation through catabolite repression ¹⁸⁶ .
<i>hns</i>	Histone like proteins ¹⁹¹	H-NS reduces adhesion in anoxic condition ¹⁸⁶ .
<i>lrp</i>	Leucine-responsive regulatory protein (Lrp) ⁴⁶	A global regulatory protein that affects biofilm formation by regulating the expression of bacterial fimbriae ^{45,46} .
<i>ihf</i>	Integration host factor ^{45,47,189}	A global regulatory protein that affects biofilm formation by regulating the expression of bacterial fimbriae and curli ^{45,189} .
<i>lrhA</i>	LysR-type regulator LrhA (LysR homologue A) ³⁷	A global regulator that induces the transition from planktonic cells to biofilm formation by repressing numerous genes (48) involved in flagellation, motility and chemotaxis ³⁷ .
<i>flhDC</i>	A DNA-binding transcriptional regulator that activates the expression of class II gene expression for flagellar assembly ^{19,189}	A central regulator of biofilm formation, which controls the expression of genes involved in flagellar assembly, motor assembly, and chemotaxis required for initial bacterial attachment ¹⁹ .
<i>fimBE</i>	FimB and FimE, two recombinases, controls the expression of type I fimbriation ⁴⁵	FimE can turn off the expression of <i>fim</i> gene cluster, while FimB can turn on or turn off the expression of <i>fim</i> gene cluster ^{45,48} .
<i>csgD</i>	Transcription regulator CsgD ¹⁸⁹	A putative transcription factor belongs to the <i>luxR</i> family and activates transcription of the <i>csgBA</i> operon encoding curli, and extracellular structures involved in bacterial adhesion ^{36,189}

2.11 REFERENCES

- 1 **Donlan, R. M.** 2001. Biofilm formation: a clinically relevant microbiological process. *Clin Infect Dis* **33**: 1387-1392.
- 2 **Walker, J., Surman, S., Jass, J.** 2000. Industrial Biofouling: Detection, Prevention and Control.1-12.
- 3 **Banerjee, I., Pangule, R. C., Kane, R. S.** 2011. Antifouling coatings: recent developments in the design of surfaces that prevent fouling by proteins, bacteria, and marine organisms. *Advanced Materials* **23**: 690-718.
- 4 **Davey, M. E., O'Toole G, A.** 2000. Microbial biofilms: from ecology to molecular genetics. *Microbiol Mol Biol Rev* **64**: 847-867.
- 5 **Donlan, R. M.** 2002. Biofilms: microbial life on surfaces. *Emerging infectious diseases* **8**: 881-890.
- 6 **Dunne, W. M.** 2002. Bacterial adhesion: seen any good biofilms lately? *Clinic Microbiology Review* **15**: 155-166.
- 7 **Stoodley, P., Sauer, K., Davies, D. G., Costerton, J. W.** 2002. Biofilms as complex differentiated communities. *Annu Rev Microbiol* **56**: 187-209.
- 8 **Van Houdt, R., Michiels, C. W.** 2005. Role of bacterial cell surface structures in *Escherichia coli* biofilm formation. *Res. Microbiol.* **156**: 626-633.
- 9 **Bullitt, E., Makowski, L.** 1995. Structural polymorphism of bacterial adhesion pili. *Nature* **373**: 164-167.
- 10 **Thomas, W. E., Nilsson, L. M., Forero, M., Sokurenko, E. V., Vogel, V.** 2004. Shear-dependent 'stick-and-roll' adhesion of type 1 fimbriated *Escherichia coli*. *Mol Microbiol* **53**: 1545-1557.
- 11 **Karatan, E., Watnick, P.** 2009. Signals, Regulatory Networks, and Materials That Build and Break Bacterial Biofilms. *Microbiol Mol Biol R* **73**: 310-347.
- 12 **Palmer, J., Flint, S., Brooks, J.** 2007. Bacterial cell attachment, the beginning of a biofilm. *Journal of industrial microbiology & biotechnology* **34**: 577-588.
- 13 **Marshall, K. C., Stout, R., Mitchell, R.** 1971. Mechanisms of the initial events in the absorption of marine bacteria to surfaces. *J. Gen. Micro.* **68**: 337-348.
- 14 **Das, T., Manefield, M.** 2012. Pyocyanin promotes extracellular DNA release in *Pseudomonas aeruginosa*. *PLoS One* **7**: e46718.
- 15 **Renner, L. D., Weibel, D. B.** 2011. Physicochemical regulation of biofilm formation. *MRS bulletin / Materials Research Society* **36**: 347-355.
- 16 **Harmsen, M., Yang, L., Pamp, S. J., Tolker-Nielsen, T.** 2010. An update on *Pseudomonas aeruginosa* biofilm formation, tolerance, and dispersal. *FEMS Immunol Med Microbiol* **59**: 253-268.
- 17 **Jayaraman, A., Wood, T. K.** 2008. Bacterial quorum sensing: signals, circuits, and implications for biofilms and disease. *Annu Rev Biomed Eng* **10**: 145-167.
- 18 **Ma, L. et al.** 2004. Assembly and development of the *Pseudomonas aeruginosa* biofilm matrix. *PLoS pathogens* **5**: e1000354.
- 19 **Eisenbach, M. et al.** 2004. *Chemotaxis*. (Imperial College Press).
- 20 **Adler, J., Templeton, B.** 1967. The effect of environmental conditions on the motility of *Escherichia coli*. *J. Gen. Microbiol.* **46**: 175-184.
- 21 **Uchida, K., Dono, K., Aizawa, S. I.** 2013. Length control of the flagellar hook in a temperature-sensitive *flgE* mutant. *J. Bacteriol.*

- 22 **Soutourina, O. A. et al.** 2002. Regulation of bacterial motility in response to low
pH in *Escherichia coli*: the role of H-NS protein. *Microbiology* **148**: 1543-1551.
- 23 **Maurer, L. M., Yohannes, E., Bondurant, S. S., Radmacher, M., Slonczewski,
J. L.** 2005. pH regulates genes for flagellar motility, catabolism, and oxidative
stress in *Escherichia coli* K-12. *J Bacteriol* **187**: 304-319.
- 24 **Shin, S., Park, C.** 1995. Modulation of flagellar expression in *Escherichia coli* by
acetyl phosphate and the osmoregulator OmpR. *J Bacteriol* **177**, 4696-4702.
- 25 **Kunin, C. M., Hua, T. H., Bakaletz, L. O.** 1995. Effect of salicylate on
expression of flagella by *Escherichia coli* and *Proteus*, *Providencia*, and
Pseudomonas spp. *Infect Immun* **63**: 1796-1799.
- 26 **Zhao, K., Liu, M., Burgess, R. R.** 2007. Adaptation in bacterial flagellar and
motility systems: from regulon members to 'foraging'-like behavior in *E. coli*.
Nucleic. Acids. Res. **35**: 4441-4452.
- 27 **Kitamura, E., Nakayama, Y., Matsuzaki, H., Matsumoto, K., Shibuya, I.**
1994. Acidic-phospholipid deficiency represses the flagellar master operon
through a novel regulatory region in *Escherichia coli*. *Biosci Biotechnol Biochem*
58: 2305-2307.
- 28 **Kunin, C. M., Hua, T. H., Guerrant, R. L., Bakaletz, L. O.** 1994. Effect of
salicylate, bismuth, osmolytes, and tetracyclin resistance on expression of
fimbriae by *Escherichia coli*. *Infect. Immun.* **62**: 2178-2186.
- 29 **Li, C., Louise, C. J., Shi, W., Adler, J.** 1993. Adverse conditions which cause
lack of flagella in *Escherichia coli*. *J Bacteriol* **175**: 2229-2235.
- 30 **Mizushima, T. et al.** 1995. Control by phosphatidylglycerol of expression of the
flhD gene in *Escherichia coli*. *Biochim Biophys Acta* **1245**: 397-401.
- 31 **Prüss, B. M.** 1998. Acetyl phosphate and the phosphorylation of OmpR are
involved in the regulation of the cell division rate in *Escherichia coli*. *Arch.*
Microbiol. **170**: 141-146.
- 32 **Shi, W., Bogdanov, M., Dowhan, W., Zusman, D. R.** 1993. The *pss* and *psd*
genes are required for motility and chemotaxis in *Escherichia coli*. *J. Bacteriol.*
175: 7711-7714.
- 33 **Shi, W., Li, C., Louise, C. J., Adler, J.** 1993. Mechanism of adverse conditions
causing lack of flagella in *Escherichia coli*. *J Bacteriol* **175**: 2236-2240.
- 34 **Hong, S. H., Wang, X. X., Wood, T. K.** 2010. Controlling biofilm formation,
prophage excision and cell death by rewiring global regulator H-NS of
Escherichia coli. *Microbial Biotech.* **3**: 344-356.
- 35 **Soutourina, O. et al.** 1999. Multiple control of flagellum biosynthesis in
Escherichia coli: role of H-NS protein and the cyclic AMP-catabolite activator
protein complex in transcription of the *flhDC* master operon. *J Bacteriol* **181**:
7500-7508.
- 36 **Prigent-Combaret, C. et al.** 2001. Complex regulatory network controls initial
adhesion and biofilm formation in *Escherichia coli* via regulation of the *csgD*
gene. *J Bacteriol* **183**: 7213-7223.
- 37 **Lehmen, D. et al.** 2002. LrhA as a new transcriptional key regulator of flagella,
motility and chemotaxis genes in *Escherichia coli*. *Mol. Microbiol.* **45**: 521-532.

- 38 **Francez-Charlot, A. et al.** 2003. RcsCDB His-Asp phosphorelay system negatively regulates the *flhDC* operon in *Escherichia coli*. *Mol Microbiol* **49**: 823-832.
- 39 **Tart, A. H., Blanks, M. J., Wozniak, D. J.** 2006. The AlgT-dependent transcriptional regulator AmrZ (AlgZ) inhibits flagellum biosynthesis in mucoid, nonmotile *Pseudomonas aeruginosa* cystic fibrosis isolates. *J Bacteriol* **188**: 6483-6489.
- 40 **Lauriano, C. M., Ghosh, C., Correa, N. E., Klose, K. E.** 2004. The sodium-driven flagellar motor controls exopolysaccharide expression in *Vibrio Cholerae*. *J. Bacteriol.* **18**: 4864-4874.
- 41 **Klemm, P., Vejborg, R. M., Hancock, V.** 2010. Prevention of bacterial adhesion. *Appl Microbiol Biotechnol* **88**: 451-459.
- 42 **Connell, I. et al.** 1996. Type 1 fimbrial expression enhances *Escherichia coli* virulence for the urinary tract. *Proc Natl Acad Sci U S A* **93**: 9827-9832.
- 43 **Martinez, J. J., Mulvey, M. A., Schilling, J. D., Pinkner, J. S., Hultgren, S. J.** 2000. Type 1 pilus-mediated bacterial invasion of bladder epithelial cells. *EMBO J* **19**: 2803-2812.
- 44 **Prüss, B. M., Besemann, C., Denton, A., Wolfe, A. J.** 2006. A complex transcription network controls the early stages of biofilm development by *Escherichia coli*. *J Bacteriol* **188**: 3731-3739.
- 45 **Blomfield, I. C., Kulasekara, D. H., Eisenstein, B. I.** 1997. Integration host factor stimulates both FimB- and FimE-mediated site-specific DNA inversion that controls phase variation of type 1 fimbriae expression in *Escherichia coli*. *Mol Microbiol* **23**: 705-717.
- 46 **Hung, S. P., Baldi, P., Haltfield, G. W.** 2002. Global gene expression profiling in *Escherichia coli* K12. The effect of leucine-responsive regulatory protein. *J. Biol. Chem.* **277**: 40309-40323.
- 47 **García-Contreras, R., Zhang, X. S., Kim, Y., Wood, T. K.** 2008. Protein translation and cell death: the role of rare tRNAs in biofilm formation and in activating dormant phage killer genes. *PLoS One* **3**: e2394.
- 48 **Hommais, F. et al.** 2001. Large-scale monitoring of pleiotropic regulation of gene expression by the prokaryotic nucleoid-associated protein, H-NS. *Mol Microbiol* **40**: 20-36.
- 49 **Blumer, C. et al.** 2005. Regulation of type 1 fimbriae synthesis and biofilm formation by the transcriptional regulator LrhA of *Escherichia coli*. *Microbiology* **151**: 3287-3298.
- 50 **Oshima, T. et al.** 2002. Transcriptome analysis of all two-component regulatory system mutants of *Escherichia coli* K-12. *Mol Microbiol* **46**: 281-291.
- 51 **Blumer, C. et al.** 2005. *Global regulatory networks in enteric bacteria* 75-92.
- 52 **Vidal, O. et al.** 1998. Isolation of an *Escherichia coli* K-12 mutant strain able to form biofilms on inert surfaces: involvement of a new *ompR* allele that increases curli expression. *J. Bacteriol.* **180**: 2442-2449.
- 53 **Maurer, J. J., Brown, T. P., Steffens, W. L., Thayer, S. G.** 1998. The occurrence of ambient temperature-regulated adhesins, curli, and the temperature-sensitive hemagglutinin tsh among avian *Escherichia coli*. *Avian Dis* **42**: 106-118.

- 54 **Barnhart, M. M., Chapman, M. R.** 2006. Curli biogenesis and function. *Annu Rev Microbiol* **60**: 131-147.
- 55 **Gerstel, U., Römling, U.** 2003. The *csgD* promoter, a control unit for biofilm formation in *Salmonella typhimurium*. *Res Microbiol* **154**: 659-667.
- 56 **Arnqvist, A., Olsén, A., Pfeifer, J., Russell, D. G., Normark, S.** 1992. The Crl protein activates cryptic genes for curli formation and fibronectin binding in *Escherichia coli* HB101. *Mol Microbiol* **6**: 2443-2452.
- 57 **Olsén, A., Arnqvist, A., Hammar, M., Sukupolvi, S., Normark, S.** 1993. The RpoS sigma factor relieves H-NS-mediated transcriptional repression of *csgA*, the subunit gene of fibronectin-binding curli in *Escherichia coli*. *Mol Microbiol* **7**: 523-536.
- 58 **Olsén, A., Arnqvist, A., Hammar, M., Normark, S.** 1993. Environmental regulation of curli production in *Escherichia coli*. *Infect Agents Dis* **2**: 272-274.
- 59 **Hammar, M., Arnqvist, A., Bian, Z., Olsén, A., Normark, S.** 1995. Expression of two *csg* operons is required for production of fibronectin- and congo red-binding curli polymers in *Escherichia coli* K-12. *Mol Microbiol* **18**: 661-670.
- 60 **Brombacher, E., Dorel, C., Zehnder, A. J., Landini, P.** 2003. The curli biosynthesis regulator CsgD co-ordinates the expression of both positive and negative determinants for biofilm formation in *Escherichia coli*. *Microbiology* **149**: 2847-2857.
- 61 **Vianney, A. et al.** 2005. *Escherichia coli* *tol* and *rcs* genes participate in the complex network affecting curli synthesis. *Microbiology* **151**: 2487-2497.
- 62 **Ferrieres, L., Clarke, D. J.** 2003. The RcsC sensor kinase is required for normal biofilm formation in *Escherichia coli* K12 and controls the expression of a regulon in response to growth on a solid surface. *Mol. Microbiol.* **50**: 1665-1682.
- 63 **Jubelin, G. A. et al.** 2005. CpxR/OmpR interplay regulates curli gene expression in response to osmolarity in *Escherichia coli*. *J. Bacteriol.* **187**: 2038-2049.
- 64 **Zheng, D., Constantinidou, C., Hobman, J. L., Minchin, S. D.** 2004. Identification of the CRP regulon using in vitro and in vivo transcriptional profiling. *Nucleic. Acids. Res.* **32**: 5874-5893.
- 65 **Brown, P. K. et al.** 2001. MlrA, a novel regulator of curli (AgF) and extracellular matrix synthesis by *Escherichia coli* and *Salmonella enterica* serovar Typhimurium. *Mol Microbiol* **41**: 349-363.
- 66 **Prüb, B. M. et al.** 2003. FlhD/FlhC is a regulator of anaerobic respiration and the Entner-Doudoroff pathway through induction of the methyl-accepting chemotaxis protein Aer. *J. Bacteriol.* **185**: 534-543.
- 67 **Wang, S., Fleming, R. T., Westbrook, E. M., Matsumura, P., McKay, D. B.** 2006. Structure of the *Escherichia coli* FlhDC complex, a prokaryotic heteromeric regulator of transcription. *J Mol Biol* **355**: 798-808.
- 68 **Cai, S. J., Inouye, M.** 2002. EnvZ-OmpR interaction and osmoregulation in *Escherichia coli*. *J Biol Chem* **277**: 24155-24161.
- 69 **Gottesman, S., Trisler, P., Torres-Cabassa, A.** 1985. Regulation of capsular polysaccharide synthesis in *Escherichia coli* K-12: characterization of three regulatory genes. *J Bacteriol* **162**: 1111-1119.
- 70 **Harman, J. G.** 2001. Allosteric regulation of the cAMP receptor protein. *Biochim Biophys Acta* **1547**: 1-17.

- 71 **Kenney, L. J., Bauer, M. D., Silhavy, T. J.** 1995. Phosphorylation-dependent conformational changes in OmpR, an osmoregulatory DNA-binding protein of *Escherichia coli*. Proceedings of the National Academy of Sciences of the United States of America **92**: 8866-8870.
- 72 **Stout, V.** 1994. Regulation of capsule synthesis includes interactions of the RcsC/RcsB regulatory pair. Res Microbiol **145**: 389-392.
- 73 **Stewart, P. S., Franklin, M. J.** 2008. Physiological Heterogeneity in Biofilms. Nature Rev. Microbiol. **6**: 199-210.
- 74 **Wimpenny, J., Manz, W., Szewzyk, U.** 2000. Heterogeneity in Biofilms. FEMS Microbiol Rev **24**: 661-671.
- 75 **Nyvad, B., Fejerskov, O.** 1997. Assessing the stage of caries lesion activity on the basis of clinical and microbiological examination. Community Dent Oral Epidemiol **25**: 69-75.
- 76 **Stewart, P. S.** 2003. Diffusion in Biofilms. J. Bacteriol. **185**: 1485-1491.
- 77 **Wessel, A. K., Hmelo, L., Parsek, M. R., Whiteley, M.** 2013. Going local: technologies for exploring bacterial microenvironments. Nature Reviews Microbiology **11**: 337-348.
- 78 **Yarwood, J. M., Bartels, D. J., Volper, E. M., Greenberg, E. P.** 2004. Quorum sensing in *Staphylococcus aureus* biofilms. J Bacteriol **186**: 1838-1850.
- 79 **De Kievit, T. R., Iglewski, B. H.** 1999. Quorum sensing, gene expression, and *Pseudomonas* biofilms. Methods Enzymol **310**: 117-128.
- 80 **Hammer, B. K., Bassler, B. L.** 2003. Quorum sensing controls biofilm formation in *Vibrio cholerae*. Mol Microbiol **50**: 101-104.
- 81 **Gonzalez Barrio, A. F. G. et al.** 2006. Autoinducer 2 Controls Biofilm Formation in *Escherichia coli* through a Novel Motility Quorum-Sensing Regulator (MqsR, B3022). J. Bacteriol. **188**: 305-316.
- 82 **Flickinger, S. T. et al.** 2011. Quorum Sensing between *Pseudomonas aeruginosa* Biofilms Accelerates Cell Growth. J Am Chem Soc **133**: 5966-5975.
- 83 **Danese, P. N., Pratt, L. A., Kolter, R.** 2000. Exopolysaccharide production is required for development of *Escherichia coli* K-12 biofilm architecture. Journal of Bacteriology **182**: 3593-3596.
- 84 **Ghigo, J. M.** 2001. Natural conjugative plasmids induce bacterial biofilm development. Nature **412**: 442-445.
- 85 **Mah, T. F., O'Toole, G. A.** 2001. Mechanisms of Biofilm Resistance to Antimicrobial Agents. Trends Microbiol **9**: 34-39.
- 86 **Lewis, K.** 2001. Riddle of Biofilm Resistance. Antimicrob Agents Ch **45**: 999-1007.
- 87 **Sorensen, S. J., Bailey, M., Hansen, L. H., Kroer, N., Wuertz, S.** 2005. Studying Plasmid Horizontal Transfer In Situ: A Critical Review. Nat Rev Microbiol **3**: 700-710.
- 88 **Hausner, M., Wuertz, S.** 1999. High rates of conjugation in bacterial biofilms as determined by quantitative in situ analysis. Appl Environ Microb **65**: 3710-3713.
- 89 **Wuertz, S., Hendrickx, L., Kuehn, M., Rodenacker, K., Hausner, M.** 2001. In situ quantification of gene transfer in biofilms. Methods Enzymol **336**: 129-143.

- 90 **Haagensen, J. A., Hansen, S. K., Johansen, T., Molin, S.** 2002. In situ detection
of horizontal transfer of mobile genetic elements. *FEMS Microbiol Ecol* **42**: 261-
268.
- 91 **Wuertz, S., Okabe, S., Hausner, M.** 2004. Microbial communities and their
interactions in biofilm systems: an overview. *Water Sci Technol* **49**: 327-336.
- 92 **Molin, S., Tolker-Nielsen, T.** 2003. Gene transfer occurs with enhanced
efficiency in biofilms and induces enhanced stabilisation of the biofilm structure.
Curr Opin Biotechnol **14**: 255-261.
- 93 **Christensen, B. B. et al.** 1998. Establishment of new genetic traits in a microbial
biofilm community. *Appl Environ Microbiol* **64**: 2247-2255.
- 94 **Ryu, J. H., Beuchat, L. R.** 2005. Biofilm formation by *Escherichia coli* O157:H7
on stainless steel: effect of exopolysaccharide and Curli production on its
resistance to chlorine. *Appl Environ Microbiol* **71**: 247-254.
- 95 **Prigent-Combaret, C., Prensier, G., Le Thi, T. T., Vidal, O., Lejeune, P.,
Dorel, C.** 2000. Developmental Pathway for Biofilm Formation in Curli-
producing *Escherichia coli* Strains: Role of Flagella, Curli and Colanic acid.
Environ. Microbiol. **2**: 450-464.
- 96 **Tischler, A. D., Camilli, A.** 2004. Cyclic diguanylate (c-di-GMP) regulates
Vibrio cholerae biofilm formation. *Mol Microbiol* **53**: 857-869.
- 97 **Berk, V. et al.** 2012. Molecular architecture and assembly principles of *Vibrio
cholerae* biofilms. *Science* **337**: 236-239.
- 98 **Banin, E., Vasil, M. L., Greenberg, E. P.** 2005. Iron and *Pseudomonas
aeruginosa* biofilm formation. *Proceedings of the National Academy of Sciences
of the United States of America* **102**: 11076-11081.
- 99 **Wang, X., Preston, J. F., 3rd, Romeo, T.** 2004. The *pgaABCD* locus of
Escherichia coli promotes the synthesis of a polysaccharide adhesin required for
biofilm formation. *J Bacteriol* **186**: 2724-2734.
- 100 **Jackson, D. W. et al.** 2002. Biofilm Formation and Dispersal under the Influence
of the Global Regulator CsrA of *Escherichia coli*. *J. Bacteriol.* **184**: 290-301.
- 101 **Cucarella, C. et al.** 2001. Bap, a *Staphylococcus aureus* surface protein involved
in biofilm formation. *J Bacteriol* **183**: 2888-2896.
- 102 **Pierce, C. G., Uppuluri, P., Lopez-Ribot, J. L.** 2013. A Method for the
Formation of Candida Biofilms in 96 Well Microtiter Plates and Its Application to
Antifungal Susceptibility Testing. *Laboratory Protocols in Fungal Biology Fungal
Biology* 217-223.
- 103 **Pratt, L. A., Kolter, R.** 1998. Genetic analysis of *Escherichia coli* biofilm
formation: roles of flagella, motility, chemotaxis and type I pili. *Mol Microbiol*
30: 285-293.
- 104 **Klausen, M. et al.** 2003. Biofilm formation by *Pseudomonas aeruginosa* wild
type, flagella and type IV pili mutants. *Mol Microbiol* **48**: 1511-1524.
- 105 **Whitchurch, C. B., Tolker-Nielsen, T., Ragas, P. C., Mattick, J. S.** 2002.
Extracellular DNA required for bacterial biofilm formation. *Science* **295**: 1487.
- 106 **An, Y. H., Friedman, R. J.** 1998. Concise review of mechanisms of bacterial
adhesion to biomaterial surfaces. *J Biomed Mater Res* **43**: 338-348.

- 107 **MacKintosh, E. E., Patel, J. D., Marchant, R. E., Anderson, J. M.** 2006. Effects of biomaterial surface chemistry on the adhesion and biofilm formation of *Staphylococcus epidermidis* *in vitro*. *J. Biomed. Mater. Res. Part A* **78**: 836-842.
- 108 **Agladze, K., Wang, X., Romeo, T.** 2005. Spatial Periodicity of *Escherichia coli* K12 Biofilm Microstructure Initiates During a Reversible, Polar Attachment Phase of Development and Requires the Polysaccharide Adhesin PGA. *J. Bacteriol.* **18**: 8237-8246.
- 109 **Weibel, D. B., Diluzio, W. R., Whitesides, G. M.** 2007. Microfabrication Meets Microbiology. *Nature Rev. Microbiol.* **5**: 209-218.
- 110 **O'Toole, G. A., Kolter, R.** 1998. Flagellar and twitching motility are necessary for *Pseudomonas aeruginosa* biofilm development. *Mol Microbiol* **30**: 295-304.
- 111 **Heydorn, A. et al.** 2002. Statistical analysis of *Pseudomonas aeruginosa* biofilm development: impact of mutations in genes involved in twitching motility, cell-to-cell signaling, and stationary-phase sigma factor expression. *Appl Environ Microbiol* **68**: 2008-2017.
- 112 **Reisner, A., Haagensen, J. A., Schembri, M. A., Zechner, E. L., Molin, S.** 2003. Development and maturation of *Escherichia coli* K-12 biofilms. *Mol Microbiol* **48**: 933-946.
- 113 **Corona-Izquierdo, F. P., Membrillo-Hernandez, J.** 2002. A mutation in *rpoS* enhances biofilm formation in *Escherichia coli* during exponential phase of growth. *FEMS Microbiol Lett* **211**: 105-110.
- 114 **Ling, H., Kang, A., Tan, M. H., Qi, X., Chang, M. W.** 2010. The absence of the *luxS* gene increases swimming motility and flagella synthesis in *Escherichia coli* K12. *Biochem Biophys Res Commun* **401**: 521-526..
- 115 **Davies, D. G. et al.** 1998. The involvement of cell-to-cell signals in the development of a bacterial biofilm. *Science* **280**: 295-298.
- 116 **Baca, H. K. et al.** 2006. Cell-directed assembly of lipid-silica nanostructures providing extended cell viability. *Science* **313**: 337-341.
- 117 **Harper, J. C. et al.** 2010. Cell-Directed Integration into Three-Dimensional Lipid-Silica Nanostructured Matrices. *Acs Nano* **4**: 5539-5550.
- 118 **Lu, Y. F. et al.** 1999. Aerosol-assisted self-assembly of mesostructured spherical nanoparticles. *Nature* **398**: 223-226.
- 119 **Carnes, E. C. et al.** 2010. Confinement-induced quorum sensing of individual *Staphylococcus aureus* bacteria. *Nat Chem Biol* **6**: 41-45.
- 120 **Falconnet, D., Csucs, G., Grandin, H. M., Textor, M.** 2006. Surface engineering approaches to micropattern surfaces for cell-based assays. *Biomaterials* **27**: 3044-3063.
- 121 **Leong, K., Boardman, A. K., Ma, H., Jen, A. K.** 2009. Single-cell patterning and adhesion on chemically engineered poly(dimethylsiloxane) surface. *Langmuir* **25**: 4615-4620.
- 122 **Takeuchi, S., DiLuzio, W. R., Weibel, D. B., Whitesides, G. M.** 2005. Controlling the shape of filamentous cells of *Escherichia coli*. *Nano Lett* **5**: 1819-1823.
- 123 **Hochbaum, A. I., Aizenberg, J.** 2010. Bacteria pattern spontaneously on periodic nanostructure arrays. *Nano Lett* **10**: 3717-3721.

- 124 **Kim, S. H., Yamamoto, T., Fourmy, D., Fujii, T.** 2011. An electroactive microwell array for trapping and lysing single-bacterial cells. *Biomicrofluidics* **5**: 24114.
- 125 **Rettig, J. R., Folch, A.** 2005. Large-scale single-cell trapping and imaging using microwell arrays. *Anal Chem* **77**: 5628-5634.
- 126 **Lovchik, R., von Arx, C., Viviani, A., Delamarche, E.** 2008. Cellular microarrays for use with capillary-driven microfluidics. *Anal Bioanal Chem* **390**: 801-808.
- 127 **Di Carlo, D., Aghdam, N., Lee, L. P.** 2006. Single-cell enzyme concentrations, kinetics, and inhibition analysis using high-density hydrodynamic cell isolation arrays. *Anal Chem* **78**: 4925-4930.
- 128 **Probst, C., Grunberger, A., Wiechert, W., Kohlheyer, D.** 2013. Polydimethylsiloxane (PDMS) Sub-Micron Traps for Single-Cell Analysis of Bacteria. *Micromachines* **4**: 357-369.
- 129 **Balaban, N. Q., Merrin, J., Chait, R., Kowalik, L., Leibler, S.** 2004. Bacterial persistence as a phenotypic switch. *Science* **305**: 1622-1625.
- 130 **Boedicker, J. Q., Vincent, M. E., Ismagilov, R. F.** 2009. Microfluidic confinement of single cells of bacteria in small volumes initiates high-density behavior of quorum sensing and growth and reveals its variability. *Angew Chem Int Ed Engl* **48**: 5908-5911.
- 131 **Churski, K. et al.** 2012. Rapid screening of antibiotic toxicity in an automated microdroplet system. *Lab Chip* **12**: 1629-1637.
- 132 **Schmitz, C. H., Rowat, A. C., Koster, S., Weitz, D. A.** 2009. Dropspots: a picoliter array in a microfluidic device. *Lab Chip* **9**: 44-49.
- 133 **Leung, K. et al.** 2012. A programmable droplet-based microfluidic device applied to multiparameter analysis of single microbes and microbial communities. *Proceedings of the National Academy of Sciences of the United States of America* **109**: 7665-7670.
- 134 **Bai, Y. P. et al.** 2013. Intra-Species Bacterial Quorum Sensing Studied at Single Cell Level in a Double Droplet Trapping System. *Int J Mol Sci* **14**: 10570-10581.
- 135 **Kim, J. H., Lee, D. Y., Hwang, J., Jung, H. I.** 2009. Direct pattern formation of bacterial cells using micro-droplets generated by electrohydrodynamic forces. *Microfluid Nanofluid* **7**: 829-839.
- 136 **Eun, Y. J., Utada, A. S., Copeland, M. F., Takeuchi, S., Weibel, D. B.** 2011. Encapsulating Bacteria in Agarose Microparticles Using Microfluidics for High-Throughput Cell Analysis and Isolation. *Acs Chem Biol* **6**: 260-266.
- 137 **Voskerician, G. et al.** 2003. Biocompatibility and biofouling of MEMS drug delivery devices. *Biomaterials* **24**: 1959-1967.
- 138 **Song, H., Ismagilov, R. F.** 2003. Millisecond kinetics on a microfluidic chip using nanoliters of reagents. *J Am Chem Soc* **125**: 14613-14619.
- 139 **Thorsen, T., Roberts, R. W., Arnold, F. H., Quake, S. R.** 2001. Dynamic pattern formation in a vesicle-generating microfluidic device. *Phys Rev Lett* **86**: 4163-4166.
- 140 **Baret, J. C. et al.** 2009. Fluorescence-activated droplet sorting (FADS): efficient microfluidic cell sorting based on enzymatic activity. *Lab Chip* **9**: 1850-1858.

- 141 **Ahn, K. et al.** 2006. Dielectrophoretic manipulation of drops for high-speed
microfluidic sorting devices. *Appl Phys Lett* **88**: 024104-1-024104-4.
- 142 **Zeng, Y., Novak, R., Shuga, J., Smith, M. T., Mathies, R. A.** 2010. High-
Performance Single Cell Genetic Analysis Using Microfluidic Emulsion
Generator Arrays. *Anal Chem* **82**: 3183-3190.
- 143 **Weibel, D. B. et al.** 2005. Bacterial printing press that regenerates its ink:
Contact-printing bacteria using hydrogel stamps. *Langmuir* **21**: 6436-6442.
- 144 **Yamazoe, H., Tanabe, T.** 2009. Cell micropatterning on an albumin-based
substrate using an inkjet printing technique. *J Biomed Mater Res A* **91A**: 1202-
1209.
- 145 **Merrin, J., Leibler, S., Chuang, J. S.** 2007. Printing multistrain bacterial
patterns with a piezoelectric inkjet printer. *PLoS One* **7** e663: 1-7.
- 146 **Liberski, A. R., Delaney Jr., J. T., Schuber, U. S.** 2011. “One Cell-One Well”:
A New Approach to Inkjet Printing Single Cell Microarrays. *ACS Comb. Sci.* **13**:
190-195.
- 147 **Choi, W. S., Ha, D., Park, S., Kim, T.** 2011. Synthetic multicellular cell-to-cell
communication in inkjet printed bacterial cell systems. *Biomaterials* **32**: 2500-
2507.
- 148 **Kaehr, B., Shear, J. B.** 2007. Mask-directed multiphoton lithography. *J Am
Chem Soc* **129**: 1904-1905.
- 149 **Connell, J. L. et al.** 2010. Probing Prokaryotic Social Behaviors with Bacterial
“Lobster Traps”. *mBio* **1**: e00202-00210.
- 150 **Connell, J. L., Ritschdorff, E. T., Whiteley, M., Shear, J. B.** 2013. 3D printing
of microscopic bacterial communities. *Proceedings of the National Academy of
Sciences of the United States of America* **110**: 18380-18385.
- 151 **Timp, W., Mirsaidov, U., Matsudaira, P., Timp, G.** 2009. Jamming prokaryotic
cell-to-cell communications in a model biofilm. *Lab Chip* **9**: 925-934.
- 152 **Meyer, A. et al.** 2012. Dynamics of AHL mediated quorum sensing under flow
and non-flow conditions. *Phys Biol* **9**: 1-10.
- 153 **Hill, R. T., Lyon, J. L., Allen, R., Stevenson, K. J., Shear, J. B.** 2005.
Microfabrication of three-dimensional bioelectronic architectures. *J Am Chem
Soc* **127**: 10707-10711.
- 154 **Kaehr, B., Allen, R., Javier, D. J., Currie, J., Shear, J. B.** 2004. Guiding
neuronal development with in situ microfabrication. *Proceedings of the National
Academy of Sciences of the United States of America* **101**: 16104-16108.
- 155 **Kaehr, B., Shear, J. B.** 2008. Multiphoton fabrication of chemically responsive
protein hydrogels for microactuation. *Proceedings of the National Academy of
Sciences of the United States of America* **105**: 8850-8854.
- 156 **Mashburn, L. M., Jett, A. M., Akins, D. R., Whiteley, M.** 2005.
Staphylococcus aureus serves as an iron source for *Pseudomonas aeruginosa*
during in vivo coculture. *J Bacteriol* **187**: 554-566.
- 157 **Dilanji, G. E., Langebrake, J. B., Leenheer, P. D., Hagen, S. J.** 2012. Quorum
Activation at a Distance: Spatiotemporal Patterns of Gene Regulation from
Diffusion of an Autoinducer Signal. *J Am Chem Soc* **134**: 5618-5626.
- 158 **Quist, A. P., Pavlovic, E., Oscarsson, S.** Recent advances in microcontact
printing. *Anal Bioanal Chem* **381**: 591-600.

- 159 **Sgarbi, N. et al.** 2004. Self-assembled extracellular matrix protein networks by
microcontact printing. *Biomaterials* **25**: 1349-1353.
- 160 **Hou, S. et al.** 2007. Inhibition of *Escherichia coli* biofilm formation by self-
assembled monolayers of functional alkanethiols on gold. *Appl Environ*
Microbiol **73**: 4300-4307.
- 161 **St John, P. M. et al.** 1998. Diffraction-based cell detection using a microcontact
printed antibody grating. *Anal Chem* **70**: 1108-1111.
- 162 **Morhard, F., Pipper, J., Dahint, R., Grunze, M.** 2000. Immobilization of
antibodies in micropatterns for cell detection by optical diffraction. *Sensor Actuat*
B-Chem **70**: 232-242.
- 163 **Howell, S. W., Inerowicz, H. D., Regnier, F. E., Reifenberger, R.** 2003. Pattern
protein microarrays for bacterial detection. *Langmuir* **19**: 436-439.
- 164 **Suh, K. Y., Khademhosseini, A., Yoo, P. J., Langer, R.** 2004. Patterning and
separating infected bacteria using host-parasite and virus-antibody interactions.
Biomed Microdevices **6**: 223-229.
- 165 **Sun, K. et al.** 2012. Mussel-Inspired Anchoring for Patterning Cells Using
Polydopamine. *Langmuir* **28**: 2131-2136.
- 166 **Love, J. C., Estroff, L. A., Kriebel, J. K., Nuzzo, R. G., Whitesides, G. M.**
2005. Self-assembled monolayers of thiolates on metals as a form of
nanotechnology. *Chem Rev* **105**: 1103-1169.
- 167 **Rowan, B., Wheeler, M. A., Crooks, R. M.** 2002. Patterning bacteria within
hyperbranched polymer film templates. *Langmuir* **18**: 9914-9917.
- 168 **Rozhok, S. et al.** 2005. Methods for fabricating microarrays of motile bacteria.
Small **1**: 445-451.
- 169 **Hou, S., Burton, E. A., Wu, R. L., Luk, Y. Y., Ren, D.** 2009. Prolonged control
of patterned biofilm formation by bio-inert surface chemistry. *Chem Commun*
(Camb) 1207-1209.
- 170 **Gu, H., Hou, S., Yongyat, C., De Tore, S., Ren, D.** 2013. Patterned biofilm
formation reveals a mechanism for structural heterogeneity in bacterial biofilms.
Langmuir **29**: 11145-11153.
- 171 **Teughels, W. N. V. A., Sliepen, I., Quirynen, M.** 2006. Effect of Material
Characteristics and/or Surface Topography on Biofilm Development. *Clin. Oral*
Impl. Res. **17**: 68-81.
- 172 **Bollen, C. M. L., Lambrechts, P., Quirynen, M.** 1997. Comparison of Surface
Roughness of Oral Hard Materials to the Threshold Surface Roughness for
Bacterial Plaque Retention: A Review of the Literature. *Dent Mater* **13**: 258-269.
- 173 **Taylor, R. L., Verran, J., Lees, G. C., Ward, A. J. P.** 1998. The Influence of
Substratum Topography on Bacterial Adhesion to Polymethyl Methacrylate. *J*
Mater Sci-Mater M **9**: 17-22.
- 174 **Hilber, L. R., Bagge-Ravn, D., Kold, J., Gram, L.** 2003. Influence of Surface
Roughness of Stainless Steel on Microbial Adhesion and Corrosion Resistance.
International Biodete & Biodegr **52**: 175-185.
- 175 **Whitehead, K. A., Verran, J.** 2006. The effect of surface topography on the
retention of microorganisms. *Food Bioprod Process* **84**: 253-259.
- 176 **Machado, M. C., Cheng, D., Tarquinio, K. M., Webster, T. J.** 2010.
Nanotechnology: pediatric applications. *Pediatric research* **67**: 500-504.

- 177 **Chung, K. K. et al.** 2007. Impact of engineered surface microtopography on
biofilm formation of *Staphylococcus aureus*. *Biointerphases* **2**: 89-94.
- 178 **Friedlander, R. S. et al.** 2013. Bacterial flagella explore microscale hummocks
and hollows to increase adhesion. *Proceedings of the National Academy of
Sciences of the United States of America* **110**: 5624-5629.
- 179 **Mitik-Dineva, N. et al.** 2008. Impact of nano-topography on bacterial
attachment. *Biotechnology journal* **3**: 536-544.
- 180 **Satrianoa, C., Messinaa, G. M. L., Carnazzab, S., Guglielminob, S.,
Marlettaa, G.** 2006. Bacterial adhesion onto nanopatterned polymer surfaces.
Materials Science & Engineering C **26**: 942-946.
- 181 **Cassie, A. B. D., Baxter, S.** 1994. Wettability of porous surfaces. *Trans. Faraday
Soc.* **40**: 546-551.
- 182 **Genzer, J., Efimenko, K.** 2007. Recent developments in superhydrophobic
surfaces and their relevance to marine fouling: a review. *Biofouling* **22**: 339-360.
- 183 **Young, K. D.** 2010. Bacterial shape: two-dimensional questions and possibilities.
Annu Rev Microbiol **64**: 223-240.
- 184 **Volle, C. B., Ferguson, M. A., Aidala, K. E., Spain, E. M., Nunez, M. E.** 2008.
Spring constants and adhesive properties of native bacterial biofilm cells
measured by atomic force microscopy. *Colloids and surfaces. B, Biointerphases* **67**:
32-40.
- 185 **Copeland, M. F., Weibel, D. B.** 2009. Bacterial Swarming: A Model System for
Studying Dynamic Self-assembly. *Soft matter* **5**: 1174-1187.
- 186 **Beloin, C., Ghigo, J. M.** 2005. Finding gene-expression patterns in bacterial
biofilms. *Trends Microbiol* **13**: 16-19.
- 187 **Suzuki, K. et al.** 2002. Regulatory circuitry of the CsrA/CsrB and BarA/UvrY
systems of *Escherichia coli*. *J Bacteriol* **184**: 5130-5140.
- 188 **Ferrieres, L., Clarke, D. J.** 2003. The RcsC sensor kinase is required for normal
biofilm formation in *Escherichia coli* K-12 and controls the expression of a
regulon in response to growth on a solid surface. *Mol. Micro.* **50**: 1665-1682.
- 189 **Niba, E. T., Naka, Y., Nagase, M., Mori, H., Kitakawa, M.** 2007. A genome-
wide approach to identify the genes involved in biofilm formation in *E. coli*. *DNA
Res* **14**: 237-246.
- 190 **Jackson, D. W., Simecka, J. W., Romeo, T.** 2002. Catabolite repression of
Escherichia coli biofilm formation. *J Bacteriol* **184**: 3406-3410.
- 191 **Belik, A. S., Tarasova, N. N., Khmel, I. A.** 2008. Regulation of biofilm
formation in *Escherichia coli* K12: effect of mutations in HNS, StpA, Ion, and
rpoN genes. *Molekuliarnaia genetika, mikrobiologiiia i virusologiiia* 3-5.

CHAPTER 3

PATTERNED BIOFILM FORMATION REVEALS A MECHANISM FOR STRUCTUREAL HETEROGENEITY IN BACTERIAL BIOFILMS AND IMPORTANT INFORMATION OF BIOFILM- ASSOCIATED ANTIBIOTIC RESISTANCE

Part of this chapter has been published as Huan Gu, Shuyu Hou, Chanokpon Yongyat, Suzanne De Tore, and Dacheng Ren. 2013. Patterned biofilm formation reveals a mechanism for structural heterogeneity in bacterial biofilms. *Langmuir*. 29(35):11145–11153. Reproduced by permission of American Chemical Society Publication.

Shuyu Hou initiated this study. The experimental results of the *E. coli* RP437/pRSH109 and *E. coli* KX1485 ($\Delta luxS$) /pDsRed co-culture biofilms in this study were obtained by Chankpon Yongyat and Suzanne De Tore.

3.1 ABSTRACT

Bacterial biofilms are ubiquitous and are the major cause of chronic infections in humans and persistence biofouling in industry. Despite the significance of bacterial biofilms, the mechanism of biofilm formation and associated drug tolerance is still not fully understood. A major challenge in biofilm research is the intrinsic heterogeneity in biofilm structure, which leads to temporal and spatial variation in cell density and gene expression. To understand and control such structural heterogeneity, surfaces with patterned functional alkanthiols were used in this study to obtain *E. coli* cell clusters with systematically varied cluster size and distance between clusters. The results from quantitative imaging analysis revealed an interesting phenomenon that multicellular connections can be formed between cell clusters depending on the size of interacting clusters and the distance between them. In addition, significant differences in patterned biofilm formation were observed between the wild-type *E. coli* RP437 and some of its isogenic mutants, indicating that certain cellular and genetic factors are involved in interactions among cell clusters. In particular, autoinducer-2 mediated quorum sensing was found to be important.

Inspired by these results, antibiotic treatment of *E. coli* biofilm cells during biofilm formation was monitored to understand the development of biofilm related resistance to antibiotics during biofilm formation. The results revealed that the antibiotic susceptibility of biofilm cells increased in the first two hours and then gradually decreased to the level of overnight planktonic cultures. This finding suggests that the metabolic activity of biofilm cells changes over time. In addition, *E. coli* RP437 cells between square patterns were found more sensitive to ampicillin compared to the cells in

the square pattern. This supports the finding that active interaction between all clusters is involved during biofilm formation. Collectively, these results provide missing information that links cell-to-cell signaling and interaction among cell clusters to the structural organization of bacterial biofilms.

3.2 INTRODUCTION

Biofilms are surface-attached complex bacterial communities encased in the self-produced extracellular polymeric matrix^{1,2}. Biofilms have unique structural characteristics with phenotypic and biochemical properties that are distinct from its free swimming counterparts³. One of the best-known biofilm-specific properties is the high antibiotic resistance of biofilm cells that can be up to 1,000-fold higher than planktonic cells⁴. The high resistance of biofilms against antimicrobial agents makes them hard to be eradicated in medical and industrial settings and causes serious problems such as chronic infections and persistent biofouling⁵⁻⁸. Although exciting progress has been made in identifying biofilm genes⁹⁻¹¹, mechanistic understanding of biofilm formation and biofilm-associated high resistance to antibiotics is still hindered by some unmet challenges especially the heterogeneity in biofilm structure and associated spatial variation in cell density and gene expression.

As stated in Motivation section (Page 2), biofilm formation is a dynamic process influenced by many environmental factors such as bacterial surface structures, the property of the surface that biofilms are formed, and environmental conditions. Therefore, biofilms has significant heterogeneity in its structure (Fig. 3-1A). The heterogeneity in biofilm structure also plays an important role in the development of high antibiotic resistance in biofilms. For example, the diffusion rate of antibiotics and solutes such as nutrients and metabolic products depends on the size, shape, and cell density of biofilm cell clusters^{9,12}. Such concentration gradients of solutes can lead to the formation of slow-growing cells that are more resistant to antibiotics^{9,12,13}. However, the role of

biofilm heterogeneity during the development of biofilm associated high resistance to antibiotics is still not fully understood.

Besides the above challenges presented by biofilm structural heterogeneity, the mechanism of such spatial organization of cell clusters in biofilms itself is also an interesting but largely unanswered question. To reveal the underlying mechanism, it is necessary to study with rigorously controlled size and shape of cell clusters as well as the distance between them, which cannot be achieved by using conventional systems.

Recently, we reported that biofilm morphology can be controlled by tailoring surface chemistry with specific patterns of self-assembled monolayers (SAMs) of long-chain alkanethiols presenting functional groups^{14,15}. These well-defined surfaces provide a useful platform to obtain unique information about interactions among bacterial cell clusters during biofilm formation.

In this study, we investigated adhesion and early stage biofilm formation of *E. coli* on chemically patterned surfaces (Fig. 3-1B) with systematically varied pattern size and distance between adjacent square patterns. The results demonstrate that interactions among cell clusters play an important role in biofilm structural organization and cell-to-cell signaling is involved in such interactions. To understand if such interactions can lead to different metabolic levels and subsequent antibiotic resistance among cell at different locations, we also characterized the antibiotic susceptibility of cells in and between the square shaped patterns.

3.3 MATERIALS AND METHODS

3.3.1 Bacterial strains and growth media

Bacterial strains, plasmids, and associated genotypes are summarized in Table 3-1. *E. coli* RP437¹⁶, one of the model strains for biofilm formation^{14,17-20} and its five isogenic mutants [*motB* (strains with point mutation and deletion mutation were both tested), *cheY*, *tap*, and *luxS*; see Table 3-1 for details] were used to investigate bacteria-surface interactions. *E. coli* HM22²¹ was used to study the development of biofilm resistance in biofilm formation. *E. coli* wild-type strain RP437 and its mutants were routinely grown at 37°C with shaking at 200 rpm in Lysogeny Broth (LB) containing 10 g/L tryptone, 5 g/L yeast extract and 10 g/L sodium chloride²². *E. coli* RP437/pRSH109, *E. coli* KX1485/pDsRed, *E. coli* RP3087/pDsRed, and the *E. coli* KX1485/pRHG01 were grown at 37°C with shaking at 200 rpm in LB medium supplemented with 100 µg/mL ampicillin. *E. coli* HM22 was grown 37°C with shaking at 200 rpm in LB medium supplemented with 25 µg/mL of diaminopimelic acid (DPA).

3.3.2 Genetic complementation of the *luxS* mutant

The *luxS* mutant was complemented with pCR®2.1 TOPO® (Fig. 3-2A) from TOPO TA cloning® kit (Life Technologies Inc., Carlsbad, CA, USA). The *luxS* gene and its native promoter were amplified with the primers: 5' TGCTTCGAATCCCCGATCTGACTTTC 3' (forward primer) and 5' GGCGGAAAGCTTCTTGCGCACTAAGTACA A 3' (reverse primer) (Fig. 3-2B). The 991 bp PCR product was inserted in the vector between the two *EcoRI* restriction sites (Fig. 3-2C).

3.3.3 Chemicals

Alkanethiols of $\text{HS}(\text{CH}_2)_{14}\text{CH}_3$ and $\text{HS}(\text{CH}_2)_{11}(\text{OCH}_2\text{CH}_2)_3\text{OH}$ were purchased from Sigma-Aldrich Co. (St. Louis, MO, USA). The alkanethiols were dissolved in ethanol (200 proof) to 2 mM and stored at 4°C. SYLGARD[®]184 Silicone Elastomer kit (Dow Corning Co., Midland, MI, USA) was used to prepare polydimethylsiloxane (PDMS) stamps for micro-contact printing as described previously²³.

3.3.4 Preparation of the surfaces

To prepare the surfaces with square patterns of CH_3 -SAM and background of tri(ethylene glycol) (TEG)-SAM, the techniques of photolithography and micro-contact printing were used by following previously reported procedures^{24,25} (Fig. 3-3). The dimension of the square patterns and the distance between adjacent patterns were systematically varied using the software L-Edit (Tanner Research, Monrovia, CA, USA). The side width (W) of the square patterns was set to be 5, 10, 20, 30, 40, or 50 μm and the distance (D) between adjacent patterns was set to be 2, 5, 10, 15, 20, 30, 40, or 50 μm (Fig. 3-4). A silicon master mold was fabricated first to obtain topographic patterns (10 μm deep) with above designs, which was performed at the Cornell NanoScale Science & Technology and Facility at Cornell University (Ithaca, NY, USA). More details are listed in the protocol in APPENDIX. I. Then, a PDMS stamp was prepared by casting SYLGARD[®]184 Silicone Elastomer against the master mode to obtain complementary patterns. The stamp was then dipped in 2 mM of $\text{HS}(\text{CH}_2)_{14}\text{CH}_3$ and inked on a bare gold surface (coated with 0.7 nm titanium and 2.8 nm gold or 0.5 nm titanium and 0.5 nm gold) for 15 s. Thus, CH_3 -SAM was formed only in the pattern area contacted with the stamps. The slide was immediately washed with ethanol (190 proof) and soaked in 2 mM

solution of HS(CH₂)₁₁(OCH₂CH₂)₃OH in ethanol (200 proof) overnight to form the background with TEG-SAM. The slide with chemical patterns was cleaned with ethanol (190 proof), dried with a sterile air stream, and stored in a sterile petri dish at room temperature until use (more details are available in APPENDIX. II).

To study the antibiotic susceptibility of biofilm cells in biofilms formed on surfaces without well-controlled surface chemistry, glass wool (Corning Inc., Corning, NY, USA; 8 µm in diameter, 0.25 g in each petri dish) was used to form biofilms. It was sterilized by autoclaving and stored in a sterile petri dish until inoculation.

3.3.5 Biofilm formation

To study biofilm formation on well-defined surfaces with chemical patterns, overnight cultures of the wild-type strain *E. coli* RP437 and its isogenic mutants were used to inoculate LB medium to an optical density at 600 nm (OD₆₀₀) of 0.05. Biofilm growth was conducted at 37 °C for 24 h. To monitor the interaction between cell clusters in batch cultures, study the antibiotic susceptibility of bacterial cells in and between cell clusters, and investigate the role of bacterial outer membrane structures during interaction using scanning electronic microscope (SEM), patterned biofilms were gently washed three times in 0.85% NaCl (wt/vol) solution after 2 h incubation and then transferred into fresh LB medium for further biofilm growth.

The chemical complementation of the *luxS* mutant was achieved by supplementing its biofilm cultures with 1, 10, 50, or 100 µM (S)-4,5-Dihydroxy-2,3-pentanedione (DPD). The cultures were incubated at 37°C without shaking for 24 h.

The co-culture biofilms were inoculated with overnight cultures of *E. coli* RP437/pRSH109 and *E. coli* KX1485 (*ΔluxS*) /pDsRed with 4:1, 1:1, and 1:4 ratios to

OD₆₀₀ of 0.05. The biofilms of co-cultures were grown under room temperature without shaking for 48 h.

To study the antibiotic resistance of bacterial cells in early stage biofilm formation, biofilms of *E. coli* HM22 biofilms on glass wool were formed in LB media. To initiate the biofilm growth, overnight cultures of *E. coli* HM22 was used to inoculate 20 mL LB medium to an OD₆₀₀ of 0.05. Biofilm growth was conducted at 37 °C without shaking.

3.3.6 Fluorescence microscopy

To visualize the biofilms formed on patterned surfaces, LIVE/DEAD BacLight Bacterial Viability Kit (Life Technologies Inc., Carlsbad, CA, USA) was used to stain biofilm cells of the wild-type strain *E. coli* RP437 and its isogenic mutants. After incubation, the surfaces with *E. coli* biofilms were transferred from cultures to 0.85% NaCl solution and gently washed three times to remove planktonic cells. Then the biofilms were stained in 0.85% NaCl containing 0.15% (vol/vol) component A and 0.15% (vol/vol) component B of the Live/Dead staining kit for 15 min in the dark. All biofilms were visualized using an Axio Imager M1 fluorescence microscope (Carl Zeiss Inc., Berlin, Germany). Five spots were randomly selected and imaged for each pattern. The biofilm surface coverage was then calculated using the COMSTAT software written on a Matlab platform²⁶.

3.3.7 Definition of Cell Cluster Interaction Index (CII)

The total surface coverage of a biofilm (TB; unit: μm^2) formed on a CH₃-SAM/TEG-SAM patterned surface is attributed by three factors: specific adhesion on CH₃-SAM patterns, nonspecific adhesion on TEG-SAM background, and surface

coverage on TEG-SAM (EB; unit: μm^2) due to interaction between cell clusters. Hence, EB can be calculated using equation (1):

$$TB = B_{\text{Methyl}} \times A_{\text{Methyl}} + B_{\text{TEG}} \times A_{\text{TEG}} + EB \quad (1)$$

where B_{Methyl} is biofilm surface coverage on pure CH_3 -SAM (unit: %); B_{TEG} is biofilm surface coverage on pure TEG-SAM (unit: %); A_{Methyl} is the area of CH_3 -SAM on the patterned surface (unit: μm^2); and A_{TEG} is the area of TEG-SAM background on the patterned surface (unit: μm^2). TB, B_{Methyl} , and B_{TEG} were obtained from imaging analysis using COMSTAT²⁶. A_{Methyl} and A_{TEG} were calculated based on the pattern design.

To quantitatively evaluate the interactions between adjacent cell clusters, a unitless term named “Cell Cluster Interaction Index (CII)” was defined as equation (2):

$$\text{CII} = \frac{EB}{A_{\text{TEG}}} \times C = \frac{TB - B_{\text{Methyl}} \times A_{\text{Methyl}} - B_{\text{TEG}} \times A_{\text{TEG}}}{A_{\text{TEG}}} \times C \quad (2)$$

where C is a constant to proportionally adjust the value of CII to be between 0 and 10 for the convenience of comparison (C = 2.2 was used for this study). Thus, CII represents the relative surface coverage on bio-inert TEG-SAM due to interaction between all clusters.

3.3.8 Differentiating seeding cells from those formed during biofilm growth

Cells from an overnight culture of the wild-type strain *E. coli* RP437 were stained with Alexa Fluor 555 carboxylic acid succinimidyl ester from Life Technologies (Carlsbad, CA, USA) as described by Turner *et al.*²⁷ An overnight culture of the wild-type *E. coli* RP437 was used to inoculate 10 mL LB to OD_{600} of 0.4 and then washed three times at room temperature by centrifugation (5000 $\times g$, 10 min) and resuspended in 10 mL of motility buffer (0.01 M KPO_4 , 0.067 M NaCl, 10^{-4} M EDTA, pH 7.0)²⁷.

Finally the cells were resuspended in 0.5 mL motility buffer to concentrate the cells by 20 times. Alexa Fluor 555 (stored as 5 mg/mL in anhydrous dimethyl sulfoxide) was added into the 0.5 mL bacterial suspension to a working concentration of 200 µg/mL along with 25 µL 1 M sodium bicarbonate to adjust the pH to 7.8. Cells were stained for 1 h at room temperature with shaking at 100 rpm, washed three times under room temperature by centrifugation ($5000 \times g$, 10 min), and resuspended in 0.5 mL motility buffer. These cells were used to inoculate 20 mL LB medium to an OD₆₀₀ of 0.5 for biofilm growth on gold surfaces modified with 20 µm × 20 µm square patterns. The modified gold surfaces were incubated at 37 °C for 2.5 h to allow cells to attach and then were gently washed three times with 0.85% NaCl before they were transferred to petri dishes containing 20 mL fresh LB medium in each for biofilm formation. Samples were taken every hour and stained with green-fluorescent SYTO[®] 9 dye from the LIVE/DEAD BacLight Bacterial Viability Kit before they were imaged with an Axio Imager M1 fluorescence microscopy.

3.3.9 Flow cell experiment

An overnight culture of the wild-type strain *E. coli* RP437 was used to inoculate LB medium in a petri dish to OD₆₀₀ of 0.05 to form biofilm on a standard microscope slide coated with gold and modified with 20 µm × 20 µm square patterns of CH₃-SAM. The gold surface was incubated at 37 °C for 2.5 h, gently washed three times with 0.85% NaCl, and then used to assemble a flow chamber (BST model FC81; Biosurface Technologies Corp., Bozeman, MT, USA) that consists of a modified gold surface with attached cells (2.5 h after inoculation) and a standard glass coverslip on the other side. The windows for observation on both sides are 47.5 mm by 12.7 mm rectangular, with a 1.6 mm gap between them. LB medium was supplied at a flow rate of 10 mL/ h. Images

were taken by using an Axio Imager M1 fluorescence microscope every 30 min. To follow the cell growth in biofilm, a representative spot ($D = 10 \mu\text{m}$) was chosen for imaging over 24 h.

3.3.10 Long-term biofilm experiment

Glass surfaces, gold surfaces, and 316L stainless steel coupons (0.6 in. by 0.3 in., with a thickness of 0.02 in.) were sterilized in ethanol (190 proof) for 30 min and dried with a sterile air stream. To form biofilms, LB medium in petri dishes containing sterile surfaces was inoculated with an overnight culture of the wild-type strain *E. coli* RP437 to an initial OD_{600} of 0.05. The medium with planktonic cells was replaced with sterile LB medium at 24 and 48 h after inoculation to provide sufficient nutrients for biofilm growth. Samples were taken at 24, 48 and 72 h after inoculation. The surfaces were washed three times with 0.85% NaCl before using an Axio Imager M1 fluorescence microscope. Gold surfaces modified with $100 \mu\text{m} \times 100 \mu\text{m}$ patterns were prepared as described before¹⁴ and were used to test 72 h biofilm growth of the wild-type *E. coli* RP437 following the same procedure.

3.3.11 Antibiotic treatment

Overnight cultures of *E. coli* HM22 were washed three times with 0.85% NaCl solution (change to fresh solution every time) and then dosed with 200 $\mu\text{g}/\text{mL}$ ampicillin and incubated with 200 rpm shaking for 3 h at 37 °C before the cells were harvested by centrifugation (10,000 $\times g$, 1 min) at room temperature and washed with 0.85% NaCl solution. A drop plate assay of CFU as described previously²⁸ was used to evaluate the viability of cells with and without antibiotic treatment. Briefly, 96 well-plates were pre-filled with 180 μL 0.85% NaCl solution. Six 20 μL samples with and without antibiotic

treatment were loaded in the first column of a sterile 96-well plate using a pipette. A series of 10-fold dilutions was made into the subsequent columns of the same 96-well plate using a multichannel pipette. CFUs were counted after loading 10 μ L of each sample on LB agar plate supplemented with 25 μ g/mL of DPA and incubated overnight at 37 °C. Drops that showed 10 to 50 CFU per 10 μ L of diluted sample were counted to calculate the number of viable cells in the original sample. Each sample was counted with at least 9 replicates.

To study the antibiotic resistance of biofilm cells during the biofilm formation, *E. coli* HM22 biofilms formed on glass wool were harvested every 30 min after inoculation and then gently washed with 0.85% NaCl solution three times to remove planktonic cells. The washed biofilm was then transferred to sterile test tubes each containing 3 mL of 0.85% NaCl solution. To release biofilm cells from the surface of coupons and glass wool and count a CFU, test tubes with coupon or glass wool soaked in 0.85% NaCl solution were sonicated for 2.5 min and vortexed for 30s. The solution with biofilm cells was transferred to a new test tube and vortexed for another 30s before being divided into 2- aliquots in microcentrifuge tubes. One microcentrifuge tube containing 1.5 mL solution was dosed with 200 μ g/mL ampicillin and incubated with 200 rpm shaking for 3 h at 37 °C. The treated biofilm cells were collected using the AcroPrepTM 96-well filter plate (350 μ L with filter pore size 0.2 μ m in diameter) and vacuum manifold (PALL Corporation, Port Washington, NY, USA). The cells were then washed three times with 100 μ L 0.85% NaCl solution and suspended in 20 μ L 0.85% NaCl solution. The number of CFU of biofilm cells with and without antibiotic treatment was counted in the same way as described above.

3.3.12 Antibiotic susceptibility of biofilm cells on patterned surfaces

To understand if biofilm structure and location of biofilm cells play a role in antibiotic resistance, patterned *E. coli* RP437 biofilms were harvested at 2, 4 and 6h after incubation and gently washed three times in 0.85% NaCl solution (change to fresh solution every time) to remove planktonic cells. Then, the surface with biofilms was transferred to 3 mL 200 µg/mL ampicillin solution and incubated for 1 h at 37 °C. Patterned biofilms were gently washed three times in fresh 0.85% NaCl solution before the Live/Dead staining to remove extra antibiotics. To visually determine the viability of *E. coli* RP437 cells in patterned biofilms, LIVE/DEAD® BackLight™ Bacteria Viability Kit (Life Technologies Inc., Carlsbad, CA, USA) was used to stain biofilms of the wild-type strain as described above after antibiotic treatment. Biofilms were stained for 15 min in dark and visualized using an Axio Imager M1 fluorescence microscope. Five spots were randomly selected and imaged for each pattern. The biofilm surface coverage of the live and dead biofilm cells was calculated using the COMSTAT software written on a Matlab platform²⁶. Each sample has at least three replicates.

The average cell viability in cell clusters of each image was calculated by circling out two representative cell clusters from each image. The surface coverage of live or dead cells in the area between cell clusters was calculated using following equation (3):

$$B_{\text{TEG(L/D)}} = \frac{B_{\text{Total(L/D)}} \times A_{\text{Total}} - B_{\text{Methyl(L/D)}} \times A_{\text{Methyl}}}{A_{\text{TEG}}} \quad (3)$$

where $B_{\text{TEG(L/D)}}$ is the surface coverage of the cell population of interest (live, dead or total); $B_{\text{Total(L/D)}}$ is the total surface coverage by that population, which was directly calculated using COMSTAT; A_{Total} is the total area of each image; $B_{\text{Methyl(L/D)}}$ is surface coverage in pattern area by that population; A_{Methyl} is the area of CH₃-SAM (for cell

cluster formation), which was calculated based on pattern design; and A_{TEG} is the area between CH_3 -SAM patterns (interaction between cell clusters), which was also calculated based on pattern design.

3.3.13 Sample preparation for scanning electron microscopy (SEM)

To study the role of bacterial outer membrane structures during interaction among cell clusters using SEM, patterned *E. coli* RP437 biofilm growth medium was incubated at 37°C without shaking for 2 h for cells to attach. Then, the gold surfaces were gently washed three times in 0.85% NaCl solution (change to fresh solution every time) and transferred to 20 mL fresh LB for another 2 and 4 h biofilm growth at 37°C. After washing, the patterned biofilms were immediately transferred into 2.5% glutaraldehyde in 1 M phosphate buffered saline (PBS) buffer to fix the cells at room temperature until dehydration. Then, the patterned biofilms incubated for another 2 and 4 h attachment (4 h and 6 h after the initial inoculation) were harvested and soaked in 2.5% glutaraldehyde in 1 M PBS buffer at room temperature to fix the cells until dehydration. Next, the 2.5% glutaraldehyde in 1 M PBS buffer was removed and 1% osmium tetroxide in 25 mM phosphate buffer was used to stain lipid for 30 min. Then, the 1% osmium tetroxide in 25 mM phosphate buffer was replaced by a graded series of ethanol washes [25%, 50%, 75%, 90%, 95%, and 100% ($\times 3$); 30 min each] to dehydrate samples. Finally, the patterned biofilms were dried using Tousimis PVT-3B critical point dryer (Tousimis, Rockville, MD) or tetramethylsilane (Sigma-Aldrich Co., St. Louis, MO, USA). Specimens were coated with platinum with DESK II (Denton vacuum Inc., Moorestown, NJ, USA) and observed with a JEOL 5800LV scanning electron microscope (N.C. Brown

Center, Syracuse, NY) or LEO 1550 FESEM (Keck SEM, Cornell Center for Material Research (CCMR), Ithaca, NY, USA).

3.3.14 Statistics

One-way and two-way ANOVA analyses Tukey tests, and correlation analysis were applied to understand the effects of surface patterns on biofilm formation. All statistical analyses were performed by using SAS 9.1.3, Windows version (SAS, Cary, NC, USA). Results with $p < 0.05$ were considered statistically significant.

3.4 RESULTS

3.4.1 Patterned biofilm formation revealed interaction among cell clusters

To get new insights in the mechanism of bacteria-surface interactions, the gold-coated glass surfaces were modified with square patterns of CH₃-SAM for cell adhesion and background with bioinert triethylene glycol-SAM (TEG-SAM) (Fig. 3-4). Representative fluorescence images of *E. coli* RP437 biofilms on 20 $\mu\text{m} \times 20 \mu\text{m}$ patterns with 2, 5, 10, or 15 μm distance between adjacent patterns are shown in Fig. 3-5. Although all patterns are 20 $\mu\text{m} \times 20 \mu\text{m}$ squares, clear patterns of *E. coli* RP437 biofilms were only observed on surfaces with patterns separated by 10 μm or more of TEG-terminated SAM. On the surfaces with 2 μm or 5 μm between patterns, the cells covered the TEG-SAM areas between adjacent patterns substantially (Fig. 3-5A&B). Because the *E. coli* RP437 cells used in this study are $2.4 \pm 0.5 \mu\text{m}$ long on average and the threshold distance for pattern integrity (sufficient separation between adjacent patterns) is 10 μm , the connection between adjacent patterns when $D < D^*$ is unlikely to be caused solely by single cells nonspecifically attached to TEG between two adjacent

square patterns. Consistently, we observed interesting multicellular connections between patterns with 2 or 5 μm distance (Fig. 3-6A). When the distance between cell clusters reached 10 μm , connections between cell clusters were only occasionally observed with cells in a single line (Fig. 3-6B). These results suggest that multicellular structures are involved in interaction between cell clusters during biofilm formation. A critical distance (D^* , Fig. 3-6C) between adjacent patterns appears to exist, beyond which the cell clusters cannot interact efficiently (seen as clearly separated patterns).

3.4.2 Pattern size and inter-pattern distance affected interactions among cell clusters

To further confirm the existence of a critical distance for interaction among cell clusters, the CII values were calculated to quantitatively compare the surface coverage on bioinert TEG-SAM background due to specific interaction between cell clusters (the higher the CII value, the more connection between cell clusters; see Experimental Methods for more details). As shown in Fig. 3-7, for all the pattern sizes studied, the CII value decreased drastically when the distance between patterns increased from 2 μm to 10 μm and then exhibited little change when the distance further increased beyond 10 μm . For example, for the 10 $\mu\text{m} \times 10 \mu\text{m}$ patterns, the CII values are 0.86 ± 0.14 , 0.49 ± 0.12 , 0.10 ± 0.03 , 0.10 ± 0.03 , 0.06 ± 0.02 , 0.06 ± 0.02 , 0.06 ± 0.02 , and 0.05 ± 0.02 for the patterns with distance of 2, 5, 10, 15, 20, 30, 40, and 50 μm , respectively.

A two-way analysis of variance (ANOVA) adjusted by Tukey test showed that, for patterns with side length of 5, 10, 15 or 20 μm , the CII values of different inter-pattern distances for a given pattern size followed a trend of: $\text{CII}_{2 \mu\text{m}} > \text{CII}_{5 \mu\text{m}} > \text{CII}_{10 \mu\text{m}} \approx \text{CII}_{15 \mu\text{m}} \approx \text{CII}_{20 \mu\text{m}} \approx \text{CII}_{30 \mu\text{m}} \approx \text{CII}_{40 \mu\text{m}} \approx \text{CII}_{50 \mu\text{m}}$. For patterns with a side length of 30, 40 or 50 μm , the CII values also decreased with inter-pattern distance (D) significantly

when D increased from 2 to 5 and 10 μm . Although CII continued to decrease with increase in D when $D > 10 \mu\text{m}$, the changes were fairly small compared to those when $D < 10 \mu\text{m}$. For example, for $40 \mu\text{m} \times 40 \mu\text{m}$ patterns, the CII value decreased from 2.34 ± 0.33 to 0.39 ± 0.05 when D increased from 2 to 10 μm ; while it only decreased to 0.16 ± 0.03 when D further increased to 50 μm . Thus, 10 μm appeared to be the critical distance (D^*) for significant interaction among cell clusters during early stage biofilm formation of *E. coli* RP437 under our experimental condition.

In addition to the effects of inter-pattern distance on CII, it was interesting to find that the size of interacting patterns also has a significant impact on CII. As shown in Fig. 3-8, the CII values increased with pattern size for patterns larger than $20 \mu\text{m} \times 20 \mu\text{m}$ regardless of the distance between adjacent patterns; while no clear trend was found for patterns smaller than $20 \mu\text{m} \times 20 \mu\text{m}$. This finding is corroborated by a Pearson correlation analysis which showed no strong correlation between CII and pattern size for the patterns smaller than $20 \mu\text{m} \times 20 \mu\text{m}$ regardless of the distance between adjacent patterns (Table 3-2). However, a strong positive correlation was observed for all patterns with a side length of 20, 30, 40, or 50 μm ($r > 0.93$ for all patterns studied, $p < 0.0001$) (Table 3-2). Thus, 20 μm appears to be a critical dimension (W^*) of square patterns to establish fruitful inter-cluster connections. The size of $20 \mu\text{m} \times 20 \mu\text{m}$ patterns is about 200 times bigger than the footprint of individual cells used in this study, suggesting that multicellular interactions within cell clusters also influences the interaction between clusters.

3.4.3 Interactions between cell clusters are involved in biofilm structural organization

Several observations indicate that the connections between cell clusters were formed because of active interaction and formation of “bridges” between clusters, rather than non-specific binding of *E. coli* cells on the bioinert TEG-SAM. First, the formation of connections between cell clusters depends on the distance between adjacent patterns. The surface coverage (per unit area) on TEG-SAM background of $20\ \mu\text{m} \times 20\ \mu\text{m}$ pattern surfaces was found to be significantly larger than that on pattern-free TEG-SAM surfaces (Fig. 3-9). Also, the coverage of TEG-SAM increased substantially as the patterns of CH₃-SAM got closer to each other especially when the distance was smaller than $10\ \mu\text{m}$, which indicates that the surface coverage between patterns was not due to non-specific binding or biofilm growth out of patterns (biofilm remained square shape when the CH₃-SAM patterns were sufficiently separately).

To obtain further evidence of direct interaction between cell clusters, the connection between adjacent *E. coli* cell clusters was monitored in real time in a batch culture. By labeling the seeding cells with Alexa Fluor 555 and all the cells in the formed biofilm with SYTO[®] 9, cells added at inoculation (with both strong orange and green fluorescence) and those formed during biofilm growth (with green fluorescence and weak or no orange fluorescence due to dilution by cell division) can be differentiated. As shown in Fig. 3-10, the cells in the patterns had both strong green and orange colors right after inoculation. After the connection between patterns was established; however, the cells between adjacent clusters were found to be mostly green without significant orange

fluorescence, indicating that these cells were formed during biofilm growth rather than non-specific binding of seeding cells.

This finding was further corroborated by a flow cell experiment to follow the formation of connection between cell clusters in real time. As shown in Fig. 3-11, it was found that as the cells in two adjacent patterns separated by 10 μm grew and divided over time, the clusters expanded across bioinert TEG-SAM toward each other. Cell dispersion and absorption at the inter-pattern area were not observed. Overall, the above results confirmed that the interaction among adjacent cell clusters was due to the growth and division of cells from clusters that were close to each other rather than nonspecific binding of planktonic cells settling from suspension on the TEG-SAM background. Besides, the interaction was preferentially formed over the shortest distance between two close cell clusters (Fig. 3-12).

It is interesting to notice that the interaction among cell clusters is affected by the size of cell clusters and distance between them. Although interaction between adjacent cell clusters can lead to significant coverage of the TEG-SAM background, the cell clusters that are far away from other clusters remained their specific square shape (Fig. 3-5). This finding suggests that bacterial cells may be able to sense the size of their clusters and distance from other clusters within a range and interact for development toward a mature biofilm.

3.4.4 Imaging cell surface structures with scanning electron microscopy (SEM)

Interestingly, we found that *E.coli* cells can interact between cell clusters within 10 μm . This threshold distance is larger than the size of *E.coli* cells used in this study. This led to our hypothesis that surface structures, such as flegalla, may be involved in

such interactions. To test hypothesis, it is important to visualize cells on patterned surfaces with high resolution. SEM has been widely used to study the assembly and function of flagella²⁹⁻³¹, curli³¹⁻³⁵, and fimbriae³⁶⁻³⁸. To study the roles of cell surface structures that can allow bacteria to adhere and move along a solid surface during the interaction, the 24 h of patterned *E. coli* RP437 biofilm formed on gold surfaces modified with size 20 $\mu\text{m} \times 20 \mu\text{m}$ SAM patterns were imaged with JEOL 5800LV SEM with 15 kV scanning voltage (Fig. 3-13). This is encouraging although there were not much extracellular structures observed in 24 h of patterned *E. coli* RP437, which was probably due to the decrease in expression of bacterial flagella, curli, and fimbriae in 24 h biofilms.

Hence, instead of imaging 24 h patterned biofilms, we imaged 2, 4, and 6 h biofilms with SEM in the second experiment. To highlight the cell surface structures under SEM, we used the osmium tetroxide staining to label the lipid molecules in cell membrane or membrane structures³⁹. By lowering the scanning voltage to 5 kV and bringing the stage closer to detector, extracellular structures were observed (Fig. 3-14A). However, due to sample preparation using critical point drier, cell membrane of some biofilm cells was damaged (Fig. 3-14B). We further modified the protocol to address this issue. Instead of using critical point drier to finish the dehydration of samples, we used a chemical tetramethylsilane (TMS) that was reported to give better results when it was used to process mammalian cells⁴⁰. The results showed that there were extracellular structures on the outer membrane of *E. coli* cells in patterned biofilms (Fig. 3-15). Meanwhile, high resolution analytical SEM were applied in some microbiological studies, which has led to the discovery of nanotubes as a new type of surface structures in *E. coli*⁴¹. This study inspired us to image patterned biofilms using a LEO 1550 FESEM

(field emission scanning electron microscope) with resolution up to 1 nm at 20 kV and 2.5 nm at 5 kV for compatible specimen. The images obtained by this SEM revealed more detailed information about the *E. coli* cells in our biofilm samples and the fine structures can be visualized (Fig. 3-16). These extracellular existed between cells in and between cell clusters, which suggests that they may play a role during cell-cell interaction. Their role during the formation of interaction need further studied.

3.4.5 Mutation of key genes affected interaction among cell clusters

To understand whether there is any genetic basis for the interactions among cell clusters, selected isogenic mutants of *E. coli* RP437 (Table 3-1) were also characterized to compare their biofilm formation on $20\ \mu\text{m} \times 20\ \mu\text{m}$ patterns with varied distance between patterns. As shown in Fig. 3-17A and Table 3-3, the wild-type *E. coli* RP437 fully covered the CH₃-SAM patterns and formed substantial connections between cell clusters (no clear patterns were seen) when the distance D was 2 or 5 μm , less than the threshold D* (10 μm). In comparison, RP3525 (Δtap) did not form cell clusters on CH₃-SAM patterns and showed CII values close to zero. RP4979 (ΔcheY) also exhibited major defects in adhesion and cell cluster formation. Interestingly, KX1485 (ΔluxS) and RP3087 (with a point mutation in *motB*) formed relatively normal cell clusters on CH₃-SAM patterns, but the levels of interactions between cell clusters were lower than that of the wild-type *E. coli* RP437. For example, on the surfaces with 5 μm of inter-pattern distance, strong interactions between cell clusters were observed for the wild-type *E. coli* RP437 but not for KX1485 (ΔluxS) and RP3087. Overall, the interactions among cell clusters as represented by CII values were found to be wild-type (RP437) > *motB* mutant (RP3087) > ΔluxS (KX1485) > ΔcheY (RP4979) \approx Δtap (RP3525) (Fig. 3-17B). The

mutation in RP3087 led to a malfunctioned MotB protein, which rendered the cells unable to interact between clusters (Fig. 3-17)⁴². In comparison, deletion of the *motB* gene showed a stronger impact since BL-19 (Δ *motB*) even failed to attach on CH₃-SAM (Fig. 3-18).

3.4.6 Interaction among cell clusters involves quorum sensing

To confirm if the defects in the *luxS* mutant (KX1485) as described above was not due to any polar effects, we complemented the mutation with plasmid pRHG01 carrying *luxS* under its native promoter. As shown in Fig. 3-19A (images) and Fig. 3-19B (CII values), the defects of KX1485 in interaction among cell clusters were fully rescued by this complementation.

The *luxS* gene is best known for its function in bacterial quorum sensing (QS), a system of bacterial gene regulation by sensing and responding to cell density⁴³. LuxS protein is responsible for the synthesis of QS signaling molecule autoinducer 2 (AI-2), which is involved in QS in both Gram-positive and Gram-negative bacteria. In addition to QS, *luxS* has also been shown to regulate other phenotypes such as cell growth, biofilm formation, motility, virulence and resistance to antimicrobial agents^{44,45}. To specifically test whether AI-2-mediated QS is involved in cell cluster interactions, the biofilm culture of KX1485 was supplemented with different concentrations of the AI-2 precursor DPD (1, 10, 50, and 100 μ M), which can spontaneously transform to AI-2 in aqueous environment⁴⁴. The interactions between cell clusters of the *luxS* mutant was fully restored when DPD was supplemented to cultures at 50 or 100 μ M (Fig. 3-20A&B). This experiment provided important evidence that QS via AI-2 is involved in interactions among *E. coli* cell clusters.

Relatively high concentrations of DPD were required to restore the phenotype of KX1485, suggesting that *luxS* may also control some other phenotypes involved in interactions among cell clusters. To test this hypothesis, we conducted a further experiment of patterned biofilm formation of co-cultures of the *E. coli* RP437 (WT) and KX1485 ($\Delta luxS$). To allow a direct comparison of bacterial distribution in the biofilms formed by those two strains, the RP437 cells were labeled with constitutively expressed green fluorescent protein (GFP, encoded by the plasmid pRSH109) and the KX1485 cells were labeled with constitutively expressed red fluorescent protein (RFP, encoded by the plasmid pDsRed). It was interesting to find that, although KX1485 is in contact with AI-2 signals produced by the wild-type *E. coli* RP437, the wild-type RP437 cells still dominated the co-culture biofilms (Fig. 3-21) except for the patterns separated by more than 10 μm with inoculation ratio of wild-type : $\Delta luxS$ = 1: 4. Collectively, these results indicate that QS via AI-2 is important to the interaction among cell clusters; while other factors controlled by *luxS* are also involved in biofilm growth in a competitive environment.

3.4.7 *E. coli* cells exhibited changes in antibiotic susceptibility during the early stage biofilm formation

To determine the susceptibility of biofilm cells to antibiotic treatment during the early stage of biofilm formation, the effects of ampicillin on *E. coli* HM22 cells on glass wool surfaces during the first 5 h of biofilm formation was investigated. This condition was chosen because it is commonly used to isolate persister cells of *E. coli* HM22⁴⁶. It was found that during the first 2h of biofilm growth, the percentage of biofilm cells that survived the 3 h ampicillin (200 $\mu\text{g}/\text{mL}$) treatment decreased with the time (Pearson

correlation analysis; $r < -0.94$ for all samples studied, $P < 0.0001$), suggesting that the cells were metabolically active (Fig. 3-22). For example, the percentage of 2 h biofilm cells that survived the treatment was about 3-fold lower than the cell in overnight cultures used for inoculation. Interestingly, when the biofilm was inoculated for more than 2 h, the percentage of survival increased with time and returned to the original level after 5h ($r > 0.94$ for all samples studied, $P < 0.0001$). These results suggest that the metabolic activities in biofilm cells change dynamically during biofilm formation. The finding that 2h is a turning point with the maximum killing is interesting. Further study is necessary to help understand the underlying mechanism.

3.4.8 Location of biofilm cells and antibiotic susceptibility

The finding that *E. coli* cells actively interact between cell clusters led to our hypothesis that the cells in clusters and between clusters may have different levels of antibiotic susceptibility. To test this hypothesis, patterned *E. coli* RP 437 biofilms were treated with 200 $\mu\text{g/mL}$ ampicillin for 1 h and the viability of biofilm cells was determined using LIVE/DEAD staining and fluorescence microscopy. As shown in Fig.3-23, for 2, 4, and 6 h *E. coli* RP437 biofilms, cells in clusters were more resistant to ampicillin than the cells between clusters. For example, the percentage of viable cells in cell clusters in 2, 4, and 6 h patterned biofilms with 10 μm between clusters was $54.8 \pm 7.5\%$, $79.5 \pm 2.4\%$, and $91.6 \pm 1.8\%$; while the percentage of viable cells between clusters in the same biofilms was $7.4 \pm 13.1\%$, $52.0 \pm 6.8\%$, and $85.0 \pm 1.8\%$, respectively. The resistance of cells in 6 h biofilms is similar to that in 24 h biofilms respectively. This result indicates that cells between cell clusters during early stage biofilm formation were more susceptible to the antibiotic ampicillin. The susceptibility

decreased over time during biofilm formation for all the tested cells. Since ampicillin is more effective against metabolically active cells, these findings support the hypothesis that the cells between clusters are more active and the metabolism of biofilm cells decrease over time. In addition to time, the distance between patterns did not appear to play a role, except for the 2 h biofilms.

3.5 DISCUSSION

Structural heterogeneity is an important challenge to biofilm research and hinders mechanistic understanding of biofilm formation^{11,47,48}. By rigorously controlling surface chemistry, the morphology of biofilms is better controlled. The patterned biofilm formation described in this study offered a new opportunity to systematically study the interaction among cell clusters at the genetic level with controlled size and shape of cell clusters.

By comparing the CII values of patterned biofilms, the results indicate that interactions among cell clusters are specific and are influenced by the size of cell clusters and the distance between them. Both the threshold distance (10 μm) and pattern size (20 $\mu\text{m} \times 20 \mu\text{m}$) are significantly larger than the size of individual *E. coli* cells used in this study, which indicates that multicellular interaction is essential for establishing connection between cell clusters. Interestingly, we recently found that *E. coli* adhesion on the top of protruding patterns of PDMS is significant only if the dimension of protruding square patterns is 20 $\mu\text{m} \times 20 \mu\text{m}$ or larger²³. Collectively, these data suggest that a threshold dimension may be required for establishing a stable cell cluster and interaction with other clusters. Although the nature of such interactions and their effects on bacterial physiology are unknown, following the early stage biofilm formation on patterns over

time provided evidence that *E. coli* cells from adjacent clusters can grow toward each other and form “bridge-like” connections. Besides, bacterial extracellular structures seem to play a role during this process. Since pattern size and inter-pattern distance have significant impacts on CII, interactions between cell clusters appear to involve active sensing of local environment by bacteria and decision making in response to related stimuli. The finding that QS via AI-2 is involved in such interactions provided promising evidence.

Based on the results of study, we propose the following model to explain the heterogeneity in biofilms. As shown in the schematic in Fig. 3-24, when bacterial cells approach a surface through reversible adhesion, the cells need to opt for adhesion or detachment. On surfaces without well-controlled surface chemistry (in most natural and experimental conditions), the initial adhesion is heterogeneous. This leads to unevenly distributed small colonies (Fig. 3-24). The findings of this study demonstrate that the cell clusters close to each other ($D \leq D^*$) can interact and grow into a bigger colony, while the cell clusters that are far away from each other ($D \geq D^*$) will remain as individual colonies if the surrounding environment, e.g., surface chemistry, does not allow them to grow big enough to interact with other colonies. For example, Hou *et al.*⁴⁹ showed recently that biofilms can be confined in specific patterns for a month. Further development of the colonies with multiple layers of cells creates more heterogeneity due to differences in nutrient transfer, waste removal, and cell-to-cell signaling caused by the existing differences in colony size and shape. Attachment of planktonic cells and dispersion of cell clusters are additional factors causing structural heterogeneity. This

model is consistent with experimental observations of heterogeneous biofilms as shown in Fig. 3-1A, and emphasizes the importance of surface condition to biofilm formation.

Ampicillin is a β -lactam antibiotic, which inhibits the synthesis of bacterial cell wall in cell division leading to bacterial death⁵⁰. Hence, it is well known that ampicillin is only effective in killing fast-growing cells and not effective in killing slow-growing cells⁵¹. The finding that ampicillin was effective in killing 2 h biofilm cells on glass wool and the cells between cell clusters on patterned surfaces suggests that these cells are metabolically active.

These results demonstrate that important missing information can be obtained by decoupling the structural heterogeneity and other chemical or physical factors. Further studies on the role of key genes can help understand the genetic basis of observed phenomenon. The effects of structural organization on cellular processes are also important to study. For example, ampicillin treatment has been reported by to reduce flagellar synthesis⁵². The study on the role of flagellar assembly during the development of biofilm high drug resistance is part of our ongoing work.

3.6 ACKNOWLEDGEMENTS

This work is supported by the U.S. National Science Foundation (CAREER-1055644, EFRI-1137186, and CMMI-0826288). I am grateful to Shuyu Hou, who initiated this work and obtained preliminary data. I also thank Chanokpon Yongyat and Suzanne De Tore for helping me with the co-culture experiments. We are grateful to Dr. John S. Parkinson at the University of Utah for providing the strain *E. coli* RP437 and its isogenic mutants, and Dr. Robert Austin at Princeton University for the strain *E. coli* KX1485. We thank Dr. Yan-Yeung Luk at Syracuse University for access to gold

deposition equipment and the Cornell NanoScale Science & Technology Facility for access to the photolithography facilities. We also thank Dr. Arne Heydorn at the Technical University of Denmark for providing the COMSTAT software.

3.7 FIGURE CAPTIONS

Figure 3-1. Representative images of *E. coli* RP437 biofilms. (A) Heterogeneous biofilms formation on glass, gold (without chemical modification), and stainless steel surfaces (Bar = 50 μm). (B) Patterned biofilms formed on gold surfaces modified with self-assembled monolayers (SAMs) presenting functional groups (Bar = 50 μm).

Figure 3-2. Genetic complementation of the *luxS* mutant. (A) Map of the pCR®2.1 TOPO® vector. (B) The gel image indicating the *luxS* gene and its promoter were obtained. (C) PCR product of the *luxS* gene amplified from the cloned plasmid.

Figure 3-3. Schematic presentation of the pattern generation through photolithograph, soft lithography and microcontact printing.

Figure 3-4. Schematic presentation of gold surfaces modified with square patterns of CH_3 -SAM and background of TEG-SAM.

Figure 3-5. Representative fluorescence images of 24 h *E. coli* RP437 biofilms on 20 μm \times 20 μm patterns with inter-pattern distance of 2 (A), 5 (B), 10 (C), or 15 (D) μm (Bar = 50 μm).

Figure 3-6. Interaction between *E. coli* cell clusters: representative cell clusters with 5 (A) or 10 (B) μm distance; and schematic illustration of interaction between adjacent cell clusters (C) (Bar = 10 μm).

Figure 3-7. Effects of inter-pattern distance on CII values of *E. coli* RP437 biofilms. N=3 biological repeats averaged; at least 15 images were analyzed for each data point.

Figure 3-8. Effects of pattern size on CII values. N=3 biological repeats averaged; at least 15 images were analyzed for each data point.

Figure 3-9. Ratios of surface coverage on TEG-SAM (EB) of 20 μm ×20 μm pattern surfaces (with varying inter-pattern distance) to that on pattern-free TEG-SAM surfaces. N=3 biological repeats averaged; at least 15 images were analyzed for each data point.

Figure 3-10. Connections between cell clusters (W = 20 μm ; D = 10 μm) were formed due to growth of cells from adjacent clusters rather than settlement of seeding cells. Representative cell clusters after 3 h of initial attachment (A) and 7 h of growth (B) are shown (Bar = 10 μm).

Figure 3-11. Representative images of cell growth during early stage of patterned biofilm formation in a flow cell (Bar = 10 μm).

Figure 3-12. Representative images of cell growth in early stage of patterned biofilm formation in batch culture (Bar = 10 μm).

Figure 3-13. SEM images of *E. coli* RP437 cells in 24 h biofilms formed on a gold surface modified with size 20 μm × 20 μm patterns. Images were taken by using a JEOL 5800LV SEM.

Figure 3-14. SEM images of *E. coli* RP437 cells in 2h (A) and 4h (B) biofilms formed on a gold surface modified with size 20 μm × 20 μm patterns. Images were obtained using JEOL 5800LV SEM.

Figure 3-15. SEM images of *E. coli* RP437 cells in a 4 h biofilm formed on a gold surface modified with size 20 μm × 20 μm patterns. Samples were

dehydrated with tetramethylsilane (TMS) as the last step of dehydration. Images were obtained using JEOL 5800LV SEM.

Figure 3-16. SEM images of *E. coli* RP437 cells in a 4 h biofilm formed on a gold surface modified with size $20\ \mu\text{m} \times 20\ \mu\text{m}$ patterns. Images were obtained using LEO 1550 FESEM.

Figure 3-17. Patterned biofilm formation of the wild-type *E. coli* RP437 and its four isogenic mutants. (A) Representative fluorescence images of biofilms formed on surfaces modified with $20\ \mu\text{m} \times 20\ \mu\text{m}$ CH_3 -SAM patterns with varying inter-pattern distance (Bar = $50\ \mu\text{m}$). (B) CII values of biofilms shown in Figure 3-17A. N=3 biological repeats averaged for this graph; at least 15 images were analyzed for each data point.

Figure 3-18. Attachment of *E. coli* BL-19 (RP437 ΔmotB) on a surface with $20\ \mu\text{m} \times 20\ \mu\text{m}$ SAM patterns after 24 h of incubation (Bar = $50\ \mu\text{m}$).

Figure 3-19. Genetic complementation of the *luxS* mutant. (A) Representative fluorescence images of patterned biofilms of *E. coli* RP437, its *luxS* mutant KX1485, and the complemented *luxS* mutant KX1485/pRHG01 (Bar = $50\ \mu\text{m}$). (B) CII values of biofilms shown in Figure 3-19A. N=3 biological repeats averaged for this graph; at least 15 images were analyzed for each data point.

Figure 3-20. Chemical complementation of the *luxS* mutant with AI-2 precursor DPD. (A) Representative fluorescence images of patterned biofilms of *E. coli* RP437, its *luxS* mutant KX1485, and KX1485 supplemented with 50 or 100

μM DPD (Bar = 50 μm). (D) CII values of biofilms shown in Figure 3-20A. N=3 biological repeats averaged for this graph; at least 15 images were analyzed for each data point.

Figure 3-21. Co-culture biofilms on 20 μm \times 20 μm patterns. (A) Representative fluorescence images of 48 h biofilms with *E. coli* RP437/pRSH109 and KX1485/pDsRed inoculated as 4:1, 1:1, and 1:4 ratios (Bar = 50 μm). (B) Relative surface coverage of the above co-culture biofilms.

Figure 3-22. Viability of biofilm cells after treatment with 200 $\mu\text{g}/\text{ml}$ ampicillin for 3h *E. coli* HM22 biofilms were formed on glass wool. The CFU of untreated cells for each condition was normalized as 100%. N=3 biological repeats averaged for this graph.

Figure 3-23. Ampicillin susceptibility of *E. coli* RP437 cells in patterned biofilms. (A) Representative images of the patterned *E. coli* RP437 biofilms (2, 4, 6, and 24 h inoculation) on gold surfaces modified with 20 μm \times 20 μm square shaped patterns with 15 μm inter-pattern distance. The biofilms were treated with 200 $\mu\text{g}/\text{mL}$ ampicillin for 1 h and labeled with LIVE/DEAD[®] BackLight[™] Bacteria Viability Kit before imaging (Bar = 10 μm). (B) Viability of cells in patterned *E. coli* RP437 biofilms (2, 4, 6, and 24 h) analyzed using COMSTAT.

Figure 3-24. Schematic description of early stage bacterial biofilm formation on uncontrolled surfaces (A) and well-defined surfaces (B).

3.8 FIGURES

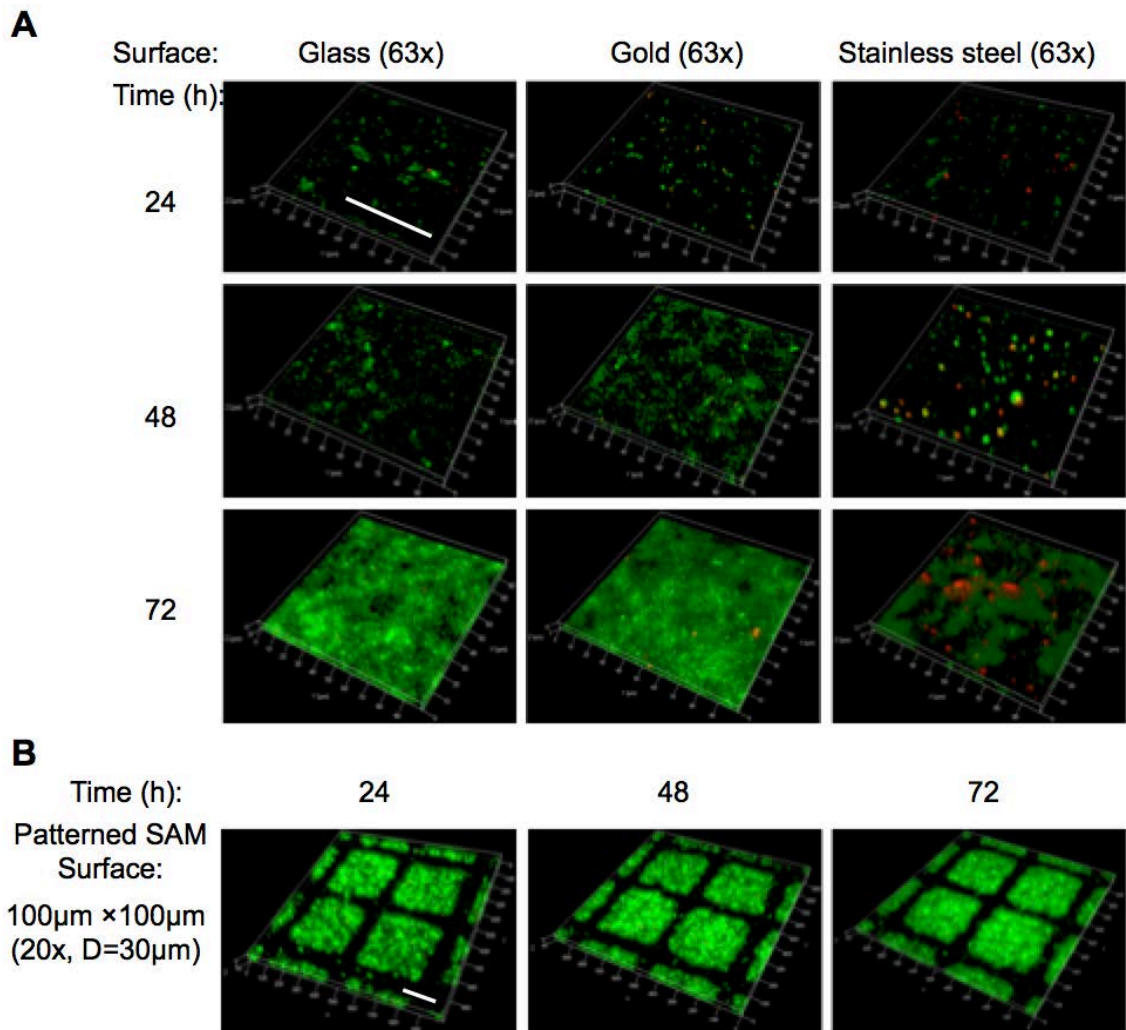


Figure 3-1

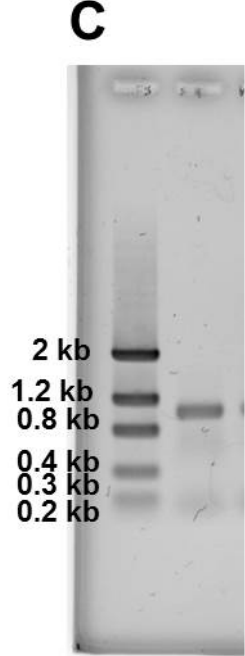
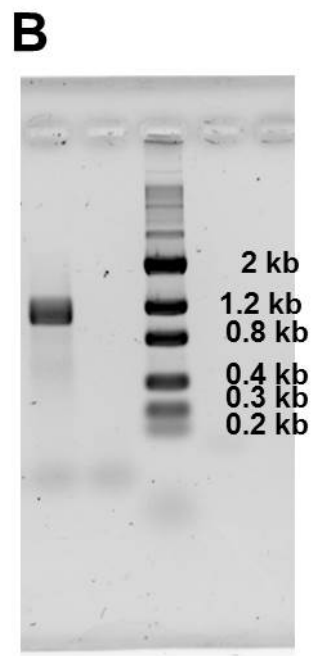
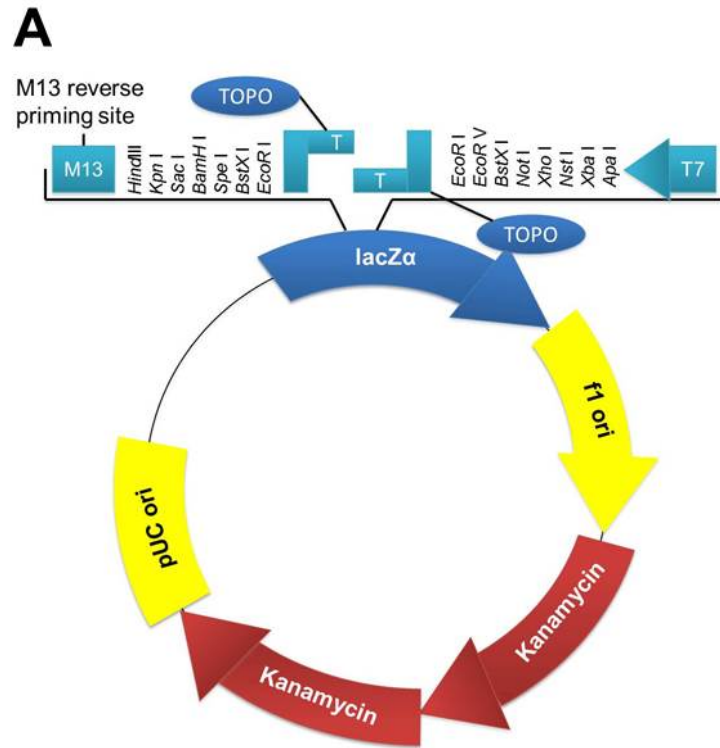


Figure 3-2

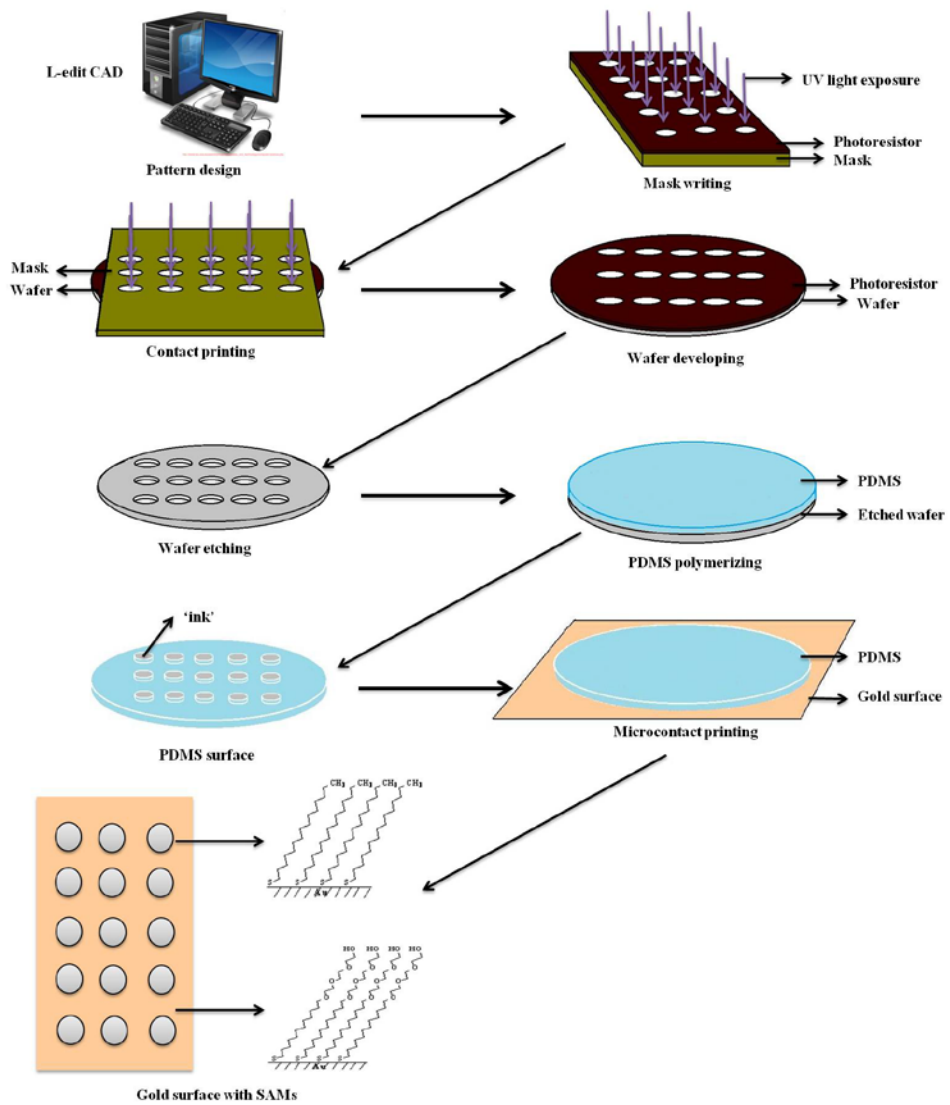


Figure 3-3

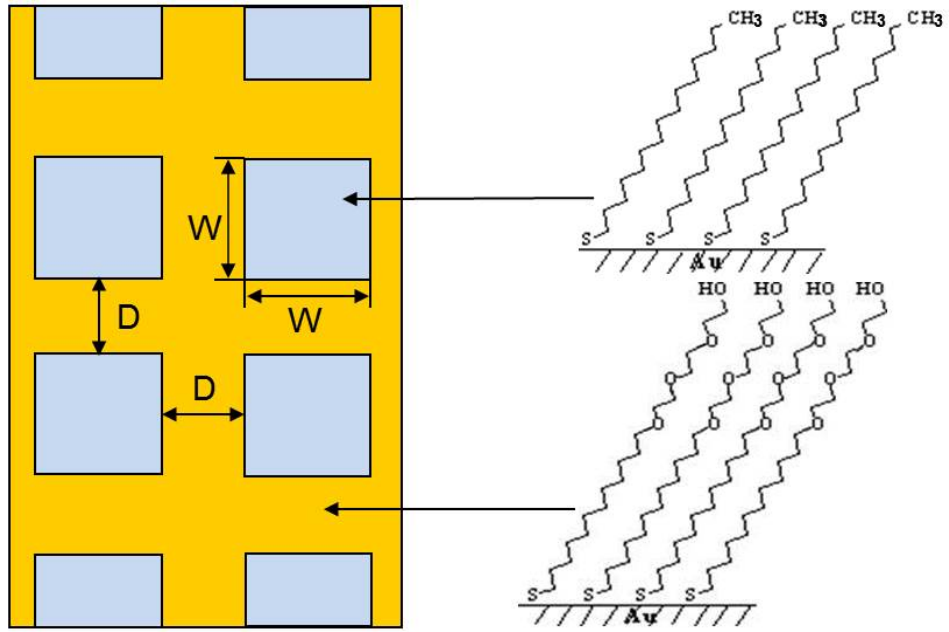


Figure 3-4

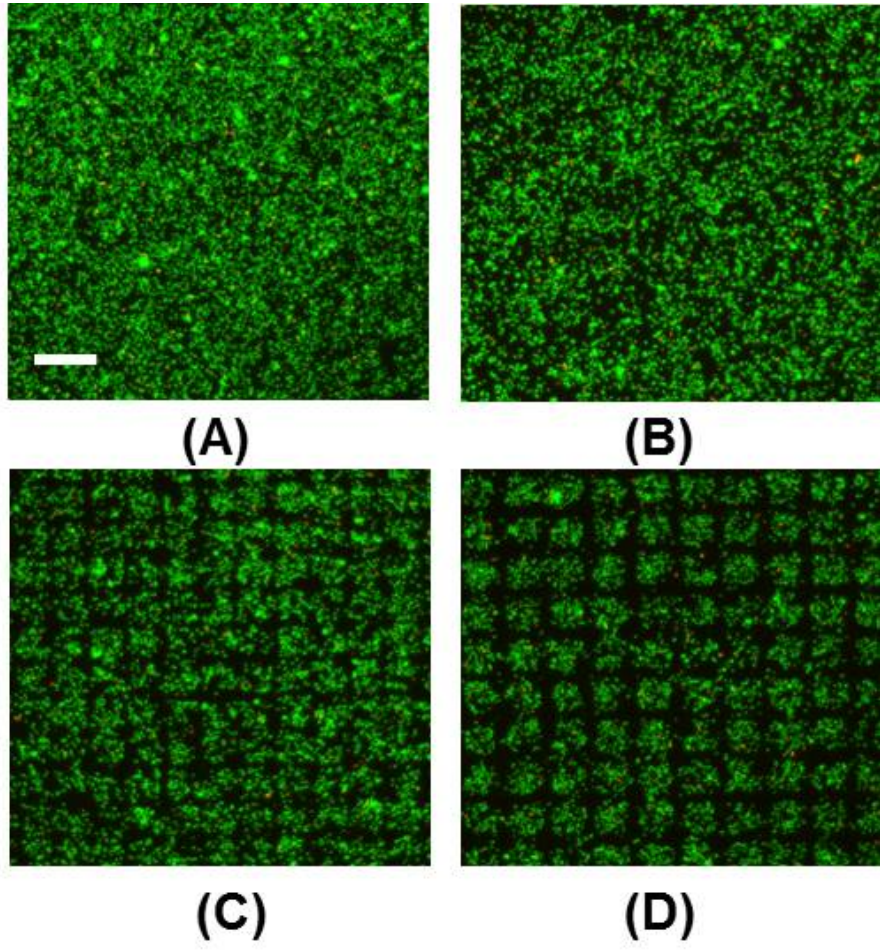


Figure 3-5

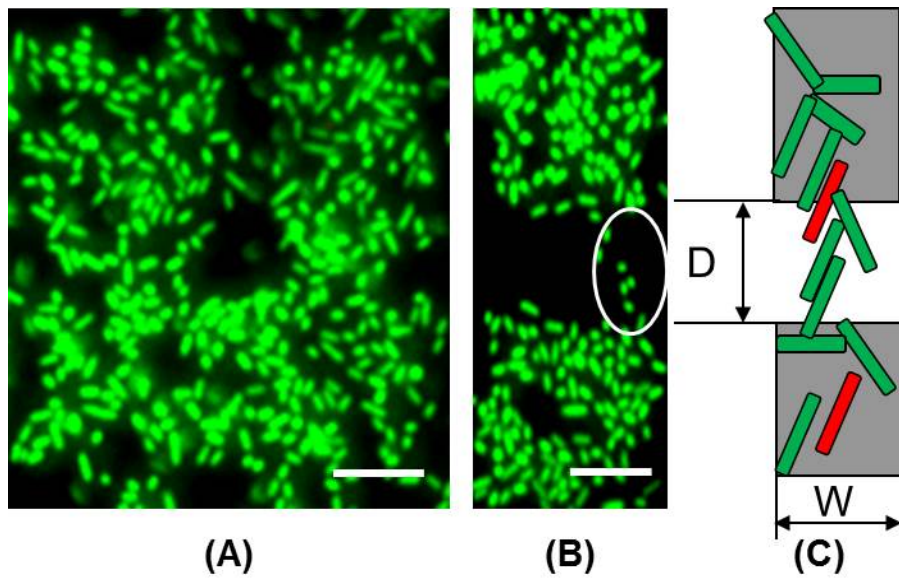


Figure 3-6

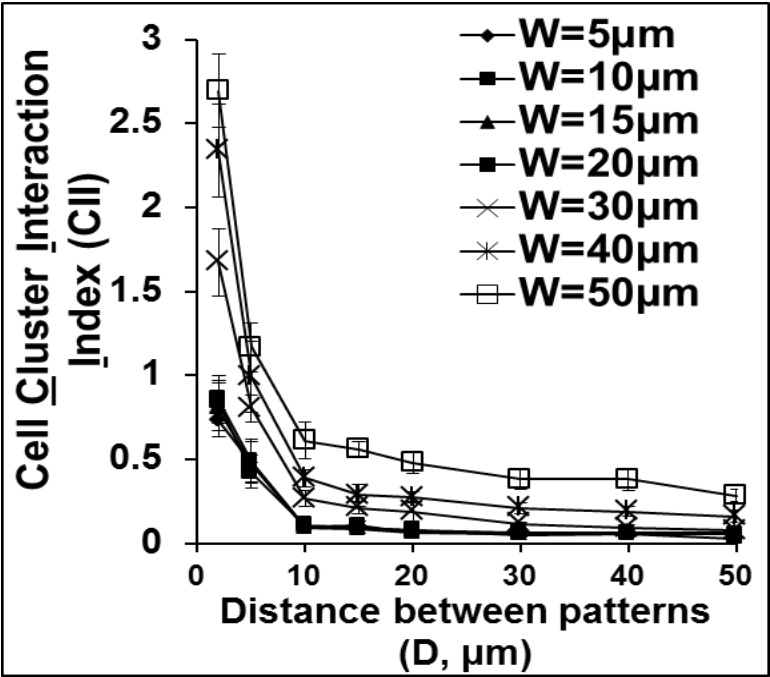


Figure 3-7

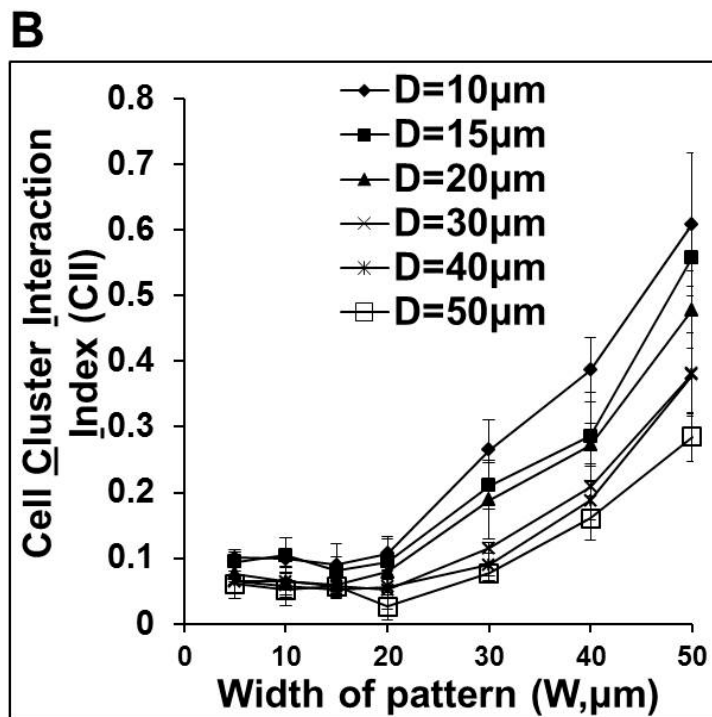
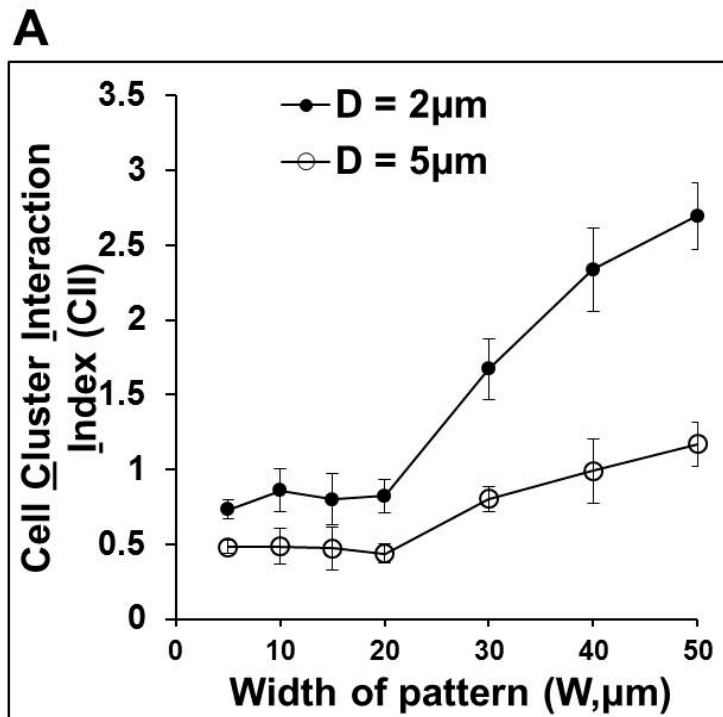


Figure 3-8

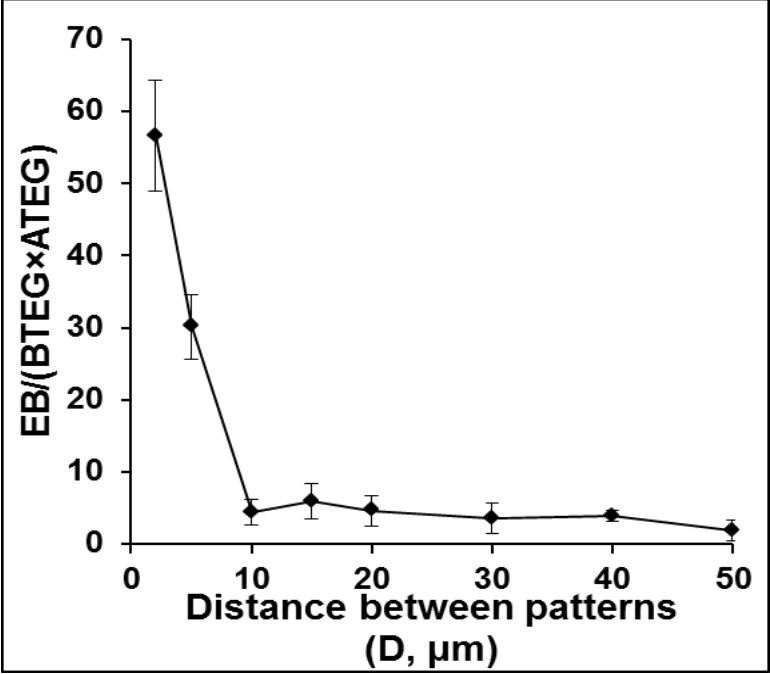


Figure 3-9

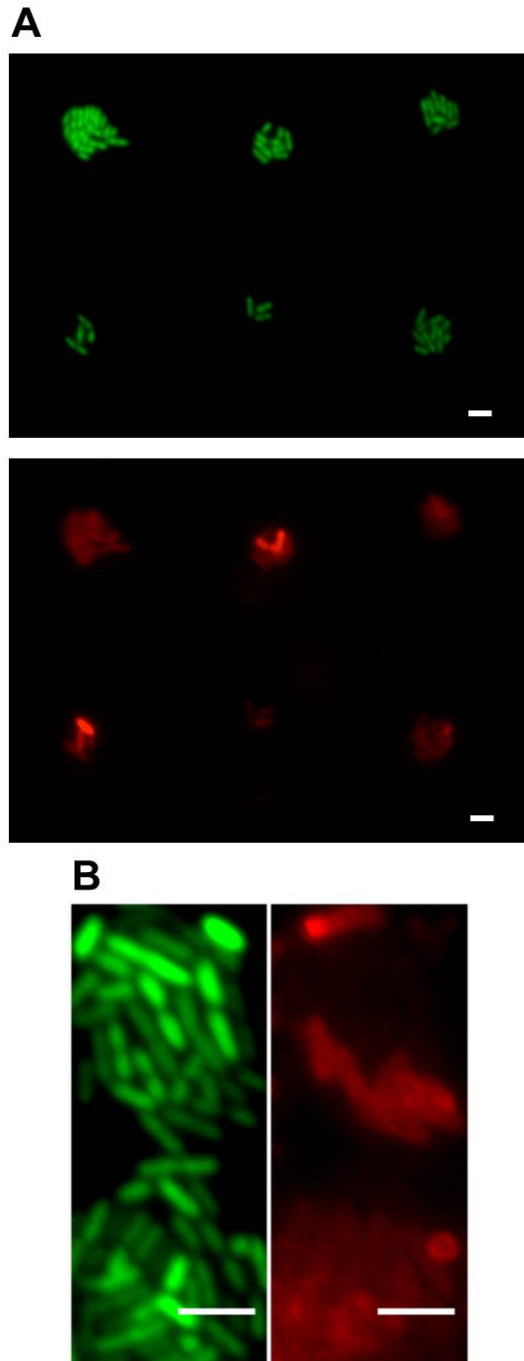


Figure 3-10

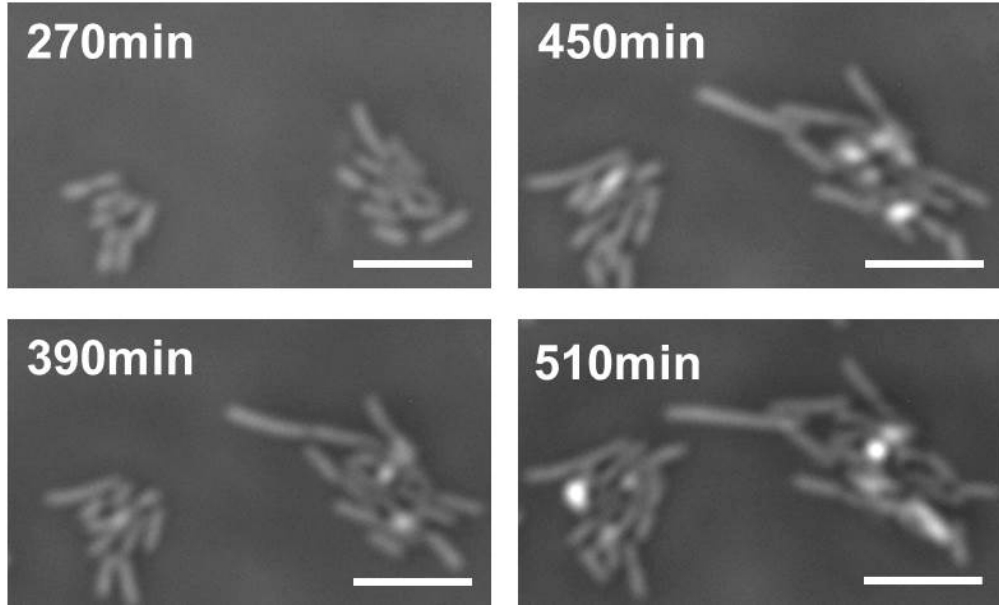


Figure 3-11

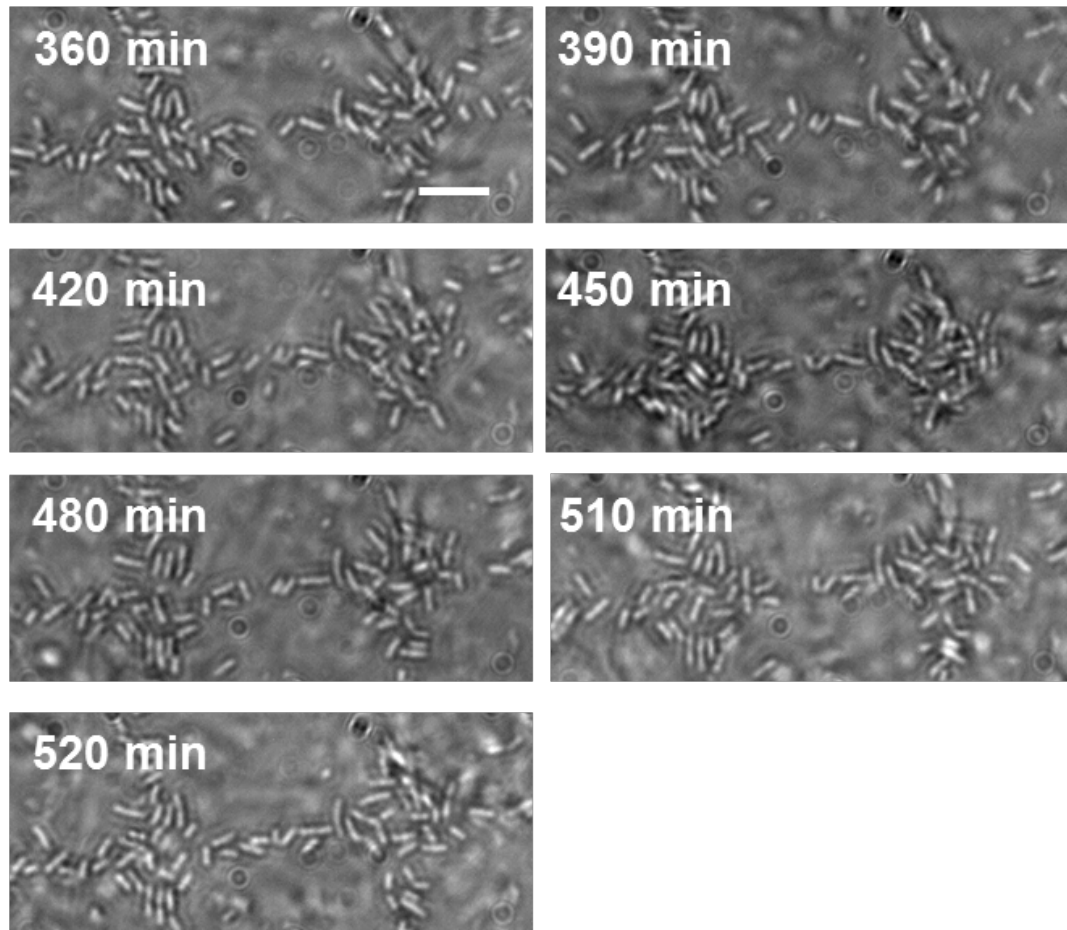


Figure 3-12

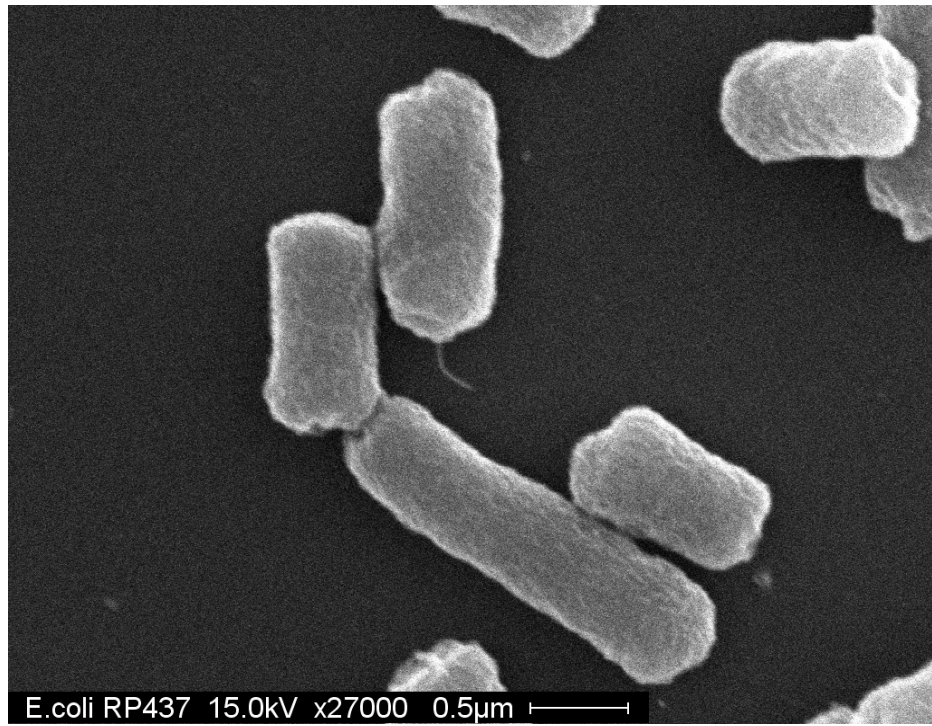
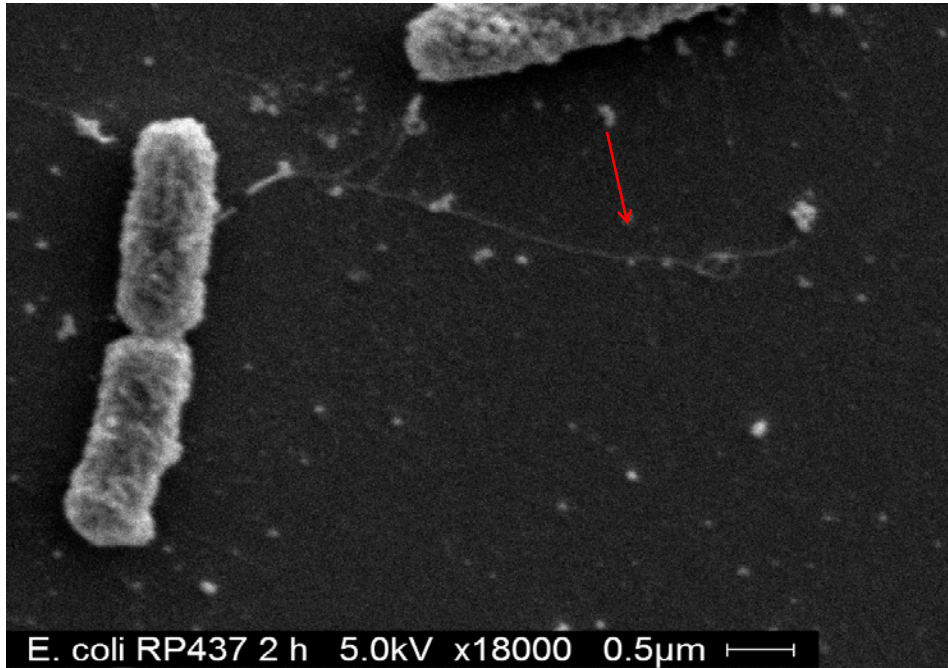


Figure 3-13

A



B

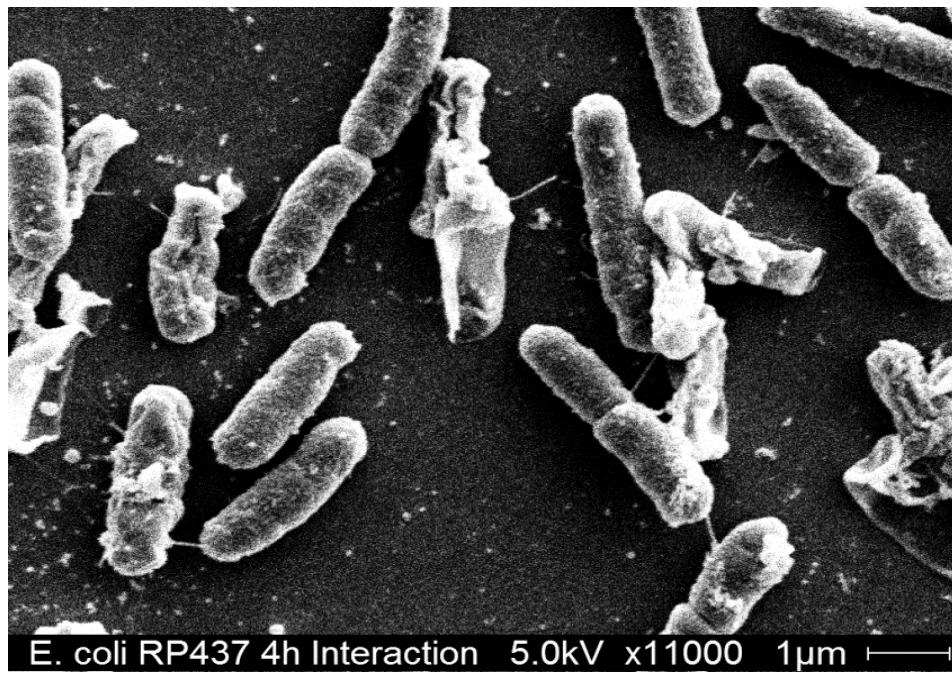
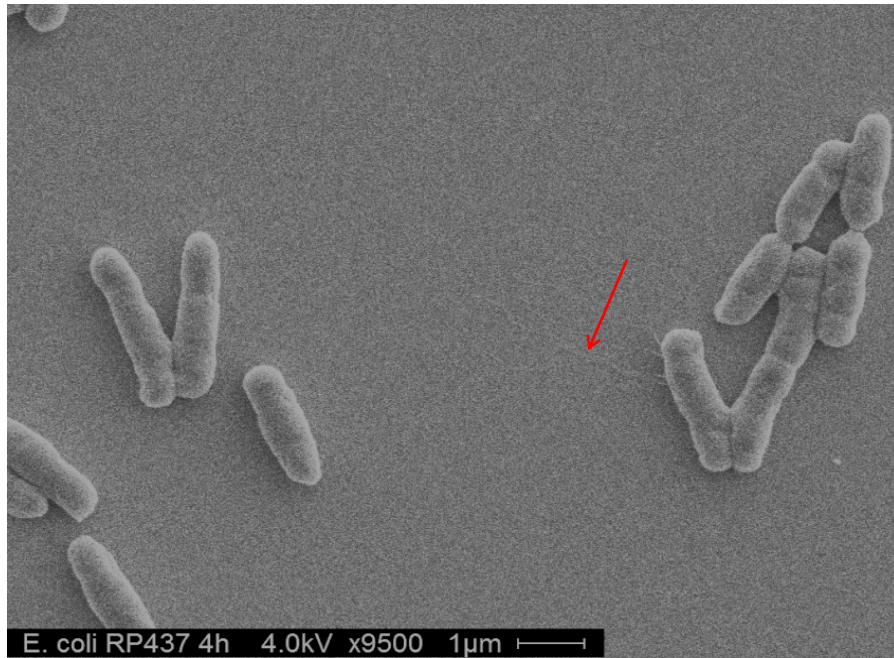


Figure 3-14

A



B

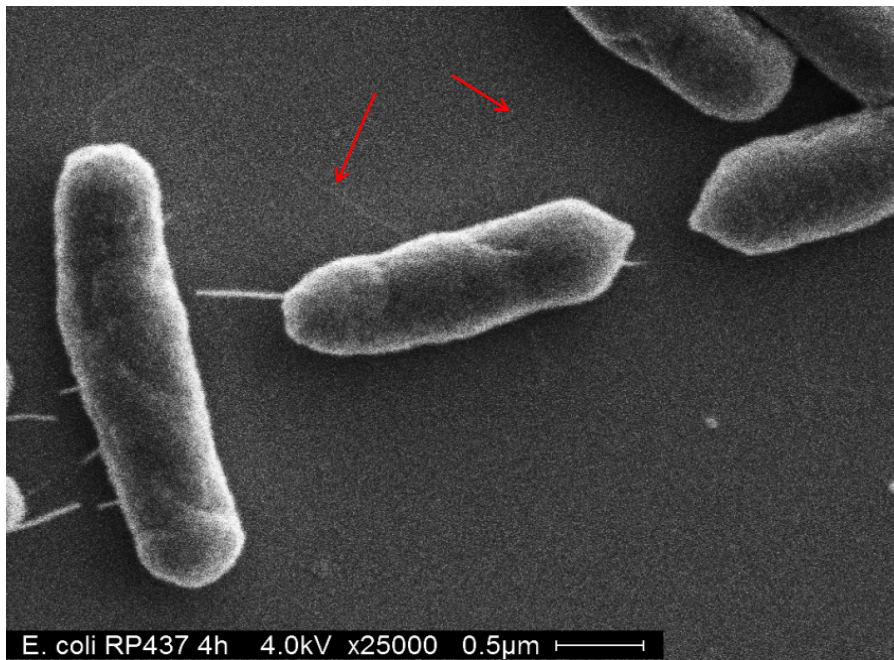


Figure 3-15

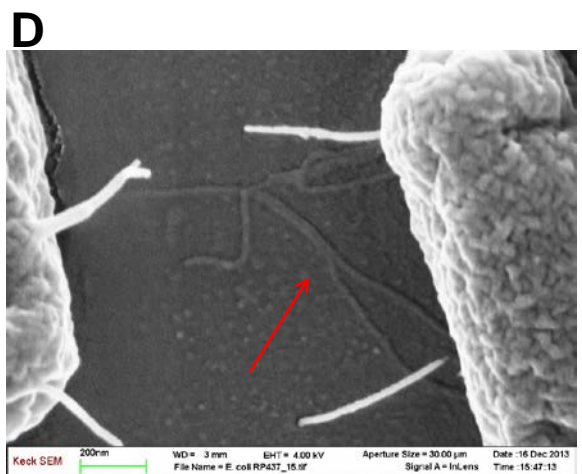
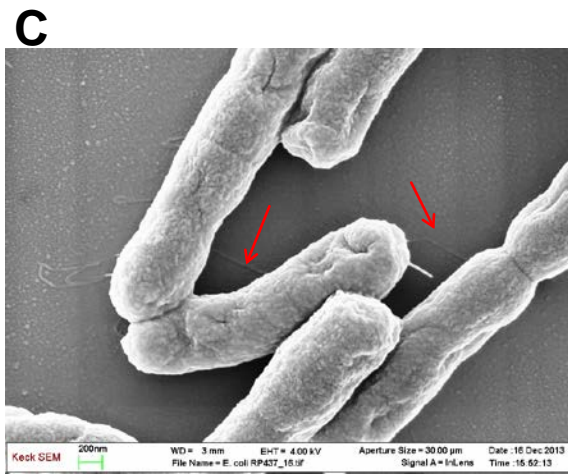
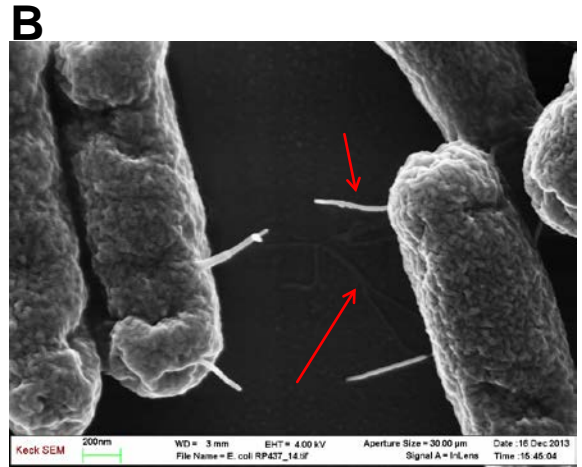
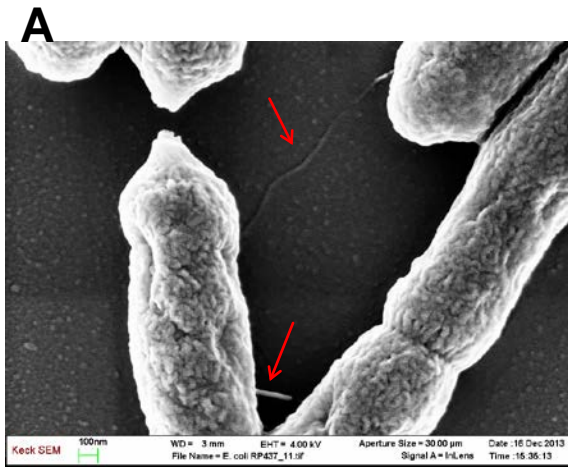


Figure 3-16

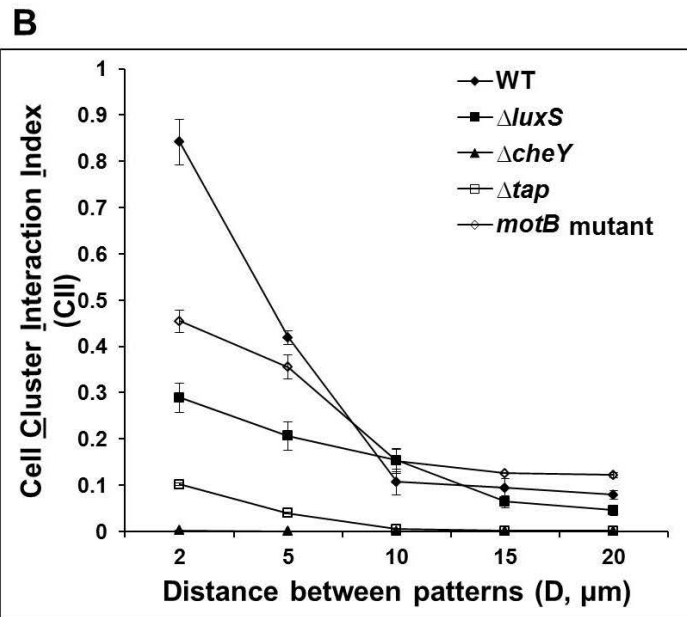
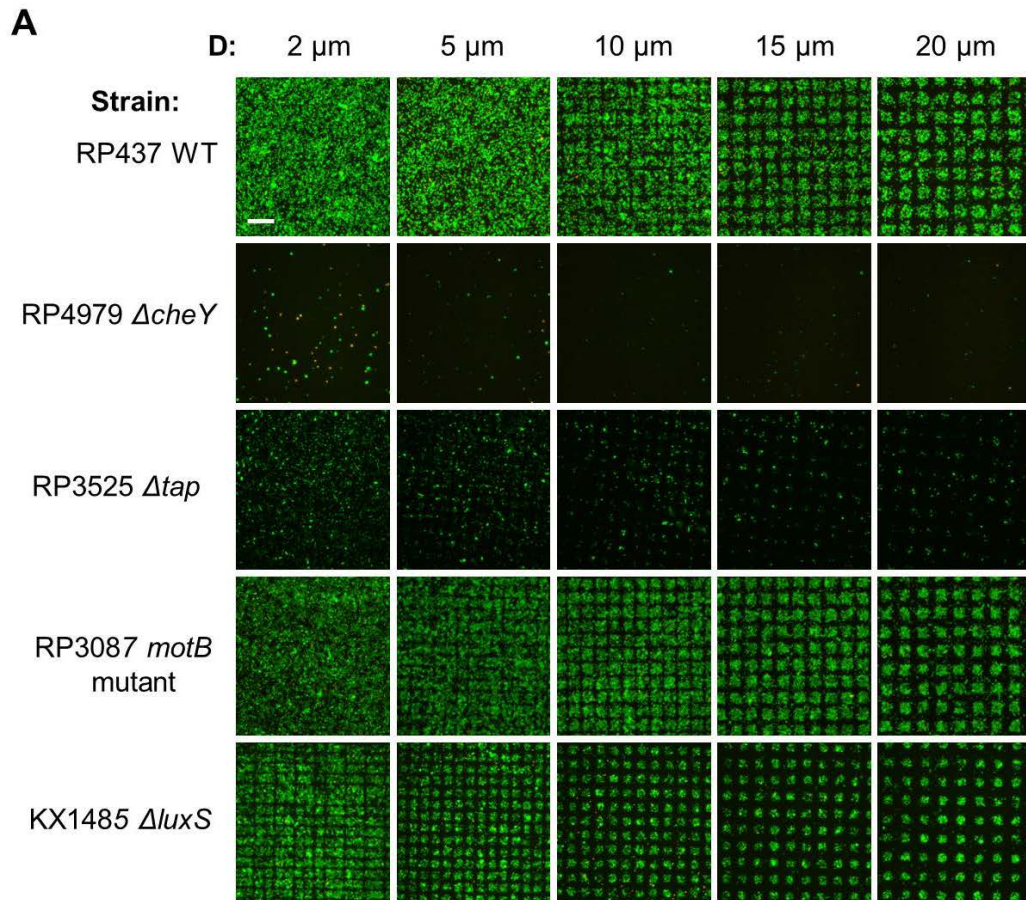


Figure 3-17

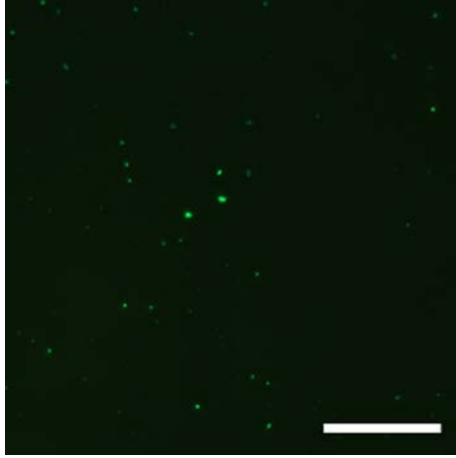


Figure 3-18

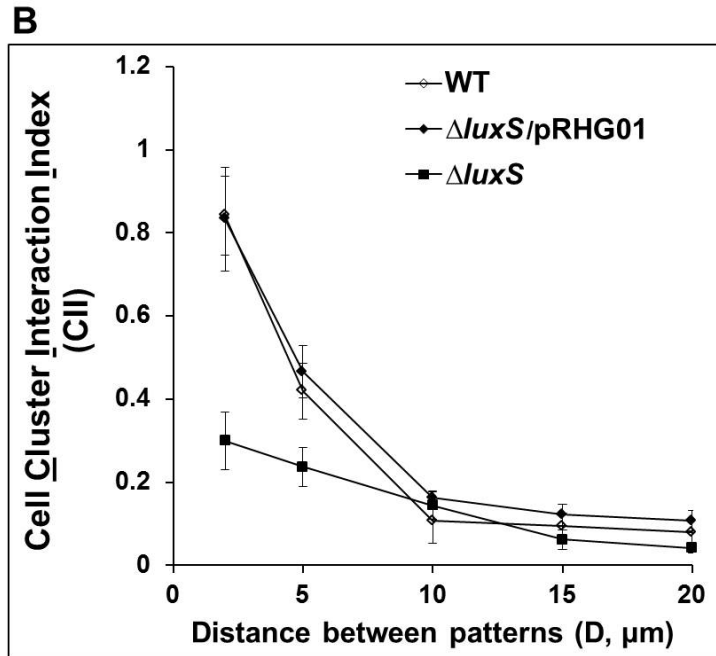
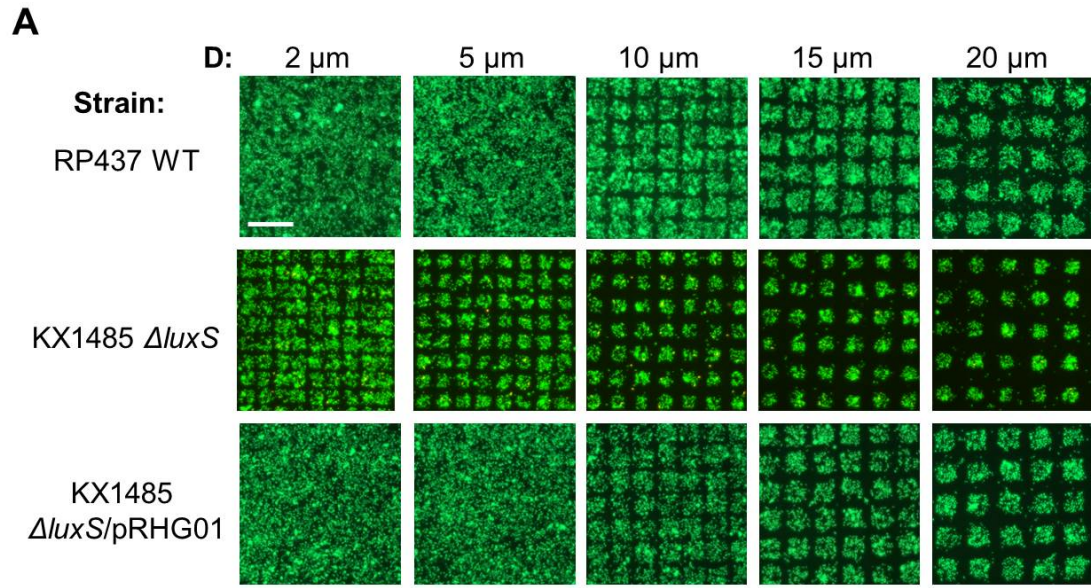


Figure 3-19

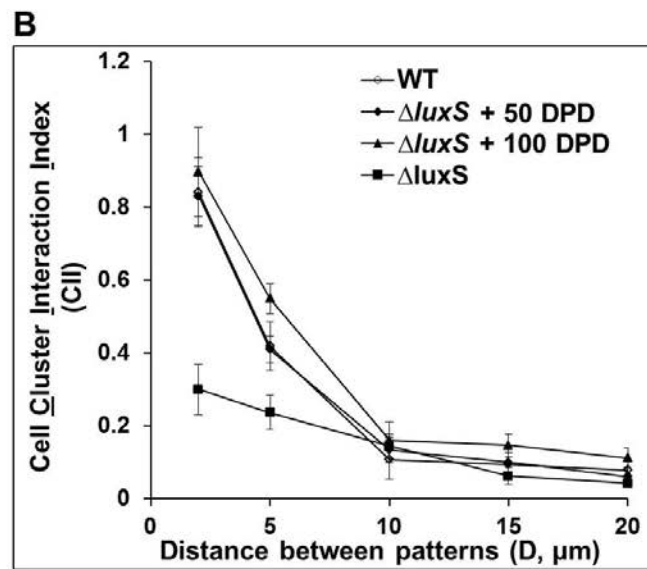
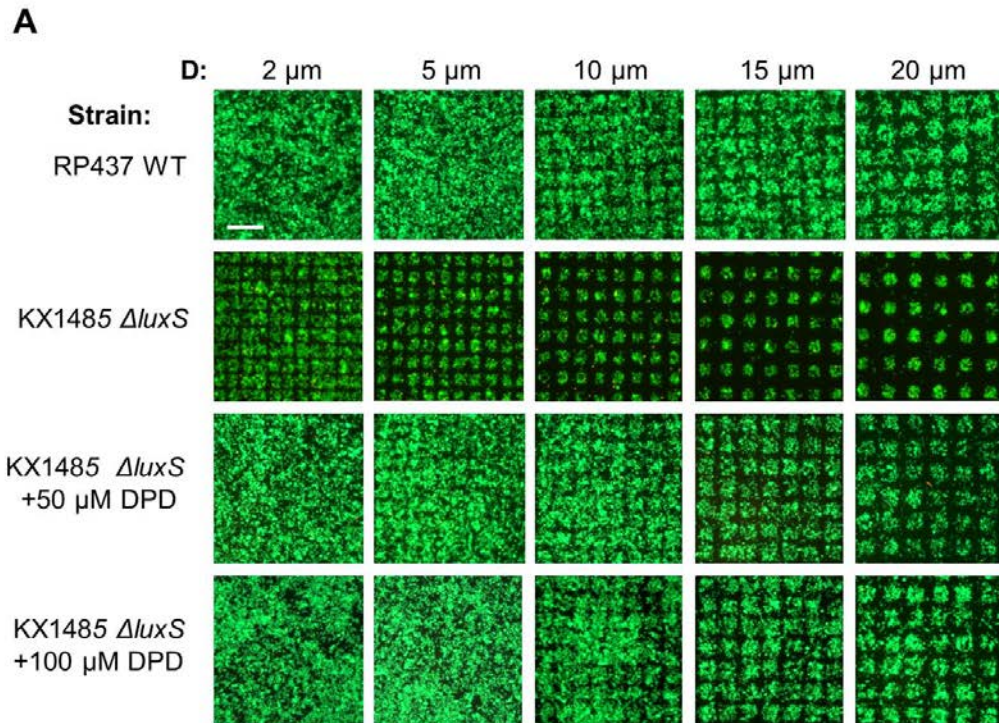


Figure 3-20

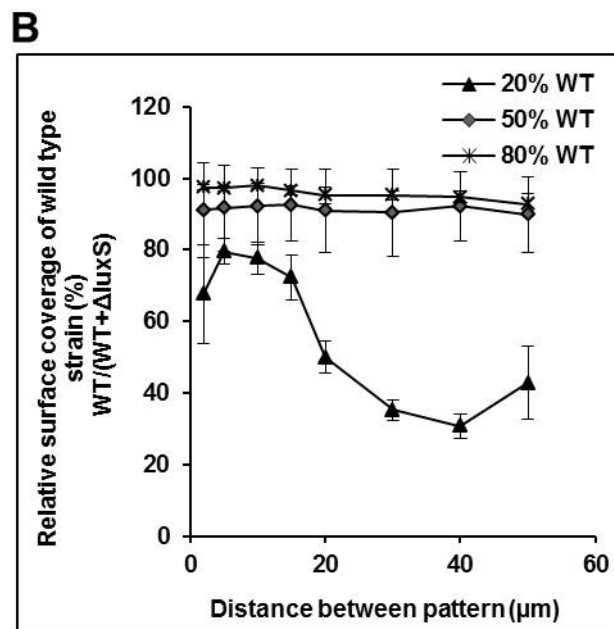
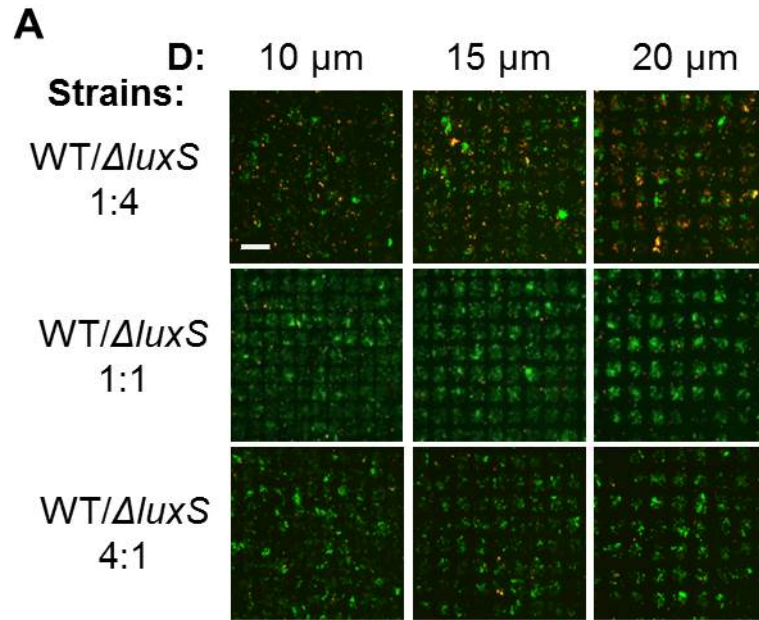


Figure 3-21 (Generated by Chanokpon Yongyat and Suzanne De Tore)

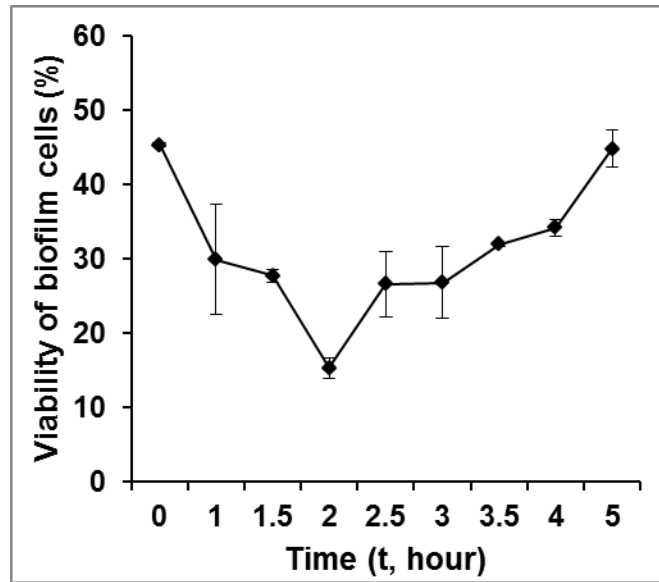


Figure 3-22

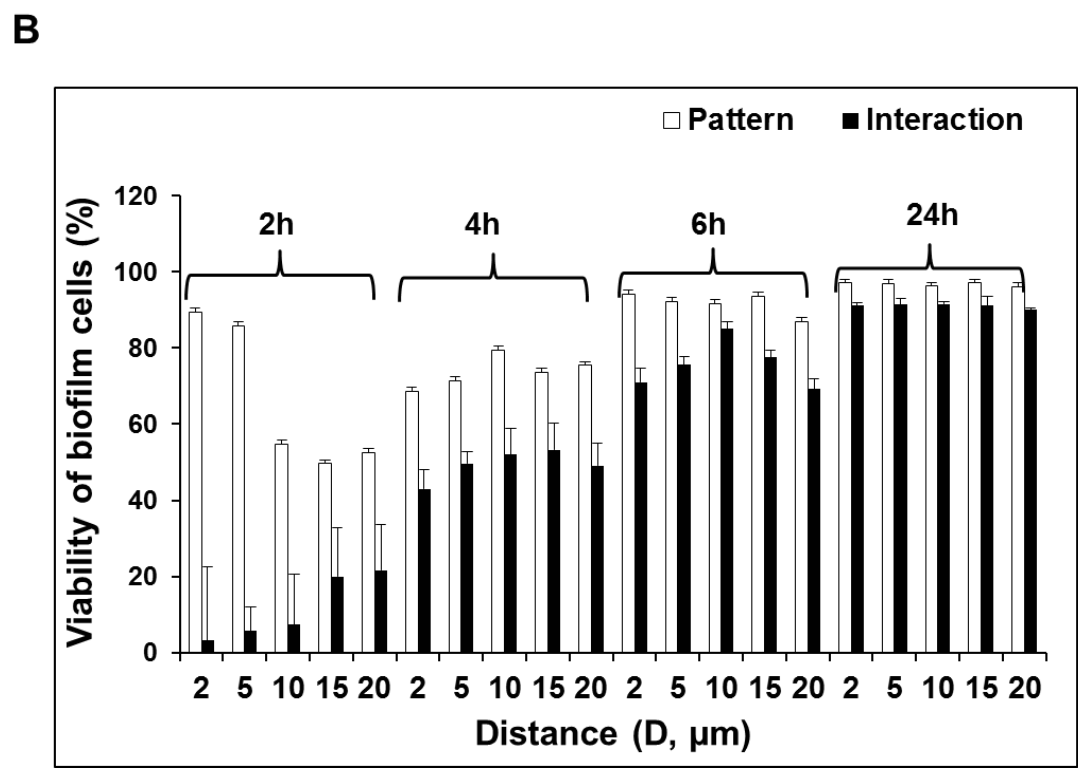
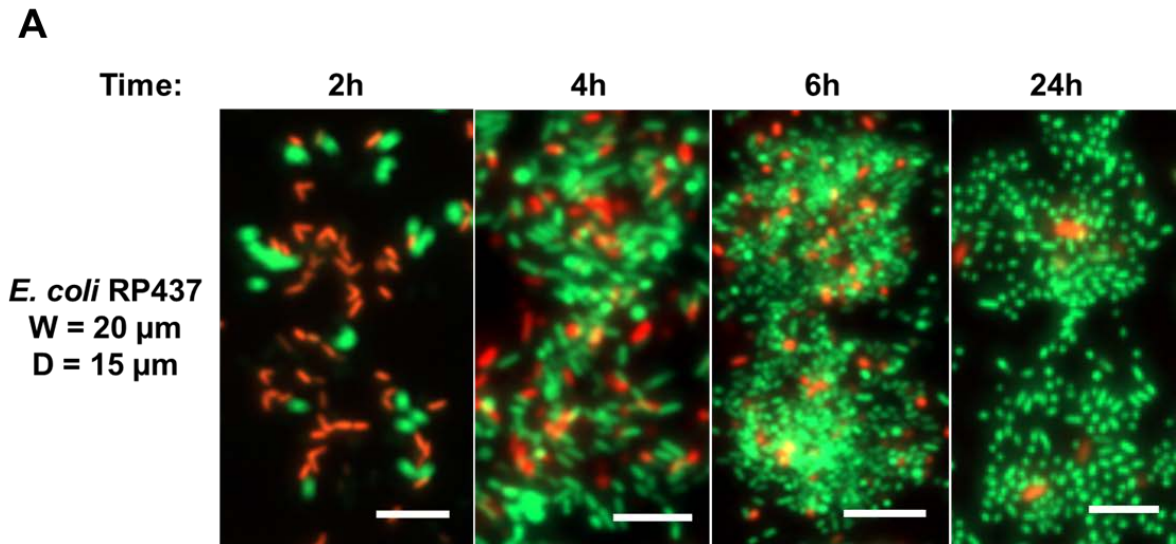


Figure 3-23

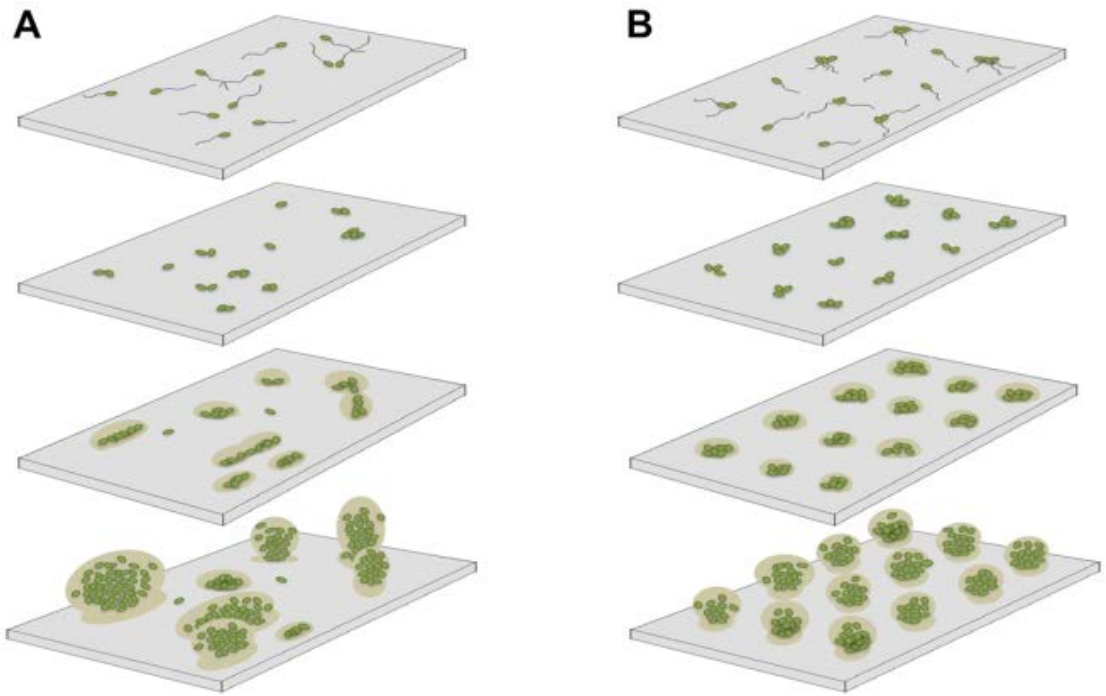


Figure 3-24

3.9 TABLES

Table 3-1. List of *E. coli* strains and plasmids used in this study.

	Genotype	Characteristics	Source/References
Strains			
RP437	<i>Wild type</i>	Wild type strain for biofilm study	16
RP3087	<i>(motB)580</i>	Motility mutant	53
RP4979	<i>eda⁺Δm43-10(cheY)</i>	Chemotaxis mutant	54,55
RP3525	<i>RP437 Δtap-365-4 Δ(lac)U169 thr⁺ leu⁺</i>	Chemotaxis mutant	56,57
KX1485	<i>luxS::Cm^r</i>	Quorum sensing mutant, unable to synthesize AI-2	58,59
HM22	<i>AT984 zde-264::Tn10 hipA7</i>	<i>hipA</i> mutant of <i>E. coli</i> AT984	21
Plasmids			
pRSH109	<i>Amp^r, gfp</i>	Label cells with constitutive GFP	This study
pDsRed	<i>Amp^r, rfp</i>	Label cells with constitutive RFP	Life Technologies Inc., Carlsbad, CA, USA
pRHG01	<i>luxS⁺, Amp^r</i>	pCR2.1 [®] -TOPO [®] with <i>luxS</i> gene and its native promoter	This study

Table 3-2. Pearson correlation coefficients between Cell Cluster Interaction Index (CII) and pattern size.

Distance (D, μm)	Pattern Size (W, μm)	Correlation Coefficient (r)
	$\leq 20 \mu\text{m} \times 20 \mu\text{m}$	-0.45**
10	$>20 \mu\text{m} \times 20 \mu\text{m}$	0.93**
	$\leq 20 \mu\text{m} \times 20 \mu\text{m}$	-0.23*
15	$>20 \mu\text{m} \times 20 \mu\text{m}$	0.94**
	$\leq 20 \mu\text{m} \times 20 \mu\text{m}$	-0.20
20	$>20 \mu\text{m} \times 20 \mu\text{m}$	0.93**
	$\leq 20 \mu\text{m} \times 20 \mu\text{m}$	-0.20
30	$>20 \mu\text{m} \times 20 \mu\text{m}$	0.93**
	$\leq 20 \mu\text{m} \times 20 \mu\text{m}$	-0.25*
40	$>20 \mu\text{m} \times 20 \mu\text{m}$	0.92**
	$\leq 20 \mu\text{m} \times 20 \mu\text{m}$	-0.47**
50	$>20 \mu\text{m} \times 20 \mu\text{m}$	0.95**

* $P < 0.05$.

** $P < 0.0001$.

Table 3-3. Biofilm formation of *E coli* RP437 and its isogenic mutants on patterned surfaces.

Genotype	Attachment on patterns	Interaction among cell clusters
Wild-type	Fully covered patterns	Normal interaction
<i>ΔcheY</i>	Barely covered	No interaction
<i>Δtap</i>	Barely covered	No interaction
<i>motB</i> point mutant	Relatively normal cell clusters (slightly less coverage than the wild type)	Significantly reduced interaction
<i>ΔmotB</i>	Barely covered	No interaction
<i>ΔluxS</i>	Relatively normal cell clusters (slightly less coverage than the wild type)	Significantly reduced interaction

3.10 REFERENCES

- 1 **Mah, T. F. et al.** 2003. A genetic basis for *Pseudomonas aeruginosa* biofilm antibiotic resistance. *Nature* **426**: 306-310.
- 2 **Hoiby, N., Bjarnsholt, T., Givskov, M., Molin, S., Ciofu, O.** 2010. Antibiotic resistance of bacterial biofilms. *Int J Antimicrob Agents* **35**: 322-332.
- 3 **Davey, M. E., O'Toole G, A.** 2000. Microbial biofilms: from ecology to molecular genetics. *Microbiol Mol Biol Rev* **64**: 847-867.
- 4 **Hoyle, B. D., Costerton, J. W.** 1991. Bacterial resistance to antibiotics: the role of biofilms. *Prog Drug Res* **37**: 91-105.
- 5 **Gilbert, P., Alison, D. G., McBain, A. J.** 2002. Biofilms In Vitro and In Vivo: Do Singular Mechanisms Imply Cross-Resistance? *J. Appl. Microbiol. Symp. Suppl.* **92**: 98S–110S.
- 6 **MacKintosh, E. E. J. D. P., Roger E. Marchant, R. E., Anderson, J. M.** 2006. Effects of Biomaterial Surface Chemistry on the Adhesion and Biofilm Formation of *Staphylococcus epidermidis* in vitro. *J. Biomed. Mater. Res. Part A* **78A**: 837-842.
- 7 **Katsikogianni, M., Missirlis, Y. F.** 2004. Concise Review of Mechanisms of Bacterial Adhesion to Biomaterials and of Techniques Used in Estimating Bacterial-Material Interactions. 37-57.
- 8 **Walker, J. Surman, S., Jass, J.** 2000. Biofilms and Biofouling. In *Industrial Biofouling: Detection, Prevention and Control* 1-12.
- 9 **Stewart, P. S., Franklin, M. J.** 2008. Physiological heterogeneity in biofilms. *Nat Rev Microbiol* **6**: 199-210.
- 10 **Weibel, D. B., Diluzio, W. R., Whitesides, G. M.** Microfabrication Meets Microbiology. *Nature Rev. Microbiol.* **5**: 209-218.
- 11 **Heydorn, A. B. E., Kato, J., Hentzer, M., Parsek, M. R., Tolker-Nielsen, T., Givskov, M., Molin, S.** 2002. Statistical Analysis of *Pseudomonas aeruginosa* Biofilm Development: Impact of Mutations in Genes Involved in Twitching Motility, Cell-to-Cell Signaling, and Stationary-Phase Sigma Factor Expression. *Appl. Environ. Microbiol.* **68**: 2008-2017.
- 12 **Mah, T. F., O'Toole, G. A.** 2001. Mechanisms of biofilm resistance to antimicrobial agents. *Trends Microbiol* **9**: 34-39.
- 13 **Lewis, K.** 2001. Riddle of biofilm resistance. *Antimicrob Agents Chemother* **45**: 999-1007.
- 14 **Hou, S. Y., Burton, E. A., Simon, K. A., Blodgett, D., Luk, Y. Y., Ren, D. C.** 2007. Inhibition of *Escherichia coli* Biofilm Formation by Self-Assembled Monolayers of Functional Alkanethiols on Gold. *Appl. Environ. Microbiol.* **73**: 4300-4307.
- 15 **Burton, E. A., Sirnon, K. A., Hou, S. Y., Ren, D. C., Luk, Y. Y.** 2009. Molecular Gradients of Bioinertness Reveal a Mechanistic Difference between Mammalian Cell Adhesion and Bacterial Biofilm Formation. *Langmuir* **25**: 1547-1553.
- 16 **Parkinson, J. S., Houts, S. E.** 1982. Isolation and Behavior of *Escherichia-Coli* Deletion Mutants Lacking Chemotaxis Functions. *J. Bacteriol.* **151**: 106-113.

- 17 **Han, Y., Hou, S., Simon, K. A., Ren, D., Luk, Y. Y.** 2008. Identifying the Important Structural Elements of Brominated Furanones for Inhibiting Biofilm Formation by *Escherichia coli*. *Bioorg Med Chem Lett* **18**: 1006-1010.
- 18 **Wu, J., Hou, S. Y., Ren, D. C., Mather, P. T.** 2009. Antimicrobial Properties of Nanostructured Hydrogel Webs Containing Silver. *Biomacromolecules* **10**: 2686-2693.
- 19 **Hou, S. Y., Zhou, C. H., Liu, Z. G., Young, A. W., Shi, Z. H., Ren, D. C., Kallenbach, N. R.** 2009. Antimicrobial Dendrimer Active against *Escherichia coli* Biofilms. *Bioorg Med Chem Lett* **19**: 5478-5481.
- 20 **Hou, S., Liu, Z., Young, A. W., Mark, S. L., Neville R. Kallenbach, N. R., Ren, D. C.** 2010. Effects of Trp- and Arg-Containing Antimicrobial-Peptide Structure on Inhibition of *Escherichia coli* Planktonic Growth and Biofilm Formation. *Appl. Environ. Microbiol.* **76**: 1967-1974.
- 21 **Keren, I., Shah, D., Spoering, A., Kaldalu, N., Lewis, K.** 2004. Specialized persister cells and the mechanism of multidrug tolerance in *Escherichia coli*. *Journal of bacteriology* **186**: 8172-8180.
- 22 **Chong, L.** 2001. *Molecular Cloning - A Laboratory Manual*, 3rd edition. Science **292**: 446-446.
- 23 **Hou, S. Y., Gu, H., Smith, C., Ren, D. C.** 2011. Microtopographic patterns affect *Escherichia coli* biofilm formation on poly(dimethylsiloxane) surfaces. *Langmuir* **27**: 2686-2691.
- 24 **Mrksich, M., Dike, L. E., Tien, J., Ingber, D. E., Whitesides, G. M.** 1997. Using Microcontact Printing to Pattern the Attachment of Mammalian Cells to Self-Assembled Monolayers of Alkanethiolates on Transparent Films of Gold and Silver. *Exp Cell Res* **235**: 305-313.
- 25 **Thery, M., Piel, M.** 2009. Adhesive Micropatterns for Cells: a Microcontact Printing Protocol. *Cold Spring Harb Protoc.*, **4**: 1-11.
- 26 **Heydorn, A., Nielsen, A. T., Hentzer, M., Sternberg, C., Givskov, M., Ersboll, B. K., Molin, S.** 2000. Quantification of Biofilm Structures by the Novel Computer Program COMSTAT. *Microbiol-Uk* **146**: 2395-2407.
- 27 **Turner, L., Ryu, W. S., Berg, H. C.** 2000. Real-Time Imaging of Fluorescent Flagellar Filaments. *J. Bacteriol.* **182**: 2793-2801.
- 28 **Chen, C. Y., Nace, G. W., Irwin, P. L.** 2003. A 6 x 6 drop plate method for simultaneous colony counting and MPN enumeration of *Campylobacter jejuni*, *Listeria monocytogenes*, and *Escherichia coli*. *Journal of microbiological methods* **55**: 475-479.
- 29 **Bertin, P. et al.** 1994. The H-Ns Protein Is Involved in the Biogenesis of Flagella in *Escherichia-Coli*. *Journal of bacteriology* **176**: 5537-5540.
- 30 **Friedlander, R. S. et al.** 2013. Bacterial flagella explore microscale hummocks and hollows to increase adhesion. *Proceedings of the National Academy of Sciences of the United States of America* **110**: 5624-5629.
- 31 **Prigent-Combaret, C., Prensier, G., Le Thi, T. T., Vidal, O., Lejeune, P., Dorel, C.** 2000. Developmental Pathway for Biofilm Formation in Curli-producing *Escherichia coli* Strains: Role of Flagella, Curli and Colanic acid. *Environ. Microbiol.* **2**: 450-464.

- 32 **Vidal, O. et al.** 1998. Isolation of an *Escherichia coli* K-12 mutant strain able to form biofilms on inert surfaces: Involvement of a new ompR allele that increases curli expression. *Journal of bacteriology* **180**: 2442-2449.
- 33 **Chapman, M. R. et al.** 2002. Role of *Escherichia coli* curli operons in directing amyloid fiber formation. *Science* **295**: 851-855.
- 34 **Kikuchi, T., Mizunoe, Y., Takade, A., Naito, S., Yoshida, S.** 2005. Curli fibers are required for development of biofilm architecture in *Escherichia coli* K-12 and enhance bacterial adherence to human uroepithelial cells. *Microbiol Immunol* **49**: 875-884.
- 35 **Saldana, Z. et al.** 2009. Synergistic role of curli and cellulose in cell adherence and biofilm formation of attaching and effacing *Escherichia coli* and identification of Fis as a negative regulator of curli. *Environmental microbiology* **11**: 992-1006.
- 36 **Hull, R. A., Gill, R. E., Hsu, P., Minschew, B. H., Falkow, S.** 1981. Construction and expression of recombinant plasmids encoding type 1 or D-mannose-resistant pili from a urinary tract infection *Escherichia coli* isolate. *Infect Immun* **33**: 933-938.
- 37 **Krogfelt, K. A., Bergmans, H., Klemm, P.** 1990. Direct Evidence That the FimH Protein Is the Mannose-Specific Adhesin of *Escherichia-Coli* Type-1 Fimbriae. *Infection and Immunity* **58**: 1995-1998.
- 38 **Austin, J. W., Sanders, G., Kay, W. W., Collinson, S. K.** 1998. Thin aggregative fimbriae enhance *Salmonella enteritidis* biofilm formation. *Fems Microbiol Lett* **162**: 295-301.
- 39 **Tinanoff, N., Brady, J. M., Gross, A.** 1976. The effect of NaF and SnF2 mouthrinses on bacterial colonization of tooth enamel: TEM and SEM studies. *Caries Res* **10**: 415-426.
- 40 **Dey, S.** 1993. A new rapid air-drying technique for scanning electron microscopy using tetramethylsilane: application to mammalian tissue. *Cytobios* **73**: 17-23.
- 41 **Dubey, G. P., Ben-Yehuda, S.** 2011. Intercellular nanotubes mediate bacterial communication. *Cell* **144**: 590-600.
- 42 **Blair, D. F., Kim, D. Y., Berg, H. C.** 1991. Mutant MotB Proteins in *Escherichia-Coli*. *J Bacteriol* **173**: 4049-4055.
- 43 **Schauder, S., Shokat, K., Surette, M. G., Bassler, B. L.** 2001. The LuxS Family of Bacterial Autoinducers: Biosynthesis of a Novel Quorum-Sensing Signal Molecule. *Mol Microbiol* **41**: 463-476.
- 44 **Heurlier, K. R. H. a. K.** 2008. Establishing Bacterial Communities by 'Word of Mouth': LuxS and Autoinducer 2 in Biofilm Development. *Nature Rev. Microbiol.* **6**: 635-643.
- 45 **Ling, H. A. K., Tan, M. H., Qi, X. B.** 2010. Mathew Wook Chang. The Absence of the *luxS* Gene Increases Swimming Motility and Flagella Synthesis in *Escherichia coli* K12. *Biochem. Biophys. Res. Commun.* **401**: 521-526.
- 46 **Chen, X., Zhang, M., Zhou, C., Kallenbach, N. R., Ren, D. C.** 2011. Control of bacterial persister cells by Trp/Arg-containing antimicrobial peptides. *Applied and environmental microbiology* **77**: 4878-4885.
- 47 **O'Toole, G. A., Kolter, R.** 1998. Flagellar and Twitching Motility are Necessary for *Pseudomonas aeruginosa* Biofilm Development. *Mol Microbiol* **30**: 295-304.

- 48 **lausen, M., Heydorn, A., Ragas, P., Lambertsen, L., Aaes-Jorgensen, A.,
Molin, S., Tolker-Nielsen, T.** 2003. Biofilm Formation by *Pseudomonas
aeruginosa* Wild Type, Flagella and Type IV pili Mutants. *Mol Microbiol* **48**:
1511-1524.
- 49 **Hou, S. Y., Burton, E. A., Wu, R. L., Luk, Y. Y., Ren, D. C.** 2009. Prolonged
Control of Patterned Biofilm Formation by Bio-Inert Surface Chemistry. *Chem
Commun* 1207-1209.
- 50 **Kohanski, M. A., Dwyer, D. J., Collins, J. J.** 2010. How antibiotics kill bacteria:
from targets to networks. *Nat Rev Microbiol* **8**: 423-435.
- 51 **Lewis, K.** 2001. Riddle of Biofilm Resistance. *Antimicrob Agents Ch* **45**: 999-
1007.
- 52 **Kaldalu, N., Mei, R., Lewis, K.** 2004. Killing by ampicillin and ofloxacin
induces overlapping changes in *Escherichia coli* transcription profile. *Antimicrob
Agents Chemother* **48**: 890-896.
- 53 **Blair, D. F., Kim, D. Y., Berg, H. C.** 1991. Mutant MotB Proteins in
Escherichia-Coli. *J Bacteriol* **173**: 4049-4055.
- 54 **Scharf, B. E., Fahrner, K. A., Turner, L., Berg, H. C.** 1998. Control of
Direction of Flagellar Rotation in Bacterial Chemotaxis. *Proc. Natl. Acad. Sci.
U.S.A.* **95**: 201-206.
- 55 **Samuel, A. D., Berg, H. C.** 1996. Torque-Generating Units of the Bacterial
Flagellar Motor Step Independently. *Biophys J* **71**: 918-923.
- 56 **Liu, X. X., Parales, R. E.** 2008. Chemotaxis of *Escherichia coli* to Pyrimidines: a
New Role for the Signal Transducer *tap*. *J. Bacteriol.* **190**: 972-979.
- 57 **Yamamoto, K., Macnab, R. M., Imae, Y.** 1990. Repellent Response Functions
of the Trg and Tap Chemoreceptors of *Escherichia coli*. *J. Bacteriol.* **172**: 383-
388.
- 58 **Park, S., Wolanin, P. M., Yuzbashyan, E. A., Lin, H., Darnton, N. C., Stock,
J. B., Silberzan, P., Austin, R.** 2003. Influence of Topology on Bacterial Social
Interaction. *P Natl Acad Sci USA* **100**: 13910-13915.
- 59 **Diao, J. P., Young, L., Kim, S., Fogarty, E. A., Heilman, S. M., Zhou, P.,
Shuler, M. L., Wu, M. M., DeLisa, M. P.** 2006. A Three-Channel Microfluidic
Device for Generating Static Linear Gradients and its Application to the
Quantitative Analysis of Bacterial Chemotaxis. *Lab Chip* **6**: 381-388.

CHAPTER 4

MICROTOPOGRAPHIC PATTERNS AFFECT *ESCHERICHIA COLI* BIOFILM FORMATION ON POLY(DIMETHYLSILOXANE) SURFACES

Part of this chapter has been published as Shuyu Hou, Huan Gu, Cassandra Smith, and Dacheng Ren. 2011. Patterned biofilm formation reveals a mechanism for structural heterogeneity in bacterial biofilms. *Langmuir*. 27 (6): 2686–2691. Reproduced by permission of American Chemical Society Publication. Shuyu Hou initiated this study.

4.1 ABSTRACT

Biofilm cells are highly resistant to antibiotics and biofilms are involved in 80% of human bacterial infections. To better understand the mechanism of bacteria-surface interaction and biofilm formation, a series of poly(dimethylsiloxane) (PDMS) surfaces with microtopographic patterns were created to systematically vary the pattern size and inter-pattern distance. *E. coli* biofilm formation on these surfaces was studied to understand the effects of surface topography on bacterial adhesion and subsequent biofilm formation. In a previous study in Ren lab¹, *E. coli* RP437/pRSH103 with constitutive expression of red fluorescence protein was found to preferentially attach and form biofilms in the valleys on upright PDMS surfaces regardless the size of protruding features and inter-pattern distance. In addition, significant biofilm formation on the top of plateaus was only found when the plateaus were larger than $20\ \mu\text{m} \times 20\ \mu\text{m}$. In this study, the biofilm formation on inverted patterned surfaces was investigated to specifically study bacterial adhesion without gravity driven settlement. It was found that *E. coli* cells also prefer to attach and form biofilms in valleys. A threshold dimension was also found for biofilm formation on top of plateaus, although it is $40\ \mu\text{m} \times 40\ \mu\text{m}$ for inverted surface. This finding suggests that a critical dimension of a flat surface is required for biofilm formation without physical confinement. Inspired by these results, we prepared PDMS surfaces with hexagon shaped microtopographic patterns smaller than the critical dimension with $2\ \mu\text{m}$ inter-pattern distance. Biofilm formation on these surfaces was significantly reduced compared to the flat PDMS surfaces.

4.2 INTRODUCTION

Biofilms are sessile communities of microorganisms attached to solid surfaces and encased in self-produced extracellular polymeric substrate (EPS)²⁻⁵. Biofilm formation is a dynamic process that includes initial attachment, microcolony formation, maturation, and dispersion⁶⁻⁹. The process of biofilm formation involves numerous changes in gene and protein expression, which are highly sensitive to environmental conditions such as surface chemistry and topography^{10,11}. Surface topography can be described using surface roughness (two-dimensional) and configuration (three-dimensional). Surface roughness, Ra, is the arithmetical mean deviation of the distance between the peak and valley¹². Surface roughness has been reported to influence bacterial adhesion. For example, Taylor *et al.*¹³ reported that the attachment of *P. aeruginosa* and *S. epidermidis* on polymethyl methacrylate (PMMA) increased significantly when Ra increased from 0.04 to 1.24 μm and bacterial adhesion decreased when Ra increased from 1.86 to 7.89 μm . In comparison, Hilbert *et al.*¹² reported that the increase of Ra from 0.01 to 0.9 μm has no effects on the adhesion of *P. sp.*, *L. monocytogenes*, and *C. lipolytica* on stainless steel surfaces. The different effects of surface roughness on bacterial adhesion reported to date could be due to the differences in the property of surfaces and the intrinsic characteristics of biofilm formed by different bacterial strains. Although these studies provide valuable information about the correlation between surface roughness and cell adhesion, these studies examined surfaces that were randomly roughened and they did not examine surfaces with specific features.

To better describe the topographic features in three dimensions, a well-defined surface configuration is needed. Thanks to the development of microtechnology, soft

materials with well-defined micro-structures can be generated and used to study the effects of surface topography on bacterial adhesion and biofilm formation¹⁴. Surface topography was reported to be able to influence bacterial adhesion and subsequent biofilm formation¹⁵⁻¹⁹. Recently, surface topography was also used in the engineering of anti-adhesive surfaces as an important environmental factor. For example, Chung *et al.*¹⁹ used engineered poly (dimethylsiloxane) elastomer (PDMS_e) surfaces with microtopography (2 μm tall, 4 μm to 6 μm long rod-shaped microstructures with 2 μm inter-pattern distance) to disrupt the colonization and biofilm formation of *S. aureus* for up to 21 days. Despite the increasing number of studies on the overall attachment of bacteria on surfaces with repeating geometric topographic patterns, the mechanism of the observed effects is still not well understood.

Recently, a former student (Shuyun Hou) in Ren lab used poly(dimethylsiloxane) PDMS surfaces with systematically varied microtopographic patterns to study the effects of surface microtopography on bacterial adhesion and biofilm formation. The shape and size of topographic patterns and the inter-pattern distance were systematically varied. Hou *et al.*¹ reported that *E. coli* preferentially attach and form biofilms in the valleys on these surfaces and a threshold of 20 $\mu\text{m} \times 20 \mu\text{m}$ was found for significant biofilm formation on top of the square shaped plateaus. In this study, we further investigated the effects using inverted pattern and designed new surfaces for antifouling activities.

4.3 MATERIALS AND METHOD

4.3.1 Bacterial strains and medium

E. coli RP437²⁰, a chemotaxis wild-type strain that is commonly used in biofilm study, and its motility mutant RP3087²¹ tagged with constitutive *rfp* on plasmid pRSH103^{1,22} were used to investigate bacteria-surface interactions. The wild-type *E. coli* and its motility mutant were routinely grown at 37 °C with 200 rpm shaking in Lysogeny Broth (LB) containing 10 g/L trypton, 5 g/L yeast extract, and 10 g/L sodium chloride²³. Tetracycline (30 µg/mL) was supplemented in the growth medium to maintain the plasmid pRSH103.

4.3.2 PDMS surfaces preparation

The PDMS surfaces with microtopographic patterns used in this study were obtained by transferring the complementary 10 µm deep (H) negative topographies from the silicon wafers etched via photolithography as reported previously^{1,24}. Both square shaped and hexagon shaped topographic patterns were designed. The side width (W) of square shaped protruding features was set to be 2, 5, 10, 15, 20, 30, 40, 50, or 100 µm and the inter-pattern distance (D) was systematically varied (2, 5, 10, 15, 20, 30, 40, 50, or 100 µm). The side width (W) of hexagon shaped topographic patterns and the inter-pattern distance were also systematically varied as 2, 5, 10, 15, or 20 µm and all combination were tested.

4.3.3 Biofilm formation and imaging analysis

To study the effects of surface topography on bacterial cell-surface interactions and biofilm formation, the biofilms of *E. coli* RP437/pRSH103 were formed on PDMS surfaces modified with microtopographic patterns. The PDMS surfaces were sterilized by

soaking in 190 proof ethanol for 30 min, dried in a 50°C oven for 40 min, and transferred to a sterile petri dish containing 20 mL LB medium supplemented with 30 µg/mL tetracycline. An overnight culture of *E. coli* RP437/pRSH103 was used to inoculate 20 mL LB medium into optical density at 600 nm (OD₆₀₀) of 0.05. Biofilms were grown at 37 °C for 24 h.

In addition to the wild-type strain, biofilm formation of the motility mutant *E. coli* RP3087/pRSH103 on the PDMS surfaces with 100 µm × 100 µm square shaped microtopographic patterns was also studied by following the procedure described above to understand the role of motility during bacterial cell-surface attachment.

Biofilms of the wild-type strain were also grown on inverted PDMS surfaces to study in the absence of gravity driven settlement. The PDMS surfaces and two pieces of small microscopic glass slides were sterilized as described above. The sterilized PDMS surfaces were put on the bottom of a petri dish with microtopographic patterns facing down and supported with two sterilized microscope slides to create a 1 mm gap between the PDMS surface and the bottom of the dish. The petri dish was incubated at 37°C for 24 h.

After incubation, the PDMS surfaces were gently washed three times with 0.85% NaCl solution (change to fresh solution every time) and visualized with a Zeiss Imager M1 fluorescence microscope (Carl Zeiss Inc., Berlin, Germany). The surface coverage and biomass of biofilms were quantified using the COMSTAT software written on a Matlab platform²⁵. At least five spots were randomly picked and imaged from each surface. Each sample had at least three biological replicates and consistent results were obtained.

4.4 RESULTS

4.4.1 Effects of surface topography on bacterial cell-surface interaction

To study the effects of surface topography on bacterial adhesion and biofilm formation, PDMS surfaces with systematically varied microtopographic patterns were prepared (Fig. 4-1). By challenging these PDMS surfaces with *E. coli* RP437/pRSH103 for 24 h, it is found previously that *E. coli* cells prefer to attach and form biofilms in the valleys between close topographic patterns (Fig. 4-2A&B). Besides, there appeared to be a threshold dimension of protruding features to allow significant bacterial adhesion and biofilm formation on top of upright protruding features (Fig. 4-2C). The threshold dimension was $20\ \mu\text{m} \times 20\ \mu\text{m}$ in this experimental system.

To understand if the higher cell density in the valleys between close topographic patterns was due to gravity-driven settlement or because bacterial cells can actively choose where to attach, *E. coli* RP437/pRSH103 biofilm was also formed on inverted PDMS surfaces with systematically varied microtopography in this study. The surface coverage of *E. coli* RP437/pRSH103 biofilm cells on inverted PDMS surfaces were significantly lower compared to that on upright PDMS surfaces. For example, the surface coverage on flat upright PDMS surface was $11.6 \pm 1.0\%$ but the surface coverage on inverted PDMS surface was $2.6 \pm 0.3\%$. Consistent with the results obtained from upright PDMS surfaces¹, *E. coli* cells also preferred to attach to the valleys than on the top of topographic patterns. A threshold dimension for significant bacterial adhesion on the top of topographic patterns was also observed for inverted PDMS surfaces (Fig. 4-3). However, instead of $20\ \mu\text{m} \times 20\ \mu\text{m}$ for upright pattern, the threshold dimension of

protruding patterns for bacterial adhesion and biofilm formation was $40\ \mu\text{m} \times 40\ \mu\text{m}$ on inverted PDMS surfaces (Fig. 4-4).

To further corroborate the results that the influence of surface topography on bacterial adhesion was not simply due to gravity-driven settlement, we also test the bacterial adhesion and biofilm formation of an isogenic nonmotile mutant, *E. coli* RP3087/pRSH103, on both upright and inverted PDMS surfaces with $100\ \mu\text{m} \times 100\ \mu\text{m}$ topographic patterns. The surface coverage of the mutant on upright $100\ \mu\text{m} \times 100\ \mu\text{m}$ patterns was lower than that of the wild-type strain. For example, the surface coverage was $3.2 \pm 0.5\%$ (Fig. 4-5A&B) and $10.2 \pm 1.7\%$ (Fig. 4-2) for the nonmotile mutant and the wide-type strain, respectively. The defects of this mutant in adhesion were also observed for inverted PDMS surfaces because the mutant cells barely attached to either the valleys or the top of topographic patterns (Fig. 4-5C).

4.4.2 Reducing biofouling by changing surface topography

As described above, we observed that there is a threshold dimension of protruding patterns that can allow bacteria to attach to the top of the topographic patterns. Bacteria barely attached to the top of topographic patterns with size smaller than the threshold dimension. This suggests that bacterial adhesion on a flat surface requires a minimum surface area, which is 200 times of the foot print of each individual of each individual cell in our study. This finding inspired us to design antifouling surfaces by engineering specific topographic features with a size smaller than the threshold dimension and inter-pattern distance less than the length of a single bacterial cell. We expect that the biomass on these surfaces can be significantly reduced. By testing the biofilm formation of *E. coli* RP437/pRSH103 on PDMS surfaces with hexagon patterns, we found that the biomass of

biofilms formed on PDMS surfaces with hexagon patterns was smaller than that on flat PDMS surfaces (Fig. 4-6). For example, when the side width of the hexagon shaped pattern was 15 μm and the inter-pattern distance was 2 μm , the biomass of the biofilms was $0.1 \pm 0.04 \mu\text{m}^3/\mu\text{m}^2$ that was 7-fold lower than the biomass of the biofilms formed on the flat PDMS surfaces ($0.8 \pm 0.2 \mu\text{m}^3/\mu\text{m}^2$) (Fig. 4-7A). Consistent with the results obtained using PDMS surfaces with square shaped microtopographic patterns, *E. coli* RP437/pRSH103 cells also preferred to attach to the valleys between hexagon features. To understand if the shape of protruding features also plays a role, we compared the biomass of the biofilms formed on PDMS surfaces with hexagon and square shaped topographic patterns of similar size (Fig. 4-7B). The biomass of biofilms formed on PDMS surfaces with 15 $\mu\text{m} \times 15 \mu\text{m}$ square shaped topographic patterns ($225 \mu\text{m}^2$) was similar to that on PDMS surfaces with hexagon shaped topographic patterns with side width of 10 μm ($259 \mu\text{m}^2$). They were all smaller than the biomass of biofilms formed on flat PDMS surfaces.

More interestingly, there appeared to be a dimension of hexagon shaped patterns that can efficiently reduce bacterial adhesion and biofilm formation when the inter-pattern distance was 2 μm (Fig. 4-7A). The lowest biomass of biofilms on PDMS surfaces was obtained when the side width of hexagon shaped patterns was 15 μm . For example, the biomass of biofilms formed on PDMS surfaces with hexagon patterns was 0.6 ± 0.08 , 0.3 ± 0.05 , 0.2 ± 0.06 , 0.1 ± 0.04 , and $0.3 \pm 0.04 \mu\text{m}^3/\mu\text{m}^2$, when the side width was set to be 2, 5, 10, 15, and 20 μm (all with 2 μm inter-pattern distance), respectively.

To test if the observed phenomenon was due to gravity-driven settlement, we also tested the biofilm formation of *E. coli* RP437/pRSH103 on inverted PDMS surfaces with microtopographic patterns. The results showed that *E. coli* RP437/pRSH103 cells still preferred to attach to the valleys between topographic patterns but the cell density in biofilms on inverted PDMS surfaces was significantly reduced (Fig. 4-8). Therefore, instead of the biomass of biofilms, cell numbers in the biofilms formed on the inverted PDMS surfaces were used to evaluate the bacterial adhesion (Fig. 4-9). There was still a threshold dimension of hexagon-shaped patterns that can efficiently reduce bacterial adhesion and biofilm formation, except that the lowest cell number was observed when the side width of the hexagon shaped patterns was 10 μm instead of 15 μm for upright surfaces (Fig. 4-9).

4.5 DISCUSSION

To study the effects of surface topography on bacterial adhesion, *E. coli* RP437/pRSH103 biofilms were formed on PDMS surfaces with systematically varied microtopographic patterns. Cells were found to prefer to attach to the valleys, which is consistent with the attachment of mammalian cells to 1 μm deep and 0.5-10 μm wide groove and the attachment of zoospores on the grooved floor of the surfaces with protruding ridges and pillars^{26,27}.

To test whether the observed phenomenon was simply a gravity-driven settlement, biofilm formation of *E. coli* RP437/pRSH103 on inverted PDMS surfaces with the same patterns was investigated. Similar results were obtained except that surface coverage on the inverted PDMS surfaces was lower than that on upright PDMS surfaces

and the threshold dimension increased to $40\ \mu\text{m} \times 40\ \mu\text{m}$. These results indicate that gravity does facilitate cell adhesion but threshold dimensions are intrinsic factors for biofilm formation, rather than simply the results of gravity. To corroborate this result, the biofilm formation of a nonmotile mutant, *E. coli* RP3087/pRSH103, on both upright and inverted PDMS surfaces was studied by following the same protocol. The results suggest that motility is critical to bacterial adhesion and the higher cell density in the valleys is not only due to gravity-driven settlement. Interestingly, there appeared to be a threshold dimension of protruding features that can allow significant bacterial adhesion on top of the topographic patterns. The threshold dimensions $20\ \mu\text{m} \times 20\ \mu\text{m}$ (for upright square patterns) and $40\ \mu\text{m} \times 40\ \mu\text{m}$ (for inverted square patterns) are significantly larger than the size of a single *E. coli* cell, which suggests that cell-cell interactions are essential for the formation of multicellular structures. Previously, by tailoring surface chemistry with self-assembled monolayers (SAMs) of alkanethiol presenting different functional groups, we observed that more interactions are formed between cell clusters when patterns are larger than $20\ \mu\text{m} \times 20\ \mu\text{m}$. This is similar to the threshold dimensions found in this study. Further study is needed to understand the mechanism of such thresholds.

Recently, surface topography has been used as a critical parameter in engineering antifouling surfaces¹⁹. The above finding of threshold also inspired us to design new surfaces to reduce bacterial adhesion. By quantifying the biomass of biofilms formed on PDMS surfaces with hexagon shaped topographic patterns, we found that PDMS surfaces with $10\ \mu\text{m}$ tall hexagon shaped topographic features can reduce the total biomass of biofilms, especially when the inter-pattern distance was set to be $2\ \mu\text{m}$. The shape of topographic features does not appear to be important. However, the fluorescence images

of the *E. coli* RP437/pRSH103 biofilms on PDMS surfaces, especially on inverted PDMS surfaces (Fig. 4-8), suggests that the reduction of total biomass of the biofilms formed on PDMS surfaces modified with hexagon shaped patterns with 2 μm inter-patterned was partially due to the interruption of cell-cell interaction. While the hexagon shape does not affect the adhesion on the top of these features, it appeared that this design prevents strong cell-cell interaction. Further studies are necessary to understand the mechanism behind this phenomenon.

While our 10 μm tall hexagon patterns can reduce biofilm formation, Frieland *et al.*¹⁷ reported that PDMS surfaces with 2.7 μm tall hexagon shape patterns with 3 μm diameter can promote biofilm formation of *E. coli* ZK2686. The differences between this study and that by Frieland *et al.*¹⁷ could be due to the difference in the heights of patterns and inter-pattern distance used, which are known to influence the hydrophobicity of a surface²⁸. The difference in the heights of pattern may also lead to results with regards to the activities of flagella. Besides, the lowest biomass in our study was observed when the side width of upright hexagon patterns was 15 μm and inter-pattern was 2 μm . The mechanism behind this phenomenon is worth of being further studied to provide better guidance for designing non-fouling surfaces.

4.6 ACKNOWLEDGMENTS

I thank the U.S. National Science Foundation (CAREER-1055644, EFRI-1037186) for financial support. We are grateful to Dr. John S. Parkinson at the University of Utah for providing the strain *E. coli* RP437 and *E. coli* RP3087. I thank Dr. Yan-Yeung Luk at Syracuse University for suggestions on preparation of PDMS surfaces, Cornell

NanoScale Science & Technology Facility for the access to the photolithography facilities, and Dr. Arne Heydorn at the Technical University of Denmark for providing the COMSTAT software. I am grateful to Dr. Shuyun Hou and Aarron Chen for conducting preliminary studies.

4.7 FIGURE CAPTIONS

Figure 4-1. SEM picture of a representative patterned PDMS surface with size $50\ \mu\text{m} \times 50\ \mu\text{m}$ patterns and $30\ \mu\text{m}$ inter-pattern distance (Bar = $20\ \mu\text{m}$).

Figure 4-2. Biofilm formation of *E. coli* RP437/pRSH103 on upright PDMS surfaces with square shaped microtopographic patterns. (A) Three dimensional view of biofilm formation on a PDMS surface with $100\ \mu\text{m}$ (W) \times $100\ \mu\text{m}$ (W) \times $10\ \mu\text{m}$ (H) patterns and $20\ \mu\text{m}$ inter-pattern distance. (B) Representative fluorescence images of *E. coli* RP437/pRSH103 biofilms on upright PDMS surfaces with systematically varied topographies (D = $10\ \mu\text{m}$) (B1-B6) and on smooth PDMS surface (B7) (Bar = $10\ \mu\text{m}$). (C) The surface coverage (mean \pm one standard error) of *E. coli* RP437/pRSH103 biofilms formed on top of face-up protruding patterns. The side width of square features (W) tested was 5, 10, 15, 20, 30, 40, 50, or $100\ \mu\text{m}$. The surface coverage was calculated using COMSTAT software²⁵.

Figure 4-3. Representative fluorescence images of *E. coli* RP437/pRSH103 biofilms on inverted PDMS surfaces with systematically varied microtopography (D = $10\ \mu\text{m}$) (A-G) and on inverted smooth PDMS surface (H) (Bar = $10\ \mu\text{m}$).

Figure 4-4. Surface coverage (mean \pm one standard error) of *E. coli* RP437/pRSH103 biofilms formed on top of inverted protruding patterns. The side width of square features (W) tested was 5, 10, 15, 20, 30, 40, 50, or $100\ \mu\text{m}$ and the inter-pattern distance was 5, 10, 15, or $20\ \mu\text{m}$. The surface coverage was calculated using COMSTAT software²⁵. N=3 biological repeats averaged; at least 15 images were analyzed for each data point.

Figure 4-5. Biofilm formation of *E. coli* RP3087/pRSH103 on PDMS surfaces with 100 $\mu\text{m} \times 100 \mu\text{m}$ topographic patterns. (A) Representative fluorescence image of *E. coli* RP3087/pRSH103 on upright PDMS surfaces (Bar = 20 μm). (B) The surface coverage (mean \pm one standard deviation) of *E. coli* RP3087/pRSH103 biofilms formed on top of upright protruding patterns. The distance was set to be 5, 10, 15, or 20 μm . The surface coverage was calculated using COMSTAT software²⁵. (C) Representative fluorescence images of *E. coli* RP3087/pRSH103 on inverted PDMS surfaces. N=3 biological repeats averaged; at least 15 images were analyzed for each data point.

Figure 4-6. Representative fluorescence images of *E. coli* RP437/pRSH103 biofilms on upright PDMS surfaces modified with hexagon shaped topographic features with different size but the same 2 μm inter-pattern distance (A-E) and on smooth PDMS surfaces (F) (Bar = 10 μm).

Figure 4-7. Biofilm formation of *E. coli* RP437/pRSH103 on upright PDMS surfaces with microtopographic patterns. (A) The biomass (mean \pm one standard deviation) of *E. coli* RP437/pRSH103 biofilms formed on PDMS surfaces with hexagon shaped topographic patterns. The width of hexagon shaped features (W) was set to be 2, 5, 10, 15, or 20 μm and inter-pattern distance (D) was set to be 2, 5, 10, 15, or 20 μm . All combinations were tested. Biomass was calculated using COMSTAT software²⁵. N=3 biological repeats averaged; at least 15 images were analyzed for each data point. (B) Comparison between the biomass (mean \pm one standard deviation) of

biofilms formed on PDMS surfaces with $15\ \mu\text{m} \times 15\ \mu\text{m}$ square shaped topographic patterns ($225\ \mu\text{m}^2$) and on PDMS surfaces with hexagon shaped topographic patterns with side width of $10\ \mu\text{m}$ ($259\ \mu\text{m}^2$). Biomass was calculated using COMSTAT software²⁵. N=3 biological repeats averaged; at least 15 images were analyzed for each data point.

Figure 4-8. Representative fluorescence images of *E. coli* RP437/pRSH103 biofilms on inverted PDMS surfaces modified with hexagon shaped patterns with side width of $20\ \mu\text{m}$ and different inter-pattern distance (A-E) (Bar = $10\ \mu\text{m}$).

Figure 4-9. The number per unit area (mean \pm one standard error) of *E. coli* RP437/pRSH103 cells on inverted PDMS surfaces with systematically varied hexagon shaped microtopographic patterns. The side width (W) of the hexagon patterns was set to be 2, 5, 10, 15, or $20\ \mu\text{m}$ and inter-pattern distance (D) was set to be 2, 5, 10, 15, or $20\ \mu\text{m}$. All combinations were tested. N=3 biological repeats averaged; at least 15 images were analyzed for each data point.

4.8 FIGURES

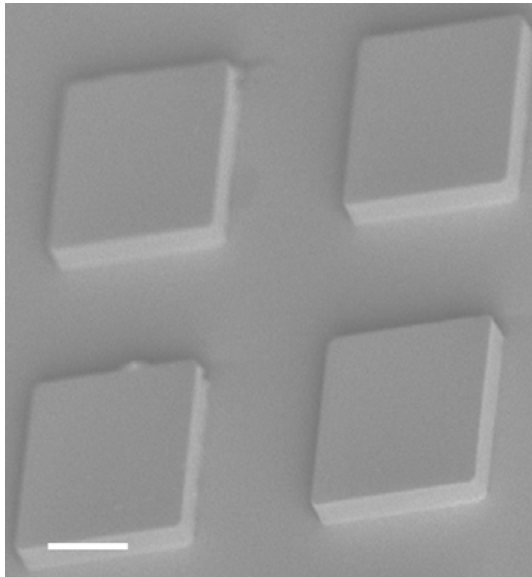


Figure 4-1

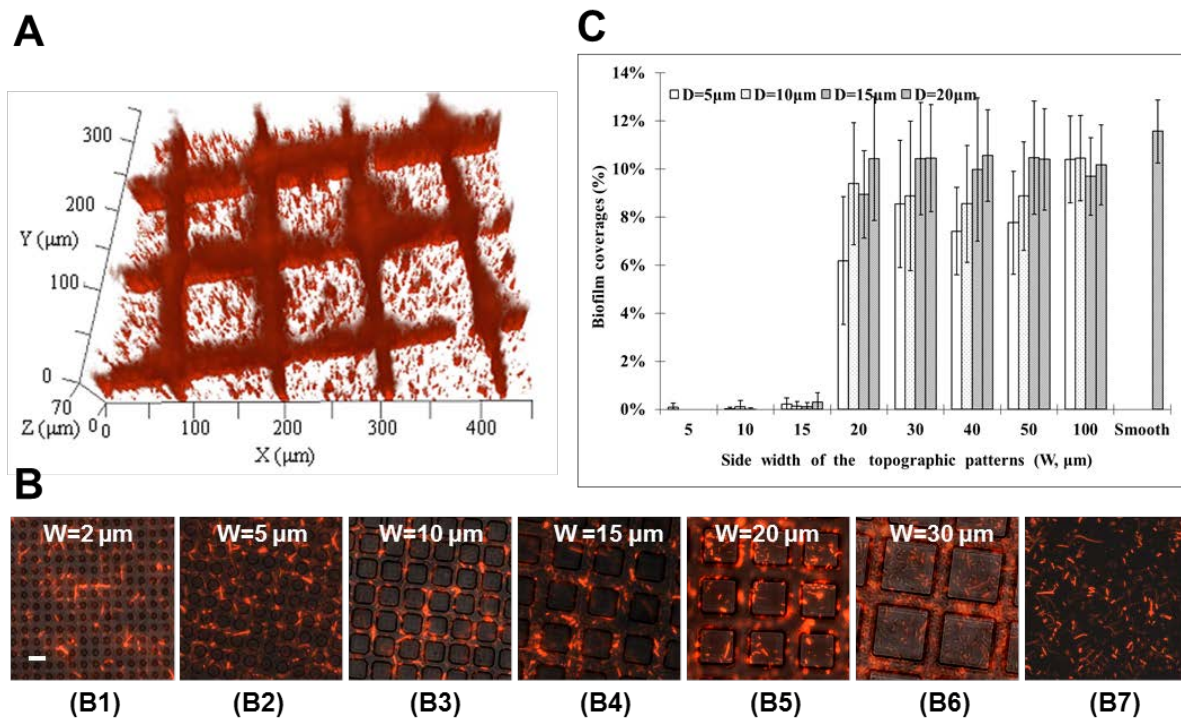


Figure 4-2 (Generated by Shuyu Hou)

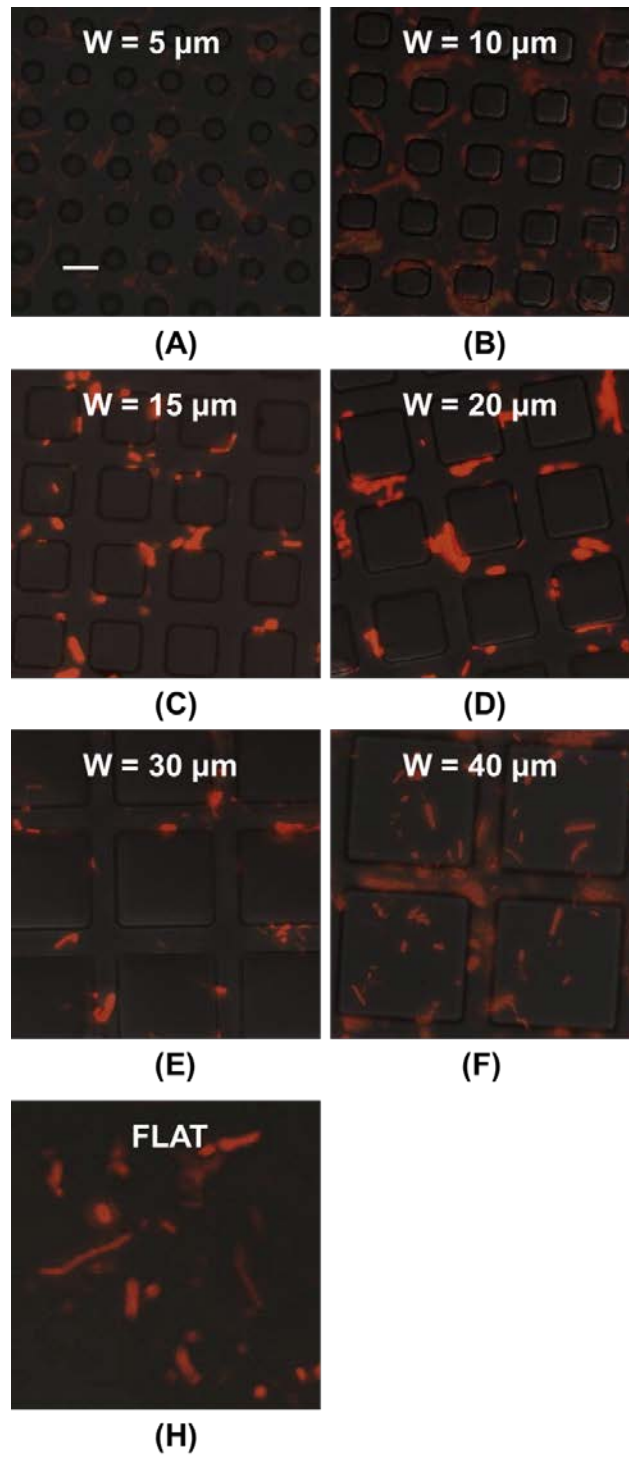


Figure 4-3

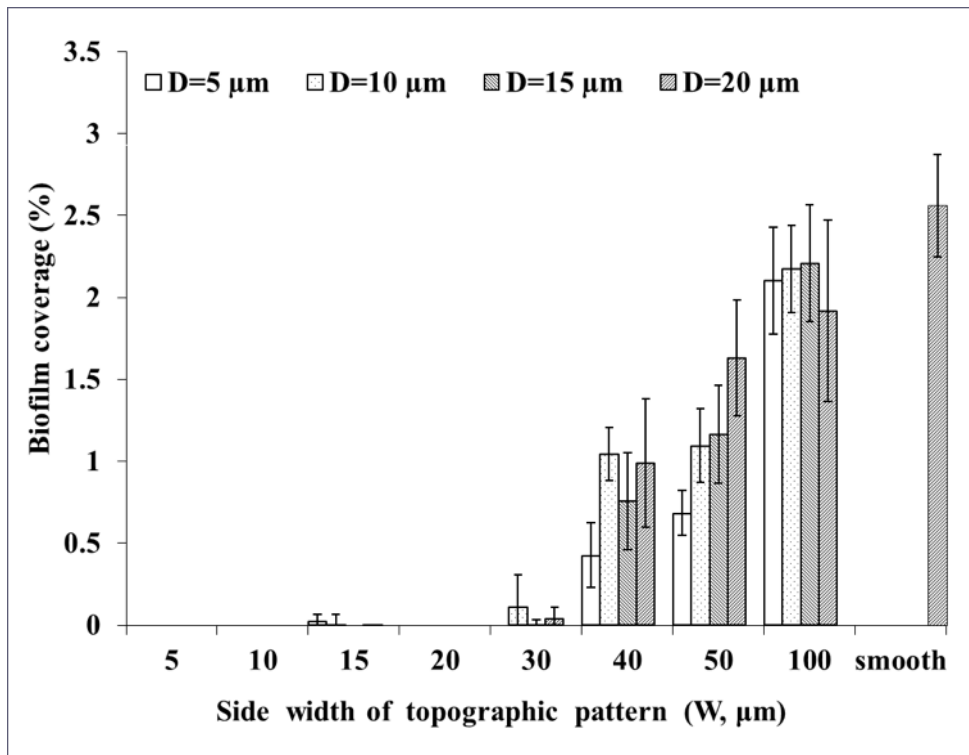


Figure 4-4

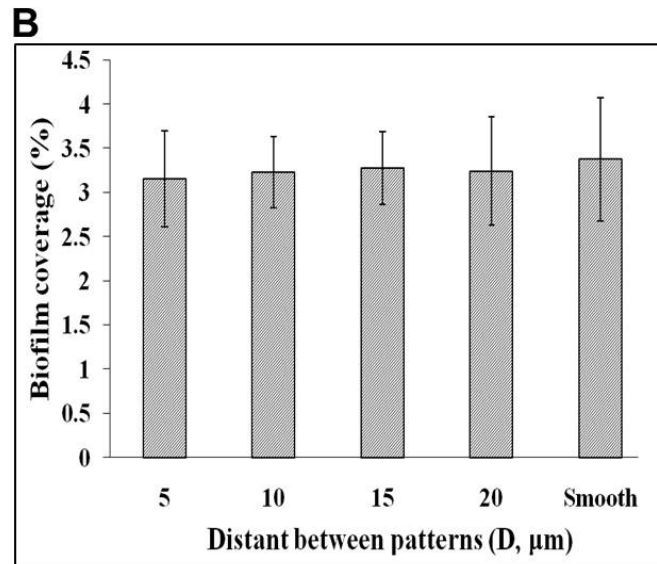
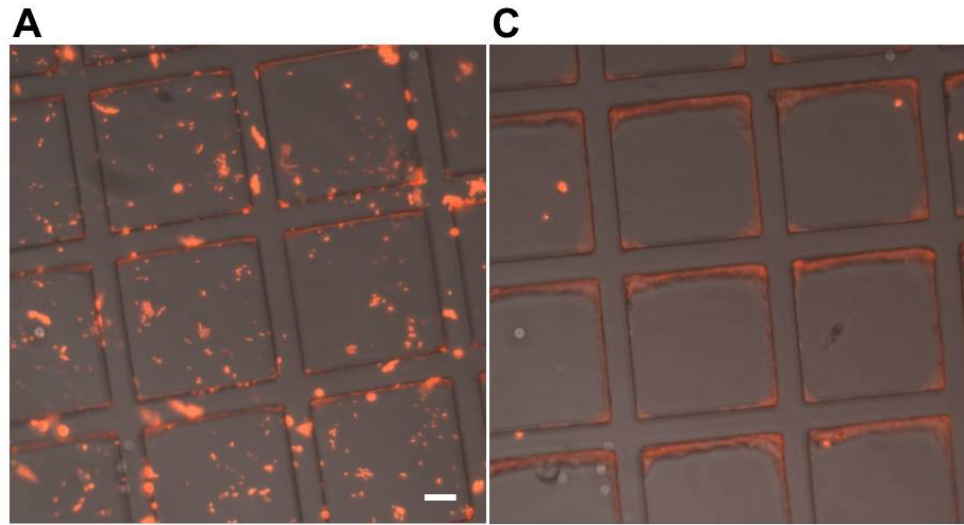


Figure 4-5

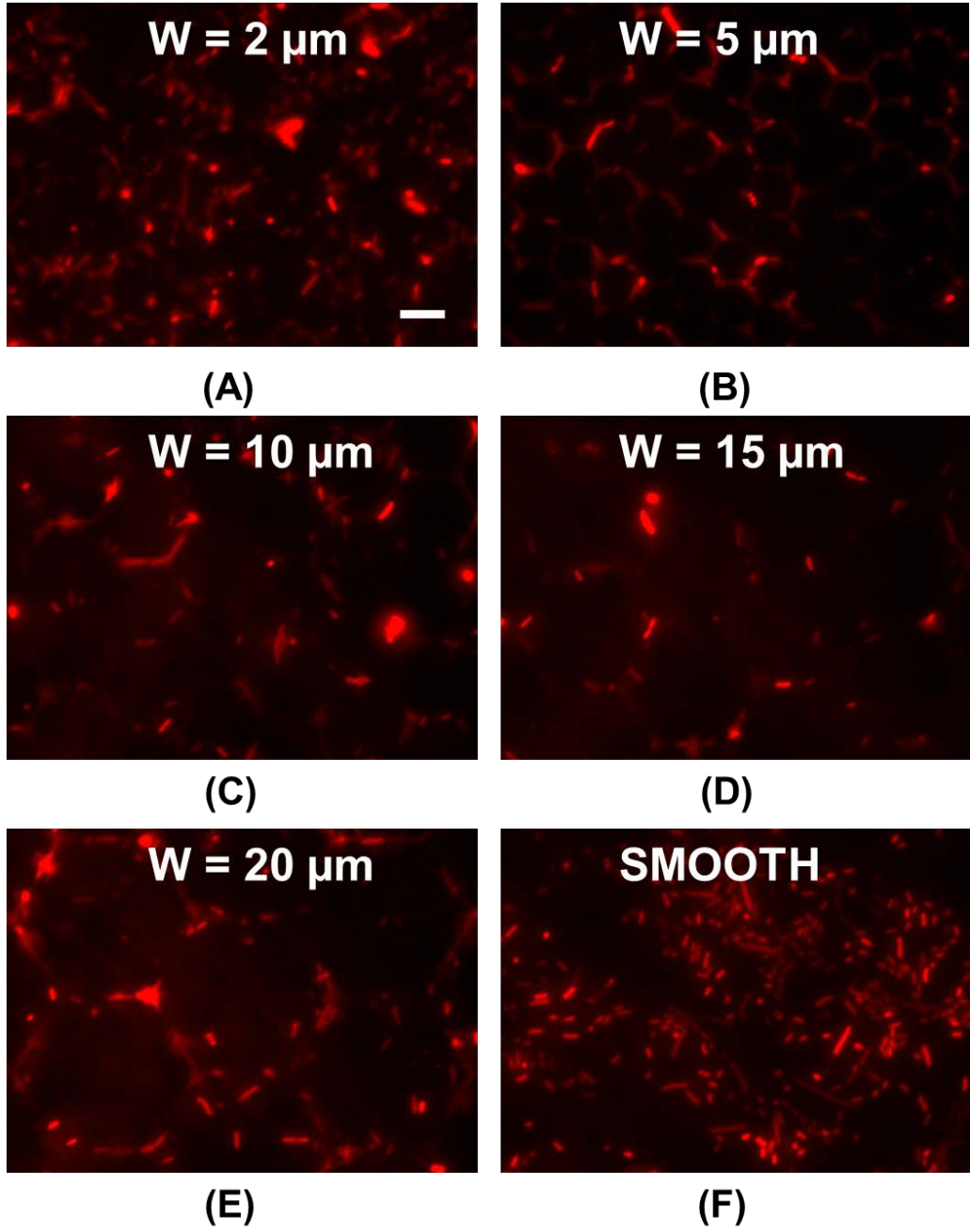


Figure 4-6

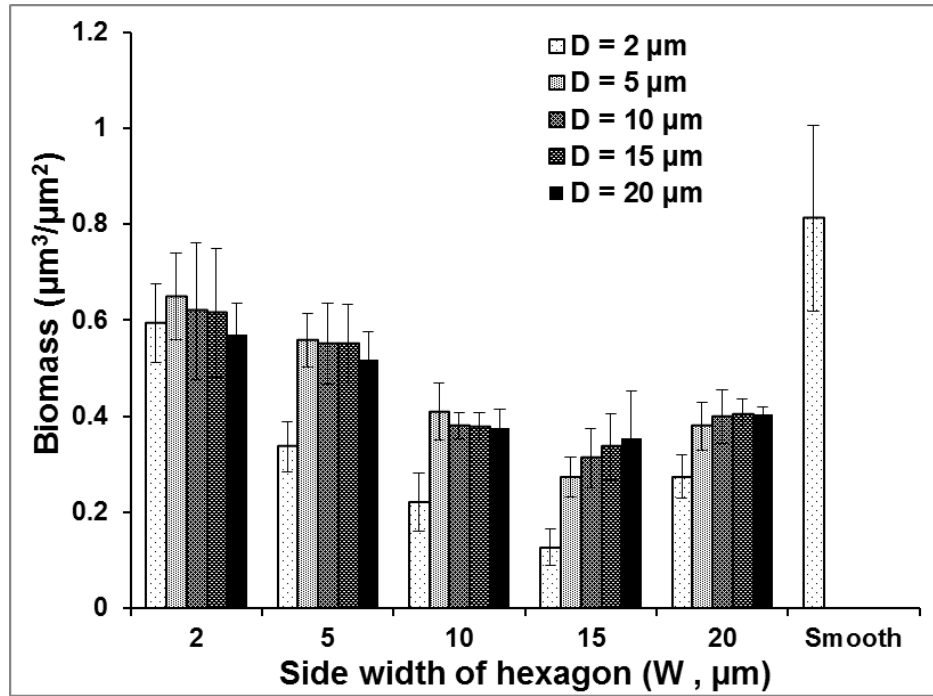
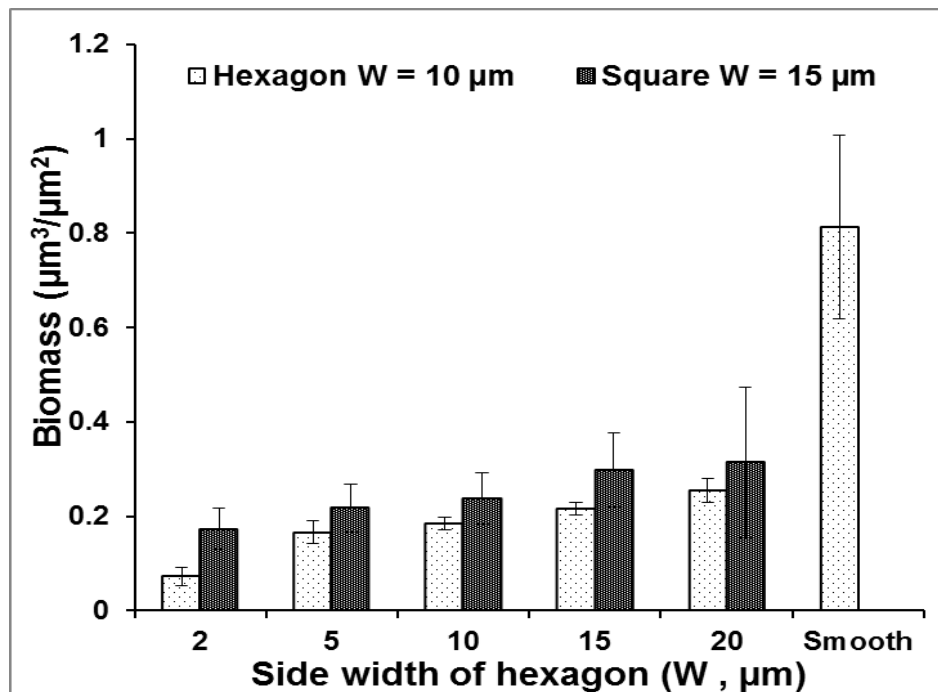
A**B**

Figure 4-7

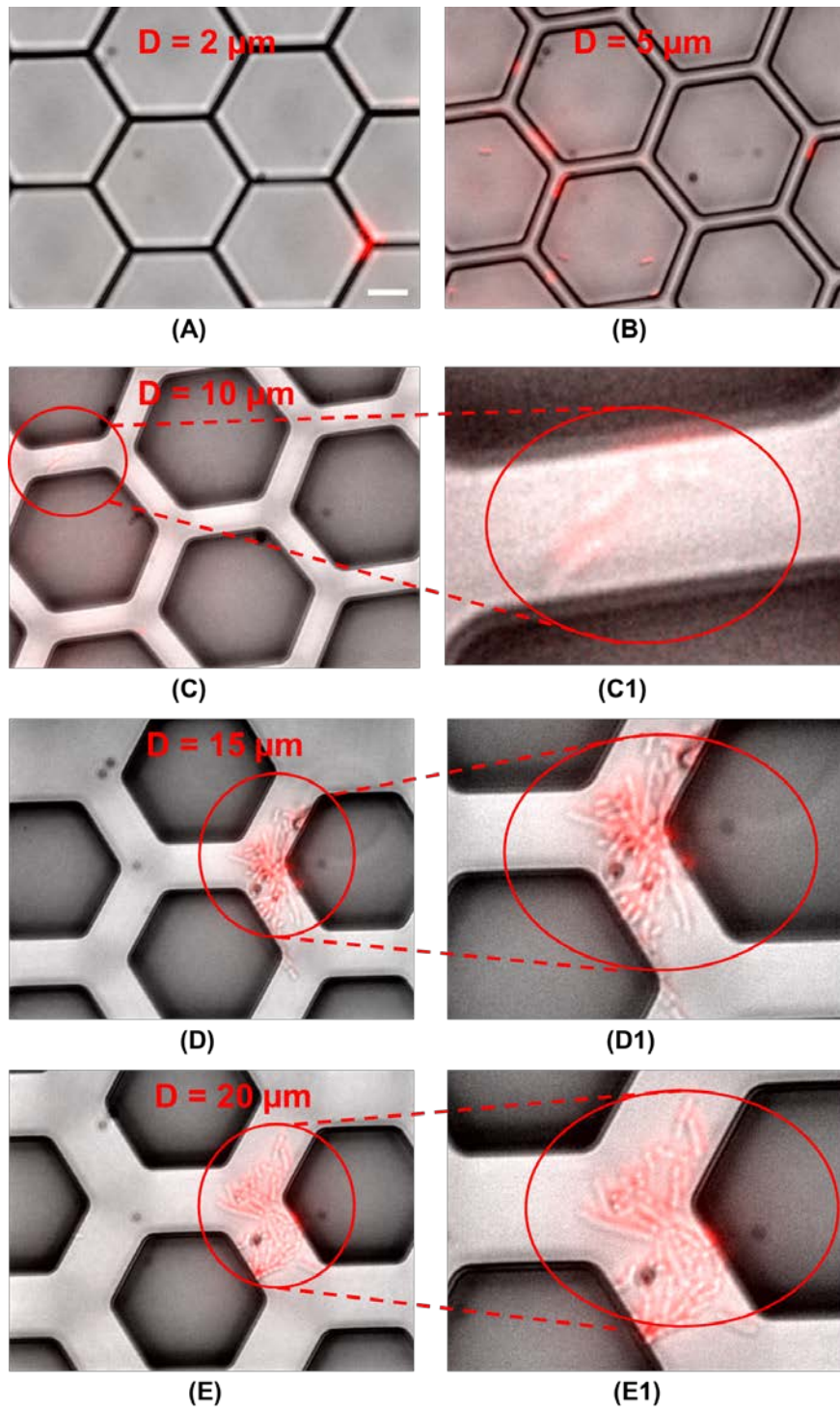


Figure 4-8

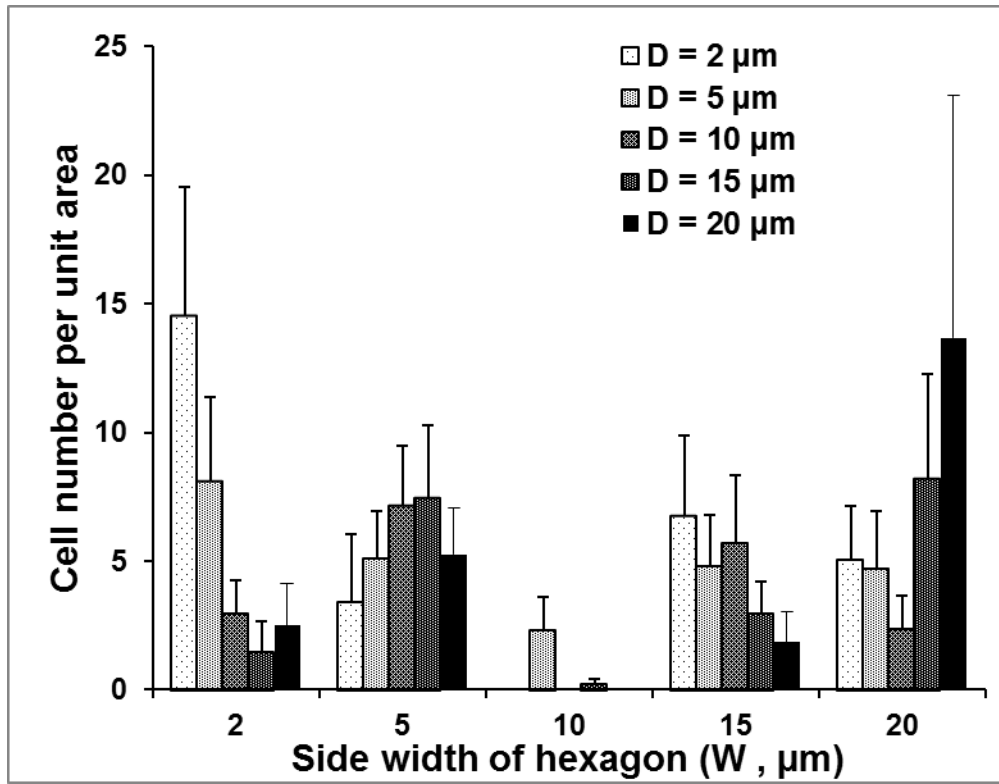


Figure 4-9

4.9 REFERENCES

- 1 **Hou, S. Y., Gu, H., Smith, C., Ren, D.** 2011. Microtopographic patterns affect *Escherichia coli* biofilm formation on poly(dimethylsiloxane) surfaces. *Langmuir* **27**: 2686-2691.
- 2 **Fux, C. A., Stoodley, P., Hall-Stoodley, L., Costerton, J. W.** 2003. Bacterial biofilms: a diagnostic and therapeutic challenge. Expert review of anti-infective therapy **1**: 667-683.
- 3 **Mah, T. F., O'Toole, G. A.** 2001. Mechanisms of biofilm resistance to antimicrobial agents. *Trends Microbiol* **9**: 34-39.
- 4 **Lewis, K.** 2001. Riddle of biofilm resistance. *Antimicrob Agents Chemother* **45**: 999-1007.
- 5 **Hall-Stoodley, L., Costerton, J. W., Stoodley, P.** Bacterial biofilms: from the natural environment to infectious diseases. *Nature reviews. Microbiology* **2**: 95-108.
- 6 **Davey, M. E., O'Toole G, A.** 2000. Microbial biofilms: from ecology to molecular genetics. *Microbiol Mol Biol Rev* **64**: 847-867.
- 7 **Donlan, R. M.** 2002. Biofilms: microbial life on surfaces. *Emerging infectious diseases* **8**: 881-890.
- 8 **Dunne, W. M.** Bacterial adhesion: seen any good biofilms lately? *Clinic Microbiology Review* **15**: 155-166.
- 9 **Stoodley, P., Sauer, K., Davies, D. G., Costerton, J. W.** 2002. Biofilms as complex differentiated communities. *Annu Rev Microbiol* **56**: 187-209.
- 10 **Bollen, C. M., Lambrechts, P., Quirynen, M.** 1997. Comparison of surface roughness of oral hard materials to the threshold surface roughness for bacterial plaque retention: a review of the literature. *Dent Mater* **13**: 258-269.
- 11 **Wim, T., Nele, W. A., Isabelle, S., Marc, Q.** 2006. Effect of material characteristics and/or surface topography on biofilm development. *Clin. Oral Implants Res.* **17**, 68-81.
- 12 **Hilbert, L. R., Bagge-Ravn, D., Kold, J., Gram, L.** 2003. Influence of Surface Roughness of Stainless Steel on Microbial Adhesion and Corrosion Resistance. *Int Biodeter Biodegr* **52**: 175-185.
- 13 **Taylor, R. L., Verran, J., Lees, G. C., Ward, A. J. P.** 1998. The Influence of Substratum Topography on Bacterial Adhesion to Polymethyl Methacrylate. *J Mater Sci-Mater M* **9**: 17-22.
- 14 **Weibel, D. B., Diluzio, W. R., Whitesides, G. M.** 2007. Microfabrication Meets Microbiology. *Nature Rev. Microbiol.* **5**: 209-218.
- 15 **Ling, J. F., Graham, M. V., Cady, N.** 2012. Effect of topographically patterned poly(dimethylsiloxane) surfaces on *Pseudomonas aeruginosa* adhesion and biofilm formation. *Nano Life* **02**: 04.
- 16 **Park, S. et al.** 2003. Influence of topology on bacterial social interaction. *Proceedings of the National Academy of Sciences of the United States of America* **100**: 13910-13915.
- 17 **Friedlander, R. S. et al.** 2013. Bacterial flagella explore microscale hummocks and hollows to increase adhesion. *Proceedings of the National Academy of Sciences of the United States of America* **110**: 5624-5629.

- 18 **Hochbaum, A. I., Aizenberg, J.** 2010. Bacteria pattern spontaneously on
periodic nanostructure arrays. *Nano Lett* **10**: 3717-3721.
- 19 **Chung, K. K., Schumacher, J. F., Sampson, E. M., Burne, R. A., Antonelli, P.
J., Brenna, A. B.** 2007. Impact of Engineered Surface Microtopography on
Biofilm Formation of *Staphylococcus aureus*. *Biointerphases* **2**: 89-94.
- 20 **Parkinson, J. S., Houts, S. E.** 1982. Isolation and Behavior of *Escherichia-Coli*
Deletion Mutants Lacking Chemotaxis Functions. *J. Bacteriol.* **151**: 106-113.
- 21 **Blair, D. F., Kim, D. Y., Berg, H. C.** 1991. Mutant MotB proteins in *Escherichia*
coli. *J Bacteriol* **173**: 4049-4055.
- 22 **Hou, S., Burton, E. A., Wu, R. L., Luk, Y. Y., Ren, D.** 2009. Prolonged control
of patterned biofilm formation by bioinert surface chemistry. *Chem Commun*
2009: 1207-1209.
- 23 **Chong, L.** 2001. *Molecular Cloning - A Laboratory Manual*, 3rd edition. Science
292: 446-446.
- 24 **Gu, H., Hou, S., Yongyat, C., De Tore, S., Ren, D.** 2013. Patterned biofilm
formation reveals a mechanism for structural heterogeneity in bacterial biofilms.
Langmuir **29**: 11145-11153.
- 25 **Heydorn, A., Nielsen, A. T., Hentzer, M., Sternberg, C., Givskov, M., Ersboll,
B. K., Molin, S.** 2000. Quantification of Biofilm Structures by the Novel
Computer Program COMSTAT. *Microbiol-Uk* **146**: 2395-2407.
- 26 **Alaerts, J. A., De Cupere, V. M., Moser, S., Van den Bosh de Aguilar, P.,
Rouxhet, P. G.** 2001. Surface characterization of poly(methyl methacrylate)
microgrooved for contact guidance of mammalian cells. *Biomaterials* **22**: 1635-
1642.
- 27 **Callow, M. E. et al.** 2002. Microtopographic cues for settlement of zoospores of
the green fouling alga *Enteromorpha*. *Biofouling* **18**: 237-245.
- 28 **Oner, D., McCarthy, T. J.** 2000. Ultrahydrophobic surfaces. Effects of
topography length scales on wettability. *Langmuir* **16**: 7777-7782.

CHAPTER 5

CONJUGATION IN *ESCHERCHIA COLI* BIOFILMS ON POLY(DIMETHYLSILOXINE) SURFACES WITH MICROTOPOGRAPHIC PATTERNS

5.1 ABSTRACT

Bacterial biofilms are less susceptible to antimicrobials and play an important role in the spread of antibiotic resistance due to close cell-to-cell contact. As an important surface character, topography has been shown to affect bacterial-surface interactions and biofilm formation. To understand if surface topography can also affect horizontal gene transfer in biofilms, we prepared (poly)dimethylsiloxane (PDMS) surfaces with 20 μm by 20 μm , 50 μm by 50 μm , and 100 μm by 100 μm protruding square-shaped patterns. Biofilm formation and associated conjugation on these surfaces were studied using fluorescently labeled donor and recipient strains of *Escherichia coli*. The results demonstrate that surface topography with inter-pattern distances larger than the length of a single *E. coli* cell can promote biofilm formation and conjugation frequency. Furthermore, motility mutant of *E. coli* exhibited defects in biofilm formation and conjugation.

5.2 INTRODUCTION

Microbes are capable of adhering to both biotic and abiotic surfaces and develop biofilms, which are multicellular communities embedded in an extracellular polymeric matrix (EPS) secreted by the attached cells¹. Biofilm cells are up to 1,000 times more resistant to antibiotics compared to their planktonic counterparts². Such high resistance plays an important role in chronic infections in human as well as biofouling and biocorrosion in industrial settings, which adversely affected human health, economy and the environment^{3,4,5,6}. The ubiquity and significance of biofilm-associated high-level drug resistance have stimulated growing interests in understanding the mechanisms of biofilm formation and developing more effective strategies for biofilm control.

Several important intrinsic mechanisms are involved in biofilm-associated antibiotic resistance including reduced penetration of antimicrobials, slow growth of biofilm cells, and enhanced extrusion of antibiotics from biofilm cells^{7,8}. In addition to the intrinsic resistance, biofilms also play an important role in acquired resistance because biofilm cells are sessile and close to each other. This provides a favorable condition for horizontal gene transfer, a process named conjugation^{9,10,11}. Bacterial conjugation occurs when the mobile genetic materials such as conjugal plasmids are transferred from donor to recipient cells through sex pili^{7,12}. The resulting transconjugants will acquire the phenotypes encoded by the mobile plasmid, which commonly lead to antibiotic resistance¹². For example, bacterial conjugation is found to be responsible for the emergence of penicillin resistance in the pathogenic *Streptococcus pneumoniae* and gentamicin resistance in *S. aureus*^{13,14}. Some conjugative plasmids have also been shown to promote biofilm formation and stabilize biofilm structure^{7,12}.

Biofilm formation is a dynamic process, including initial attachment, microcolony formation, maturation and dispersion¹⁵⁻¹⁸. The adhesion of bacteria on a solid surface is affected by many factors such as surface topography, chemistry, charge, and stiffness^{5, 19, 20}. Among these factors, surface topography has been found to affect the retention of bacteria on the surfaces^{5,19-25}. Consequently, certain topographic features have been found to either prevent or promote biofilm formation^{22,25}. For example, Chung *et al.*²⁵ reported PDMS surfaces with parallel rib patterns organized in diamond shape (inspired by shark skin) can reduce *S. aureus* adhesion by 47% compared to smooth PDMS surfaces at 14 days after inoculation. In comparison, Friedlander *et al.*²² observed that the biomass of *E. coli* biofilms on PDMS surfaces with an array of hexagonal features is approximately 30% higher than the biomass on smooth PDMS surfaces after 2 h of inoculation. Cell density is known to affect conjugation^{12,26}; however, how cell density of biofilm affects bacterial horizontal gene transfer in biofilm remains elusive. A major challenge to the mechanistic study of conjugation is the biofilm structural heterogeneity and low frequency of conjugation. We hypothesized that surface topography can affect bacterial conjugation due to its effects on biofilm formation. To test this hypothesis and understand what are the “hot spots” for biofilm-associated conjugation, we prepared PDMS surfaces with well-defined microtopographic patterns.

Using similar patterns, we reported recently that surface topography can affect bacterial initial attachment and biofilm formation²¹. There was no significant biofilm formation on top of protruding square shaped patterns of PDMS if the patterns are smaller than 20 $\mu\text{m} \times 20 \mu\text{m}$. Also, *E. coli* preferentially attach and form biofilm between protruding patterns. Thus, these well-defined topographic features can be used to study

the effects of topography on biofilm cell density as well as conjugation frequency. Thanks to a dual-labeling system developed recently, it is possible to study conjugation in real time^{27,28}. In this study, the donor strain was tagged with *gfp* downstream of a modified *lac* promoter on the conjugative plasmid regulated by a chromosomally encoded repressor (*lacIq*), while the recipient strain was labeled with constitutively expressed *rfp* on the plasmid²⁹. We chose PDMS because it is biocompatible and commonly used for medical devices^{30,31}. Using PDMS and *E. coli* also allows us to compare the results with our other studies^{22,25}.

5.3 MATERIALS AND METHODS

5.3.1 Bacterial strains and growth media

E. coli CSH26::LacIq1/pKJK10²⁹ with conjugative plasmid pKJK10 carrying a green fluorescence reporter gene (*gfp*) was used as the donor strain. *E. coli* chemotaxis wild-type strain RP437³² and its isogenic motility mutant RP3087³³ tagged with constitutive *rfp* gene on plasmid pRSH103^{21,34} were used as recipient in this work. Both strains were routinely grown overnight at 37°C in Lysogeny Broth (LB)³⁵ which contains 10 g/L NaCl, 10 g/L tryptone, and 5g/L yeast extract. Tetracycline (30 µg/mL) was added in cultures to maintain the plasmids pKJK10 and pRSH103.

5.3.2 PDMS surfaces

The PDMS surfaces with microtopographic patterns (Fig. 5-1A) used in this study were obtained by transferring complementary patterns from the silicon wafers with 10 µm deep (H) square holes etched via photolithography as reported previously^{21,36}. The side width (W) of square-shape protruding plateaus was set to be 20, 50, or 100 µm while

the distance (D) between adjacent features was systematically varied (10, 15, 20, 30, 40, or 50 μm) (Fig. 5-1A).

5.3.3 Biofilm formation and conjugation

To study the effects of surface topography on *E. coli* conjugation, the patterned PDMS surfaces were used to form co-culture biofilms of *E. coli* CSH26/pKJK10 (donor) and *E. coli* RP437/pRSH103 (recipient) or *E. coli* RP3087/pRSH103 (recipient). Each PDMS surface was sterilized by soaking in 190 proof ethanol for 30 min, dried at 50°C for 40 min, and transferred to a petri dish, each containing 20 mL LB medium supplemented with 30 $\mu\text{g}/\text{mL}$ tetracycline. *E. coli* CSH26/pKJK10 (donor) and *E. coli* RP437/pRSH103 (recipient) or *E. coli* RP3087/pRSH103 (recipient) were used to inoculate the biofilm cultures with a ratio of 3:7 (donor: recipient) to a total initial optical density at 600 nm (OD_{600}) of 0.05. The biofilm cultures were incubated at 37°C for 24 h and then the PDMS surfaces were gently washed three times with 0.85% NaCl solution (change to fresh solution every time) before imaging. To quantify the amount of donor cells, isopropyl β -D-1-thiogalactopyranoside (IPTG) (1mM) was added in some biofilm cultures to visualize the donor cells in biofilms by inducing the expression of green fluorescence protein (Fig. 5-1B).

To understand if the interaction between the donors and recipients affect biofilm formation, the biofilm formation of the recipient strains on patterned PDMS surfaces was also conducted. Overnight cultures of the recipient strains were used to inoculate the biofilm cultures to an OD_{600} of 0.035. The biofilm cultures were incubated at 37 °C for 24 h and then the PDMS surfaces were gently washed three times with 0.85% NaCl solution

(change to fresh solution every time) before imaging using Axio Imager M1 (Carl Zeiss, Berlin, Germany).

The biofilms of donor and recipient co-cultures were also grown on inverted PDMS surfaces. The PDMS surfaces and two pieces of small microscopic glass slides were sterilized with 190 proof ethanol²¹. The sterilized PDMS surfaces were put upside down on two microscope slides to provide a 1 mm gap between the PDMS surfaces and the bottom of petri dish¹⁹.

5.3.4 Conjugation frequency

The frequency of conjugation was determined by quantifying the number of transconjugants per unit biofilm area using an Axio Imager M1 fluorescence microscope. Since conjugation is a relatively low frequency event, the transconjugants in a cluster was assumed to be originated from a single conjugation event (Fig. 5-1C). Using COMSTAT³⁷, the biomass on the top of topographic patterns, the side of topographic patterns, and the channel between adjacent topographic patterns was quantified, separately. The biomass on the side of the topographic patterns was calculated using the following equation:

$$B_{Side} = \frac{B_{Total} * A_{Total} - (B_{Top} * A_{Top} + B_{Channel} * A_{Channel})}{A_{Side}} \quad (1)$$

where B represents biofilm biomass; A represents area of corresponding geometric location. The frequency of conjugation at each geometric location was normalized by the total area of corresponding location first and then further normalized by the total number of conjugation events per unit area to minimize the effects of variation among surfaces.

5.4 RESULTS

5.4.1 Surface topography affected *E. coli* conjugation in biofilm

Surface topography is known to affect bacterial initial adhesion and biofilm formation^{5,19-25}. Recently, we reported that *E. coli* adhesion on 10 μm tall protruding square patterns of PDMS is only significant when the patterns are 20 $\mu\text{m} \times 20 \mu\text{m}$ or bigger²¹. Since conjugation requires close cell-to-cell contact, we expected that surface topography can also influence bacterial conjugation. To test this, we prepared PDMS surfaces with 10 μm tall 20 $\mu\text{m} \times 20 \mu\text{m}$ square shaped topographic patterns with varying inter-pattern distance (10, 15, 20, 30, 40, or 50 μm) (Fig. 5-1). The topographic features were found to promote biofilm formation since the biomass per unit area on patterned PDMS surfaces was significantly higher than that on flat PDMS surfaces (one way ANOVA, $P < 0.001$). For example, when the distance between adjacent patterns was 10 μm , the biomass per unit area on patterned PDMS surfaces was 3.4 times higher than that on flat PDMS surfaces (Fig. 5-2). Biomass per unit area of the biofilms formed on PDMS surfaces with 50 $\mu\text{m} \times 50 \mu\text{m}$ and 100 $\mu\text{m} \times 100 \mu\text{m}$ topographic patterns was also significantly higher than that on flat PDMS surfaces (Fig. 5-2), which corroborates our conclusion that the topographic features can promote biofilm formation. The biomass per unit area decreased as the tested patterns were further separated from each other.

Since cell density is an important factor that can influence bacterial conjugation^{7,12,38}, we compared the conjugation frequency per unit area on patterned PDMS surfaces with that on flat PDMS surfaces. Consistent with the biomass data, the conjugation frequency per unit area on PDMS surfaces with 20 $\mu\text{m} \times 20 \mu\text{m}$, 50 $\mu\text{m} \times 50 \mu\text{m}$, and 100 $\mu\text{m} \times 100 \mu\text{m}$ topographic patterns was significantly higher than that on flat

PDMS surfaces when distance between patterns increased from 10 to 50 μm (Fig. 5-3) (one way ANOVA, $P < 0.05$). For example, when distance between protruding features was 10 μm , the conjugation frequency per unit area on patterned PDMS surfaces was 9.5 times higher than that on flat PDMS surfaces.

5.4.2 Conjugation at different locations of the microtopographic patterns

In our previous study using the same patterned surfaces, we have observed that *E. coli* cells preferentially attach to the valleys between neighboring protruding patterns on both upright and inverted PDMS surfaces²¹. This result suggests that bacteria can actively pursue the preferred location for adhesion and biofilm formation. It also motivated us to quantify the cells density at the different geometrical locations on the patterned surfaces and study the effects of cell density on bacterial conjugation to identify the structural factors that can cause “hot spot” of conjugation.

The biofilms formed on each PDMS surface are attributed to three sources: on top of the plateaus, on the side of plateaus and in the channel between nearby plateaus. In our experimental system, the biofilm formed on the side of the plateaus appeared to have a higher cell density than that at any other locations. To verify this, we plotted the biomass at different geometric locations versus the distances between neighbor protruding features. The results confirmed that *E. coli* prefers the side of protruding patterns for adhesion. The biomass on the side was significantly larger than on any other locations (Fig. 5-4). For example, the average unit area biomass on the side of size 20 $\mu\text{m} \times 20 \mu\text{m}$ patterns with inter-pattern distance of 30 μm was $2.1 \pm 0.1 \mu\text{m}^3 / \mu\text{m}^2$, significantly higher than that on top of patterns ($0.5 \pm 0.1 \mu\text{m}^3 / \mu\text{m}^2$) and in the channel between patterns ($0.5 \pm 0.2 \mu\text{m}^3 / \mu\text{m}^2$) (one way ANOVA, $P < 0.001$). Similar results were also obtained on

inverted PDMS surfaces with the same microtopographic patterns although the surface coverage is lower than that on upright patterns. This finding suggests that the accumulation of bacteria on the side of topographic patterns was not due to gravity (Fig. 5-5).

To understand if the difference in biomass leads to increased conjugation on the side of plateaus, we quantified the percentage of transconjugants at different geometric locations. The comparison of bacterial conjugation at different locations showed that the percentage of transconjugants among biofilm cells was significantly higher on the side of plateaus than that on top of the plateaus or in the valleys. For example, the percentage of transconjugants on the side of size $20\ \mu\text{m} \times 20\ \mu\text{m}$ patterns with inter-pattern distance $30\ \mu\text{m}$ was $72.0 \pm 20.9\%$, which is higher than that on top of the patterns ($6.1 \pm 16.5\%$) in the valleys between patterns ($21.9 \pm 21.5\%$) (one way ANOVA, $P < 0.001$) (Fig. 5-6A). Similar results were observed on the PDMS surfaces modified with $50\ \mu\text{m} \times 50\ \mu\text{m}$ and $100\ \mu\text{m} \times 100\ \mu\text{m}$ topographic patterns (Fig. 5-6B). This result suggests that surface topography does affect bacterial conjugation and the side of protruding features is the “hot spots” of conjugation.

5.4.3 *E. coli* motility mutant exhibited defects in conjugation

Our results using inverted surfaces suggest that the preference of *E. coli* attachment on the side of topographic patterns is not simply due to gravity driven settlement. To better understand this phenomenon and investigate if it involves key genes, the biofilm formation of *E. coli* RP3087/pRSH103, a motility mutant of the wild-type strain *E. coli* RP437/pRSH103, was studied using the same PDMS surfaces with microtopographic patterns. In addition, bacterial conjugation between the donors (*E. coli*

CSH26/pKJK 10) and the motility mutant strain (recipients) in co-culture biofilms was also tested to study the role of motility during *E. coli* conjugation in biofilms. By comparing biofilm formation of the wild-type strain and its motility mutant on PDMS surfaces with size $20\ \mu\text{m} \times 20\ \mu\text{m}$ patterns, we noticed that motility mutant formed less biofilms on the side of plateaus or in the channel between plateaus (Fig. 5-7A). This observation is corroborated by the COMSTAT³⁷ analysis (Fig. 5-8). For example, the biomass of the nonmotile mutant on the side of plateaus or in the channel between plateaus with $20\ \mu\text{m}$ inter-pattern distance were 0.5 ± 0.01 and $0.1 \pm 0.01\ \mu\text{m}^3/\mu\text{m}^2$ that were significantly lower than the biomass on the top of plateaus ($0.9 \pm 0.2\ \mu\text{m}^3/\mu\text{m}^2$) (one-way ANOVA, $P < 0.001$) (Fig. 5-8A). This is a drastic difference compared to the wild-type strain which formed substantial amount of biofilms at both locations (on the side of plateaus and in the channel between plateaus) (Fig. 5-7B). For example, the biomass of wild-type strain on the side of plateaus or in the channel between plateaus with $20\ \mu\text{m}$ inter-pattern distance were 0.7 ± 0.1 and $0.8 \pm 0.1\ \mu\text{m}^3/\mu\text{m}^2$ (Fig. 5-8B). Interestingly, the motility mutant preferred to form more and biofilms on the top of protruding features than the wild-type (Fig. 5-7A). The biomass of motility mutant on the top of topographic patterns with $20\ \mu\text{m}$ inter-pattern distance was two times higher than that of wild-type strain at the same location. These results further support our finding that the increased adhesion on the side of plateaus was not simply due to gravity driven settlement or artifacts in washing steps.

To understand the role of bacterial motility conjugation, we quantitatively studied the conjugation using the motility mutant, rather than the wild-type, as recipient in co-culture biofilms formed on PDMS surfaces with $20\ \mu\text{m} \times 20\ \mu\text{m}$ microtopographic

patterns (Fig. 5-8C). The conjugation frequency between donors and motility mutant is significantly low compared to the conjugation with the wild-type strain as the recipient. For example, the conjugation per unit area of the wild-type strain on PDMS surfaces with $20\ \mu\text{m} \times 20\ \mu\text{m}$ topographic patterns with $20\ \mu\text{m}$ inter-pattern distance was 4.6 ± 0.6 but the conjugation per unit area of the motility mutant was 0.2 ± 0.2 . This finding suggests that bacterial motility also plays a role in bacterial conjugation in biofilms.

5.5 DISCUSSION

Bacterial conjugation plays critical roles in biofilm-associated antibiotic resistance and other responses, allowing cells in biofilm to evolve and adapt to the hostile environments^{7,12,27}. The effects of surface topography on bacterial adhesion and subsequent biofilm formation inspired our interest in investigating the effect of this selective pressure on the DNA exchange activities in biofilm²¹. In chapter 4, we demonstrated that the side width $20\ \mu\text{m}$ is the critical dimension for *E. coli* to attach to PDMS. Thus, $20\ \mu\text{m} \times 20\ \mu\text{m}$ and bigger patterns were used in this conjugation study.

Using PDMS surfaces with square shaped microtopographic patterns of varying sizes (20 , 50 , and $100\ \mu\text{m}$) with different inter-pattern distances (10 , 15 , 20 , 30 , 40 , and $50\ \mu\text{m}$), the effects of surface topography on cell density in biofilm was investigated. The results revealed that the presence of topographic patterns promoted the biomass of biofilm. This promotion of biofilm formation on PDMS surfaces modified with microtopographic patterns was found to be due to the preferential attachment of both donors and recipients on the side of protruding patterns (Fig. 5-9 & 10). The aggregation of bacterial cells on the side of plateaus was proved to be an intrinsic phenomenon, rather than simply due to gravity-driven settlement, which is consistent with the results

observed in Chapter 4. Besides biofilm formation, PDMS surfaces with topography showed higher unit area conjugation frequency compared to flat PDMS surfaces. The side of plateaus was found to be the “hot spots” for bacterial conjugation. The higher conjugation frequency on the side of plateaus was due to the higher cell density at that location because bacterial cell density was well known as an important factor that can influence bacterial conjugation^{14,38-40}. Although cell density has been reported to be able to affect bacterial conjugation, to my best knowledge, this is the first time that a cell density related “hot spot” on surfaces with topography was revealed. This information is important for developing antifouling surfaces since virtually all the surfaces in natural environment are not smooth.

In this study, the motility of bacteria was also found to play an important role in bacterial conjugation because the *motB* mutant showed defects in bacterial conjugation. Bacterial motility was well-known to be important to bacterial movement and biofilm formation^{1,41}. However, the role of bacterial motility in bacteria during bacterial conjugation is not very well understood. The reduction of bacterial conjugation between donors and motility mutant recipients may be due to the decreased biofilm formation of the motility mutant on the side of protruding plateaus or the defects in bacterial motility. The role of bacterial motility in bacterial conjugation inside of biofilms deserves further study, which is part of our ongoing work. Overall, these results shed new lights on bacterial conjugation in biofilms.

5.6 FIGURE CAPTIONS

Figure 5-1. Bacterial conjugation on PDMS surfaces with microtopographic patterns. (A)

Schematic presentation of the PDMS surfaces with microtopographic patterns. (B) Three-dimensional image of the donors and recipients co-culture biofilms on PDMS surfaces with $50\ \mu\text{m} \times 50\ \mu\text{m}$ topographic patterns and $50\ \mu\text{m}$ inter-pattern distance. IPTG (1mM) was used to induce the expression of green fluorescence protein in donors. (C) Top-down view of the donors and recipients co-culture biofilms on PDMS surfaces with $50\ \mu\text{m} \times 50\ \mu\text{m}$ topographic patterns and $50\ \mu\text{m}$ inter-pattern distance. The expression of green fluorescence protein in donors was not induced. (Bar = $20\ \mu\text{m}$) Left: the image combines green and red fluorescence channels. Right: the image combines Differential Interference Contrast (DIC) channel, green fluorescence, and red fluorescence channels.

Figure 5-2. The comparison between the biomass in biofilms formed on PDMS surfaces modified with $20\ \mu\text{m} \times 20\ \mu\text{m}$, $50\ \mu\text{m} \times 50\ \mu\text{m}$, and $100\ \mu\text{m} \times 100\ \mu\text{m}$ microtopographic patterns with various inter-pattern distances (10, 15, 20, 30, 40, or $50\ \mu\text{m}$) and that on flat PDMS surfaces. Standard deviations are presented. N=6 biological repeats averaged; at least 30 images were analyzed for each data point.

Figure 5-3. The comparison between the unit area of conjugation frequency on PDMS surfaces modified with size $20\ \mu\text{m} \times 20\ \mu\text{m}$, $50\ \mu\text{m} \times 50\ \mu\text{m}$, and $100\ \mu\text{m} \times 100\ \mu\text{m}$ microtopographic patterns with various inter-pattern distances (10, 15, 20, 30, 40, or $50\ \mu\text{m}$) and that on flat PDMS surfaces. Standard errors

are presented. N=6 biological repeats averaged; at least 30 images were analyzed for each data point.

Figure 5-4. Biomass of *E. coli* CSH26/pKJK (donor) and *E. coli* RP437/pRSH103 (recipient) co-culture biofilms on the side and on the top of the size $20\ \mu\text{m} \times 20\ \mu\text{m}$, $50\ \mu\text{m} \times 50\ \mu\text{m}$, and $100\ \mu\text{m} \times 100\ \mu\text{m}$ microtopographic patterns with various inter-pattern distances (10, 15, 20, 30, 40, or $50\ \mu\text{m}$), in the channel between close patterns, and on flat PDMS surfaces. Standard deviations are presented. N=6 biological repeats averaged; at least 30 images were analyzed for each data point.

Figure 5-5. Biofilms of *E. coli* CSH26/pKJK (donor) and *E. coli* RP437/pRSH103 (recipient) co-culture biofilms on inverted PDMS surfaces modified with size $20\ \mu\text{m} \times 20\ \mu\text{m}$ microtopographic patterns with $10\ \mu\text{m}$ inter-pattern distance. (A) Donor and transconjugant cell clusters on the side of protruding patterns. (B) Donor and recipient cells on the side of protruding patterns. Left: the image combines Differential Interference Contrast (DIC) channel, green fluorescence, and red fluorescence channels. Right: the image combines green and red fluorescence channels.

Figure 5-6. The percentage of bacterial conjugation at different geometric locations (on the side and top of topographic patterns and in the channel between close patterns) around size $20\ \mu\text{m} \times 20\ \mu\text{m}$, $50\ \mu\text{m} \times 50\ \mu\text{m}$, and $100\ \mu\text{m} \times 100\ \mu\text{m}$ microtopographic patterns with various inter-pattern distances (10, 15, 20, 30, 40, or $50\ \mu\text{m}$). Standard errors are presented. N=6 biological repeats averaged; at least 30 images were analyzed for each data point.

Figure 5-7. Representative fluorescence images of motility mutant biofilms (A) and wild-type biofilms (B) on PDMS surfaces with size $20\ \mu\text{m} \times 20\ \mu\text{m}$ topographic patterns with $15\ \mu\text{m}$ inter-pattern distance.

Figure 5-8. Effects of motility on biofilm formation and bacterial conjugation. (A & B) The biomass of motility mutant (A) and wild-type (B) biofilms at different geometric locations (on the side and top of plateaus and in the channel between close plateaus) around size $20\ \mu\text{m} \times 20\ \mu\text{m}$ topographic patterns with various inter-pattern distances ($10, 15, 20, 30, 40,$ or $50\ \mu\text{m}$). (C) The comparison between the unit area conjugation frequency of wild-type strain, the unit area conjugation frequency of motility mutant in co-culture biofilms formed on PDMS surfaces with size $20\ \mu\text{m} \times 20\ \mu\text{m}$ topographic patterns with various inter-pattern distances ($10, 15, 20, 30, 40,$ or $50\ \mu\text{m}$), and the unit area conjugation frequency of wild-type and motility mutant biofilms on flat PDMS surfaces. $N=3$ biological repeats averaged; at least 15 images were analyzed for each data point.

Figure 5-9. The biomass of donors in biofilms formed on PDMS surfaces modified with $20\ \mu\text{m} \times 20\ \mu\text{m}$ (A), $50\ \mu\text{m} \times 50\ \mu\text{m}$ (B), and $100\ \mu\text{m} \times 100\ \mu\text{m}$ (C) microtopographic patterns with various inter-pattern distances ($10, 15, 20, 30, 40,$ or $50\ \mu\text{m}$). $N=6$ biological repeats averaged; at least 30 images were analyzed for each data point.

Figure 5-10. The biomass of recipients in biofilms formed on PDMS surfaces modified with $20\ \mu\text{m} \times 20\ \mu\text{m}$ (A), $50\ \mu\text{m} \times 50\ \mu\text{m}$ (B), and $100\ \mu\text{m} \times 100\ \mu\text{m}$ (C) microtopographic patterns with various inter-pattern distances ($10, 15, 20,$

30, 40, or 50 μm). N=6 biological repeats averaged; at least 30 images were analyzed for each data point.

5.7 FIGURES

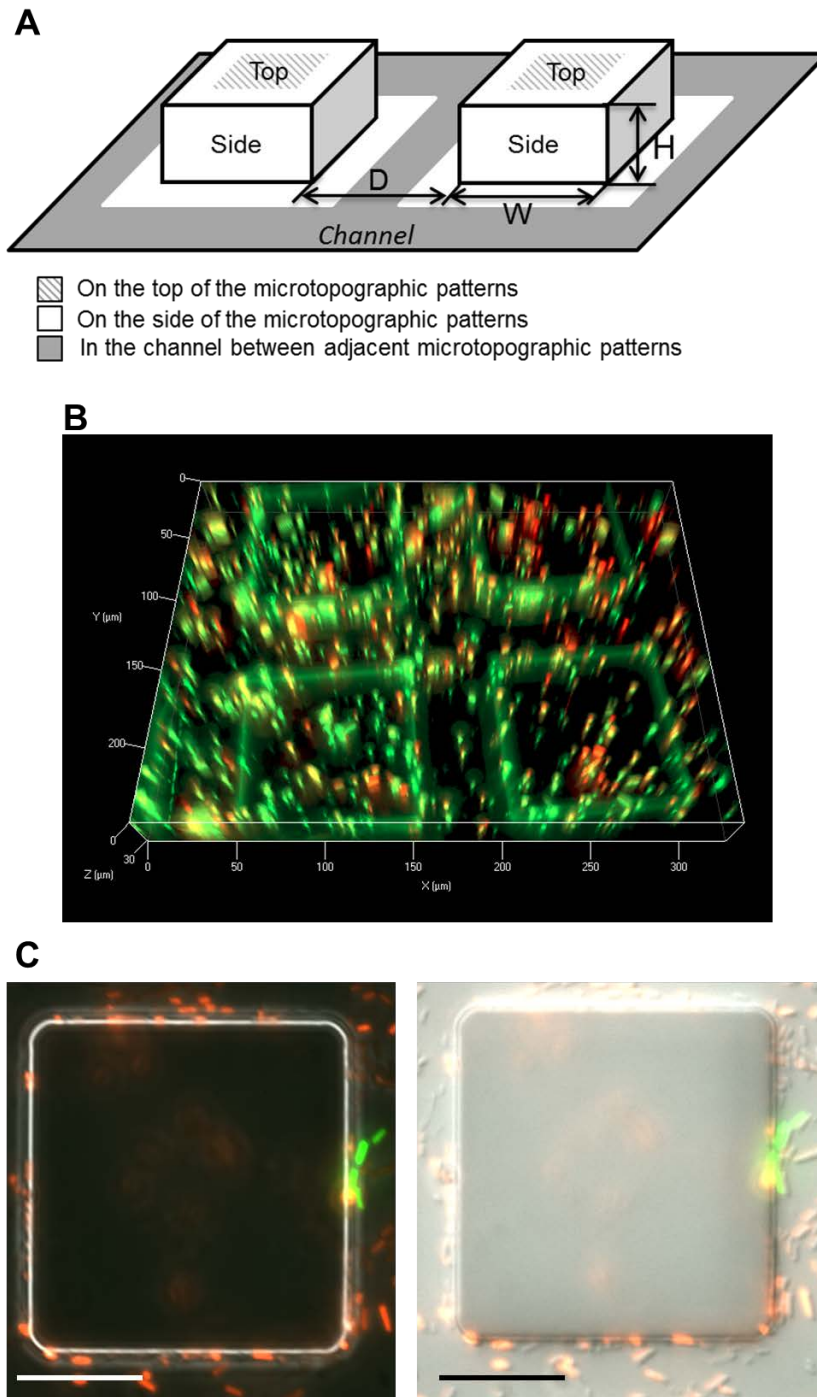


Figure 5-1

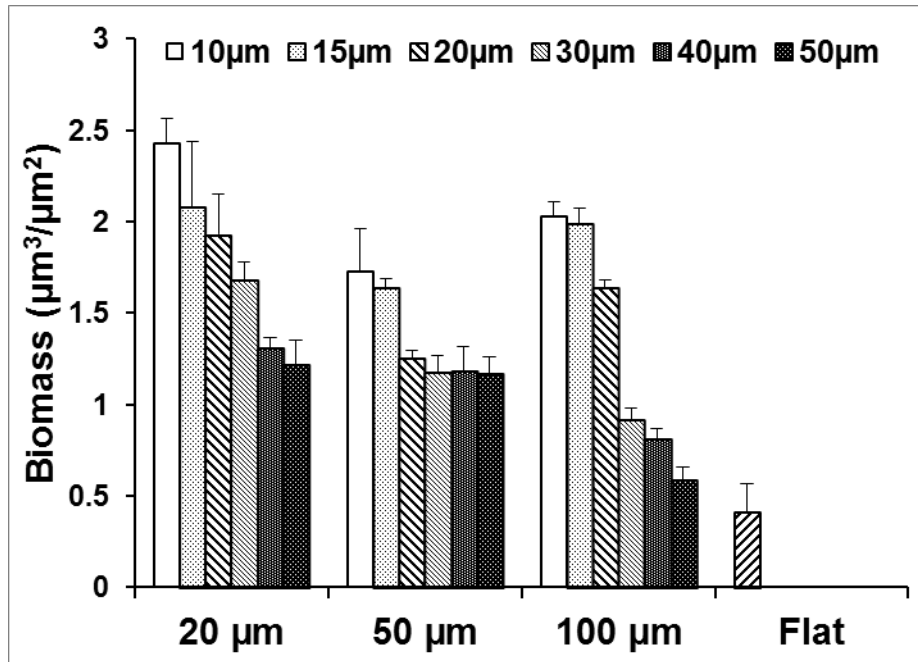


Figure 5-2

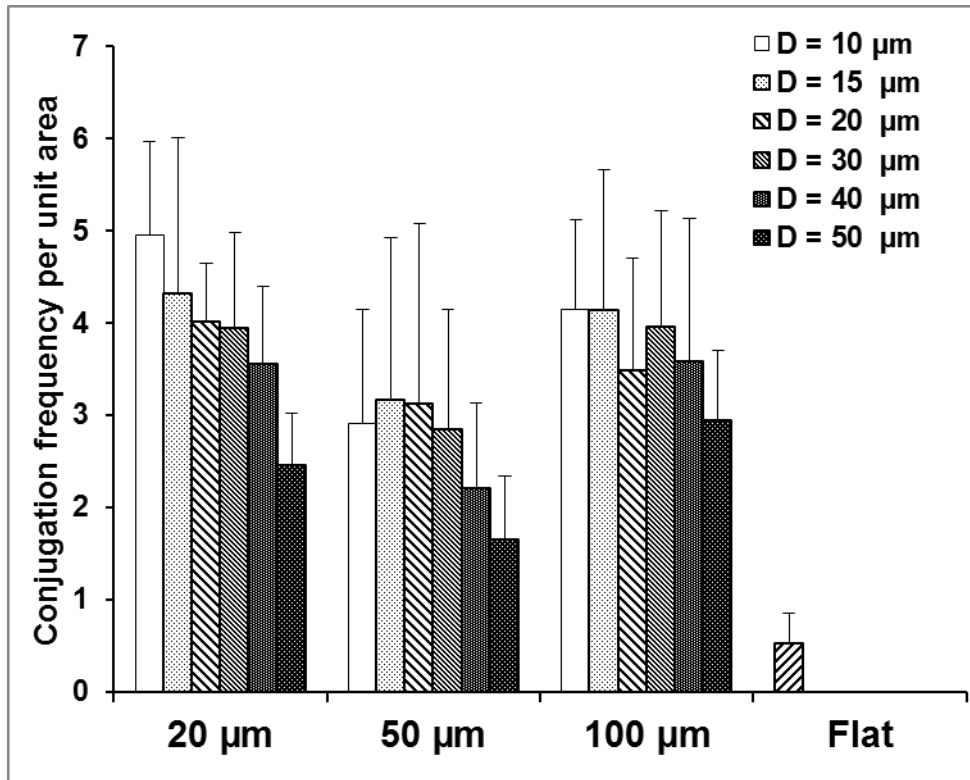


Figure 5-3

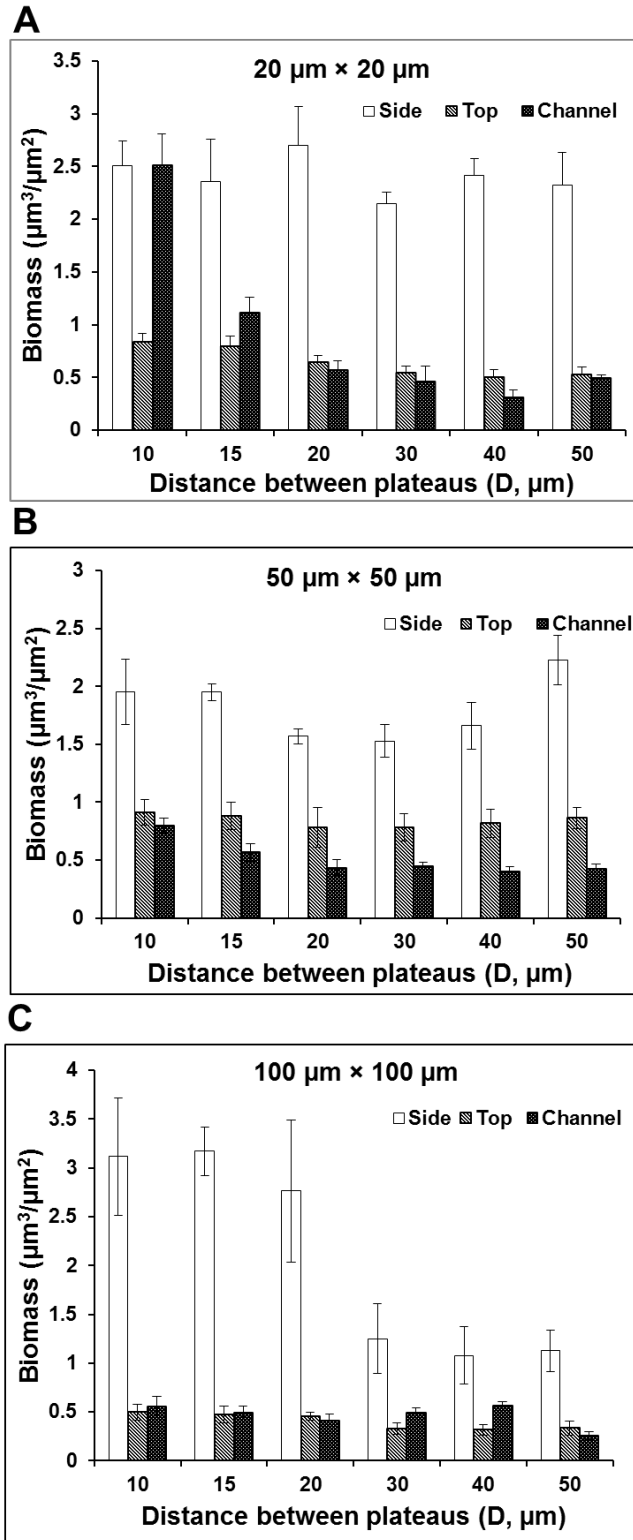


Figure 5-4

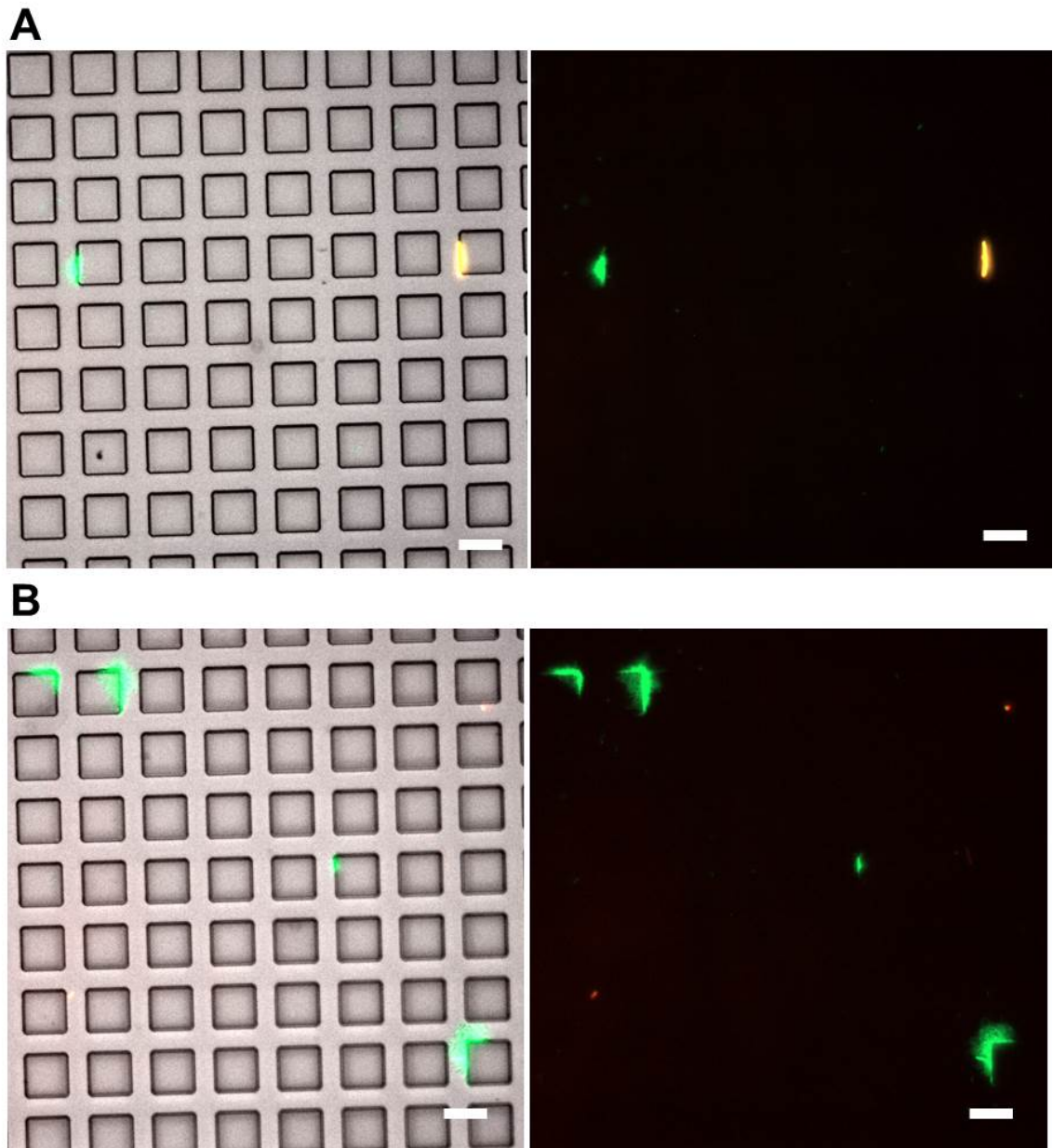


Figure 5-5

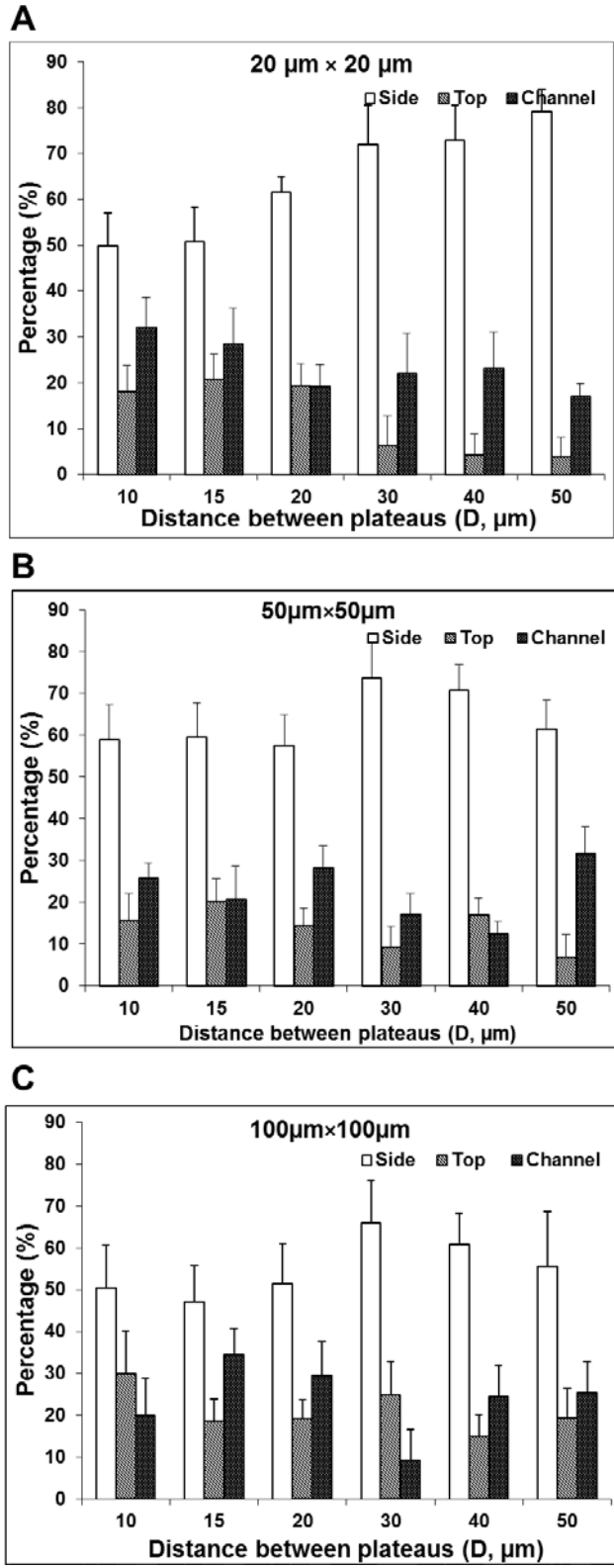
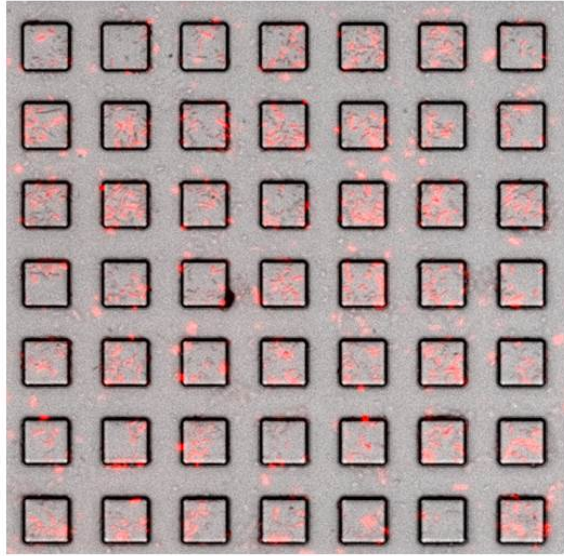


Figure 5-6

A

motB mutant
E. coli RP3087/pRSH103
W=20 μ m; D=15 μ m



B

Wild-type
E. coli RP437/pRSH103
W=20 μ m; D=15 μ m

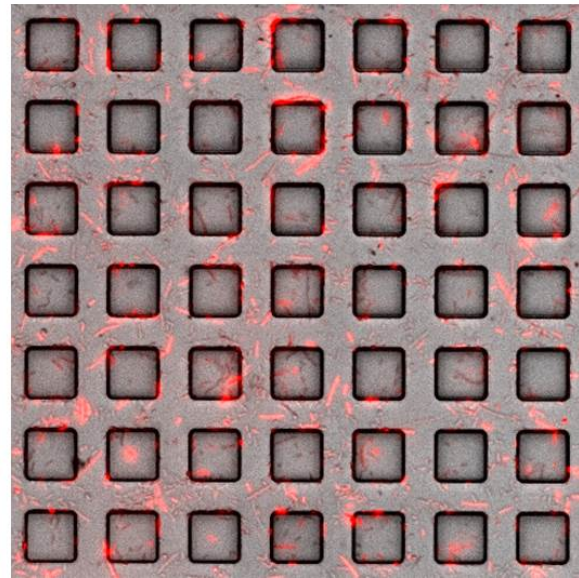


Figure 5-7

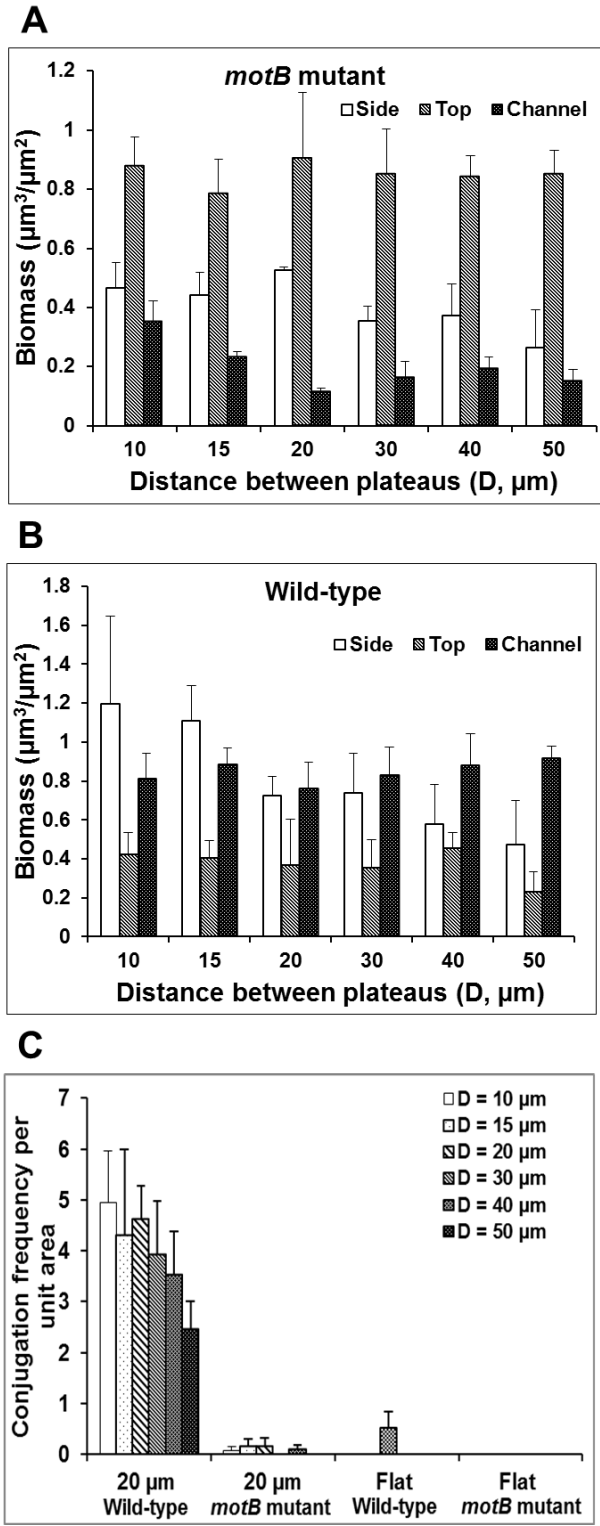


Figure 5-8

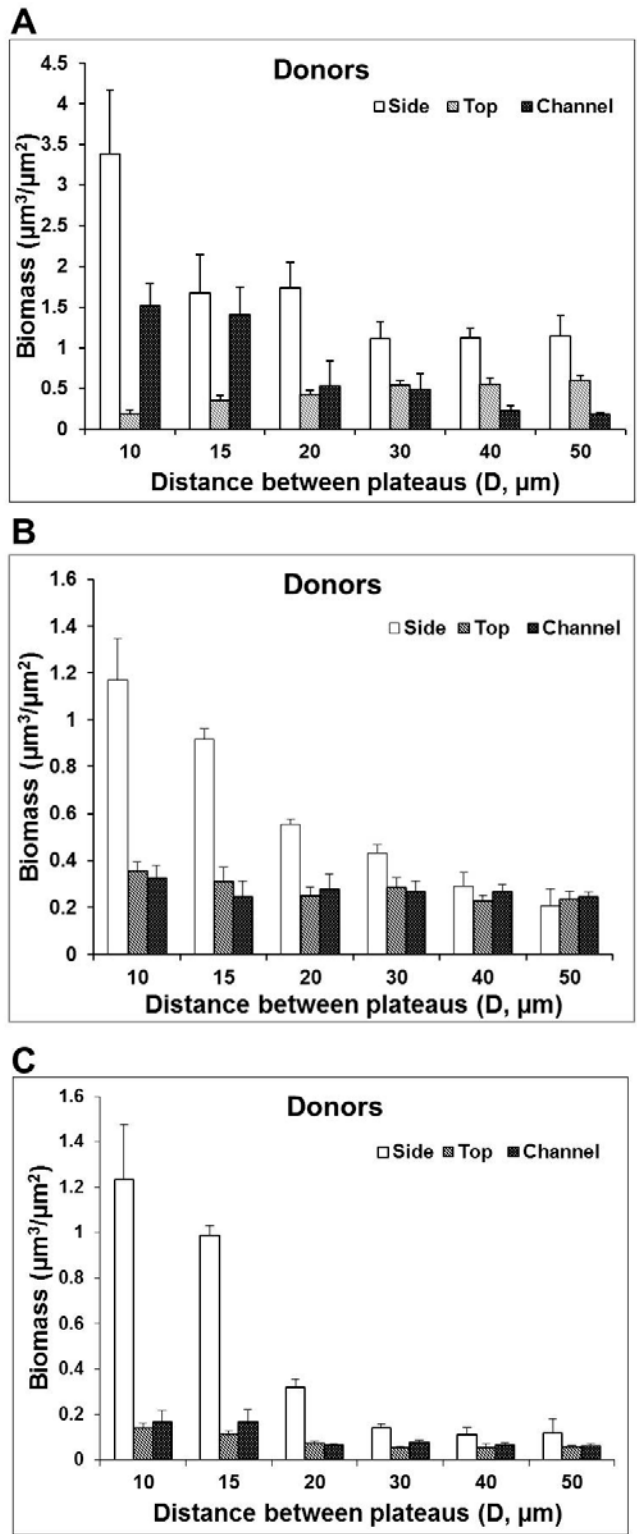


Figure 5-9

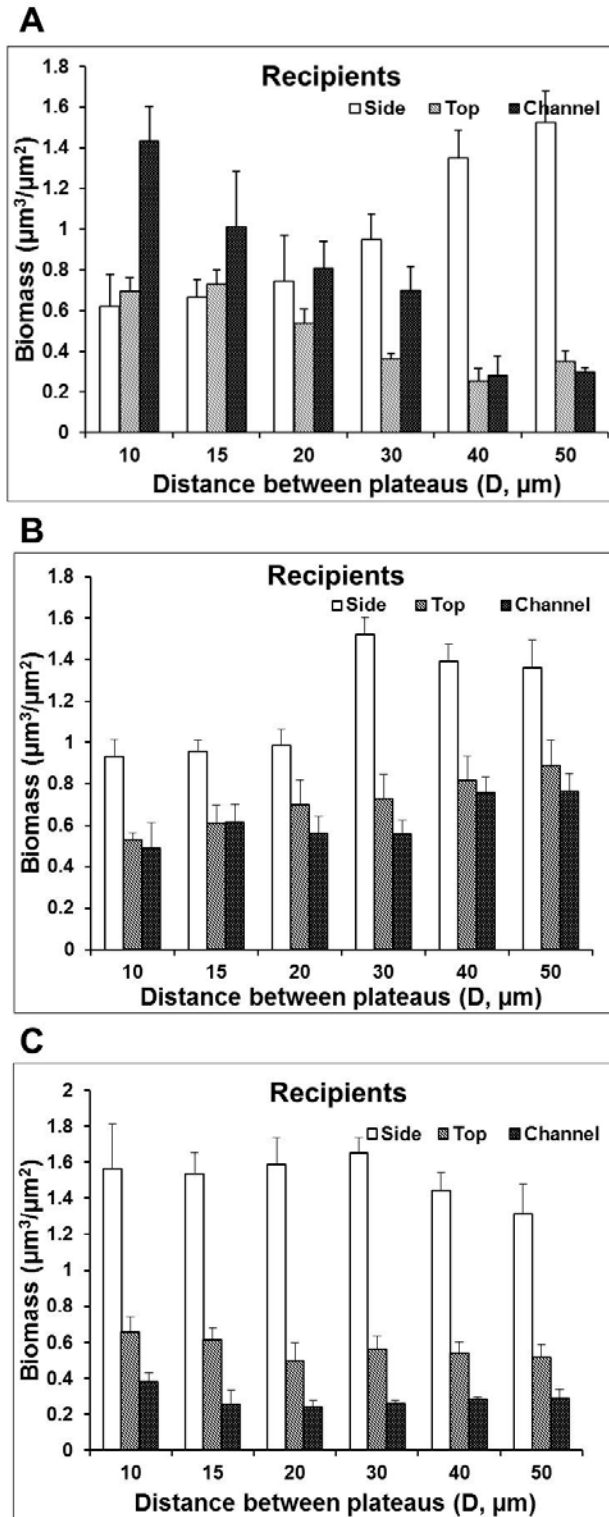


Figure 5-10

5.8 TABLE

Table 5-1. Pearson correlation coefficients between percentage of transconjugation and inter-pattern distance; as well as biomass of recipient cells and inter-pattern distance. All data were acquired on PDMS surfaces with 10 μm tall 20 μm \times 20 μm topographic patterns and varying inter-pattern distance.

Conjugation/Biomass	Location	Correlation Coefficient (r)
Percentage of conjugation	Side	0.37594**
Biomass	Side	0.94047***
Percentage of conjugation	Channel	-0.26608*
Biomass	Channel	-0.91413***

*: $P < 0.5$

** : $P < 0.05$

***: $P < 0.001$

5.9 REFERENCES

- 1 **Van Houdt, R., Michiels, C. W.** 2005. Role of Bacterial Cell Surface Structures in *Escherichia coli* Biofilm Formation. *Res. Microbiol.* **156**: 626-633.
- 2 **Mah, T. F., O'Toole, G. A.** 2001. Mechanisms of Biofilm Resistance to Antimicrobial Agents. *Trends Microbiol* **9**: 34-39.
- 3 **Gilbert, P., Allison, D. G., McBain, A. J.** 2002. Biofilms in vitro and in vivo: do singular mechanisms imply cross-resistance? *Symp Ser Soc Appl Microbiol*, 98S-110S.
- 4 **MacKintosh, E. E., Patel, J. D., Marchant, R. E., Anderson, J. M.** 2006. Effects of biomaterial surface chemistry on the adhesion and biofilm formation of *Staphylococcus epidermidis* in vitro. *J Biomed Mater Res A* **78**, 836-842.
- 5 **Katsikogianni, M., Missirlis, Y. F.** 2004. Concise Review of Mechanisms of Bacterial Adhesion to Biomaterials and of Techniques Used in Estimating Bacterial-Material Interactions. *European Cells and Materials* **8**: 37-57.
- 6 **Walker, J., Surman, S., Jass, J.** 2000. Industrial Biofouling: Detection, Prevention and Control. 1-12.
- 7 **Ghigo, J. M.** 2001. Natural conjugative plasmids induce bacterial biofilm development. *Nature* **412**: 442-445.
- 8 **Lewis, K.** 2001. Riddle of Biofilm Resistance. *Antimicrob Agents Ch* **45**: 999-1007.
- 9 **Cook, L. et al.** 2011. Biofilm growth alters regulation of conjugation by a bacterial pheromone. *Mol Microbiol* **81**: 1499-1510.
- 10 **Baharoglu, Z., Bikard, D., Mazel, D.** 2010. Conjugative DNA transfer induces the bacterial SOS response and promotes antibiotic resistance development through integron activation. *PLoS Genet* **6**: e1001165.
- 11 **Lin, A. et al.** 2011. Inhibition of bacterial conjugation by phage M13 and its protein g3p: quantitative analysis and model. *PLoS One* **6**: 1-11.
- 12 **Sørensen, J. S., Bailey, M., Hansen, H. L., Kroer, N., Wuertz, S.** 2005. Studying Plasmid Horizontal Transfer In Situ: A Critical Review. *Nature Reviews Microbiology* 700-710.
- 13 **Maiden, M. C.** 1998. Horizontal genetic exchange, evolution, and spread of antibiotic resistance in bacteria. *Clin Infect Dis* **27 Suppl 1**: S12-20.
- 14 **Al-Masaudi, S. B., Russel, A. D., Day, M. J.** 1991. Factors affecting conjugative transfer of plasmid pWG6 13, determining gentamicin resistance, in *Staphylococcus aureus*. *J. Med. Microbiol.* **34**: 103-107.
- 15 **Davey, M. E., O'Toole G, A.** 2000. Microbial biofilms: from ecology to molecular genetics. *Microbiol Mol Biol Rev* **64**: 847-867.
- 16 **Donlan, R. M.** 2002. Biofilms: microbial life on surfaces. *Emerging infectious diseases* **8**: 881-890.
- 17 **Dunne, W. M.** Bacterial adhesion: seen any good biofilms lately? *Clinic Microbiology Review* **15**: 155-166.
- 18 **Stoodley, P., Sauer, K., Davies, D. G., Costerton, J. W.** 2002. Biofilms as complex differentiated communities. *Annu Rev Microbiol* **56**: 187-209.
- 19 **Rana, D., Matsuura, T.** 2010. Surface modifications for antifouling membranes. *Chem Rev* **110**: 2448-2471.

- 20 **An, Y. H., Friedman, R. J.** 1998. Concise Review of Mechanisms of Bacterial Adhesion to Biomaterial Surfaces. *J Biomed Mater Res* **43**: 338-348.
- 21 **Hou, S., Gu, H., Smith, C. Ren, D.** 2011. Microtopographic Patterns Affect *Escherichia coli* Biofilm Formation on Poly(dimethylsiloxane) Surfaces. *Langmuir* **27**: 2686–2691.
- 22 **Friedlander, R. S. et al.** 2013. Bacterial flagella explore microscale hummocks and hollows to increase adhesion. *Proc Natl Acad Sci U S A* **110**: 5624-5629.
- 23 **Whitehead, K. A., Verran, J.** 2006. The effect of surface topography on the retention of microorganisms. *Food Bioprod Process* **84**: 253-259.
- 24 **Crawford, R. J., Webb, H. K., Truong, V. K., Hasan, J., Ivanova, E. P.** 2012. Surface topographical factors influencing bacterial attachment. *Adv Colloid Interface Sci* **179-182**: 142-149.
- 25 **Chung, K. K. et al.** 2007. Impact of engineered surface microtopography on biofilm formation of *Staphylococcus aureus*. *Biointerphases* **2**: 89-94.
- 26 **Pinedo, C. A., Smets, B. F.** 2005. Conjugal TOL transfer from *Pseudomonas putida* to *Pseudomonas aeruginosa*: effects of restriction proficiency, toxicant exposure, cell density ratios, and conjugation detection method on observed transfer efficiencies. *Appl Environ Microbiol* **71**: 51-57..
- 27 **Licht, T. R., Christensen, B. B., Krogfelt, K. A., Molin, S.** 1999. Plasmid transfer in the animal intestine and other dynamic bacterial populations: the role of community structure and environment. *Microbiology* **145 (Pt 9)**: 2615-2622.
- 28 **Christensen, B. B. et al.** 1998. Establishment of new genetic traits in a microbial biofilm community. *Appl. Environ. Microbiol.* **64**: 2247-2255.
- 29 **Sorensen, S. J., Sorensen, A. H., Hansen, L. H., Oregaard, G., Veal, D.** 2003. Direct detection and quantification of horizontal gene transfer by using flow cytometry and *gfp* as a reporter gene. *Curr Microbiol* **47**: 129-133.
- 30 **Renner, L. D., Weibel, D. B.** 2011. Physicochemical regulation of biofilm formation. *MRS bulletin / Materials Research Society* **36**: 347-355.
- 31 **Eun, Y. J., Weibel, D. B.** 2009. Fabrication of microbial biofilm arrays by geometric control of cell adhesion. *Langmuir* **25**: 4643-4654.
- 32 **Parkinson, J. S., Houts, S. E.** 1982. Isolation and behavior of *Escherichia coli* deletion mutants lacking chemotaxis functions. *J Bacteriol* **151**: 106-113.
- 33 **Blair, D. F., Kim, D. Y., Berg, H. C.** 1991. Mutant MotB proteins in *Escherichia coli*. *J Bacteriol* **173**: 4049-4055.
- 34 **Hou, S., Burton, E. A., Wu, R. L., Luk, Y. Y., Ren, D.** 2009. Prolonged control of patterned biofilm formation by bio-inert surface chemistry. *Chem Commun* **2009**: 1207-1209.
- 35 **Chong, L.** 2001. *Molecular cloning - A laboratory manual*, 3rd edition. *Science* **292**: 446-446.
- 36 **Gu, H., Hou, S., Yongyat, C., De Tore, S., Ren, D.** 2013. Patterned biofilm formation reveals a mechanism for structural heterogeneity in bacterial biofilms. *Langmuir* **29**: 11145-11153.
- 37 **Heydorn, A. et al.** 2000. Quantification of biofilm structures by the novel computer program COMSTAT. *Microbiol-Uk* **146**: 2395-2407.

- 38 **Hausner, M., Wuertz, S.** 1999. High rates of conjugation in bacterial biofilms as
determined by quantitative in situ analysis. *Appl Environ Microbiol* **65**: 3710-
3713.
- 39 **Levin, B. R., Stewart, F. M., Rice, V. A.** 1979. The kinetics of conjugative
plasmid transmission: fit of a simple mass action model. *Plasmid* **2**: 247-260.
- 40 **Normander, B., Christensen, B. B., Molin, S., Kroer, N.** 1998. Effect of
bacterial distribution and activity on conjugal gene transfer on the phyllo- plane of
the bush bean (*Phaseolus vulgaris*). *Appl Environ Microbiol* **64**: 1902-1909.
- 41 **Macnab, R. M., Aizawa, S.** 1984. Bacterial motility and the bacterial flagellar
motor. *Annu Rev Biophys Bioeng* **13**: 51-83.
- 42 **Curtiss, R., 3rd.** 1969. Bacterial conjugation. *Annu Rev Microbiol* **23**: 69-136.

CHAPTER 6

CONCLUSIONS AND RECOMMENDATIONS FOR FUTURE WORK

6.1 CONCLUSIONS

Biofilm formation is a dynamic process with vast changes in gene and protein expressions that are sensitive to many environmental factors such as surface chemistry, surface topography, and flow conditions. This dynamic process of biofilm formation and associated structural heterogeneity present a great challenge to study the mechanism of bacteria-surface interaction. In this study, we used well-defined surface chemistry and surface topography to control biofilm morphology and study bacteria-surface and bacterial cell-cell interactions. By tailoring gold surfaces with square-shaped patterns of CH₃-SAM for cell adhesion and background with bioinert triethylene glycol-SAM (TEG-SAM). The size of CH₃-SAM patterns and inter-pattern distance were systematically varied. The size of CH₃-SAM patterns was set to be 5, 10, 15, 20, 30, 40, or 50 μm and the inter-pattern distance was set to be 2, 5, 10, 15, 20, 30, 40, or 50 μm . Both the size of patterns and the inter-pattern distance were found to influence the interaction among cell clusters. In addition, critical pattern size (20 μm in this study) and inter-pattern distance (10 μm in this study) were found for significant interaction among cell clusters. Both the critical size and inter-pattern distance are larger than the size of single *E. coli* cell used in this study, which indicates that multicellular structures are involved in interaction between cell clusters during biofilm formation.

The interaction among cell clusters was found to be formed by cells grown out of cell clusters rather than those settled by gravity. Autoinducer-2 (AI-2) mediated quorum sensing (QS) was involved in such interactions since the *luxS* mutant exhibited defects in this behavior, which was complemented both chemically and genetically. Besides the *luxS* gene, the *motB* gene was also identified to be involved in the interaction among cell

clusters; In the end, *cheY* and *tap* genes were found to be important to the initial attachment of *E. coli*.

Since the critical distance for interactions between clusters is larger than the size of *E. coli* cells, we also tested the surface structures of biofilm cells. By imaging 2, 4, and 6 h biofilms with high resolution analytical scanning electron microscope (LEO 1550 FESEM, Keck SEM, Cornell Center for Material Research), nanometer-diameter structures on the surface of biofilm cells were observed. These structures appeared between cells in and between cell clusters, which suggested that they might play a role in bacterial cell-cell interaction. The protocol developed in this study can be further applied in investigating the role of these surface structures during the interaction among cell clusters on well-defined surfaces.

Inspired by the above findings, we also used the gold surfaces with engineered surface chemistry to obtain a better understanding of biofilm associated antibiotic resistance. Cells in bioinert areas between cell clusters are involved in interactions between these clusters. In 2 h patterned biofilms, these cells appeared to be more susceptible to 200 µg/mL ampicillin compared to the cells in cell clusters; while these cells gradually become more tolerant to ampicillin over time. These observations support the hypothesis that the cells between clusters are more active metabolically.

In addition to SAM surfaces, poly(dimethylsiloxane) (PDMS) surfaces modified with 10 µm tall topographic patterns were prepared in this study to investigate the effects of surface topography on bacterial cell-surface interaction. Previously, a former student in Ren lab has observed that *E. coli* RP437/pRSH103 preferred to attach and form biofilm in the valleys between close topographic patterns and there was a critical size of

plateaus to allow significant bacterial adhesion and biofilm formation on the top of protruding plateaus. The critical size is $20\ \mu\text{m} \times 20\ \mu\text{m}$ for PDMS surfaces, which is around 200 times larger than the size of a single *E. coli* cell. This conclusion indicates that bacterial cell-cell interaction is essential for the formation of multicellular structure of biofilms on those plateaus. To test whether this phenomenon was due to gravity, the biofilm formation of *E. coli* RP437/pRSH103 with constitutively expressed red fluorescence protein (RFP) was monitored using inverted PDMS surfaces modified with systematically designed microtopographic patterns. According to data, it is confirmed that there was a critical dimension for bacterial adhesion and biofilm formation on top of plateaus; however, the critical size increased to $40\ \mu\text{m} \times 40\ \mu\text{m}$ for inverted plateaus. This result indicates that gravity can facilitate biofilm formation but the critical dimensions are intrinsic factors for biofilm formation. To further corroborate the result that the adhesion on PDMS surfaces is not only due to gravity-driven settlement, the biofilm formation of the motility mutant strain *E. coli* RP3087/pRSH103 (*motB* mutant) on both upright and inverted PDMS surfaces with size $100\ \mu\text{m} \times 100\ \mu\text{m}$ patterns was tested. The results show that bacterial motility is important to bacterial adhesion on surfaces with topographies.

These results are inspiring for developing antifouling surfaces by changing surface topography. The total biomass of 24 h *E. coli* RP437/pRSH103 biofilms on PDMS surfaces with systematically designed microtopographic hexagon patterns was evaluated. The results showed that $10\ \mu\text{m}$ tall protruding hexagon features with side width of $15\ \mu\text{m}$ and inter-pattern distance $2\ \mu\text{m}$ can decrease total biomass by 70% compared to PDMS surfaces and the side width $15\ \mu\text{m}$ was found to be a critical

dimension for repelling bacterial adhesion and biofilm formation on protruding hexagon feature. This is consistent with the finding of 20 μm and 40 μm critical dimensions for square pattern.

The above results reveal that surface topography can influence cell density in biofilms. Hence, we applied this well-defined surface system to study bacterial conjugation between *E. coli* CSH26/pKJK10 (donor) and *E. coli* RP437/pRSH103 (recipient). *E. coli* CSH26/pKJK10 does not express green fluorescence protein (GFP) unless the inducer isopropyl β -D-1-thiogalactopyranoside (IPTG) presents or when the plasmid pKJK10 is transferred to recipients. *E. coli* RP437/pRSH103 constitutively expresses red fluorescence protein (RFP). Thus, by using this dual-labeling system, we could quantitatively study bacterial conjugation in biofilms formed on PDMS surfaces with systematically designed microtopographic patterns. The size of topographic patterns were set to 20, 50, or 100 μm that are equal to or larger than the critical size identified above and the inter-pattern distance was set to 10, 15, 20, 30, 40, or 50 μm . The results suggest that surfaces with microtopographic patterns in this study can promote biofilm formation and bacterial conjugation. The promotion of biofilm formation was due to the aggregation of cells on the side of protruding features, which are also found to be the 'hot spot' for bacterial conjugation on surfaces with 10 μm tall topographic features. This phenomenon was not due to gravity-driven settlement of cells because the motility mutant of recipient formed significantly less biofilms on the side of topographic patterns. The unit area conjugation frequency in biofilms formed by donors and the motility mutant recipients was also significantly lower than that in biofilms formed by donors and wild-type recipients, which indicates that motility is also important in bacterial

conjugation. Overall, by using patterned surface, this study revealed important missing information regarding bacterial-surface interactions. The results are also useful for designing new antifouling materials and surfaces.

6.2 RECOMMENDATIONS FOR FUTURE WORK

6.2.1 Role of bacterial motility in the bacteria-surface, bacterial cell-cell interactions, and bacterial conjugation

The *motB* mutant *E. coli* RP3087 that contains a malfunctioned MotB protein was found to have defects in interaction among cell clusters compared to the wild-type strain *E. coli* RP437¹. However, the isogenic *motB* deletion mutant (*E. coli* BL-19) of the wild-type strain showed major defects even in attachment. These results suggested that *motB* gene played a role in both adhesion and interaction among cell clusters. To study the role of *motB* gene in bacterial adhesion and interaction among cell clusters more specifically, the *motB* deletion mutant needs to be genetically complemented first. We recently obtained the plasmid pGM1 with *motB* gene regulated by IPTG-inducible *lac* promoter from Prof. Howard C. Berg. It can be transformed into the *motB* mutant *E. coli* BL-19 using electroporation¹⁻³. The biofilm formation of the wild-type strain, *E. coli* BL-19, and *E. coli* BL-19/pGM1 on chemically modified surfaces can be compared to study the role of *motB* gene during biofilm formation. IPTG of different concentrations can be added to induce the expression of *motB* gene and complement of the *motB* gene.

Bacterial motility was also found to affect conjugation. However, how does motility affect conjugation is unknown. The reduced bacterial conjugation frequency between donors and *motB* mutant recipients could be due to the reduction of bacterial

motility or the reduction of recipients in the biofilms formed on the side of protruding patterns. To test if bacterial motility has direct effects on bacterial conjugation, the conjugation in donors and wild-type recipients co-culture biofilms and donors and *motB* mutant recipients co-culture biofilms can be tested on filters. By eliminating topography as one of the factors, the role of bacterial motility in bacterial conjugation can be revealed.

6.2.2 Role of bacterial surface structures during interaction between cell clusters

Some cell surface structures in 2, 4, and 6 h *E. coli* RP437 patterned biofilms were visualized using LEO 1550 FESEM. To study the dynamic roles of bacterial surface structures during the interaction among cell clusters, the reporter strain of flagellar, curli, and fimbriae genes should also be used to form patterned biofilms and followed with fluorescence microscopy and SEM. This will help understand what types of structures are involved.

6.2.3 Effects of surface topography on bacterial cell-surface interaction and biofilm formation

Although we have obtained some information about the effects of surface topography on bacterial cell-surface interaction, the mechanism that governs the obtained phenomenon still needs to be further studied. We observed decrease in the biomass of biofilms formed on hexagon patterns with side width 15 μm and varying inter-patterns distance. Interestingly, Friedlander *et al.*⁴ reported that surfaces with 2.7 μm tall hexagon shaped patterns with 3 μm in diameter can promote biofilm formation. We hypothesize that the hydrophobicity of PDMS surfaces can be altered by surface topographies with different heights. This pattern dimension can lead to against or coagulation effects. Another

factor is the role of bacterial flagella in response to surface topography with different heights and dimensions. To further study, PDMS surfaces with hexagon shaped topographic patterns of different heights (2, 5, or 10 μm), size (side width, 2, 5, 10, 15, 20, 30, 40, or 50 μm), and inter-pattern distance (2, 5, 10, 15, or 20 μm) can be prepared. The hydrophobicity of these PDMS surfaces can be evaluated by measuring the contact angle. The biofilm formation of *E. coli* RP437/pRSH103 on these PDMS surfaces can be quantitatively studied to understand the effect of height, size, and inter-pattern distance on bacterial adhesion and biofilm formation. To have a mechanistic understanding of the obtained phenomenon at the genetic level, the comparison between biofilm formation of the wild-type strain and its isogenic mutants of the interested genes can be conducted. The role of flagella in bacterial adhesion on different surfaces can be monitored using FESEM.

6.2.4 Biofilm resistance to antibiotics

Biofilm resistance to antibiotics involves numerous factors. To further study the role of metabolic activity, a reporter strain of bacterial metabolic activity, *E. coli* MG-1655 ASV⁵, can be used to follow the metabolic activity of biofilm cells in patterned biofilms and correlate the results with antibiotic resistance.

6.3 REFERENCES

- 1 **Blair, D. F., Kim, D. Y., Berg, H. C.** 1991. Mutant MotB Proteins in *Escherichia-Coli*. *J. Bacteriol.* **173**: 4049-4055.
- 2 **Berg, H. C., Turner, L.** 1991. Selection of Motile Nonchemotactic Mutants of *Escherichia coli* by Field-Flow Fractionation. *Proc. Natl. Acad. Sci. USA* **88**: 8145-8148.
- 3 **Stolz, B., Berg, H. C.** 1991. Evidence for Interactions between MotA and MotB, Torque-Generating Elements of the Flagellar Motor of *Escherichia-Coli*. *J Bacteriol* **173**: 7033-7037.
- 4 **Friedlander, R. S. et al.** 2013. Bacterial flagella explore microscale hummocks and hollows to increase adhesion. *Proceedings of the National Academy of Sciences of the United States of America* **110**: 5624-5629.
- 5 **Shah, D. Z. Z., Khodursky, A. B., Kaldalu, N., Kurg, K., Lewis, K.** 2006. Persisters: a Distinct Physiological State of *E. coli*. *BMC Microbiol* **6**.

APPENDICES

APPENDIX I. PROTOCOL FOR FABRICATING SILICON WAFERS WITH MICROTOPOGRAPHIC FEATURES

This part of work was conducted at Cornell Nanoscale Facility (CNF).

Step I. Write micronscale patterns using Heidelberg Instrument DWL 2000

1. Purchase mask (5 inch) from the staff in CNF. The hour of the supply center is Monday-Thursday from 9-9:30 am and 1-1:30 pm and Friday from 10-10:30 am and 1-1:30 pm.

Converting the L-Edit file to GDSII file:

Software: L-Edit Layout Editor v13

1. Convert your L-Edit Layout File (.tdb) to GDSII file. Open your L-Edit file. Click 'File'- 'Export Mask Data'- 'GDSII...'. Change the name of the file you want to export the L-Edit Layout File into. Remember to check '**GDSII default**' instead of 'Custom' under catalog 'GDSII units' and '**Selected cell and its hierarchy**' instead of 'All cells' under catalog 'All cells'. Then click 'Export'.
2. After the export is done, check to make sure '**no error**'.
3. Reopen the .gds file that you just created in L-Edit to check whether the file only include your patterns in the GDSII file.
4. After the GDSII file is checked, the GDSII file needs to be transferred to the '**Heidelberg DWL2000**' file on the 'lab_xfer([\\image](#))(V:)' drive.

Converting the GDSII file into frame file:

Equipment: Computer 1

Software: Frame Generator

1. Go to the computer on the **left** of the Heidelberg DWL2000 machine. The conversion of the GDSII file in this computer does not require activation of the Heidelberg DWL 2000.
2. Double click on the folder '**Lab Transfer Share**' on the desktop and right click on the GDSII file you just created. Choose 'Copy To'->'Home Folder'->'gdsii'->'Copy Here'.
3. Double click the '**Frame Generator**' icon. Change the file name as 'frameDATENAMELX(1,2,3,...)'. Choose 'Contact' as 'Target'. There is **no** 'Barcode' for contact mode. Type in the 'Label' that you want to use to mark this mask (e.g., hexagon pattern). Then click 'do'. There will be a row of letters on the bottom of the box showing that 'Saved to /home/convert/gdsii/frameToday'sDateNameLX.gds', which indicates that this step is finished.
4. Close the Frame Generation application by clicking 'X' on the upright corner.

Importing the GDSII file and frame file into the computer connected to Heidelberg DWL2000:

Equipment: Computer 1

Software: X-convert

1. Double click on the '**X-convert icon**' to start the pattern conversion software.

2. Click on the icon under 'File' to initiate the conversion sequence. '**Set New Job**' window will appear.
3. Type in 'TodaysDateNameLX(1,2,3...)' in the '**Job Name**' field. Click 'OK'.
4. The '**Menu**' will appear.
5. Click '**Add**' within the 'Source File' submenu. The '**Load GDSII Design**' window will appear. Choose the **GDSII file** you saved in Heidelberg DWL2000 file on the 'lab_xfer(\\image)(V:)' drive and click 'Open'. '**GDSII Options**' will appear. Choose the 'Layer' you want to be included and unselect the other 'Layers'. Click '**Create Default**'.
6. Click '**Add**' and then '**GDSII**' within the 'Source File' submenu. '**Load GDSII Design**' window will appear. Click the frame file you created before and click 'Open'. 'GDSII Options' menu will appear. Click '**Create Default**'.
7. Under 'HMT File' submenu, click '**Merge Files**' button. The '**Merge HMT Files**' window will appear. Click '**Add all**' button, both files will be added from 'Available Files' portion of the menu to 'Merge Files' portion of menu. Click '**Generate**' and then '**Add to list**'.
8. To review your pattern, click '**OpenGL VIEWER**' button under 'HMT File' submenu.
9. Click '**Fill**' within the viewer option menu to preview your pattern. Click 'X' to exit. The patterns filled with black color are the patterns to be exposed on your mask.
10. Click 'X' to exit 'Plate 0'. This step is important for generating mirrored patterns and cannot be skipped. Click '**Add Plate**' under 'HMT File' submenu to open an empty 'Plate 0'. Click '**Add Cell**' under 'Plate 0' submenu.
11. Check the box to the left of '**Mirror**'. Click '**OpenGL**' will allow you to view the mirrored data. Click '**Complete Tasks**' and '**Save**' to save the job file. Use the same naming convention as before (TodaysDateNameLX).
12. Click '**Complete Expose Jobs**' and 'Prepare' menu will appear. Click '**Finish**' within 'Prepare' window.
13. Close the menu by clicking the red button on the upper right corner.

Writing mask:

Equipment: Heidelberg Instrument DWL2000; computer 2

1. Log into Coral and activate Heidelberg DWL 2000 to enable the keyboard and mouse of the computer to be connected with the equipment.
2. Go to computer 2 on the right of the Heidelberg DWL 2000. If the '**Exposure Map**' and '**Control Panel**' windows are not open, click the 2nd and 3rd icons under 'File' to bring up these two windows.
3. To turn on the laser, click '**Tools**' then '**Laser Control**'. '**Laser Control Panel**' window will appear. Click '**Turn Laser On**' and then '**Exit**'. The laser will be turned on and the box next to 'Laser Status' will become green.
4. Click '**Job**' in the 'Exposure Map' window and then '**Design Name**' field to highlight contents. Right click on the '**Design Name**' field and then click on '**Online**' on the pull down menu. 'Online Conversion' window will appear.

5. Double click on the pattern file you just created. You will descend into the directory structure of your pattern file. Click '**Get Design**'. The job menu will have the name of the file you chose.
6. Click '**Map**'. Check the box next to '**Laser Shutdown**' and then '**(Un)Load**' to bring the stage to the load position.
7. Open the door of the Heidelberg DWL 2000 by using the door switch located on the left hand side of the metal chamber.
8. Lift the cover of the loading stage for mask. Make sure the sensor is not right above the center of stage. Then place the L-shaped mask guide in the 4th groove for 5 inch mask. Place your mask against to the L-shaped mask guide and turn on the vacuum. Remove the L-shaped mask guide and put it on the shelf directly to the right of the stage cover. Lower the cover of the loading stage.
9. Close the door of the Heidelberg DWL 2000 by using the door switch.
10. Click '**To Center**' button in the 'Control Panel' menu. Check the position of the sensor to ensure that it has been moved to the center and then click '**Focus**'.
11. Click the 4th icon under 'File'. The stage will move and the sensor will try to find four edges of the mask. Check whether the sensor is moving to find the four edges of the mask.
12. Click '**Exposure**' in the 'Exposure Map' window. The exposure time will appear on the window. The time is not accurate because the machine cannot predict what pattern you will write.
13. **Do not** close the software after you finished.
14. After the writing is finished, open the door of the Heidelberg DWL 2000. Raise the cover of the stage, turn off the vacuum and remove your mask. Then lower the cover of the stage and close the door. **Do not** leave the door open for a long period of time. This will damage the sensitivity of the machine.
15. Turn off the laser by clicking '**Tools**' and then '**Laser Control**'. 'Laser Control Panel' window will appear. Click '**Turn Laser Off**' and then '**Exit**'. Repeat it again to make sure that the laser is turned off and the box next to 'Laser Status' becomes red.
16. Disable the machine by logging into Coral.

Mask development and etching:

Equipment: Hamatech-Steag Mask Processor HMP900

1. Mount the exposed mask in the holder (Fig. 1).
2. Develop the mask by choosing program 2 in the Hamatech-Steag Mask Processors and click 'Start'.
3. Chrome etch the mask by choosing program 1 and click 'Start'.
4. Be aware that the sequence **cannot be reversed**.
5. Remove the etched mask from the holder.

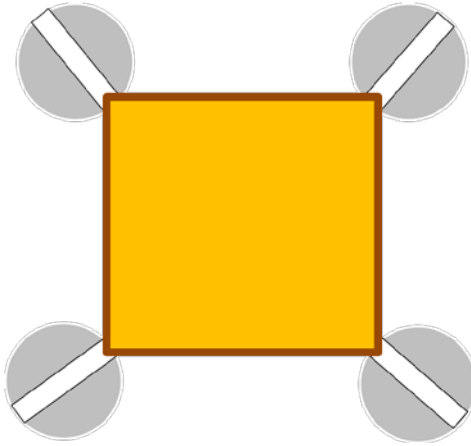


Figure 1 The top-down view of mask in Hamatech-Steag Mask Processor HMP900

Photoresist removal:

Equipment: Resist hot strip bath

1. Wear green gloves and face shield before operation.
2. Load masks onto the plastic wrack. Please make sure that the plastic wrack can be put into A108-50 before loading the masks.
3. Choose the right handle for the plastic wrack.
4. Open the lid of Tank 1 (hot bath, 75 °C). Put the plastic wrack into Tank 1 for 20 min. Avoid touching the solution in Tank 1. Lower the lid of Tank 1. **Please do not touch anything else with green gloves except the plastic wrack and handle.**
5. Transfer the plastic wrack into Tank 2 (hot bath, 75 °C) and keep for 20 min.
6. Then, transfer the plastic wrack into the tank for dump-rinse. Take off the green gloves and press the green button located above the tank. The dump-rinse cycle will start. This step is very important for the removal of photoresist.
7. When the dump-rinse cycle is finished, the safety hood will give a signal. Press the green button again to stop the alarm. Take the plastic wrack out of the tank and remove the handle.
8. Open A108-50 'Spin rinse dryer' located on the right of the safety hood for 'Hot Strip Bath'. Please kick the right side of the panel located on the bottom of the machine. There is a sign on the panel 'Lower spin dryer'. The door of the 'Spin rinse dryer' will open.
9. Load the plastic wrack into the 'Spin rinse dryer'. Click the same panel again to close the door. Press 'Start'.
10. When the process is finished, the machine will give a signal. Open the door of the 'Spin rinse dryer' and take out the plastic wrack. Close the door.
11. Remove the mask and store in the mask container for future application.

Step II. Photoresist deposition

1. Purchase wafers (3 inch) from the staff at CNF.

2. Make sure the wafers are clean before the deposition of photoresist. The wafers purchased from the supply center are considered clean. Wafers can also be cleaned with 'hot strip bath' before the deposition of photoresist.
3. To coat wafers in the spinner hood, please put face mask on during operation. Wafers are positioned in the center of a correct wafer holder and held with vacuum supplied from the bottom of the wafer holder. The wafer holder is chose based on the size of your wafer.
4. Load the program for wafer spinning. Click the 'Load' button and choose the program for the deposition of photoresist S1813 (500g (3500 rpm), 30 sec).
5. Clean wafers with P20 primer. Press the green 'Start Centering' button on the touch board screen. Measure 3 mL P20 primer with disposable pipette and then drop them in the center of the wafer. Please avoid taking P20 primer from the bottom and top layer of the P20 primer stock solution. Because there could be precipitates in the bottom layer of the stock solution and the top layer P20 primer stock solution could have been oxidized. Lower the lid. Allow P20 to spread and sit for 5 sec on the surface of the silicon wafer and then press the green 'Start Process' button. When the process is done the computer will give a signal. Press 'OK' to stop.
6. Press the green 'Start Centering' on the touch board before depositing photoresist. Measure 3 mL photoresist S1813 with disposable pipette and then drop them in the center of the wafer. Remember to push out the air on the tip of the pipette to avoid bubbles. Avoid taking the photoresist from the bottom and top layer of the stock solution as well. Lower the lid. Immediately start the deposition process by clicking the green 'Start Process' button. Wait until the process is done and stop the alarm by pressing the 'OK' button.
7. Immediately transfer the wafer onto the hot plate to bake for 60 sec and then onto a cold plate. The temperature of the hot plate is 115 °C.
8. Clean the photoresist residue in the spinner.
9. Measure the thickness of the photoresist layer on the silicon wafer using the Rudolph FTM. Three buttons are important on Rudolph FTM. The left button 'nm/micron' indicates the thickness of the photoresist you will measure. Select '**micron**' if you want to measure the photoresist of micron scale and vice versa. The middle button reflects whether film refractive index (n_f) is smaller or bigger than your substrate index (n_s). The refractive index, n_f , can be found in the reference binder located next to the instrument. The n_f of photoresist S1813 is smaller than n_s ($n_f < n_s$). The right button needs to be adjusted to the correct n_f , which is **1.59** for photoresist S1813. After these three buttons are set correctly, the thickness of the photoresist S1813 deposited on the wafer should be around **1.3 μm** .

Step III. Transfer patterns from mask to silicon wafer

1. Log into CORAL to enable the **ABM contact aligner** under the equipment list of 'Photolithography'.
2. Turn on the power of the ABM contact aligner. The red 'power' button locates at the right corner of the machine.
3. Turn on the 'Nitrogen Flow Switch' because you will use vacuum contact mode.

4. Make sure that the mask frame is not lifted. Look top-down to check whether the substrate chuck is in the center of the square-shaped hole in the center of mask frame. If it is not, adjust the knobs on the right (knob 1) and front (knob 2) of the stage to bring the substrate chuck to the center of the square-shaped hole (Fig. 2).

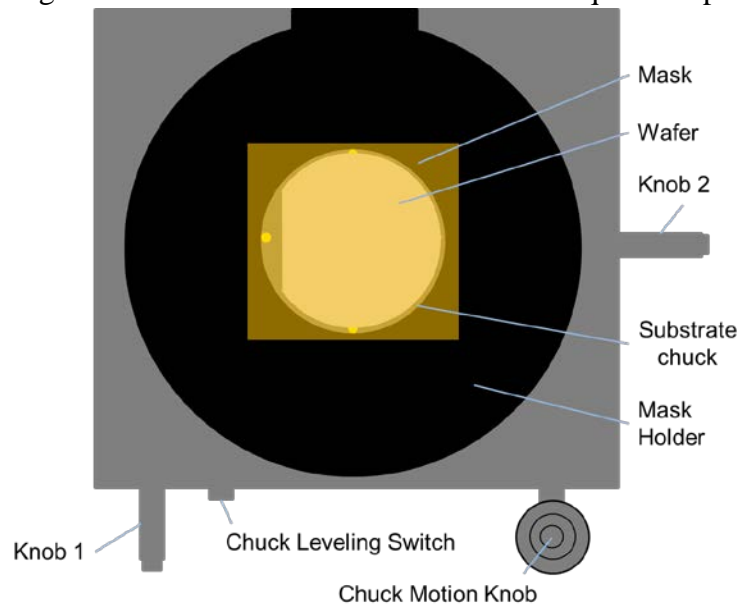


Figure 2 The top-down view of the stage of ABM contact aligner

5. Turn on 'Raise Mask Frame Switch'.
6. After the mask frame is raised, mount the mask with designed patterns to the bottom of frame with the silver side facing up and brown side facing down. Slide the mask from right to left and top to bottom until you reach the bumper on the left and bottom of the frame. Then, turn on 'mask vacuum switch'.
7. Mount wafer onto Substrate Chuck with the side coated with photoresist facing up and turn on 'Substrate Vacuum Switch'.
8. Lower the Mask Holder.
9. Bring mask to wafer by pressing and holding 'Chuck Leveling Switch' and turning 'Chuck Motion Knob' CCW (Fig. 2). Stop turning the Chuck Motion Knob when it begins slipping.
10. For alignment, bring the 'Alignment System Switch' to Align. Turn the chuck motion CW one full turn.
11. Turn off the 'Substrate Vacuum Switch' and turn on 'Contact Vacuum Switch' for Vacuum Contact Mode.
12. Move 'Alignment System Switch' back to Home position.
13. Set 'Exposure Time'. To adjust the exposure time, the same wafer can be exposed for different period of time at different area with the usage of the UV light blocker and developed (Fig. 3). Based on the developed wafer, you can determine the exposure time you need to expose the photoresist deposited on the wafer. For the photoresist S1813, the exposure time is **8 sec**.

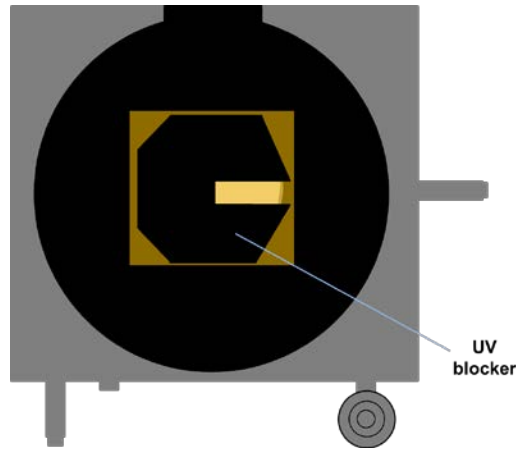


Figure 3 The top-down view of the stage of ABM contact aligner with a UV light blocker

14. Move 'Light Source Switch' to Exposure.
15. After the exposure is finished, move the 'Light Source Switch' to Home position.
16. Turn off the 'Contact Vacuum Switch' and turn on the 'Substrate Vacuum Switch'.
17. If you have another wafer, raise the Mask Frame and turn off the 'Substrate Vacuum Switch' to replace the wafer. Then go back to step 7.
18. If you don't have another wafer, turn 'Chuck Motion knob' CW to break the contact between wafer and mask.
19. Raise Mask Frame.
20. Turn off the Substrate Vacuum Switch' to remove wafer.
21. Turn off 'Mask Vacuum Switch' to remove mask.
22. Lower Mask Frame.
23. Turn off 'Power Switch' and 'Nitrogen Flow Switch'.
24. Disable the ABM contact aligner by logging into Coral.
25. Develop the mask by using program 6 in 'Wafer Developer 1' (Stage HamaTech, HMP 900). The program 6 includes '726 MIF 60 sec DP'.

Step VI. Etch silicon wafers

1. Clean the photoresist on the edge of the wafers with Q-tips cotton swabs and acetone (at least 1 inch) (Fig. 4).

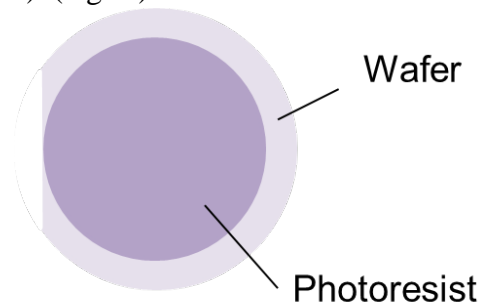


Figure 4 A silicon wafer deposited with photoresist S1813

2. Log into Coral to enable the UNAXIS 770.
3. Vent loadlock by clicking 'Utilities'->'Loadlock'->'Vent'. When the system shows 'ATOMOSPHERE', open the lid and load your wafer onto load arm with the photoresist side facing up. Locate wafer flat facing rear.
4. Click 'Process'->'Batch'->'File'->'Load'->'Obtrench.bch'->'OK'.
5. Click 'File'->'Exit'.
6. Click 'Ready' and 'Run'.
7. If there is an alarm giving by UNAXIS 770 during etching, click 'ALARM SILENCE'->'HOLD'.
8. The depth of each loop varies everytime. Everytime when you use UNAXIS 770 for etching, the first etching should only include three loops. Click 'END STEP' when the machine finishes the third loop.
9. Open the lid and remove your wafer. Click 'Utilities'->'Landlock'->'Pump'.
10. Go to P10 to measure the depth etched after three loops.
11. Disable UNAXIS 770 and enable P10 in Coral.
12. Load your wafer in the center of the stage. Press 'F7 LOAD/UNLOAD' to load your wafer. If the monitor is not showing 'PRECISION MODE', press 'F6 X-Y'. To position the sensor, press 'ZOOM'->'Z' and then down arrow to bring the sensor to the surface of your wafer.
13. After the contact is made, press 'X-Y' and use the left and right arrow to find your pattern.
14. Once your pattern is located, press 'ESC/MENU'->'CATALOG'-'ENTER'. Find your recipe for measurement. The recipe should include 'Type: 2D; V. Range: 300 μm; Profile:' Then press 'X-Y'.
15. Press 'F8 START' to apply the recipe for measurement.
16. After the measurement is finished, press 'F10 LEVEL'. Move 'L' and 'R' to the same level, press 'LEVEL' again. Move 'R' to the upper level to read the height of the etching. Use this height to calculate height/loop and the number of loop to get the height you want. Then go back to step 2.
17. Disable P10 in Coral.
18. After the etching process is finished, press 'Utilities'->'Landlock'-'Pump'-'STANDBY'.
19. Disable UNAXIS 770 in Coral.
20. Clean the photoresist on the wafers with 'Hot Strip Bath' and A182-39M.
21. The depth of patterns needs to be determined and labeled on the back of wafer for the convenience of future usage using P10 before coating with FOTS.

Step V. Coat silicon wafers with microtopographic features with antiadhesion chemical FOTS

1. Check whether the chemical FOTS is available on MVD 100 (Line 2). If FOTS is not available, contact the equipment manager of MVD 100 one week before coating to request.
2. Log into CORAL system and enable the tool MVD 100 under equipment list 'Packaging & Misc Processing'.
3. Check the chamber pressure on the touch board screen of MVD 100. The pressure should be less than 0.035 Torr.

4. Run a dummy run of your process. A dummy run is a short run of your process for about 1 min or less with an empty chamber. The operation procedure is the same as coating a real sample.
5. Vent the chamber and load your sample. Press 'Routines' button on the screen and then the green 'Vent' button. After the chamber is vented, 'VIEW SYSTEM' will show 'Chamber Vented'. Open the lid and load your samples into the chamber. There is no specific loading position for your sample in the chamber. Be aware of the two holes in the corners of the chamber floor. They should not be blocked.
6. Pumpdown the chamber. Press 'Routines' button on the screen and then the green 'Vent' button. The status of 'VIEW SYSTEM' will show 'Purge' and then 'Idle' when the pumpdown process is finished.
7. Load the program for your process. Specifically, the program of 'FOTS' needs to be loaded. Press 'Sequences' button on the touch board screen and then the arrow besides the process. There are three options available, including 'Single Layer', 'Double Layers', and 'Multiple Layers'. Press the arrow besides 'Single Layer' and the red 'Load' button on the upper right corner of the touch board screen. Chose the program 'FOTS' and press 'Yes' for loading this program.
8. Run process. Press 'Sequences' button to go back to upper screen and then the green 'Run' button for the process you have programmed/verified.
9. Abort the run. If something goes wrong, you need to abort the program. Press 'Abort' button on the upper right side of the screen and then 'Clear Fault'. Restart your program again.
10. Vent the chamber. After the program is finished, the status of 'VIEW SYSTEM' will show 'Idle'. Press 'Routines' button and then the green 'Vent' button to vent the chamber. When 'Chamber Vented' is shown, open the lid and remove your samples. If you have more samples, load them and go back to step 6. If you have finished processing your samples, go to step 11.
11. Pumpdown the chamber. Press the 'Routines' button and then the green 'Pumpdown' button. When the status of 'VIEW SYSTEM' shows 'Idle', the pumpdown process is finished.
12. Log out. It is important to remember to disable the machine MVD 100 in CORAL after the pumpdown step is over.

APPENDIX II. PROTOCOL FOR GOLD SURFACE MODIFICATION

Material:

Gold surface, tweezers, cotton swab, PDMS pattern with microtopographic pattern, microscope glass slides, cover slides, filter, air, a piece of clean paper, petri dishes

Chemicals:

Ethanol (200 proof), Pentadecanethiol 98% (Sigma-Aldrich, St. Louis, MO, USA; FW: 244.5; working concentration: 2mM), Triethylene glycol mono-11-mercaptonelecy ether 95% (Sigma-Aldrich, St. Louis, MO, USA; FW: 336.53; working concentration: 2mM), 0.85% NaCl solution.

Procedure:

Day 1

1. Practice how to cut glass slides into approximately 6 mm by 12.5 mm small pieces. Please cut on the side of microscope slides that was not coated with gold.
2. Put the small pieces of gold slides in petri dish with the side coated with gold facing up.
3. Clean your hands with 190 proof ethanol first. (Please wear gloves)
4. Sterilize your tweezers with ethanol and remove ethanol with flame. . (Please use tweezers with teeth).
5. Pick up a piece of small gold surface with your tweezers and put it on your palm with the side coated with gold facing up
6. Grab a corner of the gold slides. Wash the gold surface thoroughly with 190 proof ethanol.
7. Dry the slide with a sterile air stream.
8. Then put the gold surface on the clean paper with the side coated with gold facing up.
9. Wash a PDMS surface with microtopographic pattern with 190 ethanol and dry it with a sterile air stream.
10. Swab the PDMS surface with 2 mM CH₃-SEM using cotton swab and dry the PDMS surface with a sterile air stream.
11. Then gently drop the PDMS pattern onto sterilized gold surface with the microtopographic patterns facing down.
12. Then count for 15 seconds.
13. Grab the PDMS pattern firmly with tweezers and take it away from the gold surface.
14. Wash PDMS pattern with 190 proof ethanol, dry it with air stream and store it in a clean petri dish for further application.
15. Wash the gold surface with 190 proof ethanol to remove extra CH₃-SAM and soak it in a tube with 3 mL TEG-SAM solution.

16. Let the gold surface sit in TEG for 24 hours at room temperature.
17. Prepared overnight culture of your bacterial strain.

Day 2

1. Prepare a clean petri dish and a clean paper.
2. Clean your hands and tweezers. (Please wear gloves)
3. Take the gold surface out of TEG alkanthiol solution.
4. Wash the gold surface with 190 proof ethanol and dry it under a sterile air stream.
5. Put the gold surface into a clean petri dish with the side coated with gold facing up.
6. Measure the OD₆₀₀ of your overnight culture and then calculate how much you need to add into 20 mL LB solution to reach OD₆₀₀ of 0.05.
7. Put the petri dish in the 37°C culture room for biofilm growth after inoculation.

Day 3

1. Take three clean petri dishes and filled them with 0.85% NaCl solution.
2. Take the gold surface with biofilms out of the culture room and then wash the gold surface three times with 0.85% NaCl solution to remove planktonic cells.
3. Then transfer the gold surface onto the micoroscope glass slides.
4. Put the cover slips on top of the gold surfaces.
5. Then image the sample using the microscope.

APPENDIX III. PROTOCOL FOR LABELING BACTERIA WITH ACRIDINE ORANGE

Material: Acridine orange Powder (Sigma-Aldrich, St. Louis, MO, USA)

Stock solution: 5 mg/mL in water (Store in dark)

Staining solution (in 10 mL water):

1mL of Acridine Orange stock solution

0.5 mL of glacial acetic acid to make the staining solution to pH 3

Staining procedure:

1. Wash your sample three times in 0.85% NaCl solution (change to fresh solution every time).
2. Transfer sample into 3 mL acridine orange staining solution.
3. Let the sample stain for 2 min. Then image the sample with fluorescence microscope.

APPENDIX IV. PROTOCOL FOR THIN LAYER GOLD DEPOSITION ON COVERSLIPS

1. Clean the coverslips using the Piranha Cleaning. Load coverslips in a clean glass container with glass lid first. Fill the glass container with a mixture of 98% sulfuric acid and hydrogen peroxide with volume ratio (7:3). Then, the glass container will be brought to a hot plate until the temperature of the mixtures reaches 80°C. Maintain the temperature at 80°C for 45 min. Next, allow the temperature of mixture to decrease to room temperature. Remove the mixture and wash the coverslips with distilled water, methanol, and ethanol. Dry the coverslips with nitrogen.
2. Coat the cleaned coverslips using the Odd Hour Evaporator in CNF.
3. Load the cleaned coverslips on the sample holder.
4. Enable the Odd Hour Evaporator in Coral.
5. Turn off the Ion Gauge.
6. Press 'Stop' button on the AVC 485 and wait until you hear the gate valve close. Then press the vent button on the AVC 485.
7. Wait until the green 'Vented' light comes on and the red 'Vacuum' button goes off.
8. Once the bell jar is vented, hold the switch 'UP' to raise the bell jar and press the 'Stop' button on the AVC 485 to turn off the nitrogen vent.
9. Flip the shutter switch to the right to open the shutter and the green light on 'OPEN' will come on.
10. Quickly load your samples. Face the surface of your sample downwards the source.
11. Flip the shutter switch to the left to close the shutter and the red light on 'CLOSED' will come on.
12. Loading the titanium and gold on position '1' and '2'.
13. Check the crystal monitor life on the Operate Screen. If the reading is over 20%, the quartz crystal needs to be changed. To change, pull off the crystal holder cap and replace the old crystal with a new crystal. The reading should become 0%.
14. Hold the switch 'DOWN' to bring down the bell jar until the bell jar stop moving.
15. Press the 'Start' button on the AVC 485 to start the vacuum. The red vacuum light should come back on.
16. Turn on the ion gauge when the AVC 485 switches from roughing mode to high vacuum. Wait until the pressure reaches about 2.0×10^6 Torr before evaporating. The shorter you leave the jar open, the shorter it will take to bring down the pressure.
17. Unlock the selection switch and select 'EB Gun'.
18. Re-lock the selection switch and the red light should come back on.
19. Make sure the ion gauge is on.
20. From left to right, turn on the four switches on the right hand side of the evaporator.
21. Press one of the yellow 'Reset' buttons on the high voltage controller.
22. Press the red 'Source' button and the red 'High voltage' button.
23. Hold the up arrow to increase the power for the evaporation of the material that you want to deposit. Bring up the power to 3.5% slowly and adjust the speed by looking through the view port.
24. Adjust the location of the electron beam by adjusting the two knobs for controlling the vertical and horizontal motion of the electron beam to make sure the electron beam slowly sweep inside the center of the crucible and over the entire source.

25. Increase the power 3% per minute until the desired power threshold and deposition rate is reached.
26. To start depositing material, flip the shutter switch to the right to open the shutter and press the 'Zero' button on the XTC/2 to zero the crystal monitor.
27. When the thickness reaches the desired number, flip the shutter switch to the left to close the shutter.
28. Slowly decrease the power back to zero.
29. Let the material sit for a while to cool down and then change to the second material by press the '2' button. Then go back to step 23.
30. After you finish the deposition, press the green 'Off' button on the high voltage control panel.
31. Press the green 'Off' button on the source.
32. From right to left, turn off the four switches on the right hand side of the evaporator.
33. Turn off the ion gauge and press 'Stop' button on the AVC 485. Wait until you hear the gate valve is closed.
34. Press 'Vent' button on the AVC 485 and wait until the green 'Vented' light comes on.
35. Hold the switch 'UP' to raise the bell jar.
36. Press the 'Stop' button on the AVC 485 to turn off the nitrogen vent.
37. Remove the sample holder and source materials. Clean the whole system with vacuum.
38. Hold the switch 'DOWN' to bring down the bell jar until the bell jar stop moving.
39. Press 'Start' button on the AVC 485 to start the vacuum. The red vacuum light should come on. Wait until the vacuum switch from roughing to high-vacuum before leaving the tool.
40. Disable the Odd Hour Evaporator in Coral.

Huan Gu

121 Lafayette Road Building 2 Apt. 405
Syracuse, NY, 13205
Email: hugu@syr.edu
Cell Phone: (315)378-6001

EDUCATION

Chemical Engineering

August, 2009 - May, 2014

Ph.D. candidate, Biomedical and Chemical Engineering, Syracuse University
(anticipated)

Thesis: Patterned Biofilm Formation to Investigate Bacteria-Surface Interaction

Advisor: Dr. Dacheng Ren

Applied Chemistry

September, 2006 - July, 2009

M.S. China University of Mining & Technology, Beijing, CHINA

Exchange student in **Technical Institute of Physics and Chemistry of CAS (IPC of CAS)**

Role: Project leader, Study on the components of crude oil

Applied Chemistry

September, 2002-July, 2006

B.S. China University of Mining & Technology, Beijing, CHINA

PUBLICATIONS

Conjugation in *Escherichia coli* Biofilms on Poly(dimethylsiloxane) Surfaces with Microtopographic Patterns. **Huan Gu**, Kristopher William Kolewe, and Dacheng Ren. In preparation.

Orientation and Cluster Formation of *Escherichia coli* Cells Attached to (Poly)dimethylsiloxane Surfaces with Microtopographic Line Patterns. Aaron Chen, **Huan Gu**, and Dacheng Ren. In preparation.

Material and Surface Engineering to Control Bacterial Adhesion and Biofilm Formation: A Review of Recent Advances. **Huan Gu** and Dacheng Ren. **Frontiers of Chemical Science and Engineering (FCSE)**. 2014, 8(1): 20-33.

Patterned Biofilm Formation to Investigate Interactions among Cell Clusters: Linking Cell-to-Cell Communication to Structural Organization of *Escherichia coli* Biofilms. **Huan Gu**[†], Shuyu Hou[†], Chanokpon Yongyat, Suzanne De Tore, and Dacheng Ren. **Langmuir**. 2013, 29; 11145-11153.

Microtopographic Patterns Affect *Escherichia coli* Biofilm Formation on Poly (dimethylsiloxane) Surfaces. Shuyu Hou[†], **Huan Gu**[†], Cassandra Smith, and Dacheng Ren. **Langmuir**. 2011, 27: 2686-2691.

Recent Advances on Researches of Methods for Componental Analysis of Crude Oil. **Huan Gu**, Yao Lu, Xuzhu Shang, and Hai-yong Zhang. Physical Testing and Chemical Analysis Part

B : Chemical Analysis. 2011,47(4): 496-500.

Analysis of Paraffin after Low-Temperature Oxidization by Gas Chromatography. **Huan Gu**, Xuzhu Shang, Haiyong Zhang, Yao Lu, and Lizhuang Zhou. Chemical Engineering of Oil & Gas. 2009,02: 164-166.

Application of Ant Colony Algorithm to Optimization of Monomer Ratios in Emulsion Polymerization. Xiangkun Guo, Xiaoling Wang, and **Huan Gu**. Computers and Applied Chemistry. 2007, 24(7):925-928.

Preparation and Mechanical Properties of Polyacrylate Latex Modified Fly-Ash/Cement Mortar. Xiangkun Guo, Lizhuang Zou, and **Huan Gu**. Acta Scientiarum Naturalium Universitatis Sunyatseni. 2007, 46(plus27):167-168.

Preparation and Mechanical Properties of Polyacrylate Latex. Xiangkun Guo, **Huan Gu**, and Xiaoyong Li. Acrylic acid chemical engineering and application. 2007,20(2):16~19.

Research on Polymer Modified Mortar Based on MATLAB. Xiangkun Guo, Xiaoling Wang, and **Huan Gu**. Sichuan Building Science. 2008,34(2):159~162.

Pareto Ant Colony Optimization to Batch Free-radical Polymerization Reactors. Xiangkun Guo, Lizhuang Zou, **Huan Gu**. Proceedings of International Conference on Informatics and Control Technologies 2006. 12 Shenzhen, China. 335-340.

PRESENTATIONS

The Stevens Conference on Bacteria-Material Interactions. Hoboken, NJ.

June 9, 2011

Talk on June 9th: Microtopographic Patterns Affect *Escherichia coli* Biofilm Formation on Poly(dimethylsiloxane) Surfaces.

AIChE's 2011 Meeting, Minneapolis, MN.

November 8, 2010

Talk on November 8th: Effects of Microtopographic Patterns on *Escherichia Coli* Biofilm Formation on Polydimethylsiloxane Surfaces.

LABORATORY SKILLS/EQUIPMENTS

Microscopy

- Upright and inverted fluorescence microscopy (Upright: Zeiss Imager M1; Inverted: Zeiss Observer Z1)
- Confocal microscopy (Zeiss LSM 710)
- Atomic force microscopy (CNF, AFM Veeco Icon)
- Scanning electron microscopy (CNF, Zeiss Ultra SEM; CCMR, Keck SEM; JEOL JSM-5800 LV)

Software

- Imaging software (Zen and Axiovision)
- Image analysis software (MATLAB based COMSTAT)

Biotechniques

- Polymerase Chain Reaction (PCR)
- Cloning
- DNA/RNA Isolation
- Plasmid Isolation and Transformation
- Northern Blotting

Cornell Nanofabrication Facility (CNF)

- ABM Contact Aligner (ABM)
- Hamatech-Steag Mask Processors
- Hamatech-Steag Wafer Processors
- Manual Resist Spinners
- PG Mask Writer
- Resist Hot Strip Bath
- SU-8 Hotplates
- MVD100
- MOS Clean
- L-Edit CAD Software
- P10 Profilometer
- Unaxis 770 Deep Si Etcher
- CVC Sputter Deposition

SELECTED AWARDS

Student Travel Grant Award

The 6th ASM Biofilms Conference, Miami, FL.

September 29 - October 4, 2012

The Stevens Conference on Bacteria-Material Interactions, Hoboken, NJ.

June 9 - June 10, 2011

Research Assistantship (RA)

Department of biomedical and chemical department, Syracuse University.

September, 2009 - Now

Teach Assistantship (TA)

Department of biomedical and chemical department, Syracuse University.

September, 2009 - May, 2010

SELECTED POSTERS

Patterned Biofilm Formation Reveals Critical Information of

September, 29 - October 4, 2012

Bacteria-Surface Interactions.

The 6th ASM Conference on Biofilms. Miami, FL.

Horizontal Gene Transfer in *Escherichia coli* Biofilms on (Poly)dimethylsiloxane

June 16 - 19, 2012

Surfaces with Micotopographic Patterns.

ASM 2012 General Meeting, San Francisco, CA.

Patterned Biofilm Formation Reveals Critical Information of

June 16 - 19, 2012

Bacteria-Surface Interactions.

ASM 2012 General Meeting, San Francisco, CA.

**Effects of Microtopographic Patterns on *Escherichia coli* Biofilm Formation on
June 9 - 10, 2011
Polydimethylsiloxane Surfaces.**

The Stevens Conference on Bacteria-Material Interactions. Hoboken, NJ.

TEACHING EXPERIENCES

Heat and Mass transfer

January, 2010 - May, 2010

TA, Primary responsibility for grading, consultations, students, and recitation.

Introduction to Chemical Engineering Principles

September, 2009 - December, 2009 TA, Primary responsibility for grading and consultations.